Investigating the actin regulatory activities of Las17, the WASp homologue in *S. cerevisiae*

A thesis submitted for the degree of Doctor of Philosophy

By

Liemya E. Abugharsa

Department of Molecular Biology and Biotechnology

University of Sheffield

March 2015

Abstract

Investigating the actin regulatory activities of Las17, the WASp homologue in *S. cerevisiae*

Clathrin mediated endocytosis (CME) in *S. cerevisiae* requires the dynamic interplay between many proteins at the plasma membrane. Actin polymerisation provides force to drive membrane invagination and vesicle scission. The WASp homologue in yeast, Las17 plays a major role in stimulating actin filament assembly during endocytosis. The actin nucleation ability of WASP family members is attributed to their WCA domain [WH2 (WASP homology2) domain, C central, and A (acidic) domains] which provides binding sites for both actin monomers and the Arp2/3 complex. In addition, the central poly-proline repeat region of Las17 is able to bind and nucleate actin filaments independently of the Arp2/3 complex. While Las17 is a key regulator of endocytic progression and has been found to be phosphorylated in global studies, the mechanism behind regulation of Las17 actin-based function is unclear. Therefore, the aims of this study were to investigate the post-translation modification of Las17 by phosphorylation, and to determine how this modification impacts on Las17 function both in vivo and in vitro. Mass Spec analysis was employed and allowed identification of further phosphorylation sites in Las17. Through the studies described here I was able to demonstrate that Las17 is phosphorylated, and that one specific phosphorylation event was of importance in endocytosis. Ser588 mutants were shown to affect an early stage of endocytosis whereby S588D mutant had a negative impact on growth, actin organisation, and endocytic invagination. The overall results suggest a regulatory model in which Las17 is subjected to intramolecular interaction that supports Arp2/3-independent actin nucleation mediated by its PP region. Phosphorylation must then be relieved to allow Arp2/3-dependent actin polymerisation to take place to drive invagination. These data establish a novel regulatory model of Las17 and have increased our understanding on the mechanism of actin nucleation during early endocytosis in yeast.

Table of contents

Table of contents

Table of contents

Table of contents

Chapter 3: *in vivo* Analysis of Las17 Phosphomutants

Chapter 4: *in vitro* Analysis of Las17-S588 Mutants

Chapter 5: Further Analysis of Las17 Phosphorylation

Table of contents

List of figures

List of figures

List of Tables

Abbreviations

A	acidic domain
ABP	actin binding protein
ADF	actin depolymerisation factor
ADP	adenosine diphosphate
ATP	adenosine triphosphate
Aip1	actin interacting protein 1
ANTH	AP180 N-Terminal Homology domain
APS	ammonium persulfate
Arp2/3 complex	actin related protein 2/3 complex
ADP	adenosine diphosphate
ATP	adenosine triphosphate
B	Basic domain
C	Central domain
CRIB	Cdc42/Rac interactive region
Cryo-EM	Cryo-electron microscopy
DMSO	dimethyl sulphoxide
DTT	dithiothreitol
E.coli	Escherichia coli
ECL	enhanced chemi-luminescence
Ent1/2	epsin-like protein 1/2
ENTH	Epsin N-terminal homology domain
ER	endoplasmic reticulum
F-actin	filamentous actin
G-actin	globular actin
GBD	GTP-ase binding domain
GFP	Green fluorescent protein
GST	glutathione-S-transferase

Abbreviations

Grb2	Growth factor receptor-bound protein 2
IPTG	isopropyl β-D-1-thiogalactopyranoside
JMY	junction mediating and regulatory protein
Ka	association constant
Kd	disassociation constant
kDa	kilodalton
LatA	Latrunculin A
LiAc	Lithium acetate
LY	Lucifer Yellow
MATα	Mating type α
MAT a	Mating type a
Nck	non-catalytic kinase
NPF	Nucleation promoting factor
N-terminus (Nt)	amino-terminus
N-WASP	Neuronal Wiskott-Aldrich syndrome protein
PEG	Polyethylene glycol
pH	Potential of hydrogen
pI	Isoelectric point
PIP	Phosphatidylinositol 4-phosphate
PIP2	Phodphatidylinositol4,5-biphosphate
PMSF	Phenylmethanesulfonylfluoride
ppm	Parts per million
PRD	Proline rich domain
Rac	alpha serine/threonine-protein kinase
Rho1	Ras-like GTP-binding protein Rho1
S. cerevisiae	*Saccharomyces cerevisiae*
SD	Standard deviation
SH3 domain	Src-homology 3 domain
SHRC	WASH regulatory complex

Abbreviations

Sjl	Synaptojanin
Src	proto-oncogene tyrosine-protein kinase Src
Srv2/CAP	Suppressor of RasVal19/Cyclase associated protein
Tmp1/2	Tropomyosin
TRIS	Tris(hydroxymethyl)aminomethane
Tβ4	Thymosin β4
Vrp1	Verprolin
WASH	WASP and Scar homology protein
WASP	Wiskott-Aldrich syndrome protein
WAVE	WASP family Verprolin-homologous protein
WCA	WH2, C and A domains
WH1	WASP homology domain 1
WH2	WASP homology domain 2
WHAMM	WASP homologue associated with actin, membranes and microtubules
WHD	WAVE homology domain
WIP	WASP interacting protein
WMD	WHAMM membrane interacting protein
Yap1801/2	homologues of epsin and AP180/CALM proteins
YPD	Yeast peptone dextrose
α-factor	alpha factor mating pheromone
Å	Ångeström , symbol for 0.1 nm length
Δ	deletion

Chapter 1:

Introduction

Chapter: 1

1.1 Introduction

The cytoskeleton is a network of protein filaments that function together to preserve the integrity and stability of the cell. The cytoskeleton in eukaryotes is composed of three major structures: microtubules, intermediate filaments, and actin filaments (figure 1.1). These ordered structures are evolutionarily conserved, but intermediate filaments are absent in yeast cells.

Microtubules are thick structures, formed from an assembly of tubulin heterodimers, comprised of, alpha- and beta-tubulin (α/β-tubulin). Continuous polymerisation of the heterodimer results in chains of tubulin subunits called protofilaments. In microtubules, 13 protofilaments are joined side-by-side to form a hollow tube of 25 nm in diameter. Microtubules are polar, they have a minus (-) end containing α-tubulin, and positive (+) end containing β-tubulin. Polymerisation of microtubules occurs when subunits of β-tubulin bound–GTP are assembled at the (+) end; this stimulates GTP to hydrolyse into GDP and phosphate, thus increasing microtubule instability. If the rate of polymerisation is faster than the rate of GTP hydrolysis, the microtubules grow, but if the rate of polymerisation is slower than GTP hydrolysis (i.e. the GTP-cap is lost) this leads to microtubules disassembly and therefore causing them to shrink. Microtubules are important for vesicle trafficking, movement of organelles and cell division (Erickson and O'Brien., 1992; Howard and Hyman., 2009 and 2003).

Intermediate filaments are composed of monomeric strands that can combine to form dimers and tetramers. Two α-helical strands of monomers join together to form a coiled-coil dimer, and two of these dimeric strands can join to form a staggered tetramer. Two tetramers are packed together laterally to generate rope-like filaments of 10 nm in diameter. Unlike microtubules, intermediate filaments are non-polar structures (Strelkov et al., 2003). The main function of intermediate filaments is to provide a mechanical strength to the cells by bridging cell junctions within the nucleus (Herrmann et al., 2007; Dey et al., 2014).

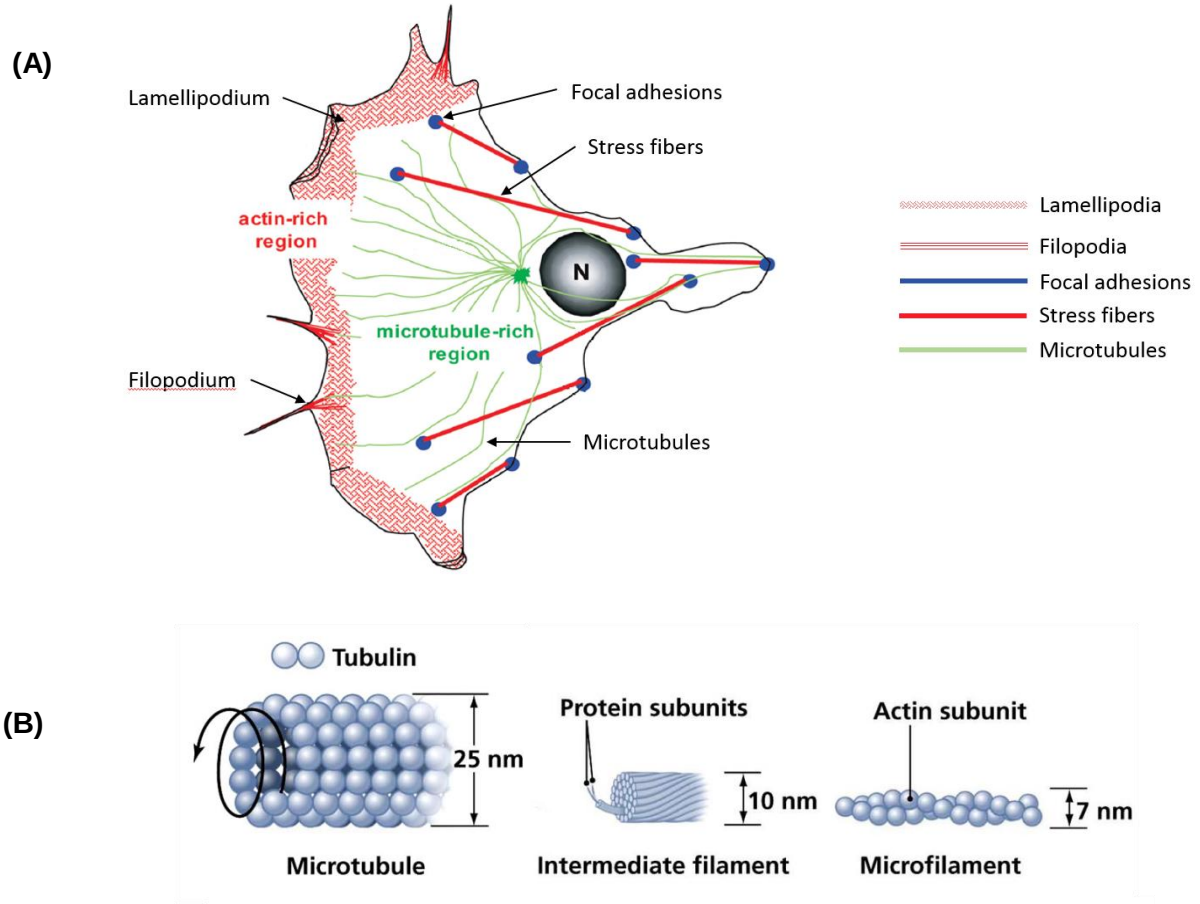

Figure 1.1: Cytoskeleton in eukaryotic cells

(A) A diagram of eukaryotic cell showing actin–rich regions (red) organised into filopodia, and ruffling lamellipodia, and microtubules–rich regions where microtubules radiate from the centrosome (green star) with their + ends directed towards the plasma membrane. Other actin structures in cells are include stress fibres (thick red lines), which are anchored to the substrate via focal adhesions (blue dots) (Manneville, 2004).

(B) The subunit compositions of microtubules, intermediate filaments, and actin filaments (Walter and Boron, 2003).

Chapter: 1

Actin filaments also called microfilaments structures of 7nm in diameter. Actin filaments are composed of actin monomers (G-actin) that polymerise to form actin filaments (F-actin). Like microtubules, actin filaments are polar, as the ATP-G-actin assembles at the barbed end (the fast growing end) of the actin filament, whereas the loss of the ADP-G-actin primarily occurs at the pointed end (the slow growing end) of the filament. When the rate of G-actin addition and loss of an actin filament are at in equilibrium, this is called treadmiling (Pollard et al., 1986; Carlier and Pantaloni 1986; 1997; Pantaloni et al., 2001). More details about polymerisation of actin will be discussed in section 1.2.3. Various different structures that mediate cell movement are dependent on actin dynamics; these include lamellipodia (Ridley et al., 1992), filopodia (Kozma et al., 1995), stress fibres, and focal adhesions (Baily and Condeelis, 2002). In cells, remodelling of actin filaments is controlled by a plethora of actin binding proteins (ABPs) that function in response to certain signals. ABPs are often highly conserved proteins and regulate different aspects of actin cytoskeleton assembly and architecture, including actin filament nucleation or, actin filament elongation, capping or severing of F-actin, actin monomer sequestering or, F-actin bundling or cross-linking (Pollard et al., 2003).

Understanding the molecular basis of regulation of the actin cytoskeleton is the major focus of this study, which requires critical understanding of the molecular mechanisms of actin binding proteins (ABPs). This chapter will give insights into many aspects of actin remodelling and regulation by different ABPs.

1.2 Actin

Actin is one of the most conserved proteins in eukaryotes, playing critical roles in the dynamics of the actin cytoskeleton. In mammalian cells, actin exists in different isoforms which are expressed in a tissue dependent manner. The actin isoforms include alpha (α)-actin isoforms, beta (β)-actin isoforms and gamma (γ)-actin isoforms. The α-actin is mainly expressed in muscle cells whereas; β-actin and γ-actin isoforms are expressed in both the muscle and the non-muscle cells (Tomasevic et al., 2007). The differences in properties of the actin isoforms are mainly attributed to processing and modification of their amino (N)-terminal end. The α-actin isoforms contain an N-terminal methionine residue followed by cysteine and then aspartate or glutamate. However, β-actin and γ-actin isoforms present terminal N-acetyl aspartic or glutamic acid residues. As with β- and γ-actin isoforms, the methionines and cysteines of α-actin isoforms are acetylated and then cleaved by specific enzymes, and the new terminus is then re-acetylated (Rubenstein *et al*., 1990; Herman, 1993).

In cells actin can be present as monomers (globular (G)-actin) or polymers (filamentous (F)-actin). The transition from the G-actin to F-actin form is regulated by various factors including nucleotide hydrolysis, the presence of charged molecules, and its interaction with a number of actin binding proteins.

1.2.1 Actin structures

1.2.1.1Monomeric (G)-actin

The actin monomer is 375 residues long with molecular weight of 42kDa. Straub and colleagues, were first to purify actin from muscle tissues (Straub et al., 1942). Since then, it has been extensively studied and many attempts were made to define its tertiary structure. Binding of actin to sequestering proteins allowed actin to stay in the monomeric state during crystallisation. Thus, the structure of rabbit actin determined using X-ray analysis at 6Å resolution (Suck et al., 1981). Four years later the same structural mode

(skeletal actin:DNaseI complex) was produced but with an improvement in its resolution to 4.5Å (Mannherz and Suck, 1985). Since then, Kabsch and colleagues solved the tertiary structure of α-skeletal actin in ATP or ADP forms, at effective resolution of 2.8Å and 3Å respectively (Kabsch et al., 1990). After this, the structures of the G-actin complexed with other proteins that prevent its polymerisation were solved such as the profilin:β-actin structure, which was determined at a resolution of 2.55Å (Schutt et al., 1993), and the vitamin-D-binding protein (DBP):actin structure, solved to 2.1Å resolution (Otterbein et al., 2001).

Later, Otterbein and co-workers reported the crystal structure of ADP-G-actin after binding of the fluorescent probe tetramethylrhodamine-5-maleimide (TMR) to residue S374 in G-actin, which prevents polymerisation of actin (Otterbein et al., 2001; Hurley et al., 1996). The uncomplexed ADP-G-actin was solved to 1.45Å resolution and this model differed from that solved by Kabsch et al., (1990). Otterbein suggested that, in his model subdomain 2 forms the correct conformation for ADP-actin (see figure 1.2). Thus, it is likely that the Kabsch ADP-actin model was possibly inaccurate, because the actin monomers were bound to ATP that was hydrolysed to ADP-P_i during crystallization, which may not reflect the true conformation of ADP-actin (Otterbein et al., 2001).

The actin molecule is a flattened, bi-lobed structure consisting of two major domains (α/β domains) that are separated by a central cleft for nucleotide and divalent cation binding. Each lobe (or domain) can be subdivided into two distinct subdomains (shown in figure 1.2). Subdomain1 (residues1-32, 70-144 and 338-375) revealed extensive conservation to subdomain 3 (residues 166-169, and 286-289), therefore suggesting that both domains originated from a gene duplication early in evolution. However, subdomain 2 (residue 40-45) and subdomain4 (residues 202-204, 243-245) can be viewed as a large insertion into subdomain1 and 3. In addition, the peptide sequence of subdomain 2 contains many non-conserved residues including the DNaseI

binding loop (D loop) (figure 1.2), in particular residues 39-5 (Kabsch et al., 1990). The D-loop is a flexible structure that has two possible conformational states closed or open. The most recent model that represents the closed form of the nucleotide-dependent change of D- loop after ATP hydrolysis was reported in the Otterbein structural model of G-actin complexed with ADP (Otterbein et al., 2001).

The two major domains (α/β) are joined by the hinge region, which is formed by a polypeptide chain that passes twice between the domains, generating two central clefts. The upper cleft provides a binding pocket for ATP and divalent cation (Mg^{2+} or Ca^{2+}), whereas the lower cleft is rich in hydrophobic residues. The lower cleft is located between subdomains 1and 3, which provides a binding site for the association of ABPs and allows longitudinal contact between the actin subunits of actin filaments (Strzelecka-Golaszewska, 2001; Dominguez, 2011).

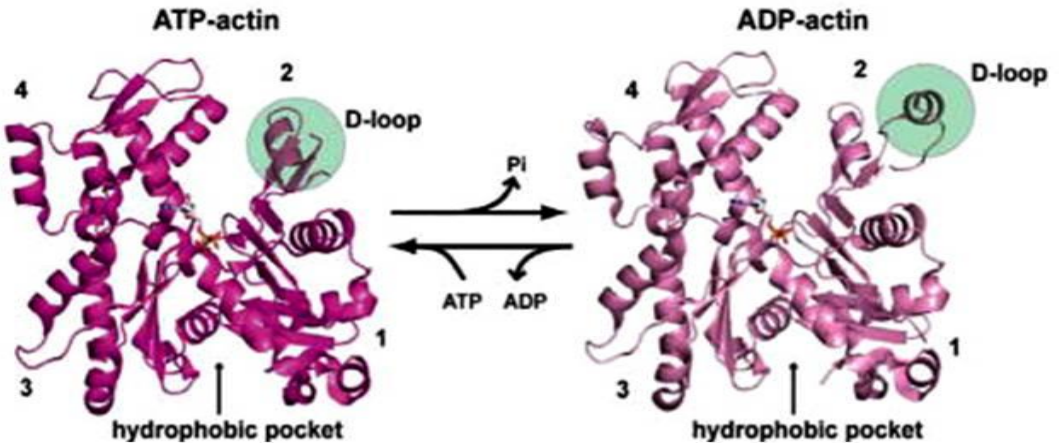

Figure 1.2: Structure of monomeric actin.

The actin monomer consists of 2 major domains that are subdivided into subdomains 1, 2, 3, and 4. The combination of these subdomains generates two clefts. The upper cleft is located between subdomains 2 and 4, provides a binding site for a nucleotide and divalent ion. The lower cleft (hydrophobic pocket) between subdomains 1 and 3 mediates the interaction of actin with ABPs. Upon nucleotide exchange, the actin monomer undergoes a conformational change, particularly in the D-loop. This alters the stability of the actin filament, which modulate the binding affinities of ABPs to actin and of actin monomers to each other within the filament.

From: Lee and Dominguez, 2010

1.2.1.2 The actin polymer (F-actin)

In 1960, Oosawa and Kasai (Oosawa and Kasai. 1962) first proposed the concept of actin monomers polymerising to form linear helical actin. Three years later, Hanson and Lowy used electron microscopy (EM) analysis of negatively stained muscles to describe the tertiary structure of actin filaments. In this model, F-actin was observed as a helical structure that could be viewed either as a two start right-handed, long pitch helix or as a single start, left-handed helix with each subunits spaced by 27.6Å (Hanson and Lowy 1964). The F-actin structure deduced by Holmes in 1990 suggested a right-handed helix with a filament diameter of 90Å, which is equivalent to the parameters found in the Hanson model (Holmes et al., 1990). For over 10 years, many F-actin models were established from the Holmes model, but the major challenge was to determine the correlation between the subunits to form the actin filaments backbone, since the actin monomers are subjected to conformational change due to nucleotide hydrolysis. Oda and his co-workers (2009) presented an F-actin model, which was obtained by high-resolution X-ray fiber diffraction of F-actin from rabbit skeletal muscle. The Oda model achieved a resolution of 3.3Å in radial direction and 5.6Å along the equator (13Å in total). This model revealed an F-actin structure with a slightly smaller radius of gyration of 23.7Å compared to 25Å in the Holmes model. The Oda model also revealed a conformational change that take place during actin polymerisation, which resulted in a 20˚ rotation of the two major domains, this causes flattening of actin protomers in F-actin by generating intra-strand connections, thus facilitating more contacts between the actin monomers to form polymer (Oda et al., 2009). A year later, Fujii and co-workers obtained an atomic model of F-actin using cryo-EM analysis, which allowed the structures of the actin domains, the D-loop and some of the extended polypeptide chains to be clearly resolved (Fujii et al., 2010). This model was not too different from the F-actin structural model described by Oda et al., 2009, except that the D-loop was in a different conformation. Moreover, the Fujji model was fitted onto the crystal structure of the uncomplexed ADP-F-actin solved by Otterbein et al., (2001) (Oda et

al., 2010; Holmes et al., 2003). The Fujji model offered good views of the axial symmetry of F-actin by rotation of the two halves of the actin subunit when fitted onto the Holmes model. The pocket dedicated to nucleotide binding is opened with 5˚ anti-clockwise rotation of domain 1, and such rotation allows the Gln137 residue to come closer to the γ-phosphate-binding site to facilitate ATP hydrolysis (Figure 1.3). In addition, it was shown that the connection between salt bridges formed between the major domains was not as extensive as it was thought to be in Oda model. However, subsequent rotation of domain1 by 20˚ would disrupt the hydrophobic interaction with subdomain 3, which would alter the actin conformation, but that would probably be stabilized by the longitudinal contact between the actin molecules of F-actin(Gelkin et al., 2001; reviewed in Bugyi and Carlier, 2010)..

1.2.2 Actin polymerization

Assembly and disassembly of actin filaments is a dynamic process that requires energy for ATP hydrolysis. In cells, it was found that actin polymerisation is enhanced by certain conditions including high concentrations of Mg^{2+}, low concentrations of Ca^{2+}, elevated temperature, high concentrations of KCl (>50 mM) and neutral or slightly acidic pHs. Actin polymerisation in vitro is stimulated by similar conditions as those found physiologically (Strzelecka-Golaszewska et al., 2001; Carlier, 1991; Zimmer and Frieden, 1986; Frieden, 1983)

Figure 1.4 shows the process of actin polymerisation which consists of three stages: Actin nucleation, F-actin elongation, and treadmiling.

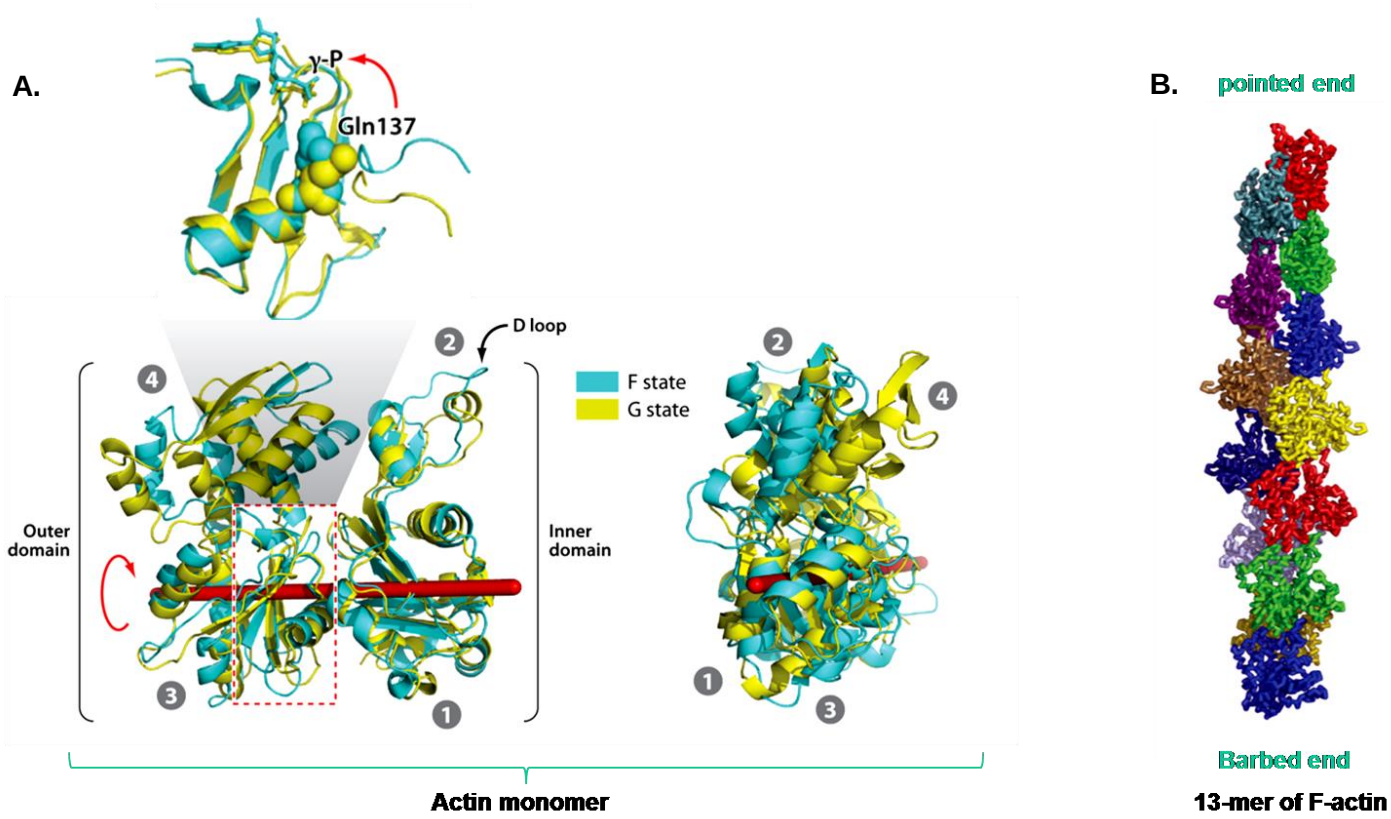

Figure 1.3: Structural changes of the actin monomer associated with polymerisation and ATP hydrolysis

(A) front (left) and side (right) view of the actin monomer in G-actin (yellow) and F-actin(cyan) states, the two structures are interconvertible between these two states by rotation of the two major domains (outer and inner domains) of actin around the axis. Subdomains are identified by numbers 1, 2, 3 and 4(gray circles). The red dotted box is enlarged in the top panel to show the D-loop in G and F-actin states. Rotation of the two major domains brings Gln137 (spheres) closer to the γ-phosphate of ATP (sticks).

(B) Structure of a 13-mer of F-actin derived from the Oda F-actin model.
From: Bugyi and Carlier, 2010

1.2.2.1 Nucleation

The first step of actin filament formation is nucleation of monomeric actin. Actin nucleation is a spontaneous process that involves assembly of actin monomers into dimers and then trimers or tetramers. This reaction is relatively slow (K_a = 3.4-12.3 $\mu M^{-1}s^{-1}$), and requires subsequent addition of actin monomers to initiate filaments (Pollard et al., 1986; Kuhn and Pollard, 2005). The formation of actin dimers is energetically unfavourable. However, incorporating a third subunit to the dimer results in a more stable complex called a nucleus, which promotes further addition of actin subunits to extend into filaments (F-actin). In cells, different nucleators are essential to drive actin nucleation, such as the Arp2/3 complex and formins (see section 1.4.6). These proteins facilitate the formation of stable nuclei from which actin filaments are developed. The formation of actin filaments can only occur when the level of actin monomers is above the critical concentration (Cc), otherwise the monomeric state of actin is favoured. The critical concentration is the level of G-actin at which the number of G-actin subunits is in equilibrium with the number of actin filaments. At actin concentrations below Cc no polymerisation takes place, whereas at monomer concentrations above the Cc, assembly of actin filaments can proceed (Wegner and Engel. 1975; Pantaloni et al., 1986).

It was shown that addition of Mg^{2+} induces a conformational change in actin subunits, which promotes polymerisation. However, the dissociation constant of Mg^{2+} binding to actin is quite high (K_d = 5 mM) in the absence of Ca^{2+}, suggesting weak affinity to the actin. However, Ca^{2+} addition prolonged the lag time of polymerisation (lag phase) prior to the onset of actin polymerisation (see figure 1.4). The lag phase of actin polymerisation is believed to occur partially due to the time taken for divalent Mg^{2+} to bind to the actin cleft in the absence of nucleators (Frieden, 1983).

Determining the association and dissociation rate constants allows for characterisation of actin polymerisation kinetics using Brownian dynamics simulation (BD) applied on the Holmes model (McCammon et al., 2001, Holmes et al., 1990). BD showed that the disassociation constant of actin

dimers is considerably high (K_d = 4.6 mM) but when another actin subunit is added to the dimer, the dissociation value of the reaction dropped to K_d = 0.6 mM. This suggests that, trimeric actin is the critical size of the nucleus (McCammon et al., 2001). This conclusion was in agreement with the experimentally estimated rate constant of the nucleation pathway that was previously described (Wegner and Engel. 1975; Frieden, 1983).

The kinetics of actin filament assembly and disassembly were also determined in real time using total internal reflection fluorescence (TIRF) microscopy, allowing observation of nucleation and growth of filaments from both ends (Amann and Pollard, 2001; Fujiwara et al., 2002). Kuhn and Pollard estimated the rate of association and dissociation constants of both ends of single F-actin filament labelled with Oregon green at Cys374. Real-time (TIRF) measurements demonstrated that, the association constant (K_a) of the Mg-ATP-actin at the barbed end is approximately 10 times greater than that at pointed end (7.4$\pm$ 0.5 μM $^{-1}s^{-1}$ at the barbed end and, 0.56$\pm$ 0.10 μM $^{-1}s^{-1}$ at the pointed end) (Kuhn and Pollard, 2005). The estimated rate of monomers association at the barbed end was comparable to the value obtained by Pollard and co-workers (K_a = 3.4-12.3 μM $^{-1}s^{-1}$) (Pollard et al., 1986). In the same experiment, the dissociation constant of monomers at barbed end pointed ends of the filament were also measured in the presence of actin sequestering protein vitamin D. Mg-ADP-F-actin (aged filaments) were generated by mixing F-actin formed from Mg-ATP-G-actin: at this point ATP bound subunits catalyse nucleotide exchange within the filament to form Mg-ADP-P_i-F-actin, as a result most of the filaments are converted to Mg-ADP-actin. Thus, the mean dissociation constant (K_d) of Mg-ADP-actin was 1.4s^{-1} at the barbed ends, which is identical to the value reported by Pollard (Pollard et al., 1986), whereas a K_d of ~0.16s^{-1} was estimated for a monomer dissociation from the pointed ends (Kuhn and Pollard, 2005).

1.2.2.2 Elongation

Extension of actin filaments during actin polymerisation is called the elongation stage (depicted in figure 1.4). Elongation of F-actin involves continuous addition of actin subunits, which occurs preferentially at the barbed end. Addition of actin subunits to the opposite end is much less than that at the barbed ends (Pollard, 1986; Kuhn and Pollard. 2005). Incorporation of monomeric actin to the barbed end requires nucleotide exchange of ADP-G-actin to ATP-G-actin. Conformational change of actin subunits due to ATP hydrolysis to ADP and P_i destabilise the contacts between the monomers in the filament resulting in up to 5-10 fold increase in actin dissociation from the barbed end. The dissociated monomers would then be recycled and used for further rounds of polymerisation (Carlier et al., 1991).

During actin polymerisation, the rate of actin filament elongation is rapid and dependent on the availability of monomers in the actin pool (which must be above the critical concentration for elongation to take place). In vitro, actin polymerisation occurs spontaneously, and as the number of actin monomers incorporated into filament increases, the rate of filament elongation increases to the stage at which the number of newly formed filament ends becomes greater than the number of the monomers in solution. At elongation stage, polymerisation of actin monomers proceeds until the concentration of actin pool reaches to critical concentration, which is equal to ~0.1 μM of unpolymerised G-actin (Oosawa and Asakura, 1962). At this point, the rate of actin elongation stays at a constant level leading to treadmilling stage.

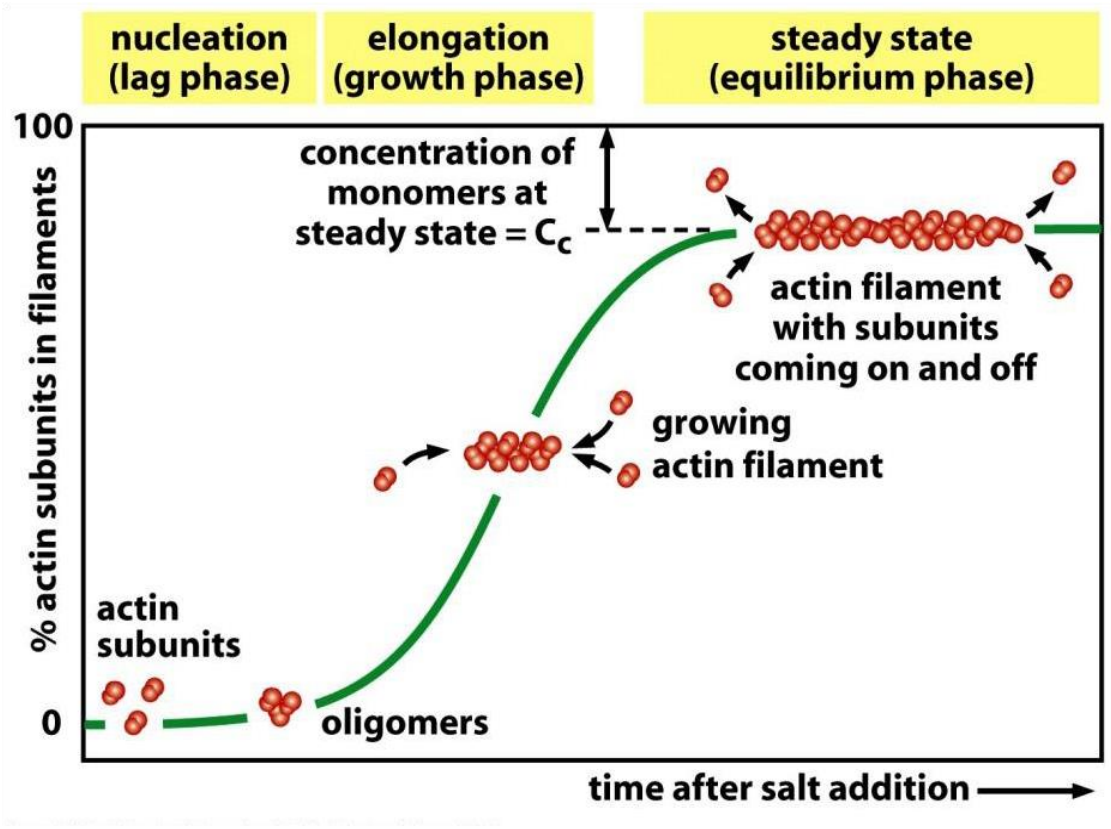

Figure1.4: Representative graph showing the stages of actin polymerisation in vitro.

Upon addition of salt, the dimeric form of G-actin assemble into oligomers (lag phase). The actin filament grows from either side in the growth phase. At the steady state the actin subunits within the filament start coming off and on at the same rate (equilibrium phase).

Figure 16-10b Molecular Biology of the Cell (© Garland Science 2008)

1.2.2.3 Treadmilling

The steady state of actin polymerisation is the period at which no further subunits are available to extend the filaments as the concentration of actin monomers is at the critical concentration of the barbed end, as shown in figure 1.4. At the steady state, the number of actin subunits assembling at the barbed end is equivalent to the number of the subunits disassembling from the pointed end, a process known as treadmilling (Wegner, 1976). Treadmilling can be controlled by the availability of free actin subunits added to the barbed end and the loss of actin monomers from the pointed end. As a result of treadmilling, no further growth of filamentous actin is observed.

1.3 Cytoskeleton in prokaryotes

Bacteria have a primitive cytoskeleton that plays several regulatory roles. Like the cytoskeleton in eukaryotes, the bacterial cytoskeleton provides a support to the cell shape and anchorage to cellular organella. Bork and colleagues were the first to determine the structure of bacterial actin-like proteins MreB, FtsZ, and ParM (Bork et al., 1992). Since then these actin-like proteins in bacteria were shown to posses conserved folds in their domain structures similar to those observed in eukaryotic actin (van den Ent and Lowe, 2000; van den Ent et al., 2001 and 2001). MreB, ParM, and FtsZ were therefore classified as members of the actin superfamily. However, because of the diversity of actin-like proteins sequences in bacteria more than 35 different families were discovered according to their phylogenetic and functional significances (Derman et al., 2009).

MreB is an actin-like protein from *Bacillus Subtitles*, which maintains the integrity of the cell wall of rod-shaped-bacteria. MreB is able to form protofilaments under the same conditions as actin in vitro (Esue et al., 2005). Under EM, these polymers appear as two protofilaments, which are both single stranded helix. The spacing between the subunits is 51.1Å in the protofilament. Unlike human actin, MreB lacks the helical twist as shown in figure 1.5 (van den Ent et al., 2001). Depletion of MreB results in rounded-shaped cells due to cell morphological defects (Daniel and Errington, 2003).

MreB was shown to form membrane-bound complexes in conjunction with other actin-like proteins including MreC, MreD, and RodZ. This complex is also required for cell shape in *E. coli* (Divakaruni et al., 2005; Kruse et al., 2005; Shiomi et al., 2008). In addition, MreB appears to play a role in chromosome segregation (Gitai et al., 2005).

ParM is a plasmid-borne bacterial actin-like protein that showed low sequence homology to MreB. ParM generates F-actin-like protofilaments. The crystal structure obtained from ParM protofilaments revealed twisted left-handed helices, which is the opposite twist direction to F-actin (depicted in figure 1.5) (van den Ent et al., 2002; Orlova et al., 2007). In cells, ParM shows different behaviours, it can be visualised as a filamentous structure along the cell span or can be distributed randomly at foci. ParM dynamics are directly associated with plasmid segregation during the cell cycle (Moller-Jensen et al., 2003; Campbell and Mullins, 2007).

The bacterial homologue of tubulin, FtsZ is essential for *E. coli* cell division (de Bore et al., 1992). Like MreB, the FtsZ primary sequence has only 10% identity to its human homologue (tubulin), but it displayed significant folding homology to tub (Löwe and Amos, 1999). FtsZ depends on GTP hydrolysis during polymerisation, but is unable to form microtubule-like structures. Instead, the protofilaments generated by FtsZ are joined laterally to produce distinct structures in vitro (Bramhill and Thompson, 1994; Mukherjee and Lutkenhaus, 1994)

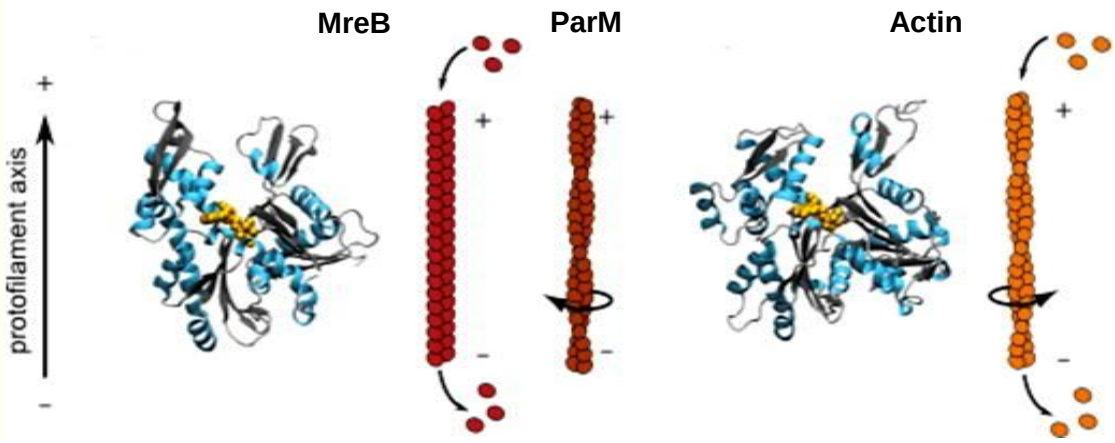

Figure 1.5: Prokaryotic actin-like proteins.

The MreB monomer (left panel) has a similar tertiary structure to eukaryotic actin (left panel), but the two protofilaments formed by MreB appear as an untwisted helix- stands (red circles), unlike actin (orange circles) ParM (right panel and actin form similar helical structures with ParM twisted in a left-handed direction (brown circles), whereas F-actin forms a right-handed twist (orange circles).

From: Wickstead and Gull, 2011

In vivo, polymerised FtsZ forms a Z-ring during bacterial cytokinesis, at this stage FtsZ interacts with FtsA , a protein that belongs to the actin/HSP70 family proteins (Bork et al., 1992) and recruits other components required for inner-membrane remodelling (Adam and Errington, 2009).

1.4 Actin binding proteins (ABPs)

An overview of how actin binding proteins (ABPs) influence actin assembly and disassembly is depicted in figure 1.6. Cellular actin is regulated by many ABPs that affect actin filament turnover, these proteins often contain distinct domains that allow them to interact with other proteins to modulate actin organisation. ABPs can be classified into different sub-groups according to their function, though some ABPs can be part of more than one sub-group. This section describes examples of the ABPs that have been shown to have pronounced effects on actin filament turnover in vivo and in vitro.

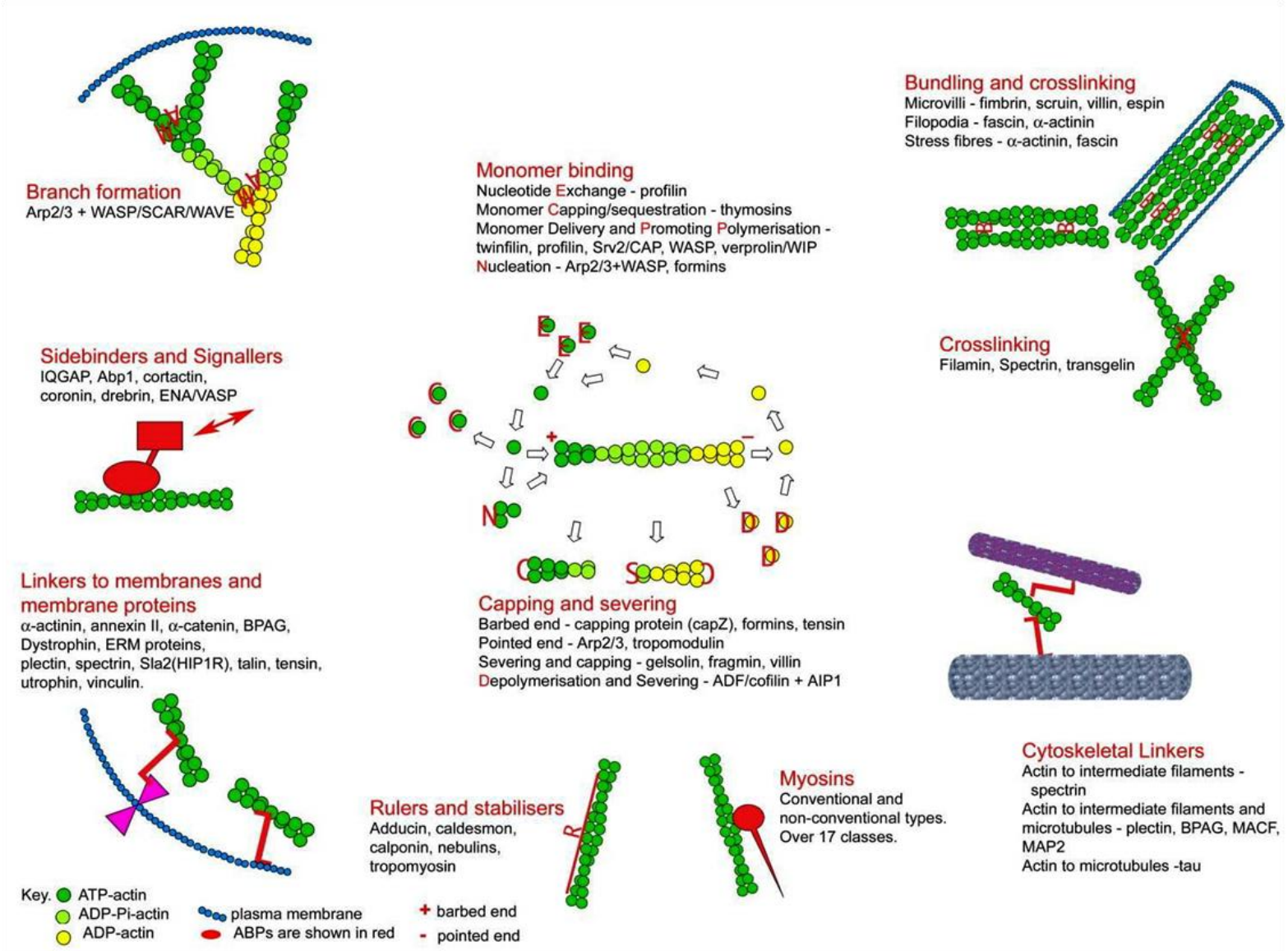

Figure 1.6: An overview of different types of actin binding proteins that influence actin dynamics.
From: Winder and Ayscough, 2005

1.4.1 G-actin binding proteins

1.4.1.1 Profilin family

Profilins are small proteins with a molecular mass of 19 kDa. Profilins are ubiquitous proteins required for actin filament elongation (Ampe et al., 1988). They bind to ATP-G-actin and deliver it to the barbed of filaments, thus allowing continuous growth of the filament and preventing the association of monomeric actin to the pointed end (Pollard and Cooper, 1985). Profilin-mediated actin barbed end elongation is induced when the number of free ATP-G-actin subunits is higher than the critical concentration (Pantaloni et al., 1993; Pollard et al., 2000). Profilin can also act as sequestering factor; when there are no free barbed ends available for polymerisation (e.g. when the barbed ends are capped) then profilin induces actin depolymerisation (Carlsson et al., 1977).

Profilin exists in high molar concentrations at regions where actin turnover is active, and its biological importance is also attributed to the ability of profilin to interact with many F-actin nucleation ligands. Profilin interacts with the polyproline-rich domains of many actin regulatory proteins such as N-WASP and VASP, which allows ATP-G-actin delivery to drive actin filament formation (Witke, 2004; Pollard et al., 2003). Profilin activity is also regulated by the membrane lipids phosphatidylinositol 4-phosphate (PIP) and phosphatidylinositol 4,5-bisphosphate (PIP_2). These phospholipids are thought to be responsible for dissociation of profilin from ATP-G-actin as the PIP binding site of profilin overlaps with its actin binding site (Lassing and Lindberg, 1990; Dos Remedios et al., 2003; Goldschmidt-Clermont et al., 1990).

1.4.1.2 Thymosin β4

Thymosin β4 (Tβ4) is an actin monomer sequestering protein with a molecular weight of 5 kDa. Tβ4 inhibits actin polymerisation when complexed with actin at a 1:1 stoichiometry through its conserved WASP homology 2 (WH2) domain (Safer et al., 1991). Hence, Tβ4 binds G-actin and prevents F-actin assembly from either end, but in the presence of profilin the Tβ4:actin complex can dissociate, allowing elongation of the actin filament (Ballweber, et al., 2000; Pantaloni and Carlier 1993). When, Tβ4 levels are at molar excess (≥ 20 μM) a weak cooperative interaction with F-actin is also observed, but the physiological significance of this interaction is unclear (Carlier et al., 1996). Tβ4 binds preferentially to the ATP-actin form and prevents nucleotide exchange on G-actin by preventing its conformational change (Goldschmidt-Clermont et al., 1992; Carlier et al., 1996).

1.4.1.3 Twinfilin

Twinfilin is an actin binding protein that is present in eukaryotic cells ranging from mammals to yeast. However, this protein is not expressed in plants. Twinfilin contains two actin depolymerisation factor-homology (ADF-H) like domains (which are cofilin actins binding domain) that are separated by a linker region, followed by a C-terminal tail with 35 residues. Twinfilin can bind and sequester actin monomers and has a high affinity for ADP-actin (K_d = 0.05 μM) (Palmgren et al., 2002). One of the ADF-H domains is at the N-terminal end of twinfilin whereas the second one is at the C-terminal end. The N-terminal ADF-H acts as an actin entry domain that that promotes ADP-G-actin delivery to the ADF-H in the C-terminus through a conformational change of the twinfilin molecule. Twinfilin also prevents actin filament assembly by inhibiting nucleotide exchange on actin monomers, forming a stable complex of with ADP-actin monomers (Palmgren et al., 2002).

1.4.2 F-actin binding proteins

Upon actin nucleation, actin filaments grow rapidly due to continuous addition of actin monomers. The rapid extension of the filaments is controlled by various mechanisms including capping, F-actin depolymerisation, and severing of F-actin.

1.4.2.1 Capping-CapZ

CapZ is a heterodimeric protein composed of an α- and β-subunit. Each subunit has multiple isoforms, and both subunits are required for capping barbed ends of actin filaments (Casella, 1994). CapZ is one of the key factors that regulate the dynamics and organisation of actin filaments in cells. It binds tightly to the barbed ends of filaments, thereby allowing no further addition or loss of actin subunits at these ends. CapZ is mainly localised to barbed ends in the dynamic regions of cells. Therefore, upon certain stimulation, capping proteins can promote the rapid growth of non-capped filaments in areas where most filaments are capped (Pantaloni et al., 2001). CapZ can dissociate from the barbed ends of filaments upon binding of PIP or PIP_2 to CapZ. As a result, a large number of free F-actin barbed ends are generated, which allows actin polymerisation to continue in areas where PIP or PIP_2 are localised (Schafer et al., 1996).

1.4.2.2 F-actin depolymerisation-ADF/cofilin

Actin depolymerisation factor (ADF)/cofilin family members are small proteins (15-18 kDa), that play roles in enhancing actin depolymerisation (Lappalainen et al., 1998; Lappalainen and Drubin, 1997). ADF/cofilin contains a single ADF-homology domain (ADF-H), which can bind and sequester actin monomers (Nishida et al., 1984), and also has the ability to interact with F-actin. Cofilin is a multifunction of protein which functions via two mechanisms: F-actin depolymerisation, and severing of actin filaments. The latter property will be described in section 1.4.2.3. Depolymerisation of F-actin by ADF is allowed when dissociation of the G-actin from the pointed ends of the filament, and the presence of profilin (which catalyses nucleotide exchange

on G-actin) accelerates the rate of pointed end dissociation by cofilin **(**Didry et al., 1998). Thus, the activity of ADF/cofilin causes the concentration of ADP-G-actin to become elevated in the cytoplasm, and this ADP-G-actin is recycled by conversion to ATP-G-actin by profilin then reassembled at barbed end of the filaments (shown in figure 1.6). The depolymerising protein cofilin promotes ADP-G-actin disassembly from filament pointed ends, providing actin monomers to incorporate into free barbed ends. This effect stimulates the changing of ADP for ATP on the G-actin:profilin complex, which results in raised equilibrium rates of assembly and disassembly of actin filaments (Van Torys et al., 2008; Carlier et al., 1997; Didry et al., 1998).

1.4.2.3 F-actin severing

Actin severing activity breaks the actin filaments into short filaments. Two examples of severing proteins are gelsolin and ADF/cofilin. Gelsolin is an actin regulatory protein that belongs to the gelsolin superfamily. The molecular mass of gelsolin is 80 kDa, and gelsolin consists of two tandem homologous halves (segments G1-G3 and G4-G6). The N- linker joins the N- and C-terminal halves of gelsolin (Kwiatkowski et al., 1986). Gelsolin activity in cells is regulated by many factors including Ca^{2+} levels, the pH, and the presence of PIP_2. Severing by gelsolin is initiated when it binds to the side of the filament, which leads to the generation of a new barbed end. However, its activity for severing is slow (Selden et al., 1998); the delay in severing may reflect the time required to re-arrange the gelsolin segments (McGough et al., 1998). The severing mechanism of gelsolin is regulated by Ca^{2+} level in vivo. The N-terminus has a single Ca^{2+} binding site, whereas the C-terminal tail (which is named as the latch helix) contains two Ca^{2+} binding sites. After severing, gelsolin remains associated with the newly formed actin filament as a cap, which prevents filaments from reannealing at their barbed ends (Gremm and Wegner, 2000; Choe et al., 2002). The phospholipid PIP_2 inhibits gelsolin by inducing uncapping of the filament barbed end, thereby permitting

actin polymerisation to proceed. Severing and capping by gelsolin can create many short actin filaments, which increases the number of barbed ends that can be elongated when the gelsolin cap is removed (Seldon et al., 1998).

The severing activity of cofilin takes place when it binds to the side of an aged actin filament (ADP-F-actin). This process is accompanied by a conformational change of cofilin which causes a shift in the mean twist of the filament in the region where cofilin is bound. As a result, a longitudinal and lateral alteration takes place between the monomers of the filament takes place leading to filament destabilization (Bertling et al 2004; Bamburg, 1999; McGough et al., 1997). ADF/cofilin activity is regulated by several ABPs that share similar actin binding sites. Gelsolin G1domain competes with ADF/cofilin for actin binding, suggesting that both proteins bind to the same region on actin (Ballweber et al., 1997). The mammalian protein coronin interacts with ATP-F-actin and prevents its severing by ADF/cofilin. Therefore, coronin increases the affinity of ADF/cofilin towards aged filaments rich in ADP-actin (Cai et al., 2007; Gandhi et al., 2010). ADF/cofilin also interacts with phospholipids, which inhibit its actin binding activity due to overlapping of the PIP binding site of cofilin with its actin binding site (Kusano and Obinata, 1999).

1.4.3 Actin-crosslinking/bundling proteins

The arrangement of actin polymers into higher order F-actin structure is achieved by two types of proteins: F-actin crosslinking proteins and F-actin bundling proteins (depicted in figure 1.6). Orthogonal networks arrays and bundles of F-actin are formed by these proteins, and these arrangements are found in subcellular protein complexes that coordinate cell migration and spreading. Examples of cellular architectures containing these higher order structures include lamellipodia, filopodia, and stress fibres (Tojkander et al., 2012; Yang and Svitkina, 2011a; Yang and Svitkina, 2011b).

Cross-linking proteins are responsible for generating orthogonal arrays of F-actin. In these F-actin arrays, the actin binding domains of cross-linking proteins are separated by spacers, and arranged to organise actin filaments into arrays. Cross-linking proteins can be large dimeric structures such as filaments or tetrameric structures, like spectrin. The small monomeric protein transgelin is also involved in cross-linking actin filaments into a mesh-like network under certain conditions (Revenu et al., 2004).

Actin bundling proteins are responsible for parallel and anti-parallel alignments of actin filaments into linear arrays. These linear arrays are formed either by a single protein containing two actin-binding domains or by multiple protein subunits each containing a single actin-binding domain (Chahabra and Higgs, 2007). Actin bundling proteins can be subdivided into those that generate loose or tight bundles. For example, microvilli structures are mainly formed by the actin bundling protein fimbrin. The two actin binding domains of fimbrin localised in close proximity to each other, allowing tight actin bundles to be generated. In contrast, actin stress fibres are loose, as they are constituted by the anti-parallel arrangement of the dimeric protein α-actinin. The actin-binding domain of each protein subunit is separated by a helical spacer region, which confers a looser connection between the actin filaments (Falzone et al., 2012).

1.4.4 Myosins

Myosins are a large superfamily of motor proteins, which are functionally diverse. There are over 30 classes of myosins that were discovered and myosin class II was the first class identified, (also known as conventional myosin). The other classes are considered unconventional myosins (Foth et al., 2006). Most myosins use actin as a track to transport their ligands. The head domain of myosin is a force generating domain, which is capable of walking towards the barbed end of an actin filament (with the exception of myosin VI, which moves towards the pointed end). This activity requires ATP hydrolysis. The tail regions of myosin I and myosin V are associated with the plasma membrane and with membranes of organelles giving membrane-related functions, such as myosin linkage at microvilli or filopodia. In contrast, the rod-like domain tail in myosin II arranges thick filaments in bipolar organisation, which builds contractile muscles (Tyska and Warshaw, 2002, 2010).

1.4.5 Actin stabilizers

Tropomyosins (TM) are a family of F-actin binding proteins, which are classified into two groups: muscle tropomyosin isoforms and non-muscle isoforms (Helfman et al, 1986). Muscle tropomyosins regulate movement of the myosin head along the actin filament, and thus mediate muscle contraction. However, the function of non-muscle isoforms is less well understood, but they were shown to protect the filament from severing by gelsolin in vitro (Ishikawa et al., 1989). TM isoforms cooperate with actin filaments to generate more stable filaments, which are thought to regulate binding of other actin binding proteins along the actin polymer (Bryce et al., 2003). Interaction of tropomyosin with the filament affects the overall rate of actin monomer polymerisation and depolymerisation (Lal and Korn, 1986). Tropomyosin inhibits the level of spontaneous addition of ATP-G-actin resulting in, reduction of barbed ends available for polymerisation (Hitchcock-

DeGregori et al., 1988). In addition, tropomyosin does not affect the rate of filament elongation but, stabilises the pointed end by lowering actin monomer dissociation (Broschat, 1990; Broschat et al., 1989).

1.4.6 Actin nucleators

De novo actin nucleation is a spontaneous process that is kinetically unfavourable. In cells several protein families are recruited to stimulate actin filament formation at specific times and sites**.** The best studied actin filament nucleating proteins are the Arp2/3 complex and formins (Pollard, 2007). Each actin nucleator promotes actin nucleation by a distinct mechanism. The Arp2/3 complex generates branched actin filament networks from the side of pre-existing filaments, whereas formins bind to the barbed ends of filaments to build a network of unbranched actin filaments (see figure 1.7).

1.4.6.1 Arp2/3 complex

The actin related protein 2/3 (Arp2/3) complex is the major actin nucleator in eukaryotic cells. This complex consists of seven subunits with a total molecular weight of 220 kDa. The protein subunits assemble as stable polypeptides, which are highly conserved in all eukaryotes. The Arp2/3 complex is named after the main two subunits Arp2 and Arp3 and an additional five subunits called actin related complex 1-5 (ARPC1-5), shown in figure 1.8.A.

The purified Arp2/3 complex is relatively inactive, as its activation requires nucleation promoting factors (NPFs) that provide an actin subunit to the Arp2/3 complex to initiate actin polymerisation. The activated complex assembles a new (daughter) actin filament by binding to the side of a pre-existing (mother) filament at a 70˚ angle thereby forming a Y shaped branch (Amann and Pollard 2001). The Arp2/3 complex caps the pointed end of the newly branched filament, whereas addition of further actin subunits is permitted at the free barbed end of the branch (Mullins et al. 1998).

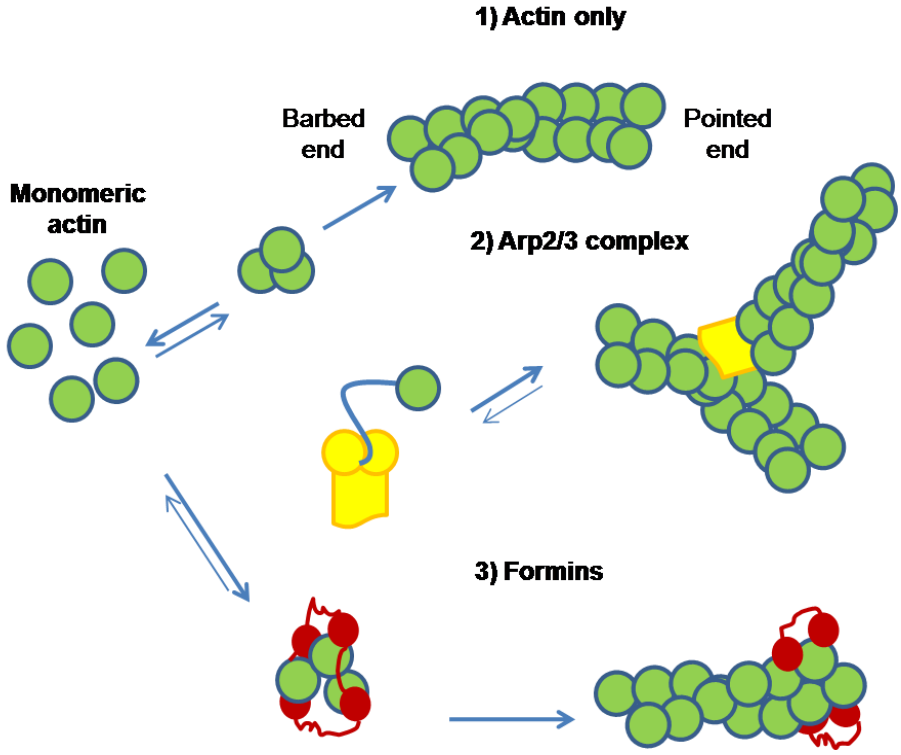

Figure 1.7: Paths of actin nucleation by Arp2/3 complex and formins.

1. Spontaneous initiation of actin filament assembly requires the formation of an actin trimer (nucleus), **2.** The Arp2/3 complex mimics an actin dimer and act as template for initiation of a new actin filament branch from a pre-formed filament, **3.** Formin stabilizes actin trimer and allows continuous growth at the barbed end of the filament.

Adapted from: Goley and Welch, 2006

The Arp2 and Arp3 subunits mimic two actin monomers, which can combine with an actin monomer to form a nucleus. The crystal structure of the inactive bovine Arp2/3 complex revealed a large separation between the Arp2 and Arp3 subunits which would prevent formation of an actin nucleus (figure 1.8.B).

In this configuration both subunits Arp2 and Arp3 contain a nucleotide binding cleft which in this case was open due to the absence of ATP (Robinson et al., 2001). Cryo-EM and 3D reconstruction studies have demonstrated that, the Arp2/3 complex undergoes a conformational change when Arp2 and Arp3 interact with the pointed end of the branched filament and Arp2 and ArpC4 contact the mother filament. These observations are in agreement with the proposal that, NPFs stimulate a conformational change of the Arp2/3 complex, which involves a subsequent rearrangement of Arp2 and/or Arp3 subunits to form a nucleus (Beltzner and Pollard, 2004; Volkmann et al., 2001). The Arp2/3 complex interacts with the acidic domain found in nucleation promoting factors (NPFs) such as those in WASP family. The Arp2/3 complex alone is a weak nucleator, but its nucleation and branching abilities are stimulated by three factors: binding to pre-existing filaments, phosphorylation of Arp2 and interaction with the WASP homology 2 (WH2), central and acidic (WCA) domains of NPFs (Suetsugu. 2013; Narayanan et al., 2011; Rodal et al., 2005). The branched actin filament forms when actin monomer delivery occurs from the WH2 domain to the barbed ends of Arp2 and/or Arp3. Upon Arp2/3 activation it was speculated that, the WCA dissociates from the complex to permit additional rounds of nucleation, but further studies are required to support this notion (Suetsugu et al., 2001; Ti et al., 2011).

In mammalian cells, the Arp2/3 complex and its activators are essential for generating a network of cross-linked filaments near ruffling membranes, which pushes against these membranes to drive cell movement.

A.

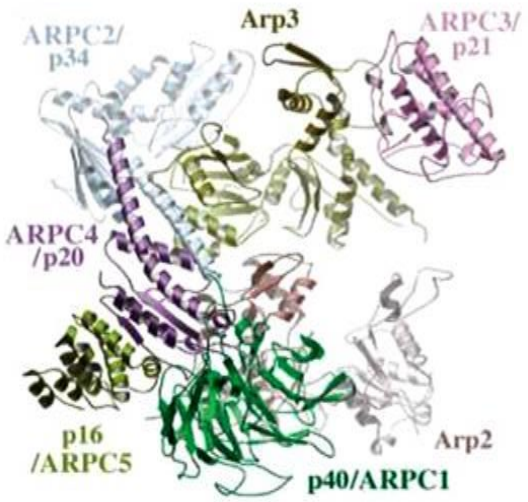

B.

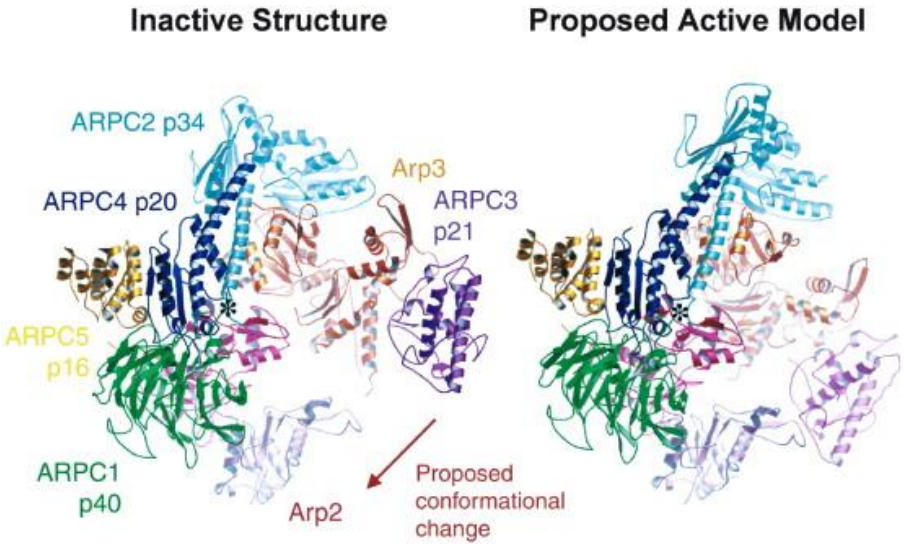

Figure 1.8: crystal structure of the Arp2/3 complex.

(A) Ribbon diagram of the Arp2/3 complex with its subunits labelled and shaded by different colours.

(B) The structural model of inactive bovine Arp2/3 complex (left panel) and the proposed active model of Arp2/3 complex (right panel). In the inactive structure, Arp2 and Arp3 are separated from each other. When activated, the complex undergoes a conformational change, so that Arp2 and Arp3 are brought close to each other.

From: Robinson et al., 2001 and Pollard, 2007

1.4.6.2 Formins

Formins are another type of actin nucleator. They are evolutionarily conserved in all eukaryotes. The actin nucleation activity of formins is attributed to the presence of two formin homology -1-and -2 domains (FH1and FH2). Some formins lack the FH1 domain but the FH2 domain is the most conserved domain in formins. In addition to the FH1 and FH2 domains, many formins contain additional functional domains including, diaphanous inhibitory (DID) domain, diaphanous autoregulatory (DAD) domain, and GTPase-binding (GBD) domain. These domains play an important role in actin regulation by formins (Goode, 2007). The intramolecular interaction between the DAD and DID domains result in inhibition of actin assembly by the FH2 domain of formins (Evangelista et al., 2003). The autoinhibitory effect of formins is released upon binding of a Rho-family GTPase to the GBD domain, which is also a property of WASP (Wallar et al., 2006).

The FH2 domains of formins can oligomerize, and two FH2 domains are able to stabilise actin dimer by binding to two actin subunits. Formins mediate unbranched-F-actin formation, which initiate by processive association of the G-actin at the filament barbed ends (Evangelista et al., 2003). Elongation of the barbed end bound by the FH2 dimer is relatively slow suggesting a transition state between the open state (where addition of actin monomer is permitted) and the closed state (where actin assembly is inhibited) (Kovar et al., 2006; Kovar and Pollard, 2004; Vavylonis et al., 2006). The transition state between the closed and open states of the formin dimer are believed to be the reason for the divergence in elongation rates between the eukaryotic species (Harris et al., 2005; Paul and Pollard, 2009).

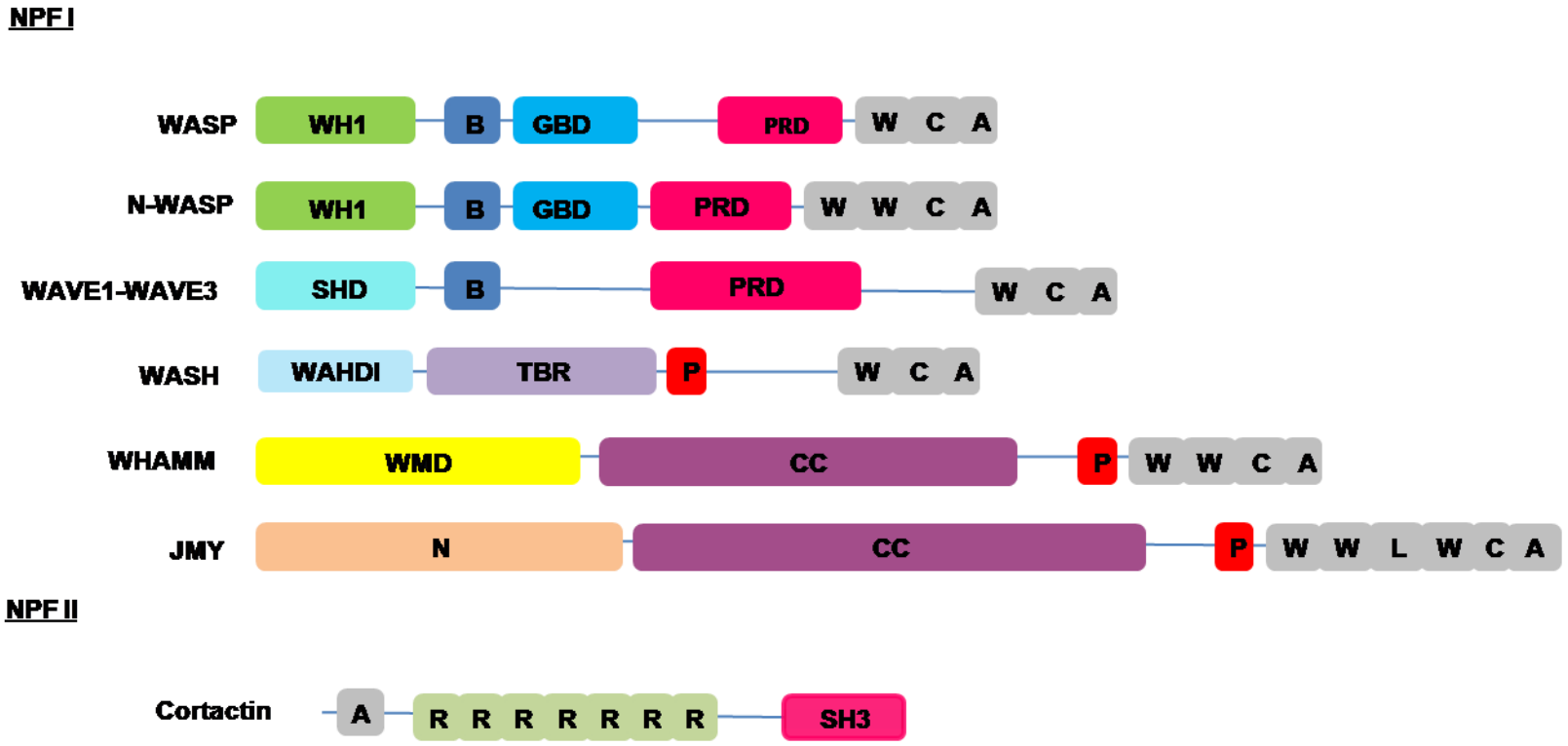

Figure 1.9: Schematic representation of mammalian nucleation promoting factors (NPFs).

WH1-WASP homology domain 1, B- basic region, GBD- GTPase binding domain, PRD- polyproline-rich domain, WCA- includes : WASP homology domain 2 (WH2), central region (C), acidic domain (A). SHD- SCAR homology domain, WHD1- WASH homology domain 1, TBR- tubulin binding region, P- PIP_2 binding motif, WMD- WHAMM membrane interaction domain, CC- coiled-coil region. N- N-terminal region of JMY, L- Linker. Central F-actin binding repeats (RxRxRxR) and SH3- Src homology domain of cortactin.

Adapted from: Campellone and Welch, 2010

1.4.7 Nucleation promoting factors (NPFs)

Nucleation of actin is mediated by the activity of the nucleation promoting factors (NPFs). In mammalian cells, NPFs interact with the Arp2/3 complex via the CA region at the C-terminus (Kelly et al., 2006; Marchand et al., 2001). The N-terminal regions of NPFs are diverse and modulate regulation of different functions in cells (Stradal and Scita, 2006). Figure 1.9 illustrates the structural domains of the mammalian NPFs, which can be categorised into two classes:

i. Class I NPFs: e.g. WASP and N-WASP (WASP subfamily), Ena/VASP family, SCAR/WAVE (WAVE subfamily), WASH, WHAMM and JMY.
ii. Class II NPFs: e.g. cortactin.

1.4.7.1 Class I

1.4.7.1.1 WASP and N-WASP

The mammalian Wiskott-Aldrich syndrome protein (WASP) is 502 residues long and highly expressed in hematopoietic cells. Mutation of the WAS gene results in a severe X-linked immunodeficiency disease in mice and humans, which is characterised by defective cell migration, cell signalling and phagocytosis (Bosticardo et al., 2009). The neuronal (N)-WASP is expressed in most cell types. Deletion of the N-WASP gene is lethal for the mice embryos due to congenital defects in neurons and cardiac cells (Snapper et al., 2001).

WASP and its homologue N-WASP serve as primary activators for the Arp2/3 complex, which mediates actin nucleation. Both have multi-functional domains that are relatively similar (shown in figure 1.9). The N-terminal of the WASPs consist of WASP homology 1 (WH1) domain, which binds to several WASP interacting proteins (WIPs), followed by a cluster of basic residues (B domain). The B domain is targeted by PIP_2, but this domain is not essential for PIP_2 binding (de la Fuente et al., 2007; Rohatgi et al., 2000). The GTPase binding domain (GBD) of WASP/N-WASP is 16 residues long, and comprises of CRIB motif (Cdc42/Rac-interactive binding) and its surrounding sequence. A CRIB

motif is also present in a number of GTPase and Rac activators (Tondeleir, et al., 2009; Burbelo et al., 1995).

The region between the GBD domain and the C-terminal region is the polyproline-rich domain (PRD), which interacts with several Src homology 3 (SH3) domain containing proteins such as Nck, Grb2 and cortactin. The C-terminal end of WASP members contains the verprolin homology domain (V) (also called WH2), central motif (C), and acidic region (A) (Welch and Mullins, 2002). The WH2 domain is important for actin monomer binding (Higgs et al., 1999), whereas the CA region reportedly binds to the Arp2/3 complex with a 1:1 stoichiometry (Marchand et al., 2001; Gaucher et al., 2012). However, another binding study suggested a 2:1 stoichiometry (Ti et al., 2011).

WASP and N-WASP proteins are inactive in the absence of other proteins due to the autoinhibitory effect that results from the intramolecular folding of the WCA domain onto the CRIB motif. This intramolecular interaction occludes actin assembly by the Arp2/3 complex (Kim et al., 2000; Prehoda et al., 2000; Miki et al., 1998a). Structural analysis suggests that the GBD domain of WASP is able to form a complex with its CA region, which causes basic Argenine477 and its surrounding residues to be buried into the intramolecular fold, causing this region to be inaccessible to the binding site of Arp2/3 complex (Kim et al., 2000).

Many accessory proteins serve as activators for WASP/N-WASP. The intramolecular interaction of WASP/N-WASP is inhibited upon Cdc42 binding to the CRIB motif. Cdc42 binding causes the GBD domain to change conformation to mediate the release of WCA to allow binding to the Arp2/3 complex (Rohatgi et al., 2000; Miki et al., 1998b). Activation of WASP/N-WASP can also occur through direct binding to single or multiple SH3 domain containing proteins such as the adaptor protein Nck, which induces the multimerization of N-WASP. This multimerization was proposed to regulate

the ordered activation of Arp2/3 complex, which could promote actin polymerisation (Ti et al., 2011), but this phenomena is yet to be described in vivo.

The well-studied WASP interacting protein (WIP) has a key role in regulating the Arp2/3 complex activation by WASPs. WIP binds to the WH1 domain of WASP and N-WASP which then stabilise the autoinhibitory structure and therefore preventing actin polymerisation in vitro (Ho et al., 2004). In an actin-based motility system in *Vaccinia*, WIP appears to mediate N-WASP recruitment to the sites of polymerisation in a Cdc42-independent manner (Moreau et al., 2000).

PIP_2 binding to the basic region (B) is thought to enhance Cdc42 binding to the GBD domain and counteracts the inhibitory conformation of the GBD-WCA interaction. Phosphorylation of tyrosine residues in the CRIB region (particularly conserved residues Y291 of WASP and Y256 of N-WASP) by tyrosine kinases also activates WASP/N-WASP to stimulate actin polymerisation mediated by Arp2/3 complex (Torres and Rosen, 2003; Suetsugu et al., 2002, 2013).

These factors collectively prime WASP/N-WASP activation of Arp2/3 complex, which in turn facilitates many cellular processes that are linked to actin polymerisation such as filopodia formation (Miki et al., 1998a), membrane ruffling (Buccino et al., 2004), and endocytosis (Qualmann and Kelly,2000).

1.4.7.1.1.1 Regulation of WASP by phosphorylation

Phosphorylation of WASP is an essential process that regulates its Arp2/3 complex-dependent actin nucleation activity. Phosphorylation of WASP by several Ser/Thr kinases is critical for regulating the autoinhibitory interaction caused by intramolecular folding between GBD and WCA domains (see section 1.4.7.1.1). The phosphorylation sites of WASP/N-WASP have been identified to tyrosine Y291 (Y291) in WASP and Y256 (Y256) in N-WASP. TheY291 and Y256 are important in filopodia formation and neurons extension in vivo (Cory et al., 2002; Suetsugu et al., 2002). Mass spec analysis identified additional serine residues at the C-terminal of WASP, which include S483 and S484. These residues are also contributed to optimal activation of Arp2/3 complex (Cory GO et al., 2003).

Y291 in WASP and its analogue Y253 in N-WASP localise in the GBD domain, which mediates Cdc42 binding when WASP is active. However, Y291 in the inactive WASP is buried in the autoinhibited conformation of GBD-WCA; this intramolecular binding protects Y291 from phosphorylation by kinases. Once Cdc42 binds to WASP, the WASP intramolecular interaction destabilises, which leads to opening the autoinhibited structure, and therefore allows the exposure of GBD to kinases (Torres et al., 2006; Torres and Rosen, 2003; Buck and Rosen, 2001; Kim et al., 2000). PIP_2 interacts with the B domain of WASP and promotes GTP hydrolysis of GTP bound to Cdc42, and Cdc42 was shown to cooperate with PIP_2 to activate WASP. However, destabilisation of the GBD-WCA interaction by Cdc42/PIP_2 is not sufficient to stimulate WASP for activation of the Arp2/3 complex (Higgs and Pollard, 1999, Rohatgi et al., 2000). This process requires further phosphorylation of WASP to be active and to prevent its dephosphorylation by the act of phosphatases. Interaction of WASP with the SH3 or SH3-SH2 domain of various kinases leads to high level of WASP activation, and thus stimulates actin nucleation mediated by Arp2/3 complex (Torres and Rosen, 2003; 2006). In vitro, the SH3-SH2 domain containing kinases can activate WASP independently of Cdc42 in vitro. Figure1.10 shows a schematic model of

WASP activation mediated by Y291phosphorylation (Fukuoka et al., 2001, Rohatgi et al., 2000). The phospho-residues of WASP S483 and S484 lie at the junction that connects the C region to the A domain in WASP. This region is critical for binding and activation of Arp2/3 complex (Zalevsky et al., 2001), and also formation of the autoinhibited structure of WASP (Suetsugu et al., 2001). Ser/Thr kinase, casein kinase 2 (CK2) mediated S483 and S484 phosphorylation was shown to enhance the affinity of Arp2/3 complex to WCA and allowed optimal actin polymerisation mediated by activation of the Arp2/3 complex in vitro and in vivo (Cory et al., 2003).

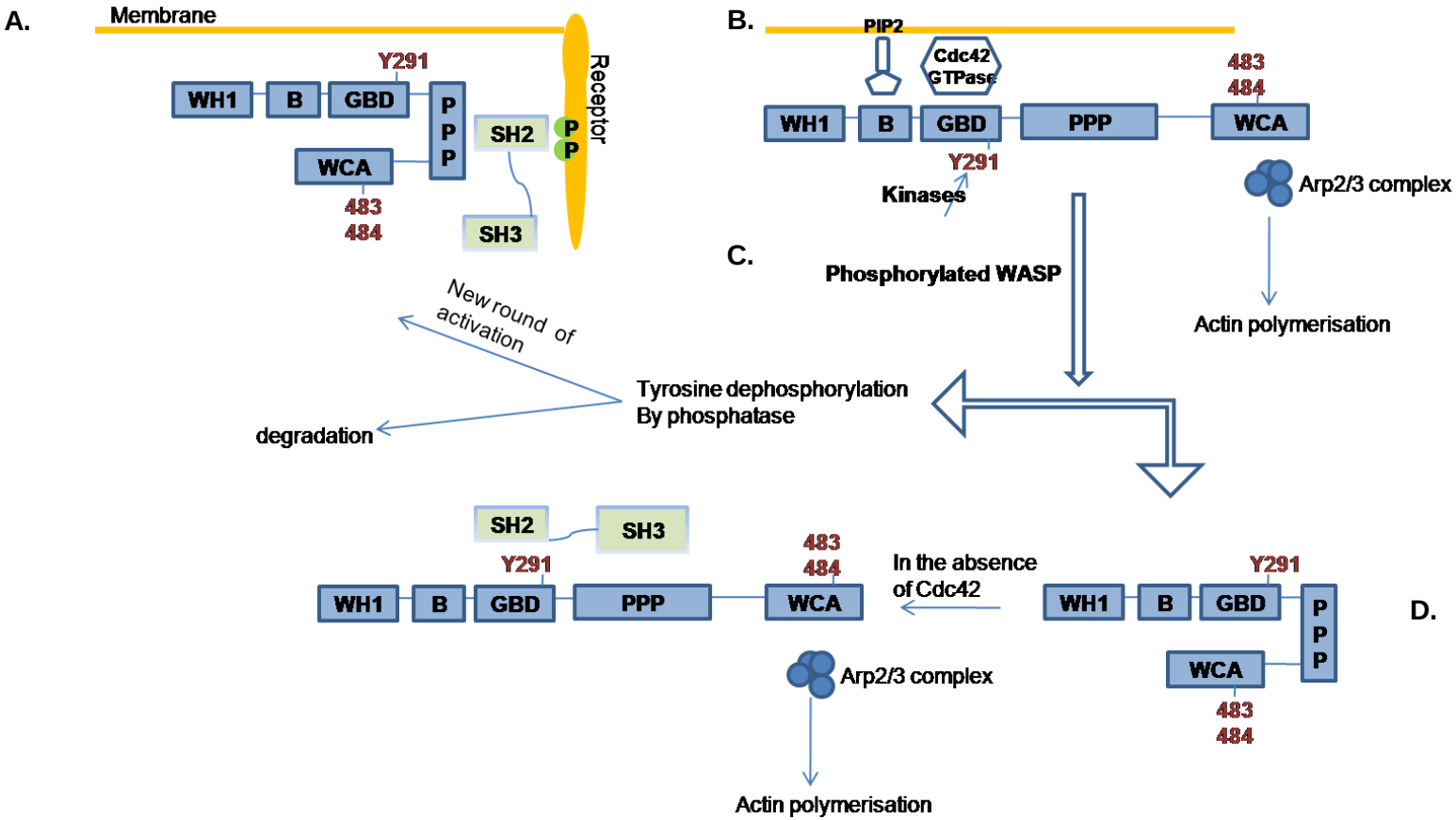

Figure1.10: Schematic model of WASP regulated by phosphorylation.

(A) The autoinhibited WASP molecule can be recruited to the region of membrane receptor signalling via SH3 domain containing proteins such as Nck. **(B)** The inactive WASP is activated by Cdc42 and PIP_2 and then phosphorylated by kinases such as Src kinases. **(C)** The phosphorylated species of WASP are regulated differently. They can be dephosphorylated by phosphatases which may undergo further cycles of phosphorylation, or be recruited for degradation. **(D)** Alternatively, in the absence of Cdc42 the phosphorylated species can be re-folded (to become an inactive structure) and then activated by SH2 and SH3 domain containing proteins, thus promoting actin polymerisation mediated by Arp2/3 complex. Model adapted from: Dovas and Cox, 2010.

1.4.7.1.2 Ena/VASP

Ena/VASP family members were first discovered in platelets, and are substrates for cAMP kinases. The protein family includes the Drosophila protein Ena and the mammalian proteins vasodilator-stimulated phosphorylation (VASP), the Mammalian Enabled (Mena) and the Ena/VASP-like (EVL) protein.

The N-terminal region of Ena/VASP contains an Ena/VASP homology 1 domain (EVH1) which is responsible for its recruitment by proteins that binds to its FPPP motif. In the centre of the Ena-VASP is a PRD, which binds to SH3 domain containing proteins. The C-terminus contains an Ena/VASP homology 2 domain (EVH2), which binds to actin monomers and F-actin, and a coiled-coil region, which is thought to mediate protein tetramerization. Additionally Ena/VASP contains multiple tyrosine and threonine residues, and phosphorylation of the sites was found to increase the stability of Ena/VASP bound to F-actin (Lanier and Gertler, 2000). Ena/VASP recruitment in vitro was found to be mediated by the binding of its PRD to short F-actin filaments, which allows processive actin filament elongation. The number of F-actin seeds was increased in the presence of cofilin, whereas actin elongation was enhanced by profilin in a concentration-dependent manner (Siton and Bernheim-Groswasser, 2014). The ability of Ena/VASP EVH2 domain to nucleate actin filaments is stimulated by addition of G- or F-actin seeds to the Arp2/3 complex (Skoble et al., 2001; Geese et al., 2002). Ena/VASP also acts as an anti-capping protein that prevents capping of filament barbed ends by capping proteins, suggesting that Ena/VASP is important in actin architecture during cell migration and ruffling formation (Samarin et el., 2004).

1.4.7.1.3 SCAR/WAVE

The WASP family verprolin homologous proteins (WAVE)/suppressor of cAR /SCAR) proteins form a subfamily within the WASP family, which is conserved in animals, protists, and plants. In mammalian cells the WAVE protein exists in three isoforms (WAVE1, WAVE2, and WAVE3), that are ubiquitously

expressed, with the highest expression in brain tissues (Stovold et al 2005). WAVEs show little sequence homology to WASP proteins, but multiple domains are conserved in all WASP family members. At the N-terminal end is the WAVE homology domain (WHD), which is followed by the B domain, PRD, and VCA (shown in figure 1.9). Like WASP proteins, the VCA domain is implicated in actin monomer and Arp2/3 complex binding which triggers actin polymerisation. The WAVE proteins lack the GBD domain, and are activated by Rac GTPase instead of Cdc42.

Cellular WAVE1 is part of a complex containing multiple binding proteins which include HSPC300 (also called Brick 1), Abi-interactor 2 (Abi2), Nck-associated protein1 (Nap1) and specifically Rac-associated1 (Sra1). This is called the WAVE regulatory complex (WRC), and WAVE is inactive in this complex. However, addition of active Rac causes subsequent disassembly of Abi2, Nap1, and Sra1 from the WRC complex. This is thought to release the trans-inhibitory state of WAVE resulting in a WAVE:HSPC300 sub-complex that activates the Arp2/3 complex to drive actin polymerisation (Derivery et al., 2009a; Eden et al., 2002; Echarri et al., 2004; Stovold et al., 2005). Recently, it has been shown that, the EVH1domain of Ena/VASP interacts with Api2, which stimulates cell migration. This interaction enables WRC activation by Rac, thus promoting Arp2/3-mediated actin polymerisation (Bisi et al., 2013 and Chen et al., 2014).

1.4.7.1.4 WASH

WASH is encoded by a human sub-telomeric gene and is conserved from vertebrates to protists (Linardopoulou et al., 2007). The modular organisation of WASH includes unique WASH-homology domain (WAHD1) and tubulin-binding region (TBR) at its N-terminal. As WASP family members, WASH also contains a middle PRD region followed by a WCA domain at the C-terminal (depicted in figure 1.9). However, the WCA domain is absent in WASH from *Trypanosomea* species (Kollmar et al., 2012).

The cellular WASH protein localises to the sorting system of endosomes and exists as a multi-protein complex known as the WASH regulatory complex (SHRC) (Derivery et al., 2009b; Duleh and Welch, 2010). It was suggested that, at least four of five SHRC complex components are structural homologues to the WCR components of WAVE (Jia et al., 2010). WASH also act as a mediator that links the tubules in retromer-mediated cargo transport from early endosomes to the Golgi via the microtubules (Gomez and Billadeau, 2009). WASH protein recruitment to the tetramer is unclear but a proposed model suggested that the FAM21 component of the SHRC complex senses the retromers on the endosomal membrane then stimulates WASH recruitment to the retromer-enriched membrane (Jia et al., 2012). *Drosophila* WASH was shown to function downstream of Rho-GTPase and was able to bundle F-actin and microtubules in a Spire (unbranched F-actin) or Arp2/3-dependent manner (Liu et al., 2012).

1.4.7.1.5 WHAMM

WASP homologue associated with actin, membrane, and microtubules (WHAMM) is only found in mammalian cells. WHAMM is able to activate the Arp2/3 complex and is involved in regulation of ER to Golgi transport (Campellone et al., 2008; Zuchero et al., 2009). The N-terminal of WHAMM consists of WHAMM membrane-interacting domain (WMD), which mediates Golgi membrane binding, and a coiled coil region, which binds to microtubules. The C-terminal contains two WH2 domains and a CA domain to mediate Arp2/3-mediated actin nucleation (shown in figure 1.9). WHAMM protein is constitutively active in vitro indicating that, like WAVE2, its activity may be regulated by a binding partner (Campellone et al., 2008). Overexpression of WHAMM causes Golgi disruption, and defects in vesicle and tubule movement, which suggests that, WHAMM supports Golgi morphology and regulates ER to Golgi transport. In addition, interaction of WHAMM with microtubules and actin filaments is able to provide the force required for membrane tubulation and dynamics (Campellone et al., 2008).

1.4.7.1.6 JMY

The junction-mediating and regulatory protein (JMY) was discovered by sequence alignment of WH2 domain containing proteins. JMY was classified as a tandem actin monomer nucleator due to the presence of three WH2 motifs. The F-actin nucleation activity of JMY is mainly Arp2/3 dependent. However, in the absence of Arp2/3 complex, JMY has lower levels of nucleation ability, which is mediated by its three WH2 domains or actin binding linker (Zuchero et al., 2009). The domain structure of JMY contains an N-terminal domain, a coiled coil region, followed by a central PRD (though some JMY isoforms lack this polyproline domain). Its C-terminus contains three repeats of WH2 domains and a CA domain (figure 1.9). The first two WH2 domains are separated from the third WH2 by a linker, which is also able to bind actin monomers. The WCA of JMY has 28% sequence identity with N-WASP and the full length protein has 35% similarity to WHAMM (Campellone and Welch, 2010; Zuchero et al., 2009). JMY localises to the nucleus, and was first discovered as a co-factor to the tumour suppressor p35 (Shikama et al., 1999). In response to DNA damage, JMY is downregulated by the protein Mdm2 (ubiquitin ligase that targets p35) causing an increase in JMY, which promotes its degradation (Coutts et al., 2009). The actin nucleation activity of JMY in vivo is unclear. However, it has been shown to play a role in multiple actin related processes. Like WHAMM, JMY was found to localise at the Golgi and influence the trafficking of vesicles (Schlüter et al., 2014). JMY is also important for promoting Arp2/3-mediated cell migration (Coutts et al., 2009). Over-expression of full length JMY revealed weak actin nucleation activity compared with its WWWH2 domain alone, suggesting that JMY is regulated by an autoinhibitory mechanism (Firat-Karalar et al 2011).

1.4.7.2 Class II- cortactin

Cortactin is a class II NPF, and was identified as a major Src kinase substrate and an actin binding protein (Wu and Parsons, 1993). Later on, it was defined by its ability to promote Arp2/3-mediated actin nucleation (Weed et al., 2000).

Cortactin plays important roles in many cellular processes such as formation of the cadherin adhesive zone, membrane remodelling in lamellipodia, and membrane ruffling (Helwani et al., 2004; Kinley et al., 2003). Unlike NPF class I proteins, cortactin contains an N-terminal domain rich in acidic residues that binds the Arp2/3 complex, and also does not contain a WH2 domain. Instead, cortactin possess central F-actin binding repeats (RxRxRxR). The C-terminal has an SH3 domain that interacts with regulatory proteins including N-WASP (Weaver et al., 2002) and WIP (Kinley et al., 2003), see figure 1.9. The NPF activity of cortactin is relatively weaker than NPF class I proteins. Nevertheless, cortactin cooperates with the WCA of N-WASP and they appear to synergise in promoting actin nucleation. Cortactin was shown to inhibit loss of filament branches nucleated by Arp2/3 complex. This suggests that, cortactin promotes nucleus stabilization (Weaver et al., 2002). Another model was proposed, in which cortactin displaces WCA binding from the branch junction after Arp2/3-mediated nucleation, this was referred as a recycling or displacement model. In the model, cortactin has no effect on actin polymerisation or Arp2/3 complex stabilisation, but it enhances the detachment of N-WASP WCA from the newly branched site. This effect causes acceleration in the branch rate driven by WCA-bound Arp2/3 complex (Siton et al., 2011).

1.5 Yeast actin

The *Saccharomyces cerevisiae* genome encodes a single essential actin (*ACT1*) gene (Shortle et al., 1982), which encodes actin-like protein Act1 that has 87-90% sequence homology to muscle actin (Gallwitz and Sures, 1980). Actin deletion revealed severe defects in yeast budding, vesicle trafficking, polarisation of actin patches during the cell cycle and chitin localisation, which reflects the key significance of the actin cytoskeleton for regulation of these processes (Gallwitz and Sures, 1980; Ng and Abelson, 1980). Yeast actin-like protein was purified from yeast cells, with a higher molecular mass of a 45kDa compared to 42 kDa for actin in mammals (Greer and Schekman, 1982). The polymerisation kinetic properties of yeast actin are relatively similar to those of muscle actin, but yeast actin has a faster rate of polymerisation when it is polymerised in the same conditions as mammalian actin. Generation of *act1* mutant alleles (*1-119*) or (*R177A*/*D179A*) using random mutagenesis made it possible to relate the cellular phenotypic consequences associated with *act1* mutants to actin polymerisation properties (Shortle et al., 1982). Drubin and co-workers analysed the effects of act1 (*1-119*) or (*R177A/D179A*) mutants on the yeast actin cytoskeleton and found that, assembled actin patches and cables could not be labelled by rhodamine phalloidin, suggesting that phalloidin may bind to monomers via R177/D179 in order to stabilise the filaments (Drubin et al., 1990). Purified (R177A/ D179A) mutants were analysed to determine their effects on actin polymerisation, these actin mutants displayed a slow rate of overall polymerisation of R117A/ D179A mutants compared to wild type actin, in which the rate of elongation was 3 fold higher than the *act1* mutants. This indicates that, the difference in the overall rate of yeast actin and muscle actin polymerisation is due to a larger rate of nucleation for yeast actin rather than a difference in the rate of elongation (Belmont et al., 1999, Buzan and Frieden, 1996). In addition, the process of nucleotide exchange in yeast actin occurs more rapidly than for muscle actin under the same conditions. Phosphate (P_i) release in yeast actin occurs following ATP hydrolysis and is concomitant with actin polymerisation

whereas; muscle actin retains its P_i following ATP hydrolysis and actin polymerisation (Yao and Rubenstein, 2001; Carlier and Pantaloni, 1986).

1.5.1 Actin architectures in yeast

Actin organisation in yeast was first visualised in chemically fixed cells, and found in three forms of actin-rich structures: actin cortical patches, actin cables, and the acto-myosin ring (Adam and Pringle, 1984). These filamentous structures undergo rearrangement throughout the stages of the cell cycle in *S. cerevisiae* (shown in figure 1.11).

1.5.1.1 Actin cortical patches

Actin cortical patches are discrete foci formed by a combination of actin filaments and actin binding proteins (Adam and Pringle, 1984). In undivided yeast cells, the actin patches are distributed randomly, whereas the actin patches in budded cells are enriched at the region of bud growth. The actin patches are therefore polarised in the bud, and this polarisation is dependent on the stages of cell cycle. The actin patches are concentrated at the growth region (tip end of the mother) which is required for polarised growth of the new bud. The mother contains few patches, which cluster at the bud neck during separation of the new bud (daughter) from the mother bud (Pruyne et al, 1998). The yeast Arp2/3 complex is required for the integrity of the actin cortical patches which are involved in both endocytosis and cell wall remodelling (; Munn and Riezman, 1994; Munn et al., 1995; Winter et al., 1997; Young et al., 2004).

1.5.1.2 Actin cables

Actin cables are polarised linear structures composed of actin filaments stabilized by various yeast proteins including: the fimbrin homologue (Sac6) and tropomyosin homologue (Tpm1 and Tpm2) (Adams and Pringle, 1984; Chant and Pringle, 1995). The Arp2/3 complex is not required for the assembly of F-actin in actin cables. Instead, Bni1 and Bnr1 (formin homologue in yeast) are responsible for nucleating actin filaments that align along the axis of the cell. Actin cables appear as slightly irregular long lines in unbudded

cells, but are more evident during bud growth (Adams and Pringle, 1984; Amberg, 1998). Actin cables are necessary for many cellular events, including mitotic spindle orientation (Theesfeld et al., 1999), vacuole inheritance, and vesicle trafficking supported by myosins (MyoV and Myo2) (Pruyne et al, 1998). Actin cables also mediate mRNA delivery to the bud, which is a process enhanced by MyoV function (Beach et al., 1999).

1.5.1.3 Acto-myosin ring

The actomyosin ring is a transient structure that plays an essential role in mammalian and yeast cytokinesis (Balasubramanian and Glotzer. 2004). The acto-myosin ring is formed from assembled F-actin, myosin II and other actin binding proteins, such as actin nucleators, actin cross-linkers or bundlers, and actin stabilizing proteins. These components form a complex that is localised in the middle of the cell plane, which generates a force required for splitting the cell during cell division (Wu and Pollard, 2005). The nature of actin filaments in the actomyosin ring is unbranched and linear, which is attributed to nucleation of F-actin by the yeast formins Bni1and Bnr1 (Lord et al., 2005). Moreover, contractile ring recruitment and position at the division site is controlled by cell cycle regulatory kinases during cytokinesis (Balasubramanian and Glotzer. 2004).

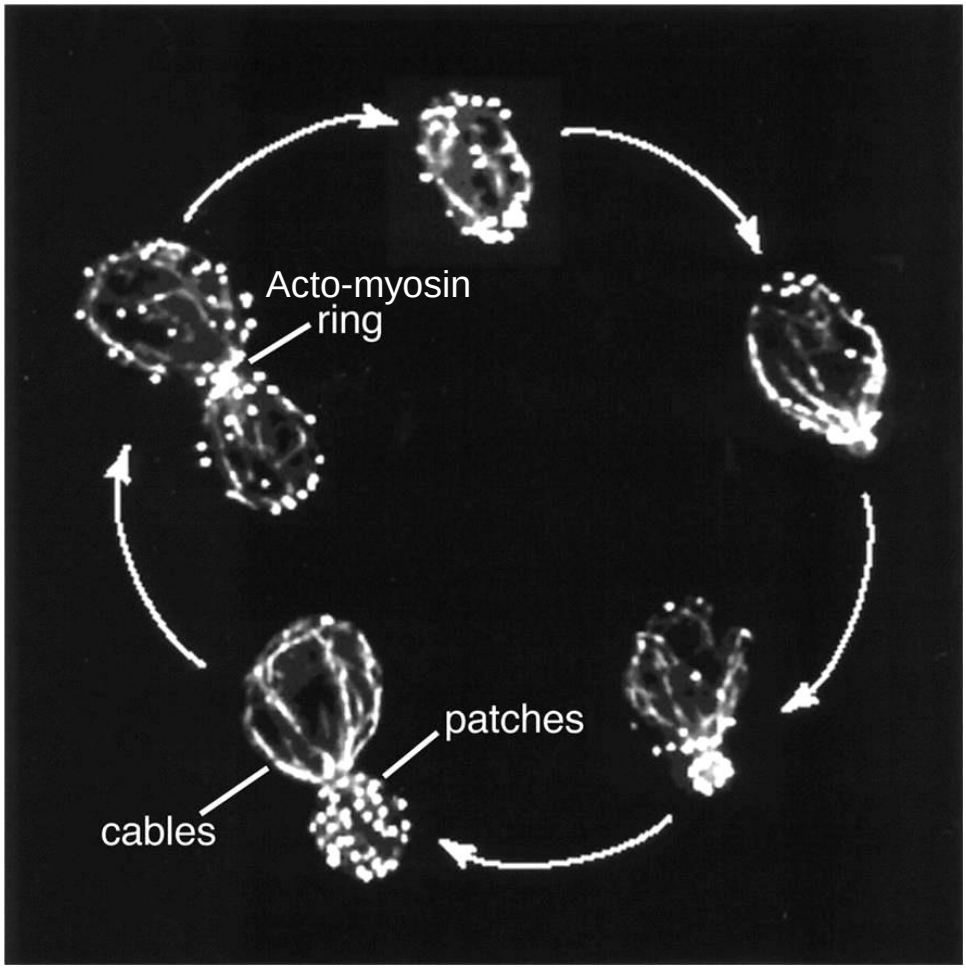

Figure 1.11: Actin structures in *S. cerevisiae*.

Diploid yeast cells were stained with rhodamine phalloidin and imaged with DeltaVision.

From: Moseley and Goode, 2006

1.6 Roles of actin in yeast endocytosis

The clearest evidence for the link between actin and endocytosis comes from studies on budding yeast. Yeast is a good model system for studying endocytosis because most of its endocytic proteins are homologues to mammalian proteins, and it is easy to delete or alter these proteins at the genetic level, since yeast cells are haploid. To determine which proteins are essential for endocytosis, genetic screens have been performed on endocytic mutants (*end* $^{--}$) in budding yeast. These mutants were defective in α-factor internalisation, and Lucifer yellow uptake, and exhibited aberrant trafficking phenotypes of FM4-64 dye. The majority of these mutants also showed defects in the actin cytoskeleton, which suggests a specific role of actin to achieve successful internalisation during endocytosis (Kübler and Riezman, 1993; Raths et al., 1993). The importance of the actin cytoskeleton in yeast was also confirmed using the drug Latrunculin-A which sequesters actin and inhibits endocytosis (Ayscough et al., 1997). In another experiment, yeast cells were treated with the F-actin stabilizing drug Jasplakinolide, which showed that F-actin alone is insufficient to establish endocytosis in yeast (Ayscough, 2002). In addition to these studies, advance in live-cell imaging have elucidated the relationship between endocytosis and actin assembly in the actin patches. Studies on the actin binding proteins Abp1 and Cap2 tagged with GFP have shown that cortical patches are very dynamic at the cell surface. Deletion of the *ABP1*, *CAP2* and *SLA1* genes caused severe defects in cortical patch movement at the endocytic sites indicating that other actin regulatory proteins may associate with cortical actin patches **(**Mulholland et al 1994; Waddle et al., 1996; Warren et al., 2002). Subsequently, more than 60 proteins associated with actin cortical patches have been identified to localise at sites of endocytosis (Galletta et al., 2010; Weinberg and Drubin, 2012).

1.7 Endocytosis in yeast

Endocytosis is a process in which the plasma membrane internalises to uptake molecules from the cell surface and then pinches off to produce a vesicle. The formed vesicle either can be delivered to lysosome for degradation or to recycle back to the plasma membrane. The functional significances of endocytosis lie on its ability to maintain cell membrane homeostasis and that through regulation of nutrient uptake, modulation of signal transduction, internalisation of cell surface receptors, lipids, or pathogens entry (Goldstein and Drubin, 2003; Doherty and McMahon, 2009). Clathrin-mediated endocytosis (CME) is the most extensively studied of all endocytic pathways, which is highly conserved from yeast to mammals. In eukaryotic cells, CME is accomplished through sequential recruitment of clathrin, endocytic adaptors, and actin binding partners at the sites of endocytosis. Clathrin, adaptor proteins and other cargoes form a protein coat at the plasma membrane, and this coated membrane bends to form vesicle which can carry various cargoes. The coated vesicle then pinches off the plasma membrane and the protein coat that surrounds the vesicle is disassembled. The uncoated vesicle is released into the cell and fuses with the membrane of an endosome. The vesicle delivers its cargoes from the early endosome to the late endosome, which fuses with lysosome to allow degradation. However, at the early endosome, cargoes can also be recycled back to the plasma membrane. In yeast, Actin and actin binding proteins have been shown to localise at the actin patches where endocytosis takes place, these actin structures are highly dynamic due to constant F-actin remodelling (Doyle and Botstein, 1996; Waddle et al., 1996). Actin is a key factor required to initiate membrane invagination, and scission of coated vesicles at endocytic sites. CME in yeast is highly dependent on Arp2/3-mediated actin nucleation to generate force that can overcome the cytosolic turgor pressure of yeast cells (Galletta et al., 2009; Aghamohammadzadeh and Ayscough, 2009). The advent of total internal reflection microscopy and live imaging of the fluorescent tags GFP and mRFP made it possible to visualise the dynamic recruitment of the proteins that are associated with the endocytic patches, and

offer an indication of which stages of the endocytic pathway these proteins might function (figure1.12).

Kaksonen and colleagues were the first to apply two-colour real-time imaging to observe various endocytic proteins and defined the change in patch dynamics during endocytic events (Kaksonen et al., 2003). Time lapse movies of fluorescently-tagged Abp1 and Sla1 expressed in 60 yeast deletion strains (each with a different constituent of actin patches deleted), revealed distinct recruitment of Abp1 and Sla1 at different stages of patch lifetime. The early recruitment of actin machinery at endocytic sites (including, Pan1 and Las17) was proposed to activate actin assembly at the stage that corresponds to membrane invagination and subsequent scission of the nascent vesicle (Kaksonen et al., 2003, 2005).

1.7.1 Actin binding proteins (ABPs) in yeast

Most of the actin binding proteins in yeast are homologues to many of the pivotal ABPs in mammals. The ABPs in yeast and their analogous in proteins in mammals are shown in table 1.1.

1.7.2 Stages of endocytosis

Cumulative data by Kaksonen and others led to the establishment of a molecular model that defines the functions and dynamics of each protein group at distinct stage of CME in yeast. Therefore, each stage is characterised by arrival of a discrete protein module (shown in figure 1.13). The first module is associated with early recruitment of clathrin, adaptor

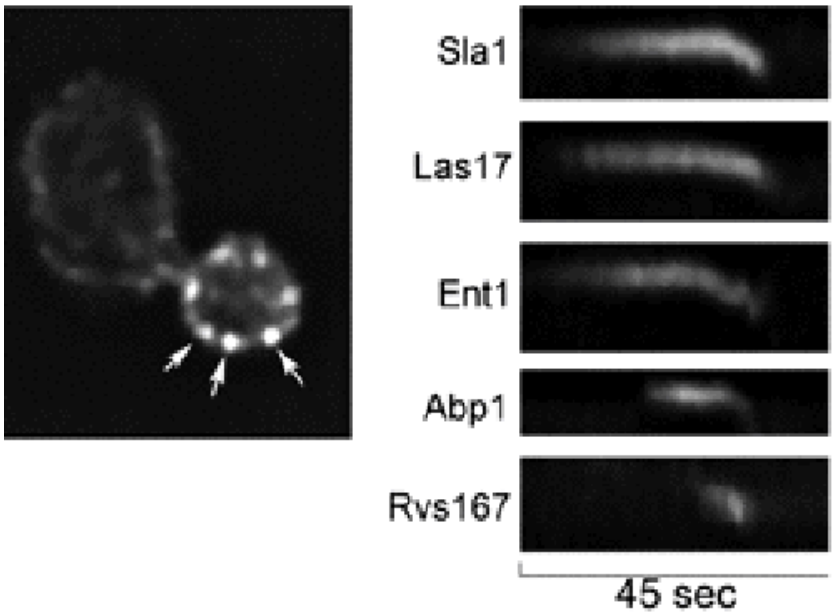

Figure 1.12: Actin and endocytic markers in budding yeast.

Left panel: Actin cortical patches visualised using rhodamine phalloidin (spots marked with arrows). Right panel: Kymographs generated from time lapse movies showing the kinetics of Sla1, Las17, and Ent1, which are recruited early and remain non-motile for most of their lifetime. Abp1 is an actin marker used to assess arrival of actin at the endocytic patch. Rvs167 arrives just after the onset of inward movement and is involved in vesicle scission.

From: Robertson et al, 2010

Yeast protein	Mammalian protein
Early	
Ede1	Eps15
Syp1	FCho1/2
Early coat	
Chc1	Clathrin heavy chain
Clc1	Clathrin light chain
Yap1801/2	AP180
Apl1/3	AP2 complex α/β subunits
Apm4	AP2 complex mu subunit
Aps2	AP2 complex σ subunit
Intermediate coat	
Sla2	Hip1
Ent1/2	Epsin
Late coat	
Pan1	Intersectin
Sla1	CIN85
End3	Eps15
Lsb3	SH3yl1
Ysc84	SH3yl1
Gts1	Small Arf GAP2
WASP/Myo module	
Las17	WASP/N-WASP
Vrp1	WIP/WIRE
Bzz1	syndapin
Scd5	-
Myo3/5	Myosin type I
Bbc1	-
Aim21	-
Actin module	
Act1	Actin
Arc15/18/19/35/40 & Arp2/3	Arp2/3 complex
Abp1	ABP1
Cap1/2	Capping proteins α/β
Sac6	Fimbrin
Scp1	Transgelin
Twf1	Twinfilin
Crn1	coronin
Ark1/Prk1/Akl1	BMP2 inducible kinase/AP2 associated kinase1/AAK1 and GAK
Cof1	cofilin
Aip1	Aip1
Pfy1	profilin
Aim3	-
Scission	
Rvs161	Amphiphysin
Rvs167	Amphiphysin/endophilin
Sjl2	Synaptojanin-1
Vps1	Dynamin

Table 1.1: Yeast endocytic proteins and their mammalian orthologues.
Adapted from: Weinberg and Drubin, 2012

proteins, and other endocytic proteins to form the endocytic coat at the site of endocytosis. At this stage the endocytic coat remains non-motile (stage 1). After 1-2 minutes, actin regulatory proteins start assembling F-actin, and this phase can be characterised by slow inward movement of the coated membrane (stage 2). Consequently, the deformed membrane undergoes fast inward movement, approximately 200 nm into the cell. This movement is proposed to correspond to invagination and vesicle scission (stage 3). The newly formed vesicle is released after arrival of the vesicle scission machinery, which include the amphiphysins Rvs161/167 and the yeast dynamin Vps1.

1.7.2.1 Stage 1: non-motile stage

The factors that drive recruitment of proteins to form the coat complex during endocytosis are still unclear. The first stage of CME involves the early arrival of clathrin (Chc1/Clc1 -heavy/light chain protein), Ede1, Ent1/2, and Yap1801/2 proteins at the site of endocytosis. The endocytic protein Ede1 is an adaptor protein and its deletion or inactivation of its ent1 interacting motif in yeast cells reduces the rate of invagination, causing defects in the process of endocytosis. This result suggests that, Ede1 might serve as a tag at the membrane to mark the site where the process of endocytosis takes place (Swanson et al., 2006; Aguilar et al., 2003). Clathrin forms the early coat but is not essential for establishing endocytosis, as clathrin deletion does not abolish endocytosis (Newpher et al., 2005; Kaksonen et al., 2003). However, clathrin was observed to localise at the distal tip of the patch, suggesting that, it may function to stabilize the curvature during invagination of the endocytic protein mesh (Idrissi et al., 2008). Similarly, the endocytic adaptor protein Yap1801/2 was also revealed to be important for stability of the endocytic protein complex (Maldonado-Báez et al., 2008). Accumulation of the clathrin and adaptor proteins at endocytic sites leads to recruitment of other endocytic proteins to join the endocytic coat network. The proteins that form this intermediate coat include Sla2 and Ent1/2 epsin-like proteins, which both bind to PIP_2 via their ENTH domain and are key factors that induce membrane

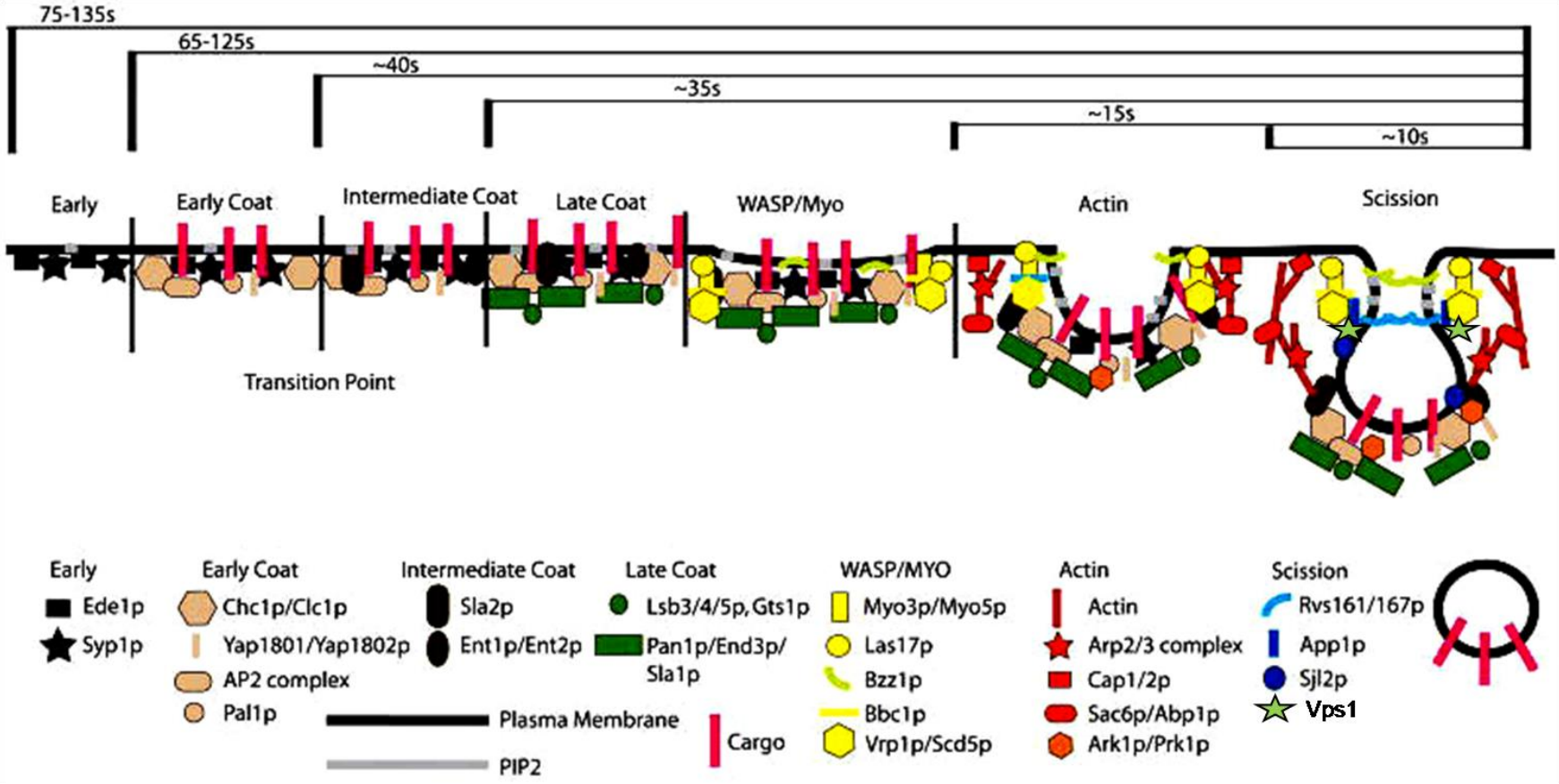

Figure 1.13: Timeline of the modular organisation of endocytic proteins.

The early and early coat proteins appear at the cell surface at different times. After cargo recruitment, actin polymerisation initiates by action of the WASP/MYO module which, generates a force together with BAR domain proteins to bend the membrane forming tubule. Sjl2p produces tension which helps to pinch off the vesicle.

Modified from: Weinberg and Drubin, 2012

curvature (Sun et al., 2005; Aguilar et al., 2003; Wendland et al 1999). Later, the coat proteins Pan1, End3, and Sla1 arrive simultaneously as a protein complex that binds to the endocytic coat components (Tang et al., 2000). Endocytic complex disassembly is dependent on phosphorylation by the Ark1/Prk1 kinase family, which will be described in section 1.8.1.3. The other coat proteins include Lsb3, Lsb4/Ysc84, Lsb5, and Gts1 proteins, which are recruited along with the WASP/Myo coat module but have different roles. Lsb3 and Ysc84 play a significant role in F-actin polymerisation and bundling (Robertson et al., 2009). On the other hand, the Lsb5 and Gts1 regulate endocytic coat disassembly at the late stage of endocytosis (Costa and Ayscough, 2005).

1.7.2.2 Stage 2: Slow movement (invagination)

The slow movement stage of endocytosis is characterised by arrival of the Las17 and myosin module (WASP/Myo). This stage is proposed to coincide with the invagination stage of endocytosis which is characterised by the constant growth of the actin network to generate the force required for bending the membrane and pinching off the nascent vesicle.

It was proposed that, slow movement of the endocytic coat is caused by the regular addition of actin monomers to polymerise actin at the plasma membrane rather than at the internalised vesicle (Kaksonen et al., 2003). Las17 is recruited prior to Myo3/5 and remains immobile at the plasma membrane for approximately 20 seconds (Kaksonen et al., 2005). A few seconds later, the myosin activator Vrp1 arrives then Myo3/5 is recruited just before invagination commences. Following Las17/Myo3/5 arrival, the actin module is recruited, which comprises actin monomers, the Arp2/3 complex, capping proteins, bundling proteins and depolymerising proteins. The onset of membrane invagination is stimulated as a result of F-actin polymerisation, which is induced by activation of the Arp2/3 complex via Las17 and Myo3/5 (Galletta et al., 2008; Sun et al., 2006). At this stage the Las17 inhibitor Sla1 moves inwards with the invaginated coat, which may remove an inhibition of Las17 (Sun et al., 2006). The Las17 and Myo3/5 module was observed to

remain in the plane of the membrane rather than being internalised with the invaginated coated vesicle (Kaksonen et al., 2005). However, immuno-EM analysis has shown that, Myo5 is located at the tip of the invaginated coat while Las17 and Bbc1 (a protein recruited with Myo5 that may inactivate Las17 and Myo5, Sun et al 2006) are localised on the sides of the tubular invagination. This suggests that, the membrane may bend prior to the onset of inward movement (Idrissi et al., 2008). However, more studies are required to support this proposal.

The actin machinery is tightly connected to the endocytic coat component through the adaptor proteins Sla2 and Sla1. Sla2 interacts with actin via its talin homology domain and acts to connect the endocytic coat to the actin filaments. Cells lacking *SLA2* displayed defective endocytosis but were able to form actin comet tails which resulted from continuous assembly of F-actin that was uncoupled from the plasma membrane. In these cells, the NPFs and endocytic coat proteins remain at the membrane whereas, actin, Arp2/3 complex, capping and bundling proteins are associated with the comet tail (Kaksonen et al., 2003). Sla1 is a key actin regulator that binds to cargo proteins. Absence of *SLA1* led to failure in NPFXD cargo uptake and actin dynamics in yeast cells, resulting in abnormal cortical patches (Ayscough et al., 1999; Holtzman et al., 1993). The interaction of Sla1 with Las17 may negatively regulate Las17 activity (Rodal et al., 2003).

1.7.2.2.1 Regulation of actin polymerisation during endocytosis

Actin polymerisation is required in yeast CME to support membrane invagination and subsequent vesicle scission. However, the mechanism of how the actin machinery is regulated at endocytic stages is still not clear. F-actin assembly is marked by arrival of the actin machinery at the endocytic coat complex and activation of Arp2/3 complex by Las17/Myo5, (shown in figure 1.14). During CME several ABPs are involved in F-actin assembly and filament organisation. The onset of actin polymerisation at the endocytic sites might be associated with removing the inhibitory effect of Las17 inhibitors Sla1and Bbc1. This step would promote inward movement of the plasma

membrane. Sun and colleagues have shown that, the addition of the yeast syndapin-Bzz1 may contribute to release of the inhibitory effect by disrupting the Las17-Sla1complex (Sun et al., 2006). These findings were discovered in vitro, but have yet to be confirmed in vivo. Abp1 and Pan1 have been found to localise at actin patches and activate the Arp2/3 complex with less potency than either Las17 or Myo5 in vitro (Duncan et al., 2001; Goode et al., 2001). Endocytic patches lacking Abp1 or Pan1 exhibit normal rates of invagination, suggesting that Las17 and Myo5 are likely to be the main activators of the Arp2/3 complex at actin patches (Sun et al., 2006). Many proteins require the presence of actin for their localisation and significantly contribute to actin polymerisation during invagination of the cell membrane. Capping proteins (Cap1and Cap2 dimer) are important for limiting further addition of monomers at the filament barbed ends. This is consistent with the idea that deletion of both *CAP1* and *CAP2* lead to a decrease in inward movement of the membrane (Amatruda et al., 1990; Kaksonen et al., 2005; Kim et al., 2006). Unlike the other ABPs, the bundling protein Sac6 (fimbrin homologue) is associated with both actin cortical patches and actin cables. Sac6 is important for stabilising the actin patch during internalisation, as deletion of *SAC6* revealed a reduced rate of membrane invagination (Gheorghe et al., 2008; Kaksonen et al., 2005). Another actin bundling and crosslinking protein that localises at the actin module is Scp1 (transgelin homologue). Expression of Scp1 in cells lacking *SAC6* caused abnormal actin organisation and defects in endocytosis indicating that Scp1 and Sac6 function together to stabilise the actin patches (Goodman et al., 2003; Winder et al., 2003). Deletion of *SAC6* and *SCP1* blocked internalisation of the actin marker Abp1-GFP, which resulted in an increase in patch longevity. However Sac6 and Scp1 function at different stages of endocytosis, Sac6 is implicated in the slow inward movement stage, whereas Scp1 functions at the fast movement stage (post-vesicle scission) (Gheorghe et al., 2008). The actin depolymerising proteins, Cof1(cofilin homologue) and its binding partner Aip1, play crucial roles in modulating actin filaments and preventing

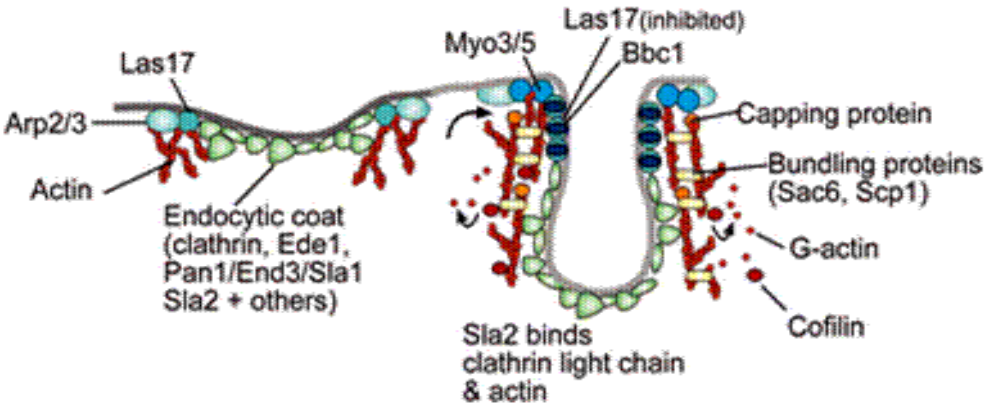

Figure 1.14: Schematic diagram showing the regulation of actin binding proteins during the invagination stage of endocytosis.

Assembly of F-actin is initiated when the Arp2/3 complex is activated by Las17, then type I myosin (Myo3/5) arrives, which functions to aid internalisation of the cell membrane. At this stage, the endocytic protein Bbc1 may inactivate Las17. Capping proteins limit the addition of new actin monomers to barbed ends and cofilin promotes F-actin disassembly. The actin bundling protein complex Sac6/Scp1 generates higher order filamentous structures, which are required for successful endocytic events.

From: Robertson et al., 2010

the elongation of aged F-actin (Moon et al., 1993; Quintero-Monzon et al., 2009).

1.7.2.3 Stage 3: vesicle scission and uncoating

Scission of the endocytic vesicle occurs after the invagination stage. In mammalian cells, the GTPase dynamin is a key factor in the scission stage during CME. The dynamin-like protein, Vps1 in yeast is proposed to be involved in scission. Vps1 was previously shown to localise with Sla1 at actin patches, and it was shown to be required for normal actin organisation in yeast cells (Yu and Cai, 2004). A study from the Ayscough lab showed that, *VPS1* deletion cells are defective in FM4-64 uptake and exhibit retracted movement of endocytic markers (Smaczynska-de Rooij et al., 2010). It was also shown that Rvs167 interacts with Vps1 in yeast two hybrid analysis, and Rvs167 induces disassembly of Vps1 oligomers in vitro (Smaczynska-de Rooij et al., 2010). Following actin polymerisation, both Rvs161 and Rvs167 form a heterodimer that localise briefly at the site of endocytosis. The Rvs161/167 module remains stationary at the membrane then exhibits a rapid 100nm inward movement. This movement was suggested to correspond to vesicle scission during endocytosis (Kaksonen et al., 2005). Like the mammalian amphiphysins, Rvs161/Rvs167 in yeast possesses a BAR domain, which is evolutionarily conserved and has the ability to induce tubulation and generate membrane curvature in vitro (Dawson et al., 2006). The yeast amphiphysins interact with many actin regulatory proteins via binding of the SH3 domain of the Rvs167 to polyproline repeats. In the absence of *RVS161/167*, cells exhibited mild defects in scission, but in combination with *VPS1* deletion, these defects were more severe indicating that Vps1 and Rvs161/167 function together in driving vesicle scission (Smaczynska-de Rooij et al., 2012).

Following scission, the endocytic coat disassembles from the nascent vesicle and this step is essential for fusion of the vesicle with the endosomal membrane. The actin regulatory kinases Ark1/Prk1 are homologues to the

AAK and GAK kinases in mammals play a central role in vesicle uncoating (Smythe and Ayscough, 2003). The kinases Ark1/Prk1 arrive at endocytic sites after invagination and their recruitment is mediated by the SH3 domain of Abp1. Yeast cells lacking both *ARK1/PRK1* were unable to disassemble the endocytic coat and had large aggregates containing many endocytic proteins and F-actin (Cope et al., 1999). At endocytic patches, the actin regulatory kinases Ark1/Prk1 phosphorylate proteins containing Lxx(Q/T)xTG motifs, including the early coat Pan1/Sla1/End3 complex. Phosphorylation of Pan1 by Prk1 down-regulates its activity to allow Arp2/3-mediated F-actin assembly and disrupts Sla1-Pan1 binding. This regulation may allow separation of the coat complex (Pan1/Sla1/End3) from the actin network. Point mutations at the Prk1 motif in Pan1 results in clumps of F-actin, a phenotype that was also seen in *ARK1/PRK1* mutants (Toshima et al., 2005; Huang et al., 2003; Zeng et al., 2001).

The PIP_2 phosphatases, synaptojanin Inp51 and Inp52 proteins are also involved in disassembly of the endocytic coat by dephosphorylation of (4,5)PIP_2 to (4)PIP which allows the ENTH and ANTH domain containing proteins (Sla2 and Ent1/2) to detach from the membrane (Sun et al., 2005; Wendland et al., 1999). In *sjl*Δ, cells have failures in Sla2 and Ent2 disassembly and exhibit inappropriate membrane invagination, which may indicate that, Sjl1 is important for uncoating PIP_2-binding proteins and may serve as a signal for scission (Sun et al., 2007). Another lipid regulatory protein is yeast Arf3 (homologue of mammalian Arf6), the endocytic role of Arf3 is suggested due to its interaction with Lsb5 and Gts1. Lsb5 binds to Sla1 and Las17, whereas Gts1 binds to Sla1, Pan1 and YAP1801/2. All of these interactions suggest that Arf3 is associated with the endocytic machinery although no direct endocytic phenotype was observed upon its deletion. However, Arf3 is an essential factor for regulating the concentration of PIP_2 (Smaczynska-de et al., 2008; Costa and Ayscough, 2005; Huang et al., 2003). Eventually, actin severing proteins including Cof1, Aip1, Crn1, and

Srv2 are recruited along with Ark1/Prk1 and Sjl2 to promote actin network disassembly. Cof1molecules bind to the sides of actin cables and develop a twist, leading to actin severing at the sites where it binds (McGough et al., 1998). Cof1 interacts with Aip1, which is an actin binding protein that caps the newly formed barbed end and prevents its elongation. The yeast coronin Crn1 stimulates Cof1 to bind to aged ADP-actin filaments, whereas Srv2 stimulates Cof1-mediated severing of actin filaments (Ono et al., 2007; Okreglak et al., 2007).

1.8 The WASp homologue/ Las17

The yeast protein Las17 (also called Bee1) is a homologue of mammalian Wiskott-Aldrich syndrome protein (WASP). Mutation of WASP in humans causes Wiskott-Aldrich syndrome (WAS), which is characterised by severe immunodeficiency and defects in blood cell morphology (Symons et al., 1996, Kim et al., 2000). In budding yeast, Las17 is a component of actin cortical patches, where it co-localises and interacts with actin cortical proteins at the site of endocytosis (Madania et al., 1999; Li et al., 1997). Las17 is not an essential gene as its function can be compensated b other NPFs to activate Arp2/3 complex in vivo. However, *las17* deletion causes defects in budding and cytokinesis due to abnormal actin organisation (Li et al., 1997). *LAS17* deletion cells accumulate post-Golgi-like vesicles in the bud, and have defective fluid-phase endocytosis and actin patch polarisation (Li et al., 1997). This suggests that, Las17 plays a critical role in multiple cellular processes associated with the actin cytoskeleton in yeast.

Furthermore, data from synthetic lethal arrays showed second site mutations which make *LAS17* an essential gene. For example, combining *arp2* and *arp3* mutant alleles with *las17*Δ is synthetically lethal at 37˚C and the cells showed a depolarised actin organisation due to the loss of interactions with Arp2/3 (Madania et al., 1999; D'Agostino and Goode, 2005). The temperature sensitivity growth defects of *arp2* and *arp3* mutants can be suppressed by overexpression of Las17 which suggests that, Las17 is a key activator of the Arp2/3 corresponding to the functions of WASP in Arp2/3

complex activation (Madania et al., 1999).

Las17 shares several functional domains with human WASP, but Las17 lacks the GBD (containing the Cdc42 binding motif). The N-terminal of Las17 contains a WASP homology-1(WH2) domain, followed by a central Polyproline (PP) rich region, which contains several repeats of five prolines. The C-terminal contains a WASP homology-2 (WH2) domain, central (C) domain and terminates with an acidic (A) region (depicted figure 1.15.A). Recent proteomic studies have identified multiple phosphosites across the Las17 primary sequence, which are either threonine or serine residues (Holt et al., 2009; Smolka et al., 2007). These phosphoresidues are located at different regions along the primary sequence of Las17, but their functional relevance has not been studied yet.

The Las17WH1domain provides a binding site for the yeast homologue of mammalian WIP (Vrp1), which binds to the C-terminal of Las17. Vrp1 arrives after Las17 at cortical patches and forms a complex with Las17, and this complex is thought to be essential for Vrp1 function and localisation to the cortical patches (Naqvi et al., 1998; Rajmohan et al., 2006). Human WASP requires WIP to restore the temperature sensitive growth defects of *LAS17* knock out yeast cells (Rajmohan et al., 2006). However, the *WAS* mutations that are located within the WH1 of WASP (Imai et al., 1999), were unable to rescue the growth defects of *LAS17* deletion at high temperature. This effect could be due to perturbing the WIP-WASP complex caused by misssense mutant which results in WAS disease in human (Rajmohan et al., 2006).

Mapping the SH3 domain-mediated interactions in yeast using a combination of phage-display and yeast two hybrid analysis has identified a large number of interactions between multiple SH3 domain containing proteins with the PP region of Las17 (Tonikian et al., 2009). A recent study has shown that, Sla1 mediates an interaction with Las17 class1/2 polyproline motifs to form a stable complex (called SLAC). Disruption of the SLAC complex leads to defects in Las17 recruitment to the site of endocytosis in vivo. These results

were confirmed by pyrene actin assembly assays, which revealed that, the SLAC complex restore the ability of Las17 to promote actin polymerisation, and sub-micromolar concentrations of the first and second SH3 of Sla1 (0.1-0.3 µM) can negatively regulate Las17 activity potentially by a mechanism whereby the first and the second SH3 of Sla1 competes with actin monomers for binding to the actin binding site in Las17PP as suggested by Robertson *et al*., 2009 (Feliciano and De Pietro, 2012). Lsb7/Bzz1 is an SH3 domain containing protein that is dependent on Las17 for its localisation in vivo. Lsb7/Bzz1 was shown to interact with Las17PP through its SH3 domain and form part of the Las17-Vrp1-Myo5 complex in vitro, which suggests that Bzz1 is involved in regulating actin polymerisation (Soulard et al., 2005; Lechler et al., 2000; Tong et al., 2002). Bzz1 may release the inhibitory effect that results from the Sla1-Las17 interaction (Soulard et al., 2002).

Ysc84 and its related protein Lsb3 (Las seventeen binding 3) were shown to interact with Las17 by yeast two hybrid analysis (Madania et al., 1999). The N-terminal of Ysc84 was shown to interact with and bundle F-actin in vitro. However, full length Ysc84 did not show any binding to F-actin, suggesting possible binding with another protein that could alter the conformation of Ysc84 to expose its actin binding site. Thus, Las17PP (residues 300-422) was shown to interact directly with the full length Ysc84 in yeast two hybrid analysis, and shown to enhance the ability of Ysc84 to bind and bundle actin. These results clearly indicate that, Las17 could possibly serve as an activator for Ysc84. This poly-proline rich fragment of Las17 was also shown to bind to the SH3 domain of Lsb3, which could suggest overlapping functions of Ysc84 and Lsb3. The interaction of Las17 with Ysc84 to activate actin bundling suggests a distinct model of actin regulation via Las17 that is Arp2/3-independent (Robertson et al., 2009). Recent work by the Ayscough lab suggest that, there are novel actin binding sites in the Las17PP region, which are able to bind and nucleate G-actin independently of Las17WCA domain (Urbanek et al., 2013). These results suggest a mechanism of actin

,

polymerisation mediated by the Las17-Ysc84 interaction whereby, the actin monomer binding site of Las17PP delivers actin to Ysc84, which in turn generates bundles of F-actin that favour polymerisation in vitro. Rvs167 contains an SH3 domain that interacts with Las17PP in yeast two hybrid screens (Tong et al., 2002; Madania et al., 1999). Phosphorylation of Rvs167 was found to inhibit its interaction with Las17 in vitro (Friesen et al., 2003). This suggests that, the phosphorylated version of Rvs167 disassociates from Las17 and therefore activates the Arp2/3 complex for polymerisation (Friesen et al., 2003).

The C-terminal of Las17 contains a WCA domain (residues 547-633), which is responsible for its NPF activity. Biochemical studies using a permeabilized cell assay revealed severe defects in actin assembly associated with yeast cells lacking *LAS17* suggesting that, Las17 is required for actin assembly (Li et al., 1997). Both Las17 and the Arp2/3 complex localise at cortical patches, but Las17 is recruited at endocytic sites 10-15 seconds prior to Arp2/3 complex suggesting, an Arp2/3-independent function (Urbanek et al., 2012). Interaction of Las17 with G-actin and Arp2/3 complex enhances actin polymerisation in vitro (Winter et al., 1999; Li et al., 1997). However, deletion of *WH2* or *CA* domain of Las17 only displays a mild phenotype, and cells have normal actin organisation in vivo (Galletta et al., 2008; Sun et al., 2006). Mutations of the PP and WCA result in defects in endocytosis and growth, suggesting sequential functions of these two domains (Urbanek et al., 2012).

A.

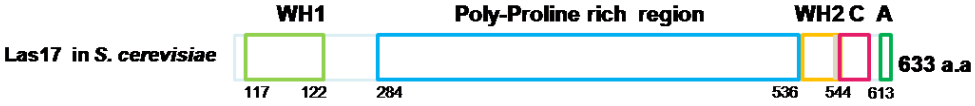


```
  1  MGLLNSSDKE  IIKRALPKAS  NKIIDVTVAR  LYIAYPDKNE  WQYTGLSGAL  ALVDDLVGNT
 61  FFLKLVDING  HRGVIWDQEL  YVNFEYYQDR  TFFHTFEMEE  CFAGLLFVDI  NEASHFLKRV
121  QKRERYANRK  TLLNKNAVAL  TKKVREEQKS  QVVHGPRGES  LIDNQRKRYN  YEDVDTIPTT
181  KHKAPPPPPP  TAETFDSDQT  SSFSDINSTT  ASAPTTPAPA  LPPASPEVRK  EETHPKHSLP
241  PLPNQFAPLP  DPPQHNSPPQ  NNAPSQPQSN  PFPFPIPEIP  STQSATNPFP  FPVPQQQFNQ
301  APSMGIPQQN  RPLPQLPNRN  NRPVPPPPPM  RTTTEGSGVR  LPAPPPPPRR  GPAPPPPPHR
361  HVTSNTLNSA  GGNSLLPQAT  GRRGPAPPPP  PRASRPTPNV  TMQQNPQQYN  NSNRPFGYQT
421  NSNMSSPPPP  PVTTFNTLTP  QMTAATGQPA  VPLPQNTQAP  SQATNVPVAP  PPPPASLGQS
481  QIPQSAPSAP  IPPTLPSTTS  AAPPPPPAFL  TQQPQSGGAP  APPPPPQMPA  TSTSGGGSFA
541  ETTGDAGRDA  LLASIRGAGG  IGALRKVDKS  QLDKPSVLLQ  EARGESASPP  AAAGNGGTPG
601  GPPASLADAL  AAALNKRKTK  VGAHDDMDNG  DDW
```

B.

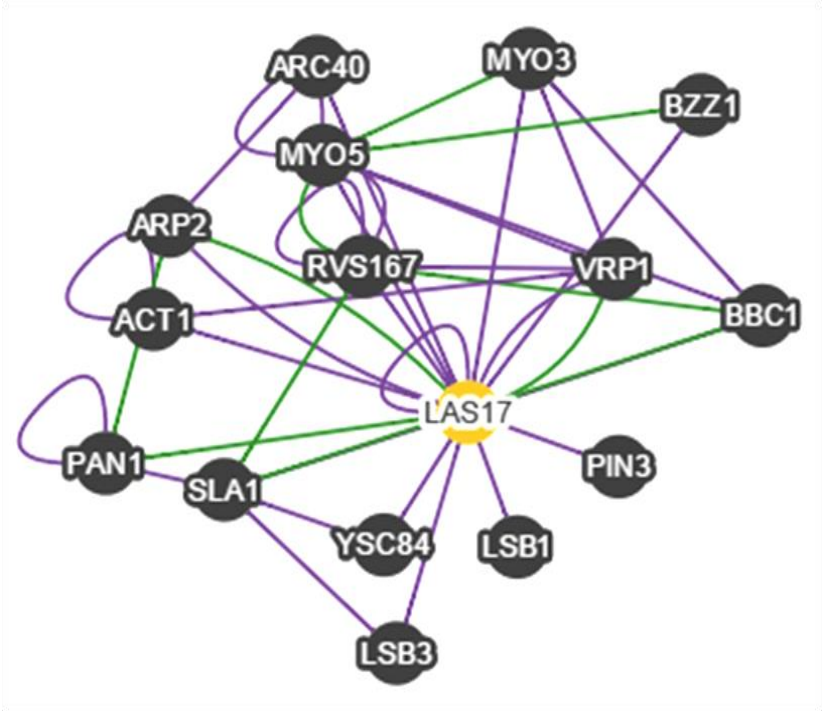

Figure 1.15: The WASP homologue Las17 in yeast

(A) Top panel: Schematic diagram of the domain structure of Las17. Bottom panel: Las17 protein sequence showing the phosphorylation sites (labelled in red), obtained from PhosphoGrid search.

(B) The Las17 interaction network. The diagram displays physical interactions (purple lines) and genetic interactions (green lines) between Las17 (yellow circle), and its interactors (dark circles). This network is based on experimental data that support these interactions. Obtained from: *Saccharomyces* genome database (http://www.yeastgenome.org/)

1.9 Roles of Las17 in endocytosis

Little is known about the regulation of Las17 during endocytosis but in vivo and in vitro studies have indicated that Las17 play distinct roles at different stages of endocytosis. Reconstitution of actin patch using Las17 functionalised beads identified over 30 proteins that are recruited at the same time or later than Las17 arrival. These observations demonstrates the central role of Las17 in formation of the actin patch structure, and may also trigger recruitment of several proteins that are associated with the formation of the actin network in the endocytic actin-patch (Michelot et al., 2010). Regulation of Las17 activity by its interactions with various endocytic proteins is depicted in figure 1.15.B.

Las17 arrives at early stage of endocytosis but it remains inactive due to binding to Sla1 and Bbc1. Syp1 protein can also negatively regulate Las17 activity in vitro, and it was proposed to function with Sla1 to keep Las7 inactive during the non-motile stage of endocytosis (Boettner et al., 2009). Las17 is considered to be the primary NPF that enhances Arp2/3-mediated actin polymerisation, which is the critical step for driving invagination of the membrane. Bzz1 arrives before the onset of membrane invagination and may release the inhibition from Las17 (Sun et al., 2006). Once the membrane invaginates, Las17 moves inward with the invaginated vesicle which is consistent with actin assembly taking place with the barbed ends oriented towards the invaginated vesicle (Idrissi et al., 2008; Galletta et al., 2008). However, regulation of the Arp2/3 complex during endocytosis is not clear, but it is proposed that the presence of pre-formed F-actin might trigger the activity of Arp2/3 complex for branching. This theory was confirmed in vitro using Las17-coated beads which provide F-actin seeds to initiate polymerisation of F-actin branching by the Arp2/3 complex (Michelot et al., 2010). On the other hand, the role of Las17 in post-scission vesicle movement is not obvious but, Las17PP was shown to mediate interaction with the SH3 domain of Rvs167. The yeast Amphiphysin (Rvs167) contains a

Bar domain which is important for connecting the membrane with the actin cytoskeleton to mediate membrane bending during scission (Friesen et al., 2003). Las17 was also observed at the scission site 100 nm away from the invaginated membrane, which could indicate that another possible role of Las17 is to couple actin dynamics to the vesicle after scission (Idrissi et al., 2008).

1.10 Summary

Actin cytoskeleton is essential to regulate various process in the cells such as cell motility, membrane trafficking and endocytosis. These cellular processes are driven by the continuous actin filament turnover which must be performed at correct time at specific sites. Polymerisation of actin is modulated by several actin binding proteins (ABPs), that are able to bind either actin monomers (G-actin) or polymer (F-actin), or both. Assembly and disassembly of ABPs at the regions whereby actin turnover is active, is controlled by signal transductions.

The fundamental requirement for actin in yeast endocytosis is more evident, whereas actin appears to be less critical in mammalian cell endocytosis. Over 60 different proteins in yeast endocytosis were found to have homologues in mammals, these proteins can interact and interplay spatially and temporally to produce distinct stages in the process. The endocytic stages include arrival of proteins that are needed for early coat assembly, late coat, membrane invagination, and membrane uncoating and vesicle scission. Actin polymerisation seems to be essential to generate a force required to drive membrane invagination into the cell against turgor pressure and also have a role in vesicle secession.

The main focus of this study is studying the actin regulatory function of Las17 in yeast. Las17 was shown to be important for regulation of actin polymerisation at the endocytic patches which binds and cooperates with the Arp2/3 complex to modulate the formation of branched-F-actin. In addition, Las17 can also nucleate actin and seeding filaments independently of the

Arp2/3 complex suggesting a second actin-regulatory function of Las17. Several phosphorylation sites have been discovered along Las17 sequence but their functional significance is not clear. Las17 lacks the GTPase binding domain, therefore it was suggested to be regulated similarly to Scar/WAVE family.

1.11 Aims of the project

At the outset of this project Las17 was shown to be a key activator of the Arp2/3 complex, and several Las17 binding partners were shown to be required for Las17 function during endocytosis. Regulation of Las17 by post-translational modifications such as phosphorylation had not been addressed. The major aims of this study were to:

- Investigate whether phosphorylation regulates Las17 function in vivo.
- Determine the effect of phosphomutants of Las17 on G-actin and Arp2/3 complex binding in vitro.
- Test the possibility that, Las17 can undergo intramolecular binding to regulate its activation using in vitro approaches.
- Define the phosphorylation species of recombinant Las17 using a western blot approach.
- Identify further phosphorylation sites and investigate phenotypic consequences of their mutation in vivo.

Chapter 2:

Materials and Methods

Chapter: 2

2.1 Materials

Chemicals used in this study come from Sigma, BDH, Fisher, Fluka, unless otherwise stated.

2.2 Yeast strains, plasmids, oligonucleotides, and antibodies

All yeast strains, plasmids, and oligonucleotides and antibodies generated and used during the research of this study are listed in tables 2.2.1, 2.2.2, 2.2.3, and 2.2.4 respectively.

Table 2.2.1 Yeast Strains

KAY	Genotype	Origin
30	Mat a, hisΔ	D. Drubin lab
31	Mat α, hisΔ	D. Drubin lab
289	Mat a,ura3-52,leu2-3,112,hisΔ200,trp1-1,lys2-801	Dewar et al., 2002
376	Mat a, ura3-52,leu2-3,112,his3,lys2,ark1::HIS	D. Drubin lab
380	Mat a, ura3-52,leu2-3-112,his3,lys2-801,prk1::LEU	D. Drubin lab
389	Mat a,Ura3-52,leu2-3,112,his3,trp1-1,lys2-801	Dewar et al., 2002
452	Mat a/α, Δlas17::KanMx/LAS17, ura3Δ/ura3Δ,his3Δ/hisΔ,leu2Δ/leu2Δ,met15Δ/met15Δ,lys2Δ/lys2Δ	Research genetics
446	Mat a, hisΔ1, leu2Δ, ura3Δ	Research genetics
472	Mat a, hisΔ1, leu2Δ, ura3Δ, las17Δ::KanMx	This study
473	Mat α, hisΔ1, leu2Δ, ura3Δ, las17Δ::KanMx	This study
480	Mata/α,ura3Δ/ura3Δ,his3Δ/hisΔ,leu2Δ/leu2Δ,met15Δ/met15Δ,lys2Δ/lys2Δ	Research genetics
711	pJ694, Mat a	P. Piper
712	pJ694α	P. Piper
1544	Mata, ura3Δ,his3Δ,leu2Δ,met15Δ,yck1::KanMx	Ayscough
1061	Mat a, Sla1-GFP::TRP	Ayscough
1644	KAY1061, Sla1-GFP::TRP, Las17::URA	Ayscough
1668	LRB758 wt, Mat a, his3,leu2,ura3-52	Ayscough
1670	LRB1517 yck1::KanMx, Mat a his3, leu2, ura3-25	Ayscough
1675	KAY446 +Las17-7xAla-3x HA::HIS	Ayscough
1676	KAY1668+Las17-7xAla-3xHA::HIS	Ayscough
1685	ΔPho85	ThermoFisher, Fermentos Ltd.

Table 2.2.2 Plasmids

Plasmid	Construction	Origin/ Reference
pKA40	MCS-3xHA- term; LEU cen.	Gift from E. Hettma
pKA 61	pRS313 HIS,CEN	Sikorski and Hieter,1989
pKA 64	pRS306 URA,CEN	Ayscough
pKA 168	pGBDU-C1, URA, CEN, empty binding domain	James et al.,1996
pKA 162	pGAD-C1,LEU,CEN,empty activation domain	James et al., 1996
pKA 260	pKA170 (pGBD) + sla1 SHD1+SHD2 2 hybrid bait	Dewar et al., 2002
pKA 263	pDW104 (pGAD) + LSB5 fragment	Dewar et al., 2002
pKA 325	pGAD- Las17 (292-536aa)	(Costa and Ayscough, 2005)
pKA 417	pGEX6P1 (GST fusion plasmid)	GE Healthcare
pKA 528	pKA527 with HA replaced by GFP from pKA525 LEU	Lab collection
pKA 475	pSM1023 4xGFP::KanMx	Lab collection
pKA 606	LAS17 (400bp 5', 246bp 3') in pKA61 HIS CEN	Urbanek et al,. 2013
pKA 607	Las17-GFP ,LEU in pKA528 (pEW416,pTpi – GFP)	Smith and Ayscough,2009
pKA670	pGEX6P1 + Las17 (300-aa end)	Urbanek et al., 2012
pKA 671	pGEX6P1 + Las17 (300-633aa end)	Urbanek et al., 2013
pKA 525	pAS52 * GFP	Lab collection
pKA 527	pEW416* pTpi - mcs - 3xHA LEU	Lab collection
pKA 872	pKA 606 –Las17S586A	This study
pKA 873	pKA 606 –Las17S586D	This study
pKA 874	pKA 606 –Las17S588A	This study
pKA 875	pKA 606 –Las17S588D	This study
pKA 876	pKA 607 –Las17S586A	This study
pKA 877	pKA 607 –Las17S586D	This study
pKA 878	pKA 607 –Las17S588A	This study
pKA 879	pKA 607 –Las17S588D	This study
pKA 895	pKA 607 –Las17SS586.588,AA	This study
pKA 896	pKA607 –Las17SS586.588,DD	This study
pKA 898	pKA 606–Las17SS586.588,AA	This study
pKA 899	pKA606–Las17SS586.588,DD	This study
pKA 900	pKA 606 –Las17T380A	This study
pKA 901	pKA606 –Las17T380D	This study
pKA 1013	pGEX6P-1+Las17WCA	This study
pKA 1014	pKA168 pGBDU-C1+Las17WCA	This study
pKA 979	pRS306: LAS17 (400bp 5' 246bp 3') in URA CEN	This study
pKA 980	pRS306: LAS17 S588A (400bp 5' 246bp 3') in URA CEN	This study
pKA 981	pRS306: LAS17 S588D (400bp 5' 246bp 3') in URA CEN	This study
pKA 1036	pEH039 MCS-3xHA-PGKterm, URA CEN	This study
pKA 1037	pEH040 MCS-3xHA-PGKterm, LEU CEN	This study

Plasmid	Construction	Origin/ Reference
pKA1043	pKA671 mutant) pGEX6P1+Las17(300-633aa end) S588A	This study
pKA1044	(pKA671 mutant) pGEX6P1+Las17(300-633aa end) S588D	This study
pKA1054	pLAS17-LAS17-3xHA (LAS17 FL+400bp promoter in pKA1037); LEU, CEN	This study
pKA1056	pGAD-C1(pKA162)+Las17 WCA domain; LEU, CEN	This study
pKA1057	pGBD (pKA168) + Las17 PP domain	This study
pKA1059	pGEX6P1+Las17WCA S588A	This study
pKA1060	pGEX6P1+Las17WCA S588D	This study
pKA1083	pKA1054 –Las17T380A	This study
pKA1084	pKA1054 –Las17T380D	This study
pKA1085	pKA1054 –Las17S588A	This study
pKA1086	pKA1054 –Las17S588D	This study
pKA1087	pKA 606 –Las17S554A	This study
pKA1088	pKA 606 –Las17S554D	This study
pKA1089	pKA1054 –Las17S554A	This study
pKA1090	pKA1054 –Las17S554D	This study
pKA1091	pKA 606 –Las17T543A	This study

Table 2.2.3 Oligonucleotides

OKA	5' to 3' Sequence	Description
1116	CTCCTTCCACAGGCCCATGGAAGAAGAGGGCC	Las17T380D_forward
1117	GGCCCTCTTCTTCCATGGGCCTGTGGAAGGAG	Las17T380D_reverse
1065	CAGGAAGCACTGGAGAAGCTGCTGCACC	Las17586,588A_forward
1066	GGTGCAGCAGCTTCTCCACGTGCTTCCTG	Las17586,588A_reverse
1067	GCAGGAAGCCGTGGAGAAGATGCTGATCCACCAG	Las17586,588D_forward
1068	CTGGTGGATCAGCATCTTCTCCACGTGCTTCCTGC	Las17586,588D_reverse
542	TGAATACGTGCGAGACGTCC	Las17check_forward
543	TCACTACCGCCTTTGAACC	Las17check_reverse
766	GATGGATCCGCTCCTTCAATGGGCATA	Las17primer5nt900 BamH1
784	GCTGCTGTCGACCCAATCATCACCATTGTCC	Las17FLno stop codon _reverse`
785	GCTGCTGGATCCTAACGCCGGCTGACGTGGACG	Las17cloning_at389 5`+BamH1
789	CAATTCGACAACAGCATCCG	Las17check_5` 618 to 637 3`
790	CCACCTCCTCCAAGAGCATC	Las17check_5` 1162 to 1181 3`
798	GCCTTATGXTTTGTAGTTGG	Las17check_3`1162 to 1181 5`
928	GATGTCGACTTAGCCTCCGGATGTTGATG	Las17cloning at 536 3`+Sal1
1034	GCACGTGGAGAATCTGCTGATCCACCAGCAGCGGC	Las17S588D_forward

OKA	5' to 3' Sequence	Description
1036	GTGGAGAATCTGCTGCACCACCAGCAGCG	Las17S588A_forward
1037	CGCTGCTGGTGGTGGTGCAGCAGATTCTCCAC	Las17S588A_reverse
1061	TCCTTCCACAGGCCGCTGGAAGAAGAGGG	Las17T380A_forward
1062	CCCTCTTCTTCCAGCGGCCTGTGGAAGGA	Las17T380A_reverse
1118	GGCTCGACTATACATTGCATCTC	Las17check_forward
1119	CCTGCAAAGCATTCTTCCATCTC	Las17check_reverse
1120	GTGGTGCAGCACTCGTCGTCG	Las17check_reverse
1264	ACCTGCCCCTCTAATTGCAGCTAAAAGTGCATCAC	Las17S544A_forward
1265	GTGATGCACTTTTAGCTGCAATTAGAGGGGCAGGT	Las17S544A_reverse
1266	GCCACCTGCCCCTCTAATATCAGCTAAAAGTGCATCACGACC	Las17S544D_forward
1267	GGTCGTGATGCACTTTTAGCTGATATTAGAGGGGCAGGTGGC	Las17S544D_reverse
1272	ACGCCTGCATCTCCAGCAGTTTCAGCGAATGAAC	Las17T543A_forward
1273	GTTCATTCGCTGAAACTGCTGGAGATGCAGGTCGT	Las17T543A_reverse
1274	GAGGCGGTTCATTCGCTGAAACTGATGGAGATGCAGG	Las17T543D_forward
1275	CCTGCATCTCCATCAGTTTCAGCGAATGAACCGCCTC	Las17T543D_reverse
1183	CGCGGATCCCCAGCTACATCAACATCCGG	Las17BamH1_P529_for
1184	GCCGACGTCGACTTACCAATCATCACCATTGTCC	Las17stop_Sal1_reverse

Table 2..2.4 Antibodies

Application	Raised in	Dilution Factor	Source
Anti –GFP monoclonal antibodies western	mouse	1:5000	Roche
anti-HA polyclonal antibody (Agarose conjugate) immunoprecipitation	Goat	20-40 µl of gel slurry per 0.1-1mg protein lysate	abcam®
anti rat-HA α primary antibodies(western)	Mouse	1:1000	Roche
Anti rat - alkaline phosphatase, secondary antibodies (western)	Rabbit	1:30000	Sigma

2.3 Molecular Biology Techniques

2.3.1 DNA plasmid mini prep

Isolation of plasmid DNA from bacterial lysates was carried out using Bioline-isolate™ plasmid mini kit. All the steps were performed according to the manufacturer instructions. The protocol was based on alkaline lysis of bacterial cells, followed by neutralization of the lysate and adsorption of the DNA onto silica membrane. The DNA was then washed with a buffer containing ethanol and eluted using 40 µl distilled water.

2.3.2 DNA Agarose Gel Electrophoresis

DNA samples were separated and visualized using flat bed agarose gel electrophoresis. The agarose gel was made by melting 0.8% agarose in TAE buffer (10 mM Tris-HCl pH7.5, 1Mm EDTA pH7.5), 5 µl of a 5 mg/ml stock ethidium bromide (BioRad) was added per 50 ml of agarose solution. The solution was then poured into a casting tray containing a comb with the required number of teeth. To visualise DNA during and after electrophoresis, DNA samples were mixed with 6x gel loading buffer (0.25% Bromophenol blue, 0.25% Xylenecynol FF, 30% glycerol). Once the gel had solidified, the samples were loaded into the wells and then electrophoresed in 1x TAE buffer at 80-120 volts. Ethidium bromide stained DNA were visualised under UV transilluminator.

2.3.3 DNA Extraction from Agarose Gel

Extraction of DNA from agarose gel was performed using Qiagen plasmid purification kit. The DNA fragment was excised from the agarose gel using a clean scalpel, and transferred into 1.5 ml tube. Three volumes of QG buffer was added to one volume of the gel slice, followed by incubation of the tube in bloke heating at 95˚C for 10 minutes in order to solubilise the agarose. The sample was then applied to QIAGEN column, and centrifuged at 13000 rpm for 30 seconds. The supernatant was carefully removed with a pipette, and column was washed with AP buffer, and then with buffer containing ethanol. The DNA was eluted with 30 µl distilled water.

2.3.4 DNA Restriction digestion

All restriction enzymes used in this study were from New England Biolabs unless otherwise mentioned. The digest was carried out as stated in the manufacturer instructions using the supplied buffers. Single or double digests of a DNA plasmid was performed using 2-10U of enzyme per reaction and this was dependent on the enzyme activity. 1x BSA and distilled water was added to make up an appropriate final volume. The digestion reaction was incubated at 37˚C for 1-2 hours. The DNA digest was run on 0.8% agarose gel in order to visualise the desired DNA fragments digests.

2.3.5 DNA Cloning

DNA ligation was performed using the Quick ligation™ kit from New England Biolab. Linearised vector was combined with three fold molar excess of linear insert in 10 µl final volume. 10 µl of 2x Quick ligation buffer was added along with 1 µl of T4 DNA ligase as stated in manufacturer instructions. The reaction sample was mixed thoroughly and then incubated at 25˚C for 5 minutes. 2 µl of ligation mix was transformed into ultracompetent XL10 Gold *E. coli* cells from Stratagene (see section 2.4.4).

2.3.6 Site directed mutagenesis of plasmid DNA using QuikChange® lightning site directed mutagenesis kit (Stratagene).

This method was used to generate Las17 phosphomutants in plasmids carrying either the full or truncations of *LAS17* gene. Site directed mutagenesis was performed as stated in the manufacturer instructions. Forward and reverse complementary oligonucleotides containing the desired mutation were designed using the QuickChange® Prime Design software.

PCR reactions were set up as below using the reagents provided with the kit:

10x reaction buffer	5 µl
5` primers (100 ng/µl)	1.25 µl
3` primers (100 ng/µl)	1.25 µl
dNTP's mix	1 µl
Quick solution reagent	1.5 µl
ddH_2O	39.5 µl
Quick Change Lightning polymerase	1 µl

Cycling Parameters:

Cycle	Temperature	Time
1	95˚C	2 min
18	95˚C	20 sec
	60˚C	10 sec
	68˚C	30 sec/kb of plasmid length
1	68˚C	5 min

The resulting PCR product was treated with 2 ul Dpn1 restriction enzyme (100U/µl) provided with Stratagene kit. This step was crucial to digest the parental methylated and hemiethylated DNA. The digest was incubated at 37˚C for 5 min, and then transformed into XL10-Gold ultracompetent cells from Stratagene (see section 2.4.4). The DNA was mini prepped and sent to be verified by sequencing.

2.3.7 Amplification of DNA using polymerase chain reaction (PCR)

2.3.7.1 Generation of DNA for genome integration, tagging, or deletion

This system was adopted from Longtine *et al*., 1998. The protocol was used to allow DNA plasmid carrying a cassette designed for deletion or tagging of gene within the yeast genome using specific oligonucleotide primers. These primers are complementary to the regions flanking the sequence of interest.

For each PCR reaction the following elements were mixed in 0.5 ml thin-walled PCR tubes. A 'hot start' reaction was required in which the Taq-polymerase was added immediately as the reaction mix had reached 94°C.

10x*Taq* reaction buffer	10 µl
$MgCl_2$ (50 mM stock)	4 µl
dNTP's mix(25 mM)	0.8 µl
5′ primer (100 ng/µl)	1 µl
3′ primer (100 ng/µl)	1 µl
DNA plasmid (1:10)	2 µl
Taq polymerase (5 U/µl)	0.4 µl
ddH_2O	80.8 µl

A 30 cycles of amplification was occurred in a MWG Biotech Primus PCR machine as follow:

Cycle	Temperature	Time
Initial denaturation	94 ºC	3 min
30x cycle	94 ºC	1 min
	55 ºC (Tm -5 ºC; if Tm of two primers are different use Tm -5 ºC of lower)	1 min
	72 ºC	1 min/kb of plasmid length+ extra 30 sec
Final extension	72 ºC	10 min
hold	4 ºC	10 min

The final PCR product was checked by running on 0.8% agarose gel electrophoresis. The amplified DNA was transformed into yeast cells allowing its incorporation into specific site in the yeast genome by homologous recombination. The grown colonies were then screened using colony PCR (see section 2.3.8).

2.3.7.2 Introducing or deletion restriction sites

Phusion ® Master Mix with high fidelity buffer (Bioline) was used to remove stop codon from 5′ to 3′ coding sequence of *LAS17* under its own promoter. Instead, the *SAL1* restriction site was inserted for cloning purposes.

50 µl PCR reactions were set up as follow:

Phusion Master mix	25 µl
5′ primer (100 ng/µl)	1.25 µl
3′ primer (100 ng/µl)	1.25 µl
Template DNA	0.5 µl
ddH_2O	22 µl

Two steps of annealing were used as both forward and reverse primers have melting temperature (Tm) of 72˚C and 71.8 ˚C respectively, thus annealing temperature for PCR reaction was set up at ≥72 ˚C.

Cycling condition for a routine PCR was as follow:

Cycle	Temperature	Time
Initial denaturation	98˚C	30 second
25-35 cycle	98˚C 45-72˚C	10 seconds 15-30 seconds per Kb
Final extension	72˚C	10 minutes
hold	4˚C	Hold

2.3.8 Screening for integration or deletion yeast strains by colony PCR

The grown colonies were struck onto appropriate agar plate, and then incubated at 30˚C (25˚C for *las17*Δ strain) overnight. Using a yellow tip, a small amount of freshly growing cells was transferred into 1.5 ml tube containing 20 mM NaOH. The cell suspension was mixed and boiled at 100˚C for 15 minutes. 2.5 µl of DNA genomic suspension was used as a template in standard PCR using primers designed to the regions flanking the insert region.

25 µl PCR reaction mix was set up as follow:

10x*Taq* reaction buffer	2.5 µl
$MgCl_2$ (50 mM stock)	1 µl
dNTP's mix (25 mM)	0.2 µl
5′ primer (100 ng/µl)	0.5 µl
3′ primer (100 ng/µl)	0.5 µl
Taq polymerase (5U/µl)	0.2 µl
ddH_2O	17.6 µl

Standard PCR cycle was employed as described in section 2.3.7.1, and the resulting products were electrophoresed in a 0.8% agarose. Yeast genomic DNA was used as a control in the PCR reaction.

2.3.9 PCR clean-up

To remove the contaminated materials from the PCR sample, QIAquick PCR purification kit to obtain a concentration of10 µg DNA. This method is based on assembly of DNA fragment into a silica membrane followed by several washing and elution steps with the buffers provided with the kit. Binding buffer containing pH indicator was applied directly to PCR sample so, if the sample had an increase in its pH the colour turns violet. In this case, 10 µl of 3 M sodium acetate was added to reverse the colour into a yellow indicating that, PCR sample at pH≤7.5 and this is the optimal pH for DNA binding to the membrane. To bind DNA, the samples were applied to QIAquick spin column and centrifuged at 13.000 rpm for 30-60 seconds. The column was washed with 750 µl PE buffer, and the DNA was eluted with distilled water. The final volume of the elution is dependent on the desired concentration of the PCR product.

2.4 Bacterial Methods

2.4.1 Bacterial growth media

The following media were used for the growth and maintenance of various *E. coli* strains that are used throughout this study.

2YT	1.6% tryptone
	1% yeast extract
	0.5% NaCl

and 2% agar for solid media.

NZY$^+$ broth	1% NZ amine (casein hydrolysate)
	0.5% yeast extract
	0.5% NaCl

The media was brought to pH 7.5 with NaOH and then autoclaved. Prior to use, the following supplements were added: 12.5 µM $MgCl_2$, 12 µM $MgSO_4$ and 0.4% glucose.

All media prepared for growth of *E. coli* strains transformed with a plasmid conferring antibiotic resistance. Ampicillin was added to the media as required to a final concentration of a 100 µg/ml. Liquid cultures were grown at 37˚C in an orbital shaking incubator (Certomat BD-1, B. Brown Biotech), whereas agar plates were grown at 37˚C Bider APT incubator.

2.4.2 Preparation of Calcium competent DH5α and BL- 21 bacterial cells

An overnight bacterial culture was diluted into 100 ml of 2x YT medium ,and incubated at 37ºC with shaking until OD_{600} = 0.5 to 0.6. Cell culture was divided into two Falcon tubes and cooled on ice for 10 minutes. The tubes were then centrifuged at 2,500 rpm for 5 minutes at 4˚C. Supernatant of each culture was discarded whilst the pellet was resuspended in 50 ml pre-

chilled 100 mM$CaCl_2$, and kept on ice for 30 minutes. After incubation, the cells were harvested as above, and the pellet of the tubes were combined and resuspended in 5 ml of pre-chilled 100 mM CaCl2 and 15% Glycerol. The suspension was aliquoted in 100 µl volume into 1.5 ml tubes and snap freezing in liquid Nitrogen. The tubes were then stored at –80°C until required.

2.4.3 Transformation of Calcium competent DH5α and BL-21(DE3) cells

Pre-prepared bacterial competent cells (see section 2.4.2) were thawed on ice for 2 minutes. 2 µl of DNA plasmid was added to the cells, mixed gently, and then incubated on ice for 30 minutes. After incubation, the cells were heat chocked at 42 ºC in water bath for 90 seconds, and then cooled on ice for 2 minutes. 500 µl of 2x YT media was added and cultured at 37˚C with shaking for an hour. The cells were centrifuged at 10.000 rpm for 1 minute, and the media was discarded while the pellet was resuspended in 150 µl 2xYT. This was spread onto 2x YT agar plate containing Ampicillin, which then incubated at 37 ˚C overnight.

2.4.4 Transformation of XL10- Gold Ultracompetent cells

The protocol used was based on manufacturer instructions (Stratagene). The XL10-Gold ultracompetent cells were thawed on ice and 1 µl of β-mercaptoethanol provided with the cells was added into 22.5 µl aliquots and incubated on ice for 2 minutes. 2 µl of DpnI treated DNA (see section 2.3.6) was added to the ultracompetent cells, the mixture was mixed gently and placed on ice for at least 10 minutes. Cells were then heat shocked at 42 °C in water bath for 30 seconds and then incubated on ice for 2 minutes.500 µl of pre-heated NZY+ broth medium was added to the cells and incubated at 37°C for 1 hour with shacking (225 rpm). The transformation reaction was then plated onto 2xYT + Amp plate and incubated at 37°C overnight. The grown Colonies were inoculated onto 5 ml of 2xYT + Amp and incubated overnight at 37°C. Overnight grown transformants was DNA isolated (see section 2.3.1) and then sent for sequencing.

2.4.5 Glycerol stock of bacterial cells

For long term storage of bacteria, 1ml culture was mixed with 1ml 50% sterile glycerol in a cryovial and then stored at –80°C freezer.

2.5 Yeast methods

2.5.1 Yeast Growth Media

The following media were used for the growth and maintenance of *S. Cerevisiae* strains used throughout this study.

YPD	1 % yeast extract (Difco)
	2 % peptone (Difco)
	0.02 % adenine (Sigma)
	For solid media, supplement with 2 % agar (Difco).

Synthetic “drop out” is a minimal SD medium, was used as a selective media for growing yeast cells to verify the auxotrophic phenotypes. To select for a plasmid carrying a gene marked with auxotrophic marker, the relevant supplement was omitted from the media (i.e. dropped out) except those required for the auxotrophic plasmid’s selection. The relevant drop out mix was used following manufacturer’s instructions (Formedium, Norwich, UK).

Drop-out media	0.67 % nitrogen base without amino acids (Difco)
	Drop-out mix (added as directed)
	For solid media, supplement with 2 % agar
Sporulation media	1% potassium acetate
	2% agar

Carbon Source:

YPD and drop-out media were routinely supplemented with 40 % glucose (Dextrose) to 2 % final concentration.

2.5.2 Crossing of two haploid *S. cerevisiae* strains

Small amount of freshly grown MAT a yeast strain were placed on top of an equal amount of MAT α strain on a fresh YPD plate, and then grown at 30 ˚C for 5 hours. Cells were then struck onto selective media that would allow the growth of diploids.

2.5.3 Sporulation and tetrad dissection of diploids on solid media

Tow strains of opposite mating type were grown overnight and then mated as described in section 2.5.2. Diploid strain to be sporulated was grown onto YPD plate overnight at 30˚C. Cells was patched onto sporulation plate and left on bench for up to 5 days. The plate was monitored daily to check for development of four-spored asci. Once four-spored asci had begun to develop, each asci was picked using a tooth pick, and resuspended in 100 µl sterile ice-cold 0.1M Potassium phosphate buffer (pH 7.4). Cells were kept on ice for 30 minutes and then spun down at 3000 rpm for 3 minutes (Boeco C-25) with the pellet being resuspended with 75 µl sterile ice-cold 0.1M Potassium phosphate supplemented with 0.5 mg/ml-100T zymolyase (ICN Biomedical). The cells were mixed and incubated at 37 ˚C for 4 minutes and then kept back to ice. Cells were diluted with 500 µl of potassium phosphate buffer and streaked on YPD plate. Tetrads were isolated using a Singer micromanipulator and dissected into rows of four spores on YPD plate using the X and Y coordinates. The plate was then incubated at 30˚C until the spores had germinated and became visible. The number of viable spores was noted and they were patched onto YPD or selective plates to test for genetic markers.

2.5.4 Determination of Yeast cell Mating Type

To determine mating type of the yeast cells, tester mating type strains (KAY30 and KAY31) were struck horizontally across *his*- plate. Each colony of unknown mating type was crossed vertically onto each tester mating type strain. The plate was then incubated overnight at 30˚C or 25˚C for the *LAS17* deletion strain, with only the cells having mated being able to grow on the plates.

2.5.5 Yeast Transformation

2.5.5.1One step transformation method, (Chen *et al*., 1992)

A 5 ml of overnight cell culture was refreshed by inoculation of 250 µl cells into 5 ml liquid media and then grown until OD_{600} = 0.6. Cells were harvested by centrifugation at 3000 rpm for 3 min, and resuspended with100 µl ONE-STEP buffer containing 0.2 M Lithium Acetate, 40% PEG 3350, pH 5.0, and 100 mM DTT. 5 µl (50 µg) of pre-boiled single stranded herring sperm (DNAssd), and 0.5-1 µl DNA plasmid were added. The tube was mixed briefly by vortexing and then incubated at 45˚C in water bath for 30 minutes. Cells were plated onto an appropriate selective agar plate and incubated at 30˚C for 48 hours. This method is inappropriate for transformation of temperature sensitive (ts) yeast strains instead, high efficiency LiAc method was undertaken (section 2.5.5.2).

2.5.5.2 High Efficiency Lithium Acetate method

Modified method from Gietz and Schiestl (2007)

An overnight culture was refreshed into 5 ml of YPD medium and grown at 30˚C until OD_{600} reached 0.5-0.6. The cells were harvested by centrifugation at 3000 rpm for 5 minutes, media was discarded while cell pellet was washed once with 5 ml 1X TE buffer ,and then once with 5 ml of 1X Lithium Acetate in 1X TE buffer. The cell pellet was resuspended in 100 µl 1X Lithium Acetate in 1X TE buffer, and then 1 µl DNA plasmid (20 µl DNA cassette was added for mutants integration or gene deletion in yeast genome), 15 µl ssDNA were added respectively to the cells. The cells were mixed and 700 µl of 40 % PEG in 1X Lithium Acetate in TE buffer was added, followed by incubation at 30˚C with shaking for 1hour. The cells were pelleted after being spun down at 3000 rpm for 5 minutes, buffer was discarded, and cells were resuspended in 150 µl SD media as required. Cells were placed on an appropriate agar plate containing appropriate drop out medium and then incubated at 30˚C until the colonies had begun to appear.

2.5.6 Temperature sensitivity of yeast cells on solid growth media

An overnight culture was diluted to 0.5 unites (U) with an appropriate synthetic medium, cells were1:10 serially diluted and 3 µl of each cell culture was spotted onto SD agar plates using multi-pipette. Plates were placed on bench to let dry and then incubated at either 30˚C or 37˚C for 48 hours. Temperature sensitivity phenotype had been characterised for the strains that were unable to grow at 37˚C.

2.5.7 Yeast cells growth rate measurement

To determine the doubling time of yeast strains, cells were grown overnight to stationary phase in synthetic medium. The OD_{600} was recorded for each cell culture which had being diluted to OD_{600}= 0.2 with fresh medium and then grown at 30˚C with shaking. The DD_{600} was measured over 6 hour using Camspec–M501 Single Beam Scanning UV/Visible Spectrophotometer.

2.5.8 β-galactosidase liquid assay of yeast (Kaisar et al., 1994)

This assay is modified method from Guarente. (1983)

Diploids carrying both Gal4-activation domain and Gal4-binding domain were grown overnight and refreshed next day by inoculation of 250 µl cells into 5 ml SD media. Cells were grown until OD_{600}= 0.5, and then harvested by centrifugation at 2000 rpm for 5 minutes. The supernatant was discarded and the pellet cell was resuspended in 1ml Z buffer. In the fume hood, three drops of chloroform and two drops of 1%SDS were added to the resuspended cells using glass pipette and then the cells were vortexed at top speed for 1 minute. The samples were incubated for 5 minutes at 28 ˚C and prior to addition of 0.2 ml o-nitrophenyl-β-D-galactoside (OPNG). Once OPNG added, the time was recorded until the samples had acquired pale yellow colour. At this stage, the reaction was stopped by adding 0.5 ml Na_2CO_3 stock solution; samples were centrifuged at 3000 rpm for 10 minutes in order to remove the cell debris. Cell pellet was discarded and OD_{420} of the supernatant was measured. β-galactosidase units were calculated using the following formula:

$$\text{β-galactosidase activity} = \frac{OD_{240}}{OD_{600} \text{ of assayed culture x volume assayed x time}}$$

OD_{240} is the optical density of the *o*-nitrophenol product.OD_{600} is the optical density of the culture at the time of assay. Volume is the amount of the culture used in the assay in ml. Time is in minutes.

Z buffer (Miller, 1972); per 100 ml:

- 1.61g $Na_2HPO_4.7H_2O$
- 0.55 g $NaH_2PO_4.H_2O$
- 0.075 KCl
- 25 mg $MgSO_4.7H_2O$
- 270 µl β-mercaptoethanol

The principal of the two hybrid assay is displayed below in figure 2.1.

2.5.9 Glycerol Stock of yeast cells

For long term storage 15% mixture of 750 µl yeast culture and 750 µl of 50% sterile glycerol was mixed in a cryovial tube and then stored at –80˚C.

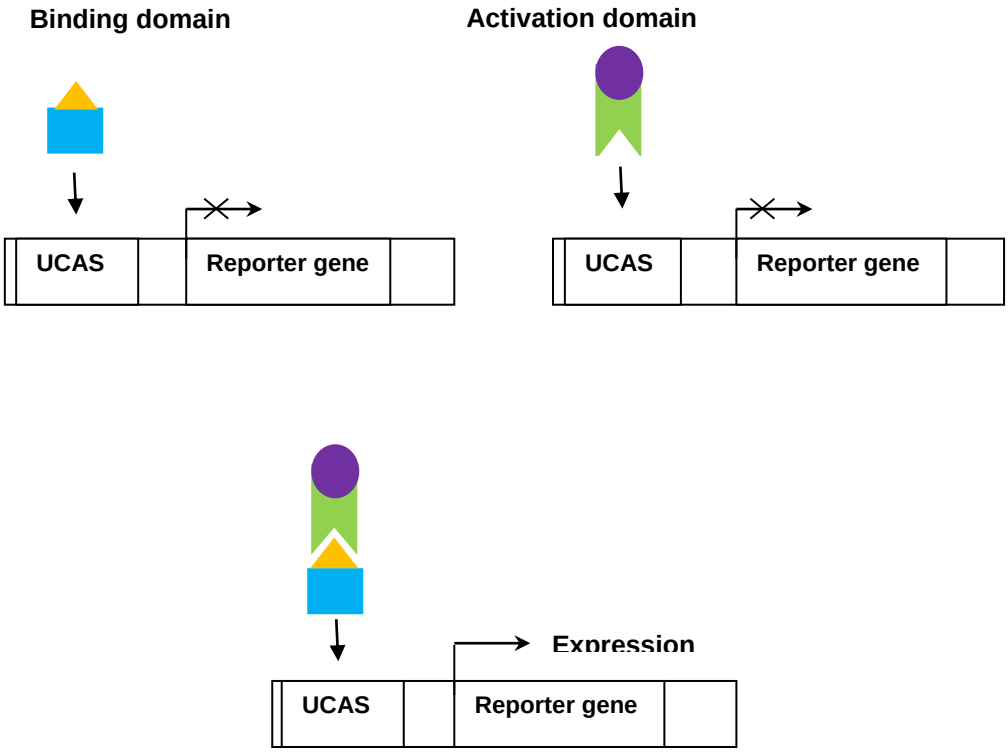

Figure 2.1 Theory of yeast two hybrids (Y2H).

Fusion proteins either Gal4-DNA binding domain or Gal4-DNA activation domain alone is unable to activate expression of the reporter gene. Expression of the reporter gene can promoted only when the proteins of interest interact and bring binding domain and activation domain together.

2.6 Protein methods

2.6.1 Small scale yeast whole cell extract prep using Glass Beads

An overnight culture of yeast cells was refreshed till OD_{600} = 0.5-0.6, and 3U of the cells was harvested by centrifugation at 3000 rpm for 5 minutes. Cell pellet was washed once with 1ml of distilled water, the supernatant was removed, and then 125 µl of 2x sample Buffer was added to the pellet. The pellet mix was transferred into clean 1.5 ml tube containing 100 µl of Acid washed glass beads. The sample was vortexed using cell disrupter for 3 minutes and then boiled in heat block at 100˚C for 3 minutes. The sample was left to cool on bench, centrifuged briefly to pellet the glass beads, and then stored immediately in –20˚C.

2x sample buffer:
- 2.5 ml 0.5 M Tris pH 6.8
- 2.0 ml Glycerol
- 2.0 ml 10% SDS (Sodium Dodecyl Sulfate)
- 2.0 ml ddH_2O
- 0.5 ml bromophenol blue solution

2.6.2 Protein extraction, using Liquid Nitrogen-Grinding method

An overnight yeast culture was diluted into 100 ml of SD medium to OD_{600}= 0.6-1.0. The cells were harvested by centrifuging at 3000 rpm for 3 minutes. The cell pellet was washed with 1ml of ddH_2O and spun down as above. The cell pellet was resuspended in 1ml of UBT Buffer freshly supplemented with protease and phosphatase inhibitors. The cell slurry was frozen drop wise into liquid nitrogen in 50 ml Falcon tube. Cells were ground in the presence of liquid nitrogen using a pestle and mortar. The yeast cell extract was collected into 1.5 ml tubes and stored at – 80˚C until required.

UBT Buffer :
- 50 mM KHEPES pH 7.5
- 100 mM KCl
- 3 mM $MgCl_2$
- 1mM EGTA
- 1% Triton X-100

Protease and phosphatases inhibitors :	40 µl EDTA free protease inhibitor cocktails 1 µM of 10 mM pepstatin-A 10 µM of 10 mM leupeptin 1mM of 500 mM NaF 0.5 mM of 100 mM Na_3VO_4

2.6.3 Immunoprecipitation (IP) from *S. Cerevisiae*

Cell extract was prepared using liquid nitrogen grinding method (see section 2.6.2). Cell lysate was centrifuged at 14,000 rpm for 20 minutes at 4˚C in a TLA100 roter (Beckman™). The supernatant was transferred onto a clean tube and precleared with 20 µl IgG mouse–Agarose conjugate if required. The pre-cleared lysate was incubated with 40 µl of the Agarose conjugated antibody at 4˚C for 2 hours on spin-mixer. Beads were pelleted and the supernatant was transferred into clean tube and mixed with equal volume of 2x sample buffer. Beads were washed 3x with 500 µl with UBT buffer supplemented with protease and phosphatase inhibitors, and kept cool during the washes. To elute the protein, the beads were resuspended in 40 µl of 2x sample buffer and boiled at 100˚C for 5 minutes. The beads were briefly centrifuged and equal volumes of supernatant and pellet (beads) were loaded onto SDS-PAGE gel (see section 2.6.6). Proteins were then analysed by Immunobloting application (see section 2.6.11).

2.6.4 Growing and induction of C41 (DE3) and BL21 *E.coli* for protein purification

A plasmid expressing GST tagged protein of interest was transformed into C41 *E. coli* or BL21 *E. coli* (see section 2.4.3). Freshly grown transformants were scrapped from the plate using scraper and suspended in 1L 2xYT (+ Ampicillin) medium (see section 2.4.1). Bacterial culture was grown at 37ºC until OD_{600} nm =0.6 to 0.8, at this point protein expression was induced by adding 0.1 mM isopropyl-β-D thiogalactopyranoside (IPTG) and cell incubation at the same conditions was continued overnight. For BL21 *E.coli* expressing GST fusion protein, induction condition was carried at 30 ºC

overnight. The overnight culture was harvested at 7700xg for 15 minutes at 4˚C. The resulting bacterial pellet either used immediately or stored at – 20˚C freezer until required.

2.6.5 Purification of GST tagged proteins

All buffers and reagents were pre-chilled and kept on ice during the whole procedures. Cell pellet was washed with 50 ml 1X PBS once and then resuspended in 10 ml of 1X PBS buffer supplemented with protease inhibitors. Whole cell lysate was prepared by 3x sonication on ice for 30 seconds each in a cell sonicator (Sanyo Soniprep 150). The lysate was then centrifuged at 21000 xg for 42 minutes at 4˚C, the supernatant was removed filtered 3x through a 0.2 µm syringe filter (Sartorius). The supernatant was transferred into a clean Falcon tube containing 250 µl 1XPBS prewashed 50 % slurry glutathione sepharose beads 4B (Amersham-EG Health care) and then incubated at 4˚C for 1hour on a rolling platform. Beads were sedimented by centrifugation at 500 g for 5 minutes. the beads pellet was washed with 10 ml of 1x PBS pH7.4, 1 % Triton x-100 , 300 mM NaCl and then with 1x PBS. 10 ml wash was performed with wash buffer (50 mM Tris pH7.0, 300 mM NaCl, 1mM EDTA pH8.0, 1 mM DTT), and then washed 3x with 10 ml elution buffer (50 mM Tris pH7.0, 50 mM NaCl, 1 mM EDTA pH8.0, 1 mM DTT) . Beads were then resuspended in 300 µl of elution buffer. GST tag cleavage was carried out when required using 10 µl pre-purified Prescission Protease in 300 µl elution buffer. The Prescission Protease cleaves between Glycine and Glutamine residue of TEV recognition sequence. The reaction was incubated at 4˚C for 8 hours on roller platform.

2.6.6 SDS-PAGE Electrophoresis

The appropriate percentage of acrylamide gel was poured according to the recipes below.

Resolving gel:

	6 %	**10 %**
Sterile water	2.7 ml	2 ml
30% acrylamide mix	1 ml	1.7ml
1.5 M Tris (pH 8.8)	1.3 ml	1.3 ml
10% APS	50 µl	50 µl
10% SDS	50 µl	50 µl
TEMED	4 µl	4 µl

5% stacking gel:

Sterile water	1.71 ml
30% acrylamide mix	0.501 ml
Stacking buffer (0.5 M Tris-HCl (pH 6.8), 0.4 % SDS)	0.75 ml
10% APS	35 µl
TEMED	3.5 µl

Running conditions: gels were run in 1x SDS running buffer at 70V through the stacking gel and then 140V in the BioRAD equipment until the dye reached the bottom edge of the gel. For purified proteins, precast BioRAD Criterion TGX precast gels (any kDa) and mini-PROTEAN TGX precast gels (any KD) were used. Criterion TGX gels were run in BioRAD Criterion cell for

35 minutes at 200 V and mini-Protean TGX gels were run in Mini protean Tetra cell for 26 minutes at 200 V in 1x SDS running buffer

2.6.7 Phos-Tag SDS-PAGE electrophoresis

A dinuclear manganese complex of acrylamide-pendant Mn^{2+}–Phos-tag™ from NARD institute ltd., was used to test for Las17 phosphorylation which can be detected by observing mobility shift of the phosphorylated species of protein. The method based on binding of Manganese molecule to two vacancy sites on the PhosTag compound forming a stable complex with phosphate group at pH 9.0. 10 % SDS PAGE resolving gel was prepared as described in section 2.6.6, and 1:1 ratio of Phos-tag™ and 10 mM $MnCl_2$ solution were added subsequently to the gel mix. Protein extracts were loaded onto Mn^{2+}–Phos-tag acrylamide gel and run in 1x running buffer, initially at 50 V through the stacking gel and then 150 V until the dye reached the bottom edge of the gel. The Las17-3x HA phosphorylation was detected by western blotting and visualised Alkaline phosphatase (see section 2.6.12).

2.6.8 Coomassie staining of SDS polyacrylamide gels

Proteins separated by SDS-polyacrylamide gel were detected using Coomassie Brilliant blue stain (Bio Rad). The electrophoresed gel was soaked in Coomasie stain solution (0.2 % (w/v) Coomasie Brilliant Blue R250, 7% (v/v) acetic acid) and then heated in the microwave for 30 seconds and left on a rocking platform with continuous movement. The gel was then destained overnight using several times changes of distilled water until the appropriate level of contrast between the protein bands and the gel was achieved.

2.6.9 Determination of protein concentration

Beer' Low method is based on determining the absorbance of the Cysteine and Tryptophan residues of protein at 280nm. However, this method would be inappropriate due to lack of tryptophan residues of Las17 peptide

sequence. Alternatively, the purified Las17 from sample containing contaminants was quantified using the following approach.

2.6.9.1 Bradford protein Assay (Colorimetric Method)

Bradford assay is based on binding of Comassie brilliant blue G-250 to unknown protein and compare this binding to that of different concentration of a standard Bovine serum albumin (BSA) protein. The Comassie solution is red-brown in its acidic solution, when the protein binds; the colour turns blue due to change in the pka value of the dye. The assay was performed by preparing duplicate aliquots of 0.5 mg/ml BSA (5, 10, 15, and 20 µl) into 1.5 ml tubes and the volume in each tube was brought to 100 µl with 0.15 M NaCl. 10 fold dilution of unknown protein was made up in the same buffer as standards protein and two blank tubes of 100 µl of 0.15 M NaCl were also included in the assay. 1 ml of Comassie solution was added to each tube, mixed thoroughly, and incubated for 2 minutes at room temperature. Each sample was A595nm measured using 1–cm path length cuvette (1 ml) and standard curve was generated by blotting absorbance versus protein concentration. The concentration of the unknown protein was calculated from the least squares of the line standard curve. This assay quantifies 1 to 10 µg protein concentration.

2.6.9.2 Determining Las17 protein concentration by densitometry

The concentration of the purified protein was also assessed by combination with standards from purified rabbit actin samples (see section 2.7.2). A series of rabbit actin was diluted in 2x sample buffer to final concentration of 0.25, 0.3, 0.5..to 5 µM. 10 fold dilution of unknown protein sample to be measured was also prepared. These standards were run alongside with purified protein of unknown concentration on precast BioRAD Criterion TGX precast gels (any KD). The gel was then Comassie stained, destained, and then viewed using ChemiDoc™XRS^{+} (BioRad)· Densitometric analysis of unknown bands were quantified using Image lab™ software (BioRad). Bands for protein bands were selected; intensity substraction of the background was applied,

and the concentration of the standards was referenced. Graph line was generated using the values of the actin standards concentrations were blotted against the value of the relative intensity of the unknown protein on the line curve.

2.6.10 Western Blotting

Proteins were separated by SDS-PAGE electrophoresis as described in section 2.6.6. These proteins are transferred using two methods: semi-dry method and wet transfer method. Semi-dry method was used to transfer protein onto TransBlot®-Torbo™ mini PVDF membrane from BioRad. The transfer was carried out using TransBlot Turbo system from BioRad. Wet transfer method was carried out using poly-vinylidene difluoride (PVDF) membrane in which PVDF membrane was soaked in 100 % methanol, then in transfer buffer (10 mM [N-cyclohexyl-3-aminopropanesulfonic acid] CAPS,10 % Methanol pH11), along with two sponges and six pieces of Whatman filter paper cut to the same size as the acrylamide gel to be transferred. A sandwich containing a sponge, three pieces of wet filter paper, PVDF membrane, the remaining sponges, and the three pieces of filter paper were assembled and then placed in the BioRad blotting apparatus with the membrane closest to the negative pole (anode). A block of ice was placed in the apparatus to keep the temperature low and the transfer was done for 3 hours at 300 mA.

2.6.11 Western blot detection using Enhanced Chemi-Luminescence (ECL)

This system is based on detecting antigen using horseradish peroxidise conjugated antibodies and the chemiluminescent substrate luminol. After plotting, the membrane was blocked in blocking solution (5% milk powder (Marvel) in 1x TBST (50 mM Tris, 50 mM NaCl, 0.05%Tween-20)) for 30 min at room temperature on rocking platform. The membrane was rinsed with in 1x TBST and then placed in plastic bag with 2 ml of blocking buffer in the presence of recommended concentration of primary antibody (see table

2.2.4), and incubated for 1 hour and room temperature or overnight at 4˚C. After incubation, the blot was washed with 1x TBST briefly and then 3x washes were carried out every 10 minutes. The membrane was placed in 15 ml falcon tube and incubated with blocking buffer containing horseradish peroxidise (HRP) conjugated secondary antibody (see table 2.2.4) for 1 hour at room temperature on rocking platform. The membrane was then washed three times with 1x TBST for 5 minutes each. In the dark room equal volumes of western blotting detection Reagents (GE Healthcare 1ml of solution (A) and 25 µl of solution (B)) plus ECL reagents including: ECL I (2.5 mM Luminol (3-Aminophthalhydrazide–Fluka no. 09253), 4.4 mM p-Coumaric acid in DMSO, 100 mM Tris pH 8.5) and ECL II (0.0192 % H_2O_2, 100 mM Tris pH 8.5) in 1:1 ratio were mixed and added to the membrane. The membrane in the developing solution was incubated for 1-2 minutes in dark. Solution mix was drained off, while the membrane was placed up side in plastic bag and developed for 30 minutes using ChemiDoc™XRS$^+$ (BioRad).

2.6.12 Western blot detection with Alkaline Phosphatase

The blotted membrane was probed with antibodies carrying Alkaline Phosphatase marker (AP) with a visibly detectable colour change. The membrane was blocked with 5 % Bovine Serum Albumin (BSA) in 1x TBST Buffer and probed with primary antibody as described in section 2.8.2.2). After washing with TBST, the blot was incubated with alkaline phosphatase conjugated secondary antibody diluted in 1xTBST at the required concentration for 1 hour at room temperature. the membrane was washed 3x for 5 minutes each and then developed in 10 ml of developing solution (100 mM NaCl, 5 mM $MgCl_2$, 100mM Tris at pH9.5) 66µl NBT made of 0.5 g NBT powder in 10 ml 50 % DMF and 66µl 5-Bromo-Chloro-3-indolyl phosphate ρ-toluidine salt (BCIP) stock of o.25 g in 10 ml 100 % DMF. The membrane was incubated in dark at room temperature until sufficient colour had developed. The reaction was then stopped by washing the membrane with water and allowed to dry on the bench overnight.

2.6.13 Two Dimensional Gel-Analyses (2D gel)

2D gel electrophoresis is proteomic analysis that involves separation, identification, and quantification of many proteins simultaneously from a single sample. The principle of 2 D gel based on two steps: first dimension and second dimension. The first dimension step is isoelectric focusing (IEF), which separates proteins according to their isoelectric points (Ip), whilst second –dimension step required for separation of proteins according to their molecular weight by SDS-PAGE gel electrophoresis. Each spot generated by two dimensional gels potentially corresponds to a single protein species in the sample.

The method described in this work is for 2-D electrophoresis using precast IPG strips (Immobiline DryStrip gels) from GE Healthcare. Immunopreciptated the 3x HA tagged Las17 was eluted with the hydration buffer to a concentration of 1mg/ml. Elution was carried out at room temperature for 30 minutes with gentle shaking. 3-10 pH Immobiline DryStrips gels (7cm) were incubated in dehydration buffer overnight in the reswelling try with the gel side down. The protein sample was reduced with 1mM DDT at room temperature for 20 minutes and then alkylated with 0.5 % ampholites and 1.2 % Destreak buffer as above. The Isoelectric focusing IEF was carried out in Peter Sudbury laboratory using Ettan IPGphor3 and the IEF parameters were set up according to the length of the Immobiline Dry Strip gel as stated in the manufacturer guideline.

IFF Program

Hydratation	0h	20ºC
300V	30 minutes	
1000V gradient	30 minutes	
5000V gradient	1 hour.20 minutes	
5000V step & hold	20 minute	
500V step & hold	2 hours	

Prior to the second dimensional gel, the strips were reduced with 2%DTT in balancing buffer (6 M urea, 50 mM Tris pH8.8, 2 % SDS, 30 % Glycerol) for 30min at room temperature with gentle shaking. Following this, alkylation step was performed with 2.5 % iodoacetamide in balancing buffer. The Dry Strip gel was washed several times with distilled water then with 1x running buffer. The strip was loaded vertically on 12 % Precast gel (Bio-Rad) and the gel was sealed with 0.5 % agarose made in running buffer. Electrophoresis was carried out at 140 V for 1.5 hour. The gel was then analysed using western blotting application (see section 2.6.11).

2.6.14 In-Gel Tryptic digests

The SDS-PAGE gel containing protein of interest was stained with safe stain (from Invitrogen) for 1 hour at room temperature. After incubation, the gel was destained by applying several washes with Milli-Q water (at 18.2MΩcm^{-1} at 25˚C) within the fume hood. Gel band containing protein of interest was excised into a siliconized eppendorf tube with clean scalpel blade, and covered with 200 µl solution I (200 mM ABC, 40 % ACN) followed by incubation at 37˚C for 30 minutes. This step was repeated 4 times with fresh solution I each time. Gel pieces were then dried down in a vacuum concentrator for approximately 15-30 minutes prior to reduction and alkylation steps. Reduction of gel pieces was carried out by adding 200 µl freshly made reduction buffer (10 mM DTT, 50 mM ABC in solution II) and then incubated at 56 ˚C for 1 hour. The samples were spun down at 13 Kg for 10 seconds, supernatant was discarded, and 200 µl alkylation buffers (55 mM IAA, 50 mM ABC made in solution II) was added to the gel pieces and incubated at room temperature for 30 minutes in the dark. Gel pieces were washed twice with 200 µl solution II (50 mM ABC) for 15 minutes each, and then washed with solution III (50 mM ABC, 50 % ACN) for 15 minutes at 37˚C. Samples were spun down at 13 Kg for 10 seconds, supernatant was removed, and the gel pieces were dried in vacuum concentrator for 15-30 minutes.

The enzymatic digest for the gel pieces was performed by adding 20 µl of Trypsin (equivalent to 0.4 µg Trypsin dissolved in solution IV (40 mM ABC, 9 % ACN)) and topped up with 50 µl of solution IV and then incubation at 37˚C was carried out overnight.

To extract the peptides, the liquid resulted from gel digest was collected onto a clean siliconized eppendorf and labelled as supernatant collection tubes (SCT). The remaining gel pieces in the tubes were covered with 20 µl solution V (100 % ACN), briefly vortexed and then incubated at 37˚C for 15minutes. After incubation, 50µl of solution VI (5 % FA) was added to the tubes, vortexed briefly and then centrifuged at 13 Kg for 15 minutes, supernatant was removed and then transferred into SCT. Washes with solution V and VI was repeated once more as described earlier.

50 µl of solution VII (50 % ACN, 5 % FA) was added to the gel pieces, shortly vortexed and then incubated at 37˚C for 30 minutes. Samples containing gel pieces were vortexed and then centrifuged at 13Kg for 10 minutes, supernatant was transferred into SCT, and the gel pieces were discarded. The supernatant collection tubes were placed in vacuum concentrator and the extracted peptides were dried at low heat overnight. Next day, the resulting peptide extracts were stored at −20˚C prior to Mass Spectroscopy analysis.

2.7 Actin Methods

2.7.1 Actin cytoskeleton Acetone powder Preparation

The protocol is based on the methods described by Perry, 1955 Methods in Enzymology 2 pg 583.

The hind leg muscles obtained from a maximum of four freshly killed rabbits was excised, sealed, and kept cool to preserve endogenous ATP. (Rabbits obtained from either the university of Sheffield animal house, University of Sheffield, or from Woldsway Foods Ltd., Spilsby, Lics., UK).

All procedures were performed at 4˚C room with all the equipment and the reagents pre-chilled. Fat and connective tissues were removed from the rabbit muscles. The muscles were minced twice in a Porkert mincer and then extracted in 3 L of Guba Straub buffer (300 mM NaCl, 100 mM NaH_2PO_4, 50 mM Na_2HPO_4, 1 mM NaN_3, 1 mM $MgCl_2$, 1 mM $Na_4P_2O_7$, 0.05 mM PMSF, 2 mM ATP, adjusted to pH 6.5) and the mixture was stirred for 10-15 minutes. The extracted mixture was then centrifuged using JLA8.1000 roter at 3000xg for 20 minutes at 4˚C. The prespun muscle residue of myosin prep was resuspended in 1 L of 10 volumes of 1 x Buffer (I [4% $NaHCO_3$, 1mM$CaCl_2$ made up in 1L distilled water]) and stirred for 15 minutes. The residue was then filtered through four layers of cheese cloth and then resuspended in 1 L of 10 volumes of 1x buffer (II [10 mM $NaHCO_3$, 10 Mm Na_2CO_3, 0.1 mM $CaCl_2$, 50 µl of 2 M buffer (I) made up in distilled water]). The mixture was resuspended manually by agitation for 10 minutes and again filtered as above. The suspension was diluted into 10 L water and quickly squeezed through cheese cloth (this step is crucial as muscle swells at low ionic strength and changing of F-actin to G-actin would be lost otherwise). The residue was resuspended in 2.5 L cold acetone (Fisher Scientific), stirred, and left to stand for 15 minutes at room temperature. The residue was then filtered through cheese-cloth and the acetone washing/filtering step was repeated 3-4 times until the supernatant becomes clear. The acetone prep was spread out on filter paper (3mm Whatman paper) and dried under the fume hood overnight. The dried acetone powder was collected and stored

in a sealed container at –80˚C until required.

2.7.2 Rabbit skeletal muscle actin preparation from acetone powder

G-actin was purified from acetone powder made from rabbit muscle based on a modified method (Winder et al., 1995) of actin purification method in (Spudich and Watt, 1971).

5 g of rabbit skeletal muscle acetone powder was resuspended in 100 ml pre-chilled G buffer (2 mM Tris-HCl pH 8.0, 0.2 mM $CaCl_2$, 1 mM NaN_3, 0.5 mM DTT, and 0.2 mM ATP) in 250 ml beaker that had placed inside a larger beaker with ice was being filled around. The suspension was left stirring slowly and continuously at room temperature for 20 minutes. The contents was then transferred into 50 ml Falcon tube and spun at 20.000xg for 35 minutes at 4˚C. Supernatant was filtered through two pinches of glass wool packed into the neck of a funnel, and then through a 4.5 µm filter and 0.22 µm filter (Minisart). A final concentration of both 0.8 M KCl and 2 mM $MgCl_2$ were added to supernatant and left stirring gently at room temperature for 30 minutes and then at 4˚C for extra 30 minutes. To pellet F-actin, actin was ultra-centrifuged at 35000 rpm using (Beckman Coulter Optima L-90K, Type 45 Ti rotor) at 4°C for 2 hours.(to prevent any collapse during the centrifugation, the tubes were topped up with F- buffer [G-buffer ,KCl and $MgCl_2$] until it is 3/4 full). Supernatant was discarded and the F- actin pellet was extracted and placed into a 15 ml glass Teflon homogeniser and then resuspended with 10 ml G-buffer. Pellet was homogenised and then dialysed against G-Buffer, at 4°C, for 3 days with three changes during the day. Actin sample was then collected into 50 ml tube and centrifuged at 35.000 rpm (Beckman Coulter OptimaMax 130K, MLA80 rotor) for 2 hours. The clear supernatant (usually the top ~2/3 of the tubes) was carefully removed and gel filtered on a Sephacryl S300 gel filtration column (Amersham XK26), equilibrated in G-Buffer. The actin peak was collected in ~3 ml fractions using an Amersham LKB RediFrac collector and stored at 4°C.

The purified actin solution contains ATP, and ATP absorbed at wave length=280 nm which adds to absorbance value given by actin. This can be avoided by using 290nm wavelength using spectrophotometer.

The actin concentration was determined using the equation:

µM actin= A_{290nm} x dilution factor/ 0.0264

Where 0.0264 is the extinction coefficient value of actin

2.7.3 Pyrene Actin preparation

All procedures were performed at reduced light at 4˚C. Pyrene (N-(1-pyrene) iodoacetamide) labelled actin was prepared using fresh actin prep from a column performed in G buffer without DTT. The peak and post peak fractions of G-actin were mixed and a concentration of A290. e= 0.63ml/(mg-cm) was determined using spectrophotometer. G-actin fraction mix was diluted to 1 mg/ml with G buffer and then polymerised by adding 100 mM KCl and 2 mM $MgCl_2$, and this was slowly stirred at room temperature for 20 minutes. Pyrene (MW385) was dissolved in DMF to make 10mg/ml and then added to polymerised actin at 10:1 molar ration while stirring. The vessel containing actin-pyrene mix was covered with foil and stirred continuously at 4˚C overnight. Dialysis step was carried out against G buffer in which 0.5 mM DTT added in smallest diameter tubing (~12-14kDa in size). For making actin more monomeric, several changes were done in hours which enable G actin be separated from pyrene precipitate. Actin-pyrene prep was spun down at 5000 rpm using MAL80 roter for 5 minutes. Extra depolymerising and stirring steps were carried out as above and, actin-pyrene prep was centrifuged at 40000 rpm at 4˚C in MAL80 roter for 1 hour. Supernatant was removed and the remaining yellow pellet was resuspended in G buffer containing DDT to final concentration of 5 mg/ml. Pellet was homogenized with loose fitting dunce plunger, and then went through gel filtration step. The pyrene-actin mixture was dialysed against G buffer at 4˚C with several changes was made. Pyrene-actin was then centrifuged at 25000 rpm for 2 hours in swinging bucket roter (Sw 41Ti). The 2/3 top of supernatant was removed

with a pipette and transferred to clean tube. The pyrene–actin was gel filtered on foil-wrapped G-150 column equilibrated with G buffer with DTT, and the prep was collected in the fraction collector covered with foil. The concentration labelling of Pyrene-actin prep was determined using the following formula:

Actin/ pyrene µM = (OD_{290} (OD_{344} × 0.127) / 0.0264
For pyrene: e at A344= 2.22×104/ (M-cm)
For actin: corrected A_{290} for actin X^{*}=X-0.127Y = 2.66×104/ (M-cm)
Where X=A_{290}, Y=A_{344}
% labelled= [pyrene] / [actin]

Working aliquots of 20 µl were subjected to rapid freezing by dropping the pyrene/actin tubes in liquid nitrogen and then stored at – 80 ˚C.

2.7.4 G-actin binding assay on GST beads

Prior to actual experiment G actin was spun down at 90K rpm for 15 minutes and spun down at 100,000 rpm using Beckman Coulter Optima Max 130K, TLA100 rotor for 15 minutes at 4°C to remove any precipitate or polymerised actin. Monomeric actin was then transferred into separate tube and left on ice to be used in the assay. GST fusion on beads were buffer exchanged by applying 3x washes with 10 ml of G buffer. GST fusion on beads was mixed with 5 µM G-actin to a final volume of 100 µl in G buffer, and then incubated at room temperature for 1 hour. After incubation, beads were spun down at 5000xg for 3 minutes, supernatant was transferred into clean tubes, and equal volume of 2x sample buffer was added to the tubes. 100 µl G buffer was added to the beads and again equal volume of 2x sample buffer was added to the beads. Supernatant and beads samples were boiled at 100˚C for 3 minutes and 15 µl of each sample was loaded on SDS-PAGE gel. The binding between GST fusion and G-actin can be detected in the pellet lane which can be observed through staining the gel with safe stain.

2.7.5 Pyrene/Actin fluorimetry assay

To determine the polymerisation kinetics of actin, pyrene-actin fluorimetry assay was carried out using a Cary Eclips fluorescence spectrophotometer (VARIAN). The fluorometer was set up as follow:

λ Excitation wavelength- 365 nm
λ Emission wavelength- 384 nm
Excitation slit width- 10nm rounds, and Emission slit width- 20nm rounds

A clean 96 wells plate was set up in 300 µl assay containing 5 µM post peak G-actin, G buffer, and pyrene actin-10% of actin volume. The fluorometer was started for 5 minutes to check the fluorescence trace is steady, and then 70 µl mix (protein of interest, 10 x KME brought to 1x concentration , and G buffer) was added to each wells using multi-pipette and mixed thoroughly. The assay was run for 2 hours and the arbitrary per time (minutes) report was analysed using GraphPad 6 Software.

2.7.6 Small scale thermophoresis (MST)

MST analysis is based on measuring the changes of the mobility of fluorescently labelled molecules along temperature gradients (22-45˚C) by detecting the changes in intrinsic properties such as size, charge, and hydration shell of the labelled molecule. Las17-PWCA fragment was purified and GST cleaved and then dialysed into G-buffer. Protein was labelled using the Monolith™ protein labelling kit RED as stated in the manufacturer instruction. The binding experiment was performed by preparing an equal volume of a 1/10 dilution of fluorescently labelled PWCA and mixed series of 2 fold dilution freshly purified G-actin in MST buffer (50 mM Tris pH 7.6, 150 mM NaCl, 10 mM $MgCl_2$, 0,05 % Tween-20, provided by the Monolith NT™ kit). Samples were loaded into glass capillaries and subjected to temperature gradients of 22-45˚C. The movement of the florescent molecule (G-actin/LAS17-PWCA) was measured by monitoring the changes in the fluorescence distribution of the complex inside the capillaries using NanoTemper Monolit -115 instrument.

2.8 Microscopy methods

2.8.1 Fluorescent microscopy

The yeast cells were viewed using an Olympus IX81 inverted fluorescent microscope with a 100W mercury lamp and oil-immersion objective. Data was collected in acquisition mode, and 3D image datasets were deconvolved.

2.8.2 Images deconvolution

AutoQuant software (Media Cybernetics®) was used to enhance signal to noise ratio of Z-stack series or image time lapse series, and data were captured as Tiff format. Live cell images were taken for 90 seconds with 1second time-lapse. The kymographs, the profile of intensity values and patch tracking were established ImageJ software by tracking the movement of a single patch on the plane of plasma membrane. Images were then assembled using image J-Fiji version and adjusted to 300 dpi using Adobe Photoshop.

2.8.3 Viewing yeast cells by fluorescence microscopy

Freshly growing yeast cells expressing a fluorescent tag were viewed after growing the cells to med-log phase in liquid SD media. 2.5 µl of cells was pipette into glass slide covered by cover slip and viewed under the fluorescence microscope.

2.8.4 Rhodamine-phalloidin actin filaments staining

1 ml actively growing yeast culture was fixed with 134 µl of 37% formaldehyde and incubated at room temperature for 30-60 minutes. Cells were spun down at 3000rpm for 5 minutes, supernatant was removed, and pellet was washed twice with 0.5 ml wash buffer I (PBS, 1mg/ml BSA, 0.1% Triton -100TX). The pellet was resuspended in 50 µl of wash buffer I and 5 µl of 40mg/ml Rhodamine phalloidin (from Molecular probes). The sample was then incubated in the dark for 30 minutes, and washed twice with 500 µl wash buffer II (PBS, 1mg/ml BSA) and then resuspended in 200 µl wash buffer II. 3 µl of suspension cells was placed on slide lid and covered with

cover-slip. Cells were viewed by fluorescence microscopy straight away or stored at 4˚C for later viewing.

2.8.5 Yeast vacuoles staining using Lucifer Yellow

This experiment is based on a method from Dulic et al., 1991.

An overnight culture was refreshed in appropriate synthetic medium and grown until OD_{600}=0.5-0.7. Cell pellet was spun down at 3000 rpm for 3 minutes and then resuspended in 30 µl synthetic medium, and 10 µl of 40mg/ml of lucifer yellow. The cells were incubated at 25˚C shaking. The duration of this incubation period is dependent on the stages of endocytosis to be assessed. Shorter incubation (30 min) time is required to assess the defect at early stage of endocytosis such as delay in dye internalisation. 90 minutes incubation is used to assess end point of endocytosis for example vesicle transport and fusion with the vacuole. After incubation, cells were 3x washed with 1ml ice-cold succinate/azide buffer and then resuspended in 10 µl succinate/azide buffer and left on ice until they are ready to be viewed by fluorescence microscopy.

2.8.6 Yeast vacuoles staining using FM4-64

FM4-64-N-(triethylammoniumpropyle)-4-(p-diethyleaminophynyl-hexatrienyl) pyridiniumdibromide is a lipophilic styryle dye which is used as a vital stain to follow bulk membrane internalization and transport to the vacuole in yeast cells (Vida and Emr, 1995). 1 ml of log phase culture (OD_{600}= 0.5-0.6) was spun down at 3000 rpm for 3 minutes. The pellet was resuspended in 250 µl of synthetic medium and then transferred into 1.5 ml eppendorf tube. 0.25 µl of 16 Mm FM4-64 made in DMSO was added and the cells were incubated for 90 min at 21˚C room temperature rotating. This incubation time is to chase the late stage of endocytosis. Following the incubation cells were harvested at 3000 rpm for 3 minutes and the pellet was resuspended in 200 µl of appropriate medium. 2.5 µl of cells were put on a slide and covered with cover-slip to be viewed under the fluorescence microscope.

Chapter 3:

In vivo Analysis of Las17 phosphomutants

Chapter: 3

3.1 Introduction

Arp2/3 complex activation is dependent on its interaction with the WCA domain at the carboxyl terminal of WASP family members. In mammalian WASP, the activity of the WCA domain is autoinhibited by intramolecular interaction with the GTPase binding domain (GBD). This autoinhibitory effect can be relieved through phosphorylation/dephosphorylation of multiple Serine/Threonine residues following an interaction with Cdc42, PIP_2 and several SH3 domain containing proteins (Cory et al, 2003; Kim et al., 2000;, Rohatgi et al., 2000; Kim et al., 2000).

The yeast homologue of WASP, Las17 plays a major role in actin cytoskeleton regulation in conjunction with Arp2/3 complex. Complete deletion of *LAS17* gene inhibits growth at high temperatures, disrupts actin cortical patch organisation, and blocks endocytosis (Madania et al., 1999; Li et al., 1997). Unlike mammalian WASP, Las17 in *S. cerevisiae* lacks a GTPase binding domain and therefore Las17 activity is subjected to other regulatory mechanisms. At the endocytic patches, Las17 interacts with the SH3-domain of several proteins; Sla1 and Bbc1, for example have been shown to inhibit Las17 activity (Rodal et al., 2003), but, the SH3 domain containing protein Bzz1 may relieve this negative effect and allow progression of membrane invagination (Sun et al., 2006). Invagination events at the endocytic sites are dependent on the activity of Las17 and Arp2/3 complex, but genetic studies by Sun and co-workers revealed that, deletion of the Las17WCA domain resulted in mild phenotypic defects whilst the overall actin organisation appeared to be normal (Sun et al., 2006). Similar phenotypes were observed upon deletion of the entire acidic (A) domain of Las17 (Galletta et al., 2009), and this led to the suggestion that, other parts of Las17 contributes to the critical function of Las17. The Ayscough lab has demonstrated that, tracts of Las17 poly-proline rich region (PP) mediate actin binding and filament nucleation independently of Arp2/3 complex suggesting that, actin binding functions of PP and WH2 domains of Las17may occur sequentially (Urbanek et al., 2013).

Multiple phosphorylated residues serine (S) and threonine (T) were identified through a PhosphoGrid search conducted along the Las17 protein sequence (www.phosphogrid.org), (depicted in figure 1.18.A). In phosphoproteomic study, Las17 was identified as a target of the DNA damage checkpoint kinases in the budding yeast. Kinases were found to target Ser586 and Ser588 residues present in the Las17 WCA domain (Smolka et al., 2007). Another study has also identified S586 and S588 as phosphorylation sites for cyclin-dependent kinase1 (Cdk1) in yeast and this was identified through combining chemical inhibition of Cdk1 with mass spectrometry (Holt et al., 2009).

In an attempt to learn more about the regulation of Las17 function through phosphorylation, phosphomutants of S586 and S588 were generated in order to analyse their phenotypic effects at the cellular level using various in vivo approaches. These included investigating the ability of phosphomutants to grow at different physiological conditions such as, elevated temperature, osmotic stress, and tolerance to the salt. The actin phenotype and endocytic functions of phosphomutants mutant cells were addressed using Rhodamine-phalloidin, Lucifer yellow and FM4-64 staining respectively. To determine at which stage of yeast endocytosis the phosphomutants are more defective, the behaviour of Sla1- GFP endocytic reporter was analysed using live-time imaging.

3.2 Generation of Las17 phosphomutants

The function of the identified Las17 phosphorylation sites S586 and S588 were investigated by generating phosphomutants. Both serines were mutagenised to Alanine (A) to generate a non-phosphorylatable protein or to aspartate (D) to create a phosphomimetic form of protein (shown in figure 3.1). The point mutation of phosphosites S586 and S588 singly or together was carried out using mutagenesis on a centromeric plasmid (pKA606) carrying full length *LAS17* under its own promoter; and the pKA607 plasmid that expresses GFP tagged full length *LAS17* under a Tpi promoter (see table 2.2.2 for plasmid description). The resulting mutagenised plasmids

were transformed into bacterial competent cells (see section 2.4.4). The transformants were grown into colonies from which plasmid DNA were isolated and verified by sequencing at Dundee sequencing DNA services. The verified phosphomutant plasmids were then re-struck, and a stock was made before analysing the effect of the mutations on yeast cells through in vivo assays.

3.3 Temperature sensitivity of Las17 phosphomutants

Deletion of *LAS17* gene from yeast genome causes the cells to be sensitive at elevated temperatures. To determine whether *S586* or *S588* phosphomutants affect the growth of yeast cells, the *las17* deletion strain was transformed with an empty plasmid (pKA61) as a negative control, and a plasmid carrying *LAS17* wild type (pKA606) as a positive control. Plasmids expressing the following phospho-mutations S586A/D (pKA 872/873), S588A/D (pKA 874/875), or double SS586, 588AA/DD (pKA 898/899) were also transformed. Overnight cultures of cells were serially diluted, and spotted onto plates containing selective synthetic media (see section 2.5.1). The temperature sensitivity properties of the phosphomutants were assessed by incubation of the plates at the permissive 30˚C and restrictive temperature 37˚C for 48 hours.

Figure 3.2.A shows that, the *las17* deletion strain expressing *LAS17* plasmid was able to grow at both permissive and restrictive temperatures. Cells expressing an empty plasmid were able to grow at 30˚C, but these cells did grow at 37˚C and this was predictable as *las17* null strains are temperature sensitive. Cells expressing single S586A/D mutations had similar growth to cells expressing wild type protein at both temperatures. This suggested that, the S586 residue is not essential for overall cell growth. The growth of cells expressing *las17-S588A* mutant was similar to that seen in wild type cells. However, cells expressing *las17-S588D* mutants were unable to grow at 37˚C, more similar to cells lacking *las17* (Figure. 3.2. A). This would indicate that, changing of S588 into alanine is important for growth at 37˚C. Cells expressing the double mutant *las17-SS586,588AA* at elevated temperature

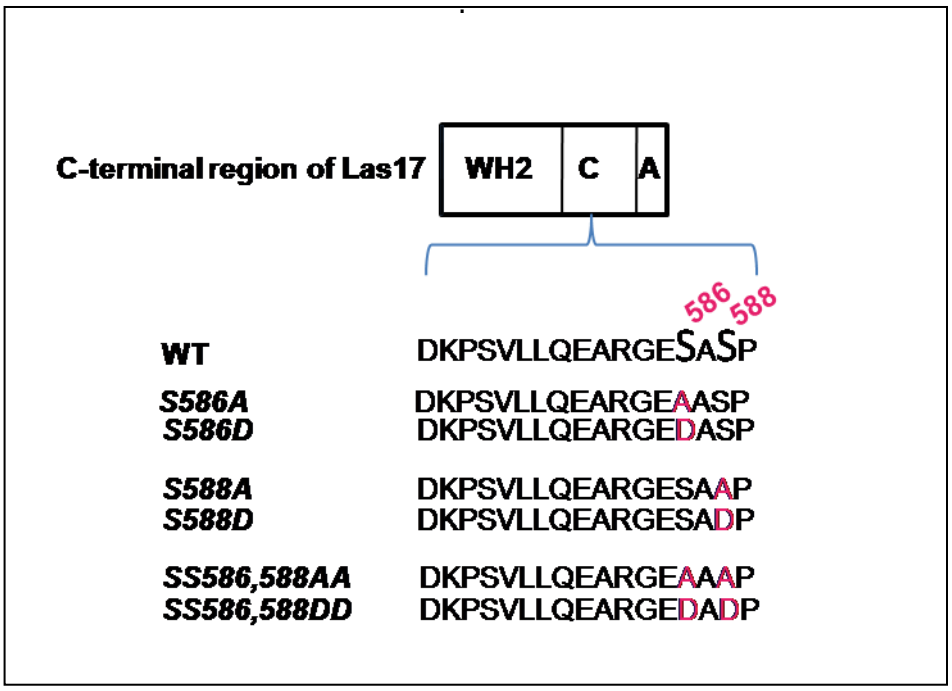

Figure 3.1: generation of Las17 S586 and S588 phosphomutants in WCA domain used in this study.

S586 and S588 phosphoresidues (labelled in magenta) localise in the junction between the WH2 domain and A domain of Las17 wild type (WT). The residues S586 and S588 respectively were changed into alanine (A) or non-phosphorylatable form, or into aspartate (D) which is the phosphomimetic form of protein. Mutations were individual in *las17-S586A/D*, *las17-S588A/D* or double in *las17-SS586,588AA/DD*.

was comparable to cells expressing *LAS17* wild type, but the growth of *las17-SS586,588DD* mutant was completely defective at 37˚C. This again suggests that, S588 site play a role in maintaining growth at elevated temperature.

To further analyse the growth of cells expressing Las17 phosphomutants, it was examined whether the growth defects caused by *S588D* mutants might be associated with actin. Thus, the *las17* deletion strains expressing the phosphomutants described above were grown in a medium containing sorbitol. Addition of sorbitol to yeast cells can alleviate phenotypes associated with actin defects (Aghamohammadzadeh and Ayscough, 2009; Whitacre et al., 2001). This has been shown to be because sorbitol acts to balance the effect of turgor pressure at the plasma membrane and reduce the requirement for actin in endocytosis. Sorbitol was added to growth plates and the plates were then incubated at 30˚C and 37˚C respectively for 3-4 days.

As depicted in figure 3.2.B, the *las17* null strain expressing wild type plasmid was grown normally either at low or elevated temperature. The *las17* null strains carrying the empty plasmid was able to grow at 30˚C, and the temperature sensitivity of these cells was slightly rescued at 37˚C in the presence of 1 M sorbitol. The growth of cells carrying *S586A* or *S5868* strains was not affected by addition of sorbitol. Cells expressing *las17-S588A* grew comparably to the wild type cells but the growth of cells expressing *las17-S588D* was fully rescued in the presence of sorbitol at 37˚C. This suggests that, *S588D* requires actin to overcome the temperature sensitivity phenotype.

In contrast, the temperature sensitivity of cells expressing the double *las17-SS586,S588DD* mutant was not fully rescued as the cells expressing this mutation showed little growth which may suggest that, S586 contributes to the overall phenotype when mutated together with S588.

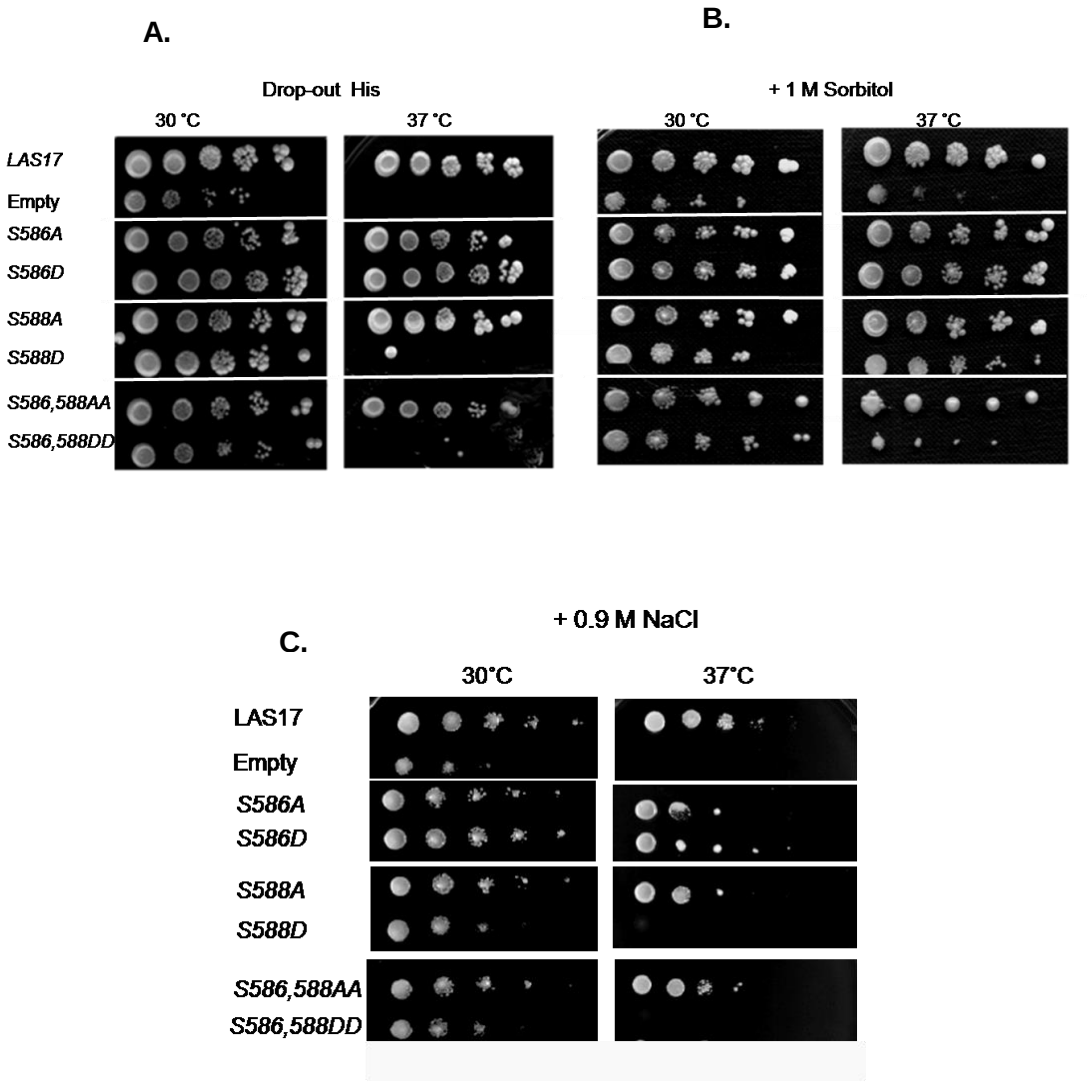

Figure 3.2: Growth analysis of *LAS17* phosphomutants.

Serial dilution of *las17* deletion strains carrying wild type, an empty plasmid or phosphomutants: either with single *S586A/D, S588A/D* mutations or double mutations *S586,588AA/DD*. Cultures were spotted onto selective SD plates **(A)**, supplemented with either 1 M sorbitol **(B)** or 0.9 M NaCl **(C)**. The plates were incubated at 30˚C and 37˚C for up to 48 hours. Interpretable results were obtained from three assays.

One more growth test of the above culture cells was undertaken. In this test the salt tolerance of the Las17 phosphomutants was assessed at 30˚C and 37˚C. Cells were diluted and spotted onto plates containing 0.9 M NaCl, as described above. Salt stress can alter the nature of actin cytoskeleton and normal actin function is required for yeast cells to grow in high osmolarity environment (Novick and Botstein, 1985; Chowdhury et al., 1992)

As shown in figure 3.2.C., cells expressing *LAS17* wild type were resistant to the hypertonic condition at either permissive or elevated temperatures. In contrast, *las17* null cells with an empty vector grew poorly grown at 30˚C, and when the temperature shifted to 37˚C they were unable to grow. Neither *S586A* nor *S586D* expressing cells were affected by the hypertonic conditions. Growth of *S588A* cells was similar to the wild type cells, while those expressing *S588D* grew very slowly at 30˚C, but at 37˚C their growth was completely abrogated. The salt tolerance of *las17-SS586*, *588AA* mutant was similar to cells expressing *LAS17* wild type, but *las17-SS586,588DD* expressing cells grew poorly at 37˚C comparable to the *S588D* mutant.

Overall, these results suggest that S586 residue mutation has no effect on growth at elevated temperatures or in high osmolarity medium. Although when mutated together with S588 into aspartate, it did appear to impair growth rescue in sorbitol medium. *S588D* and the double *SS586 588DD* mutants confer temperature and osmotic sensitivity to the cells. However, only the *S588D* single mutant was rescued by sorbitol at 37˚C possibly indicating the importance of this residue for actin based function in endocytosis.

3.4 Growth rate of yeast expressing phosphomutants

The growth rate of cells expressing *LAS17* phosphomutants was assessed by investigating their ability to grow and divide in liquid drop-out synthetic medium at 30˚C. As previously described, *las17* deletion cells expressing wild type plasmid, an empty, and phosphomutants (*S586A/D*, *S588A/D*, and *S586, 588AA/DD*) plasmids, were grown to exponential growth phase. The

cell cultures were then diluted to the same optical density as one another and incubated at 30˚C with shaking.

The OD_{600} was measured every hour for 6 hours. The top graph shown in figure 3.3 revealed that, *las17* deletion cells expressing wild type plasmid started to divide and duplicate after 4 hours and the doubling time for the wild type cells was 150 minutes. In contrast, *las17* null cells displayed a prolonged doubling time of 223 minutes indicating that, they grew slower. The growth rate of *las17-S586A, las17-S586D, las17-S588A*, and *las17-SS586,588AA* was robust revealing identical generation time as the wild type cells. In contrast, the growth rate of cells expressing *S588D* and *SS586,588DD* was reduced showing a doubling time of approximately 202 minutes. The growth rate assay was repeated with cells expressing *S588A/D* mutants only in order to confirm the phenotype. Thus, the overall growth assay would suggest that *S588D*, either single or double affected the growth rate of yeast cells, supporting the idea that, phosphorylation at S588 plays an important role in Las17 functions in vivo.

As changing of the Ser588 into aspartate revealed the most significant phenotype, the subsequent in vivo analysis was only carried on *S588A/D* phosphomutants. Single *S586A/D* or double phosphomutants were not studied further.

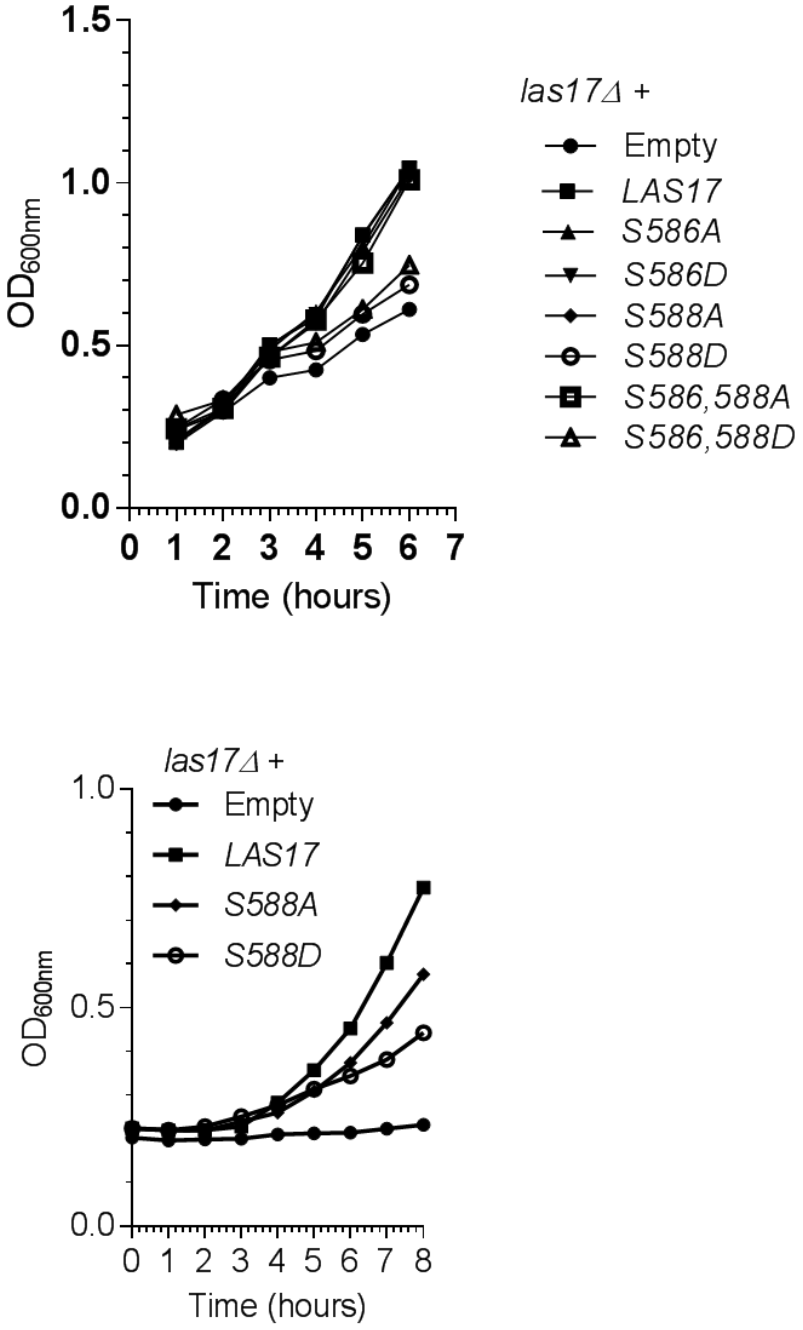

Figure 3.3: Growth rate of *LAS17* phosphomutants

Optical density of *las17*Δ strain carrying wild type, an empty plasmid or phosphomutants: *S586A/D*, *S588A/D* and *SS586 588AA/DD* was measured every hour for 6 hours at 30˚C. The graph was generated using Graphpad Prism6. The growth assay in liquid media was repeated twice, once in the presence of all the mutants (top graph) while the second assay was with *S588A/D* mutants only (bottom graph).

3.5 S588 is important for actin cortical patch assembly

From the analysis described, the S588D mutant was shown to be critical for growth of yeast cells at 37˚C and also in high osmolarity medium. Rescue of temperature sensitivity at 37˚C by sorbitol suggests a possible link to actin in endocytosis. Therefore, to determine whether S588A/D mutations affect actin organization in yeast, cells were stained with Rhodamine-Phalloidin. Phalloidin is a toxin with high affinity for filamentous actin and rhodamine is a red fluorophore conjugated to phalloidin to help visualizing of F-actin. As previously, *las17* deletion cells carrying wild type, an empty or the mutants *S588A/D* were grown to logarithmic phase, fixed with 37% formaldehyde for an hour, and then stained with Rhodamine-Phalloidin as described in section 2.10.1.

As shown in figure 3.4.A, actin cortical patches in wild type cells appeared as bright spots, more concentrated in the bud, whilst defined actin cables could be observed along the mother-bud axis (arrows indicated). In the *las17* deletion strain the actin organisation was markedly disrupted and actin appeared non-polarised in large and less numerous clumps compared to those patches found in the wild type cells. The actin cables were less defined or absent in the majority of *las17* deletion cells.

Cells expressing the *S588A* mutant exhibited wild type actin morphology, in which most of the cells contained polarized patches in the bud and visible cables in the mother cell (arrows). In contrast the cortical actin patches in cells expressing *S588D* mutant displayed an aberrant actin phenotype. Similar to the null cells, the cortical patches were large, few and dispersed throughout the mother and the bud (arrows). The actin cables were observed in some cells, but they appeared thicker than in wild type cells.

A. Rhodamine-phalloidin staining of *las17* null strains

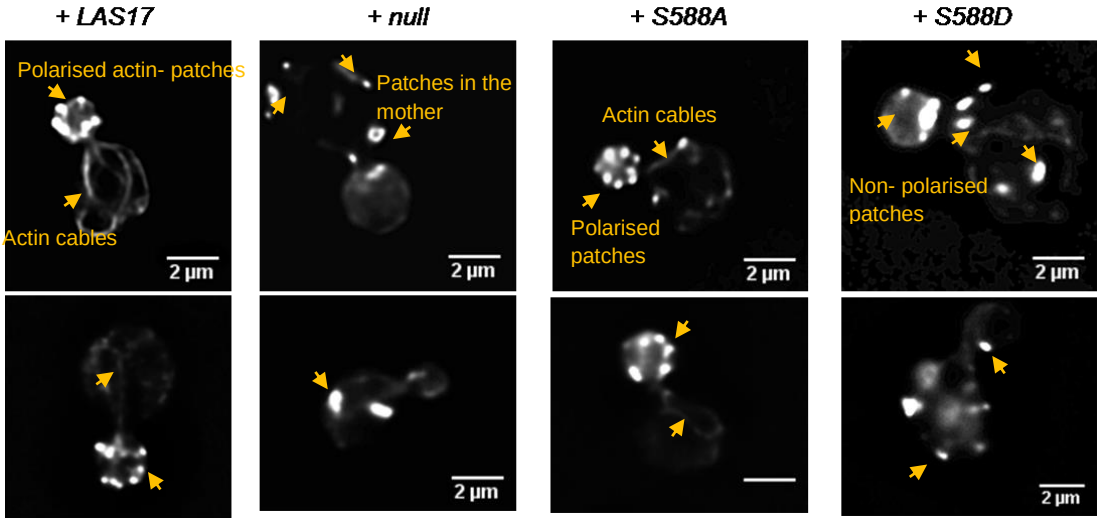

B. Distribution of actin cortical patches in *las17* null strains

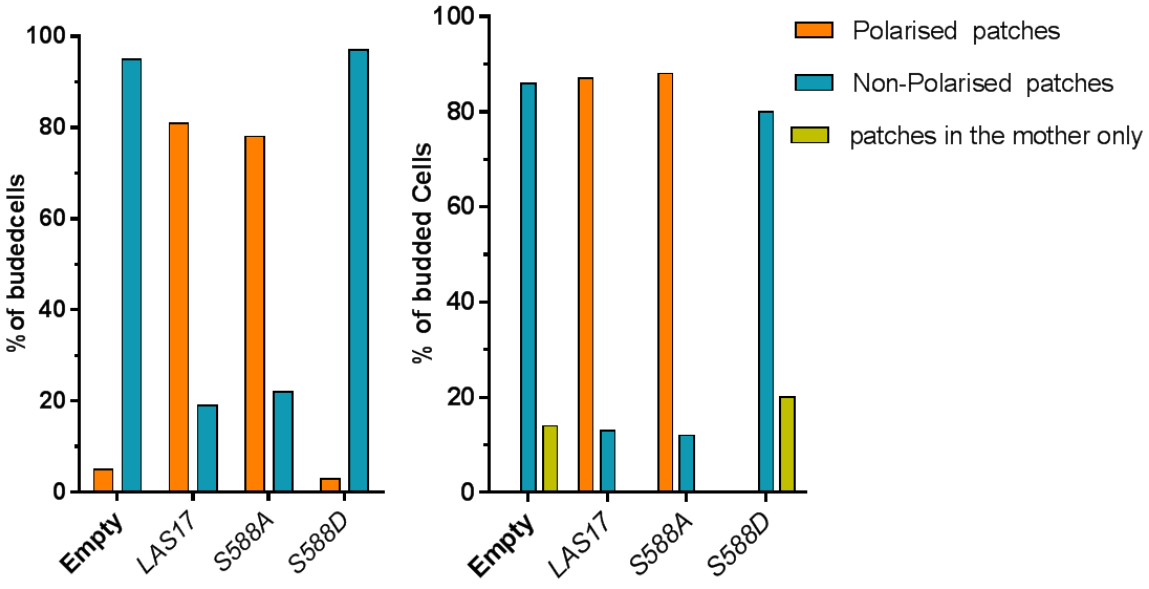

Figure 3.4: Actin cytoskeleton of *LAS17* deletion strains expressing phosphomutants.

(A) Representative images showing Rhodamine-Phalloidin staining of *las17*Δ cells carrying wt, empty plasmids, and mutants *S588A/D*, scale bar 2µm.
(B) Bar graphs showing percentage of actin patch polarisation of the above strains expressing phosphomutants (n=100). Quantifications were based on 2 sets of data obtained from 2 experiments.

To determine the extent of the defect in actin organisation caused by the *S588D* mutant, the distribution of actin cortical patches in budded yeast cells was quantified. Data from the first experiment was shown graphically in figure 3.4.B (left panel) in which the percentage of *las17* null cells with non-polarised actin patches was significantly increased up to 90 % (n=100). However, 78% of cells expressing *LAS17* wild type displayed polarised actin patches while less than 20% of these cells exhibited non-polarised patches. Above 75% of cells expressing *S588A* mutants showed polarised actin patches but 22% exhibited non-polarised phenotype. The number of cells expressing *S588D* was markedly increased to 97% with marked decrease in the number of cells with polarised actin patches (13%).

The bar graph in figure 3.4.B (right panel) showed quantification of the second experiment replicate in which 86% of *las17* null cells revealed non-polarised actin patch (n=100) whilst 14% of cells had their patches positioned in the mother only and one or no patches can be seen in the emerging bud (arrows in figure 3.4.A). Again, the percentage of cells expressing *LAS17* wild type increased to 87% whereas, 13% of these cells showed non-polarised actin patches. Cells expressing the *S588A* mutant exhibited marked increase in polarised actin patches (88%) but, 12% of these cells carried non-polarised actin patches. In contrast, cells expressing the *S588D* mutant showed a significant decrease in actin patch polarisation as 20% of these cells had their patches shifted into the mother cell (left graph), whereas 80% of these cells exhibited non-polarised actin patches.

These results would suggest that, S588 may play a role in maintaining intact actin organisation in yeast cells.

3.6 Effect of S588 phosphomutants on fluid phase endocytosis

The actin cytoskeleton in yeast is linked with endocytosis, and deletion of genes encoding one or more proteins that forms the cortical patches often leads to perturbations in both actin cytoskeleton and endocytosis (Munn et al 1995; Benedetti et al., 1994; Kübler and Riezman, 1993). The aspartate

A. Lucifer –yellow staining of *las17* null strains

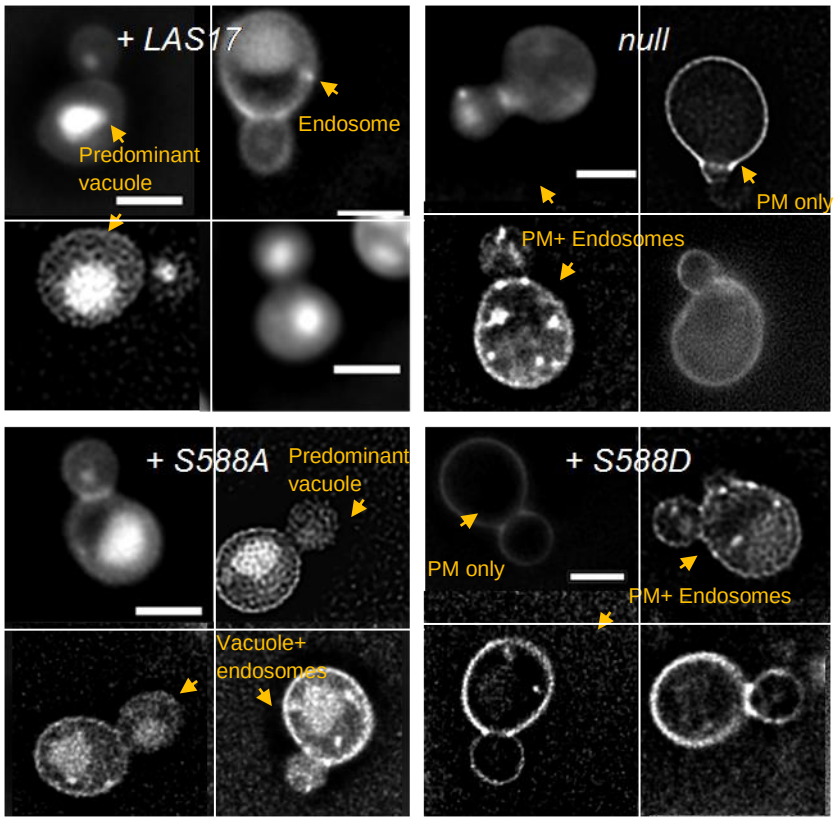

B. Quantification of LY uptake by *las17* null strains after 90 mins.

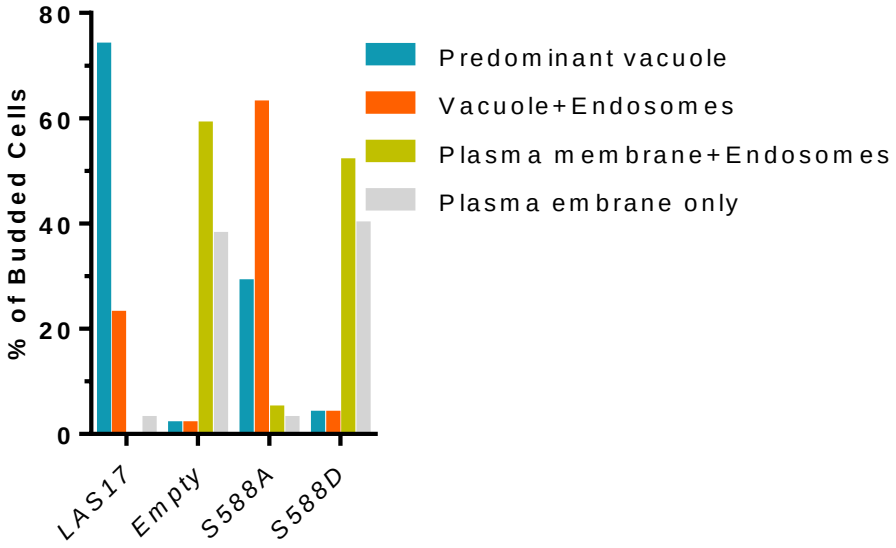

Figure 3.5: Fluid phase endocytosis of expressing phosphomutants.

(A) Representative Images shows Lucifer yellow uptake of *las17*Δ cells carrying wt, empty plasmid, S588A and S588D, scale Bar 2µm. images were obtained from two experiments.
(B) Bar graph showing percentage of Lucifer yellow uptake by cells in (A) (n=100). Phenotypic categories reflect LY uptake by the cells under fluorescent microscope (see figure 3.5.A). Quantification was based on a single set of data.

mutant *S588D* perturbed the actin cytoskeleton in yeast cells, thus it was considered worthwhile to examine whether *las17-S588A/D* phosphomutants affect fluid phase endocytosis. Lucifer yellow (LY) is a non-toxic hydrophobic molecule that was used to assess fluid-phase endocytosis in a time dependent manner. The *las17* deletion strain carrying wild type, an empty, *S588A* and *S588D* plasmids were grown to log phase and stained with Lucifer yellow for 90 minutes to allow uptake of the dye by yeast cells and accumulation into the vacuole (Dulic et al., 1991).

As shown in figure 3.5.A, in wild type cells the dye was internalised after 90 minutes and accumulated into a large vacuole in the mother cell, and a smaller vacuole in the daughter. In the absence of *las17*, there was a marked decrease in Lucifer-yellow uptake and the vast majority of cells still had stained plasma membrane. In addition punctate endosome structures were also observed in some of the *las17* null cells, indicating a delay in trafficking of the dye from the membrane into the vacuole. Cells expressing the *S588A* mutant had a similar phenotype to that observed in wild type cells. In contrast, cells expressing *S588D* mutant exhibited reduced lucifer-yellow uptake, similar to that seen in the null strain.

Subsequent quantification of Lucifer yellow internalisation was assessed as shown in the graph bar in figure 3.5.B. The phenotypic LY uptake of the above cells was divided into four categories: predominantly vacuolar; vacuolar plus endosomes; plasma membrane plus endosomes, and plasma membrane only. As shown in figure 3.5.B, 75% of cells expressing wild type *LAS17* had predominant vacuole staining but 23% of these cells revealed slower uptake with endosomes still staining. In contrast, only 4% of *las17* null cells showed vacuolar uptake of the dye. The total proportion of cells taking up LY in cells expressing the *S588A* mutant was mostly restored as 29% of these cells displayed predominant vacuole and 63% with vacuoles + endosomes. This would suggest a mild delay in LY trafficking to the vacuole. In contrast, cells expressing the *S588D* mutant showed similar proportions to

the *las17* null cells, with 52% of cells exhibiting plasma membrane and endosomal staining, and 40% of cells with no uptake.

These results would suggest that, S588 is important for trafficking from the membrane to the vacuole during endocytosis in yeast.

3.7 Effect of *las17-S588* mutants on yeast vacuolar morphology

Given the major defects in LY uptake caused by *S588D* mutants, further analysis of vacuole morphology was performed by staining the cells with FM4-64 dye.

FM4-64 is a lipophilic stain used to monitor membrane trafficking to the vacuole. As with Lucifer yellow, the uptake could be tracked over time. Logarithmic phase *las17* null cells carrying wild type, an empty plasmid, *S588A* and *S588D* were stained with the dye and incubated at room temperature for 90 minutes (see section 2.8.2).

The *las17* deletion cells carrying *LAS17* wild type, empty and *S588A/D* mutants showed a similar level of FM4-64 uptake as presented in figure 3. 6. A. However, cells exhibited different vacuolar structure, and therefore was classified as follow: normal vacuoles typical for the wild type cells, heterogeneous and fragmented-vacuoles were characteristic for *las17* null cells.

The predominant vacuolar morphology of cells expressing *LAS17* wild type was normal as the majority of these cells contained 1-3 comparable vacuoles. This phenotype was also dominant in the cells expressing *S588A* mutant (figure 3.6.A, arrows indicated). In contrast, the vacuolar system of *las17* null cells was much smaller and mostly classed as fragmented (arrows). The fragmented vacuoles are numerous-small clustered components. This phenotype was also observed in the majority of

A. FM4-64 staining of *las17 null* strains

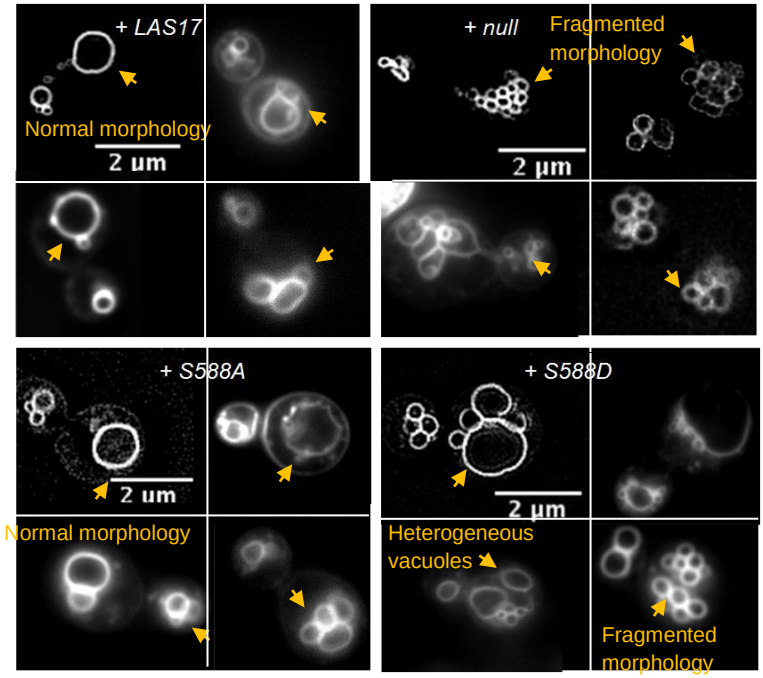

B. Quantification of *las17* null strains strained with FM4-64

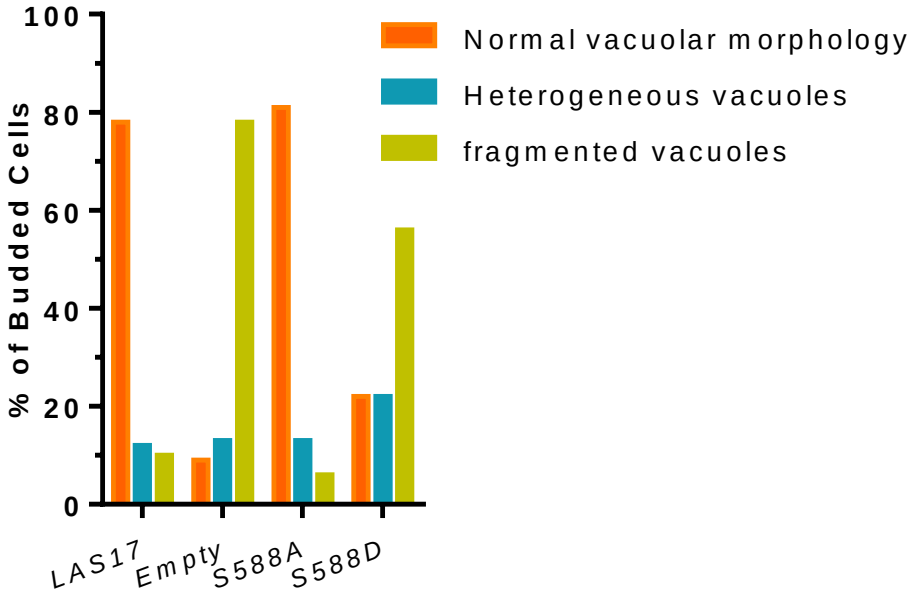

Figure 3.6: Vacuolar morphology of S588 phosphomutants.

(A) The vacuolar phenotype was assessed by FM4-64 staining of *las17*Δ cells carrying wild type, an empty and, S588A/D mutants. Images were taken by fluorescent microscopy, scale bar 2µm.
(B) Bar graph representing the percentage of normal vacuolar morphology and aberrant phenotype in the above cells (n=100). The Quantification was based on single experiment and categories were decided by observing the FM4-64 uptake phenotype in each strain. FM4-64 assay was don**)** e only once.

las17ΔS588D population (figure 3.6.A arrows). As well as fragmented vacuoles, heterogeneous vacuoles were seen in those cells in which the vacuolar system appeared as a large vacuole in the middle of the mother surrounded by smaller ones (figure 3.6.A, arrows). Quantification analysis of FM4-64 staining is depicted in figure (3.6.B) in which, 77% of the cells expressing *LAS17* wild type and 81% of *las17-S588A* mutants exhibited homogeneous vacuolar morphology. The percentage of *las17* deletion cells with fragmented vacuoles increased to 78%, whilst the number of cells expressing *S588D* mutation with fragmented vacuolar phenotype increased to 56%.

The FM4-64 staining data shown that, the vacuolar system of cells expressing *S588D* was severely disrupted which would indicate defects in vacuolar fusion and maybe as a consequence of the abnormal actin phenotype observed in these cells.

3.8 Effect of *las17-S588* mutants on the behaviour of Sla1-GFP marker

Live cell imaging analysis provides a useful tool to examine the dynamic behaviour of proteins at sites of endocytosis. To investigate whether *S588A/D* phosphomutants have an effect on individual endocytic events, the behaviour of the early endocytic coat marker Sla1-GFP was analysed in *las17* deletion cells harbouring wild type, an empty and *S588A*/*D* plasmids. Cells were grown to logarithmic phase and then viewed under fluorescent microscopy and time-lapse movies were acquired over a period of 90 seconds (section 2.8.4). The lifetime of Sla1-GFP patches was measured from the time when the patch appears to the time when it is no longer visible. The mean of at least 30 patches from 8 different cells of each strain were analysed. Kymographs patches from the same movies were generated using ImageJ; these kymographs track the movement of Sla1-GFP at the plasma membrane over time. All results were obtained from a single experiment.

As shown in figure 3.7.A. the Sla1-GFP lifetime in cells expressing *LAS17* (WT) was approximately 25.6 seconds and this value was comparable to

A. Sla1-GFP life time in *las17* phosphomutants

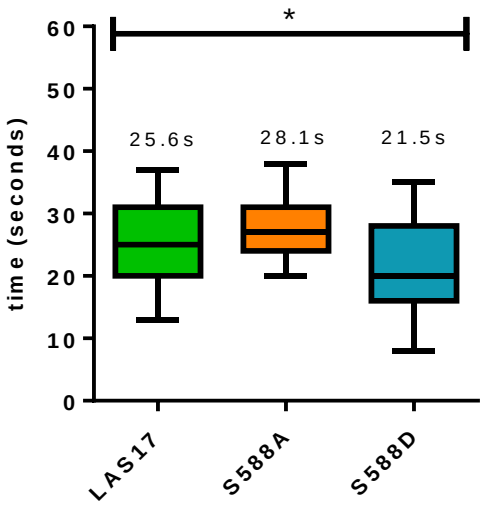

B. invagination of Sla1-GFP patches in *las17*Δ cells

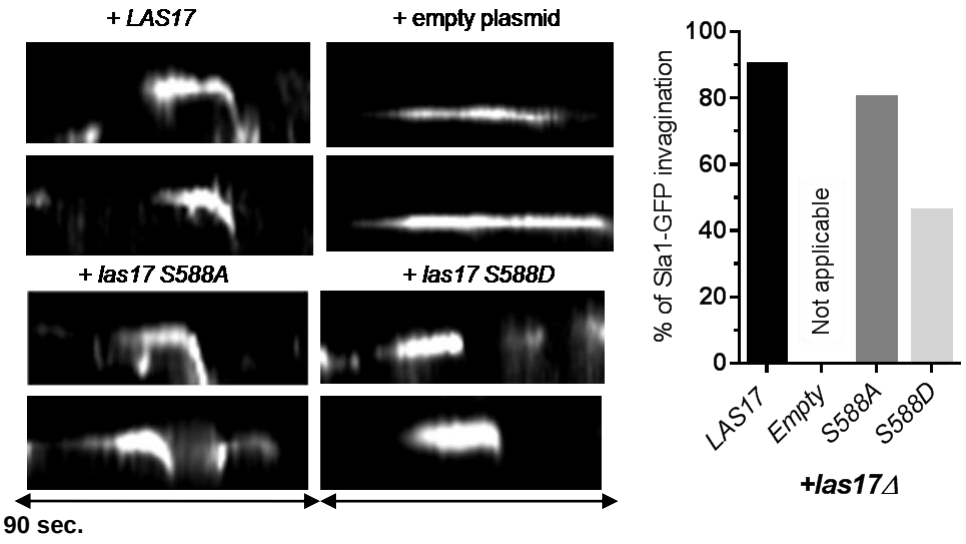

Figure 3.7: The behaviour of Sla1-GFP endocytic marker in *las17* null strains expressing phosphomutants.

(A) Analysis of Sla1GFP life time of cells expressing wt, *S588A* and *S588D*. Error bars represented standard deviation of the mean. The statistical test carried out was one tailed student's *t*-test, $p<0.0001$.

(B) Right panel shows representative kymographs of Sla1-GFP patch movement over 90 seconds in *las17* null cells carrying wt, an empty, *S588A* and *S588D* plasmids. Left panel shows the percentage of at least 30 patches was quantified and graph bar was generated using prism 6 GraphPad in order to reveal the phenotype at invagination stage.

those determined by other authors (Kaksonen et al., 2003; Urbanek et al., 2013). As the majority of Sla1 patches in a null strain were non-motile and had life span longer than the duration of the movie (90 seconds), these were not evaluated. In contrast, the lifetime of Sla1-GFP in cells expressing *S588A* mutants was around 28.1 seconds, whereas cells expressing *S588D* had their Sla1-GFP patches with a life time of 21.1 seconds suggesting a defect in Sla1-GFP function and premature disassembly of the patch.

The patch in figure 3.7.B, right panel shows kymographs from single Sla1 patches in the above cells. In cells expressing *LAS17* (wild type), the Sla1-GFP marker was stationary for several seconds followed by a subsequent steep movement. In contrast, the Sla1-GFP marker in *las17* null strain remained stable and non-motile over 90 seconds, showing no inward movement. Cells expressing *S588A* exhibited similar behavior to that in wild type cells but Sla1-GFP patch internalization in cells expressing *S588D* was defective. The extent of defect in Sla1-GFP patch internalization in each strain was analyzed statistically as shown in figure 3.7.B, left panel. The graph shows that, in wild type cells around 90% patches were able to internalize from the membrane. Similar to wt, the number of internalized Sla1-GFP patches in *S588A* mutant was increased to 80% but only 46% in *S588D* mutant exhibited some inward movement whereas over 50% persisted on the membrane. This would indicate that, *S588D* mutation caused a defect at the invagination stage of endocytosis.

To investigate the defects in Sla1-GFP lifetime in cells expressing *S588A/D* mutants further, patch tracking of a single Sla1-GFP patch was followed in strains expressing *LAS17* (wt), and *S588A/D* mutants using manual tracking in Image J. Figure 3.8.A showed patch tracking of Sla1 patches in wild type cells in which small lateral movements at the plasma membrane were observed prior to rapid invagination. In contrast, the Sla1 patch movement in cells expressing *S588A* showed patches with multiple steps at different time points during the invagination events (blue arrow heads). These observations

A. Sla1-GFP patch tracking

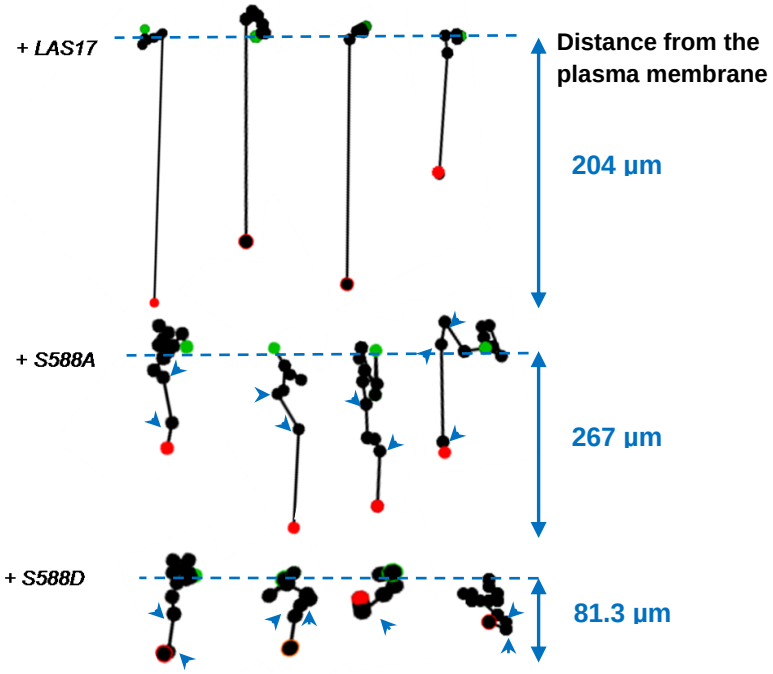

B. Patch intensity profile of *LAS17* (wt) and *S588A/D* mutants

Figure 3.8: Analysis of the dynamic of Sla1-GFP endocytic marker

(A) (Left panel) patch tracking analysis of four independent Sla1 patches in each strain was plotted indicating the initial (green spot) and ultimate (red spot) patch positions at the plane of membrane connected by a line.

(B) Intensity profile analysis of Sla1-GFP over time in cells expressing wild type, and *S588A* and *S588D* phosphomutants. Dashed line represents the time when the endocytic patch reached to the maximum intensity until they disassembled into the cytosol.

would indicate that, Sla1-GFP in cells carrying *S588A* mutation had a slower level of invagination. Sla1 patch movement was markedly affected in cells expressing *S588D* showing more extensive lateral movement at the plane of the membrane, followed by reduced inward movement (headed arrow).

Furthermore, the behaviour of patch internalisation in each strain was observed by measuring the distance the distance from the initial position of the spot to its final position. The Sla1 patches in *S588A* revealed a slow invagination and this was confirmed as the distance between the initial and the end point of Sla1 patch tracking was increased to 276.5 µm. in contrast, patches movement was markedly narrowed to 81.3 µm in *S588D* mutants. These results would suggest that, the internalisation of Sla1 patches was affected by S588A/D mutations but the phenotype was more predominant in *S588D* allele mutant.

As well as a defect in patch behaviour, mutations in components of the endocytic machinery can affect the assembly and disassembly of different proteins at the endocytic sites. This can be detected by following the fluorescence intensity of proteins. Therefore, to determine the changes in Sla1-GFP patch components in the presence of *las17* phosphomutants, an alignment of averaged and normalized intensity of 8 patches was generated using manual tracking tool in ImageJ alogarithm.

Figure 3.8.B showed that, the Sla1 patches in cells expressing *LAS17* (wt), S588A and *S588D* mutants were assembled at the plasma membrane at a similar rate (~10-11 seconds), In *S588D* expressing cells, once these patches reached maximum intensity, they rapidly moved a short distance before disassembling. This finding, would suggest a defect in patch ability to remain stable at the membrane and perform its function (3.8.B). The *S588A* expressing cells in contrast, showed a slower rate of disassembly indicating distinct defects in patch function.

Overall, as judged by patch tracking the S588A mutation causes minor defects in its behaviour but the patch can still internalise. In contrast, S588D seems to cause more marked effects on both patch behaviour and patch internalisation suggesting a link between phosphorylation state and progression through endocytosis.

3.9 Localisation of -GFP tagged Las17S588A/D mutants

To determine whether Las17S588A/D interact directly with actin, the cellular localisation of these mutants was examined using a multi-copy plasmid expressing GFP tagged Las17. Before analysing localization, the effect of GFP tagging Las17 on overall cell growth was assessed to determine whether tag addition was detrimental. *las17* deletion strains expressing Las17-GFP wild type or Las17-GFP bearing S588A/D mutations were grown to log phase and 1:10 serially diluted. Cells were spotted into plates containing synthetic media and incubated at 30˚C and 37˚C for 48 hours. As shown in figure 3.9.A, overexpression of las17 carrying S588D mutation was able to rescue the cell growth at elevated temperature as the cells exhibited similar growth to that seen in the wild type cells. This would suggest that, overexpression of Las17-S588D is required to complement the temperature sensitivity growth of *las17* null.

Further analysis was undertaken in order to determine the affect of S588A/D mutations on protein stability. Whole cell yeast extracts from the above set of cells was prepared as described in section (2.6.1). Each cell extract was loaded into SDS-PAGE gel, electrophoresed and, then western blotted. Production of the GFP tagged proteins from each cell extract was detected using primary antibodies against GFP. Immunobloting analysis in figure 3.9.B revealed that, extracts prepared from cells expressing S588A and S588D mutants were able to express the protein to a similar level as that synthesized in wild type cells. This would indicate that, overproduction of S588A/D mutants did not alter protein stability.

A. the temperature sensitivity of *S588D* mutants was fully rescued

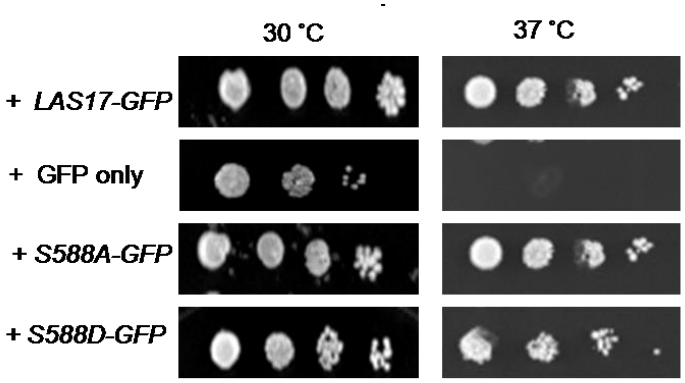

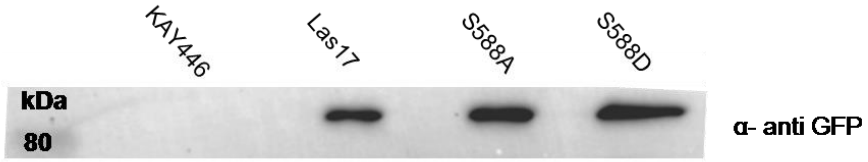

Figure 3.9: Overexpression of *Las17- S588* phosphomutants in vivo

(A) Log phase *las17* deletion strains carrying wild type, an empty plasmid or *S588A/D* mutatans were diluted 10 folds and then spotted onto selective SD plates. The plates were incubated at 30˚C and 37˚C for up to 48 hours.

(B) Immunobloting analysis of total extracts from yeast control strain (KAY446) or strains expressing wild type Las17-GFP, and S588A/D mutants.

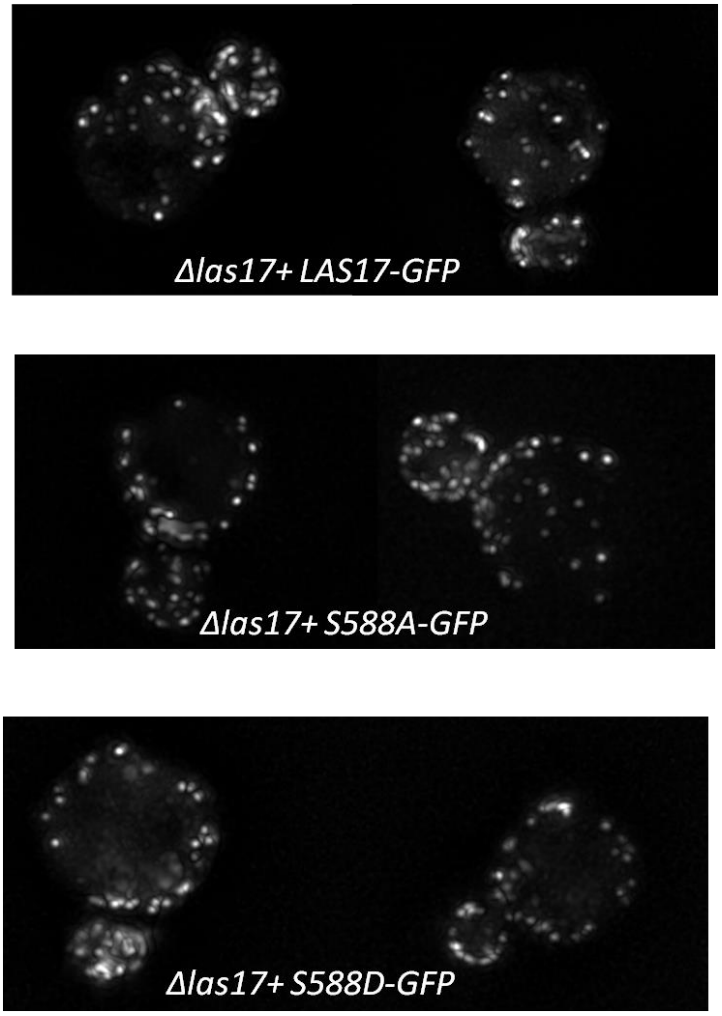

Figure 3.10: Localisation of *Las17- S588* phosphomutants in vivo

las17 deletion strains carrying wild type, an empty plasmid or *S588A/D* mutants were grown to logarithmic phase and viewed under fluorescent microscope. Z-stacks images were acquired at 100x magnification.

To investigate whether the Las17-S588A/D mutants have an impact on the localisation of actin cortical patches, the localisation of fluorescently GFP tagged Las17 in the above cells was assessed using fluorescence microscopy (described in section 2.8.4). Figure 3.10 shows the projection of Z stacks images of Las17-GFP in the wild type and S588A/D mutants. In all of these cells Las17-GFP localisation appeared as bright punctate localising at the cortex of the cell which would suggest that, overexpression of S588D mutant is required to rescue cell growth at high temperature but does not affect Las17 localisation at the endocytic patches.

3.10 Discussion

The carboxyl-terminal region of Las17 in yeast plays a major role in regulating the actin cytoskeleton through binding of monomeric actin and the Arp2/3 complex. In this chapter, the aims were to investigate whether the phosphorylation sites S586 and S588 in the WCA domain contribute to the regulation of Las17 activity in vivo. Initial work was carried out by generating phosphomutants on a plasmid expressing Las17 from its own promoter. Point mutations were generated to substitute S586 and S588 into non phosphorylatable alanine and phosphomimetic aspartate. The temperature sensitivity phenotype associated with *LAS17* deletion cells was examined in the presence of single or double versions of *S586A/D* or *S588A/D* phosphomutants. It was shown that, cells expressing *las17-S586A* or *las17-SS586,588AA* mutants can grow at elevated temperature, but the cells carrying *las17-S588D or las17-SS586,588DD* mutants were temperature sensitive at 37˚C highlighting a temperature sensitivity phenotype caused by the *S588D* mutation. Temperature sensitive growth of yeast strains is a common phenotype associated with mutations in proteins involved in the regulation of the actin cytoskeleton (Novick and Botstein, 1985; Li et al., 1986), 1 M Sorbitol was added to the growth media to analyse whether this phenotypic defect can be rescued by reducing the effects of turgor pressure. Addition of sorbitol has been shown to reduce the need for actin cytoskeleton to support endocytosis in yeast (Agamohammadzadeh and Ayscough et al.,

2009). interestingly, the temperature sensitivity of cells expressing *las17-S588D* mutants was fully rescued. The temperature sensitivity phenotype of the double *las17-SS586,588DD* mutant persisted as the growth of cells expressing this mutation was impaired. This observation led to the idea that, in addition to the role of S588D mutant, mutation of S586 to aspartate may also contribute to the cell growth at elevated temperature/osmotic pressure whereby the function of S586 could be regulated by a different pathway or mechanism to that which contributes to S588 regulation.

In addition, the growth test assessment of the phosphomutants was further analysed by addition of 0.9 M NaCl to the media. In these conditions the growth of cells expressing *las17-S588D* mutants was severely abrogated at 30˚C and 37˚C. Addition of salt can trigger activation of a cell integrity kinase pathway which may impact more indirectly on actin and cell organization, but this phenotype can be rescued by growing the cells on media containing sorbitol. Furthermore, cells expressing *las17-S588D* mutant were slow growing in liquid media as the cells displayed a prolonged generation time (202 min) comparable to null strain growth (Li et al., 1997).

in the next chapter, the connection between actin cytoskeleton and endocytosis in yeast has been widely studied and demonstrated (Munn et al 1995; Benedetti et al., 1994). Given the major defects in actin patch assembly due to the *S588D* mutation, the endocytic functions of *S588A/D* were assessed using vacuolar dyes: Lucifer yellow and FM4-64. The former dye was used to assess fluid-phase endocytosis. Vacuoles are membrane bound organelles which form part of the endocytic trafficking system in yeast, and incubation with lucifer yellow caused vesicles to internalise, fuse with endosomes and subsequently traffic contents to the vacuole. In this study, the majority of cells expressing *S588A* were able to accumulate lucifer-yellow (LY) into a vacuole with minor defects in trafficking to the early endosomal system. In contrast, *S588D* mutants were unable to uptake LY into a vacuole as well as trafficking to the vacuole seems to be severely disrupted.

The delay in trafficking of the dye from the membrane to the vacuole was judged by the prevalence of stained endosome structures. In fact endosome delivery to the vacuole also requires the ability of Las17 to stimulate Arp2/3 complex under conditions in which endocytic internalisation and actin cytoskeleton are normal (Shang et al., 2003, 2005). As cells expressing *S588D* exhibited abnormality in actin patch polarisation (see section 3.5) this would explain the extent of defects associated with endosomal and vacuolar membranes by *S588D* mutant. In addition, problems with vacuolar fusion which also was defective in *S588D* mutants pre-incubated with FM4-64. The majority of *S588D* mutants exhibited abnormal vacuolar phenotype either heterogeneous or fragmented vacuoles. The later phenotype was also observed in *las17ΔWCA* mutant in which the actin organisation was completely normal (Eitzen et al., 2002). The same study showed that, defects in purified yeast vacuoles can be reversed by excessive levels of either Las17WCA domain or calmodulin, factors that are known to interact with and stimulate Arp2/3 activity. Thus, Las17 and Arp2/3 activation was proposed to act downstream of the Rho GTPase Cdc42 and that to modulate actin assembly required for vacuole fusion (Eitzen et al., 2002). Overall results would suggest that S588 is a key residue to regulate many aspects of Las17 function.

A further in vivo study was carried out to investigate the consequences effects of *S588A/D* mutations through investigating real time association of Sla1-GFP patches that assess the invagination stage of endocytosis. Although the average timing of *las17S588A* patch appeared slightly high (28.1 seconds) from that in wild type, the difference is not statistically significant. However, as judged by monitoring individual patch tracking of Sla1-GFP in the S588A mutant, a patch revealed multiple invagination steps suggesting a defect in the ability to undergo effective membrane invagination. In contrast, changing S588 to aspartate caused a significant decrease in Sla1 lifetime with a clear defect in the ability of patches to internalise. The internalisation defects of the patches was confirmed by patch

Tracking whereby the distance from the initial and final position of the patch was reduced to 81.3 µm and this value reflects the extent of defects of Sla1 patches ability to perform intact internalisation compared to the patches in wild type cells. The data suggest that phosphorylation of Las17-S588 may be required at an early stage of endocytosis and the pronounced defects of patch movement associated with the *S588D* mutation suggest that, phosphorylation of this residue is inhibitory to protein function.

Overexpression of Las17S588D mutant allele as a GFP tagged protein was able to rescue the temperature sensitivity phenotype associated with the *las17* null strain and revealed that the mutation does not prevent Las17 localisation at the actin cortical patch. Li et al., (1997) showed that, Las17-GFP localisation was preserved at the cortical actin patches even in the absence of actin cytoskeleton needed for polarised growth, suggesting that Las17 act as stabiliser or scaffold for the actin cytoskeleton and that through its interaction with actin and other patch components (Li et al., 1997; Winter et al., 1999). This is also comparable to overexpression of WASP in tissue culture as it stimulates formation of actin rich structures at which the overexpressed WASP is localised (Symone et al., 1996). This would suggest that, generation of S588D mutation that inactivates perhaps one function of Las17 might restore the ability to interact with actin cytoskeletal proteins and that overexpression would elevate the likehood of this mutant to cause temperature sensitivity phenotype.

Actin nucleation associated with endocytic machinery in yeast is considered to be mainly mediated by the Arp2/3 complex and its strong activator the yeast WASP homologue Las17. Together these proteins promote initiation of branched actin filaments. The Las17 and Arp2/3 complex localises at the cortical actin patches in yeast, and *Las17* depletion resulted in a temperature sensitive phenotype and abnormal actin organisation. Considering all the data, the mutation S588D in the WCA domain of Las17 negatively regulates the overall function of Las17 in cells and is possibly a major regulatory post-translational modification during yeast endocytosis.

Chapter 4:

In vitro Analysis of Las17-S588 Mutants

4.1 Introduction

In cells actin nucleation is mediated by various nucleators such as Arp2/3 complex, and formins (section 1.4.6.1). Arp2/3 complex alone is a weak nucleator and its activation is dependent on NPFs. WASP is the main activator of Arp2/3 complex, and together they mediate the formation of branched actin filaments (Pantaloni et al., 2000). The C-terminus of WASP family proteins share similar domain structures, which may contain 1 or 2 WASP homology2 (WH2) domain, followed by a central (C) and an acidic domain (A). The WH2 domain mediates binding of the actin monomers whereas the (A) is the recognition motif for Arp2/3 complex (Winter et al., 1999). The central region is thought to interact with both actin monomers and Arp2/3 but it less well studied (Kelly et al., 2006).

In vitro experiments based on biochemical assays of actin polymerisation have been central in developing our understanding of the role of specific actin binding proteins in the regulation of actin dynamics. Previous work by the Ayscough lab (Urbanek et al., 2013) had shown that the proline-rich region of Las17 can function independently of Arp2/3 in actin nucleation which raises questions of how the Arp2/3 independent function of Las17 governed by Las17PP domain activity and that dependent on Arp2/3 activity are able to be modulated and function sequentially.

In vivo results presented in chapter 3 of this study showed that, mutation into aspartate at the S588 resulted in major defects in growth at 37 ˚C, and in endocytosis. These cellular processes are regulated by actin turnover suggesting that, the phosphorylation site at S588 in the Las17-WCA domain may regulate Las17 function in vivo. This chapter focuses on understanding the biochemical properties of the S588 phosphomutants through analysing the possible physical interaction of Las17 phosphomutants (S588A/D) with G-actin, and on the overall rate of actin polymerisation in the presence and absence of Arp2/3 complex. Additionally, in order to investigate whether an autoinhibitory effect is possible in Las17 similar to that found in other WASP

family members, the intramolecular interaction between the PP region of Las17 and its C-terminus (WCA) domain was experimentally tested in vitro and in vivo.

4.2 Analysis of the effect of Las17-PWCA-S588 mutants on G-actin binding using GST fusions

Recent work conducted by the Ayscough group has demonstrated that tracts of poly proline (PP) region of Las17 can trigger nucleation and polymerisation of actin (Urbanek et al., 2013). The S588 residue lies in the relatively poorly understood central region of WCA domain. To investigate whether phosphorylation at S588 contributes to the actin binding ability of Las17, glutathione S-transferase (GST) fusions of Las17-PWCA (300-633 a.a) wild type, and Las17-PWCA-S588A/D mutants were expressed and purified from C41 bacterial cells. The GST fusions on beads were incubated with 5 µM a freshly purified muscle G-actin (section 2.7.2). Interaction of the GST fusions with G-actin was detected following centrifugation of the beads as the monomeric and un-bound actin would remain within the supernatant fraction.

As shown in figure 4.1.A, when G-actin was incubated with GST only on beads, the majority of G-actin remained in the supernatant (S) fraction and did not pellet with beads indicating lack of binding. Figure 4.1.B shows that, addition of G-actin to the GST-Las17-PWCA (wt) fusion resulted in clear shift of G-actin and GST-PWCA fusion from the supernatant into the pellet (P) fraction. This binding was expected due to the presence of actin binding WH2 domain. The mutation of S588A in PWCA fragment did not appear to affect the ability of WCA to bind actin as the level of G-actin shifted to the pellet was comparable to that observed with the GST-PWCA wild type. Incubation of G-actin with the GST fusion PWCA-S588D seemed to result in a slightly reduced level of actin in the pellet possibly suggesting lower binding affinity. However, due to technical problems in accurate pipetting of beads for this assay an alternative approach was sought to investigate binding.

A. GST binding assay with G-actin

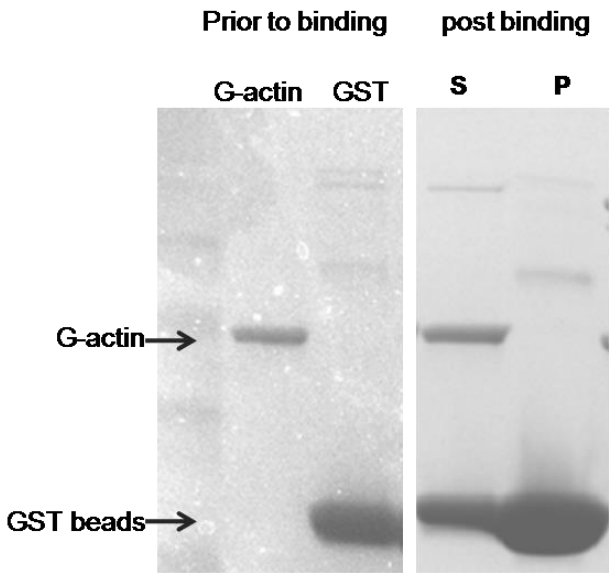

B. Binding of GST fusion PWCA and G-actin

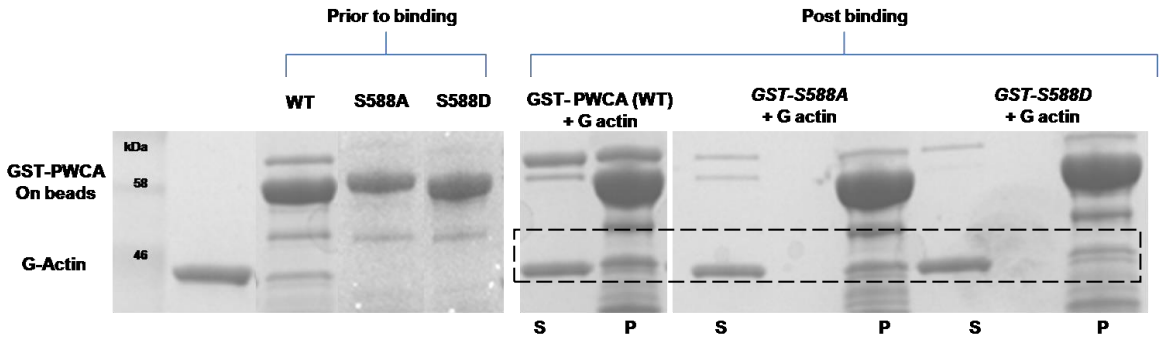

Figure 4.1: GST binding assay of Las17-PWCA phosphomutants

(A) GST only cannot bind to G-actin: 5µM of G-actin was incubated with the bead for an hour and washed with G-buffer; supernatant (S) was separated from beads pellet (P) and run on SDS-PAGE gel.

(B) GST-Las17-PWCA (wt) fragment or PWCA-S588A/D mutants on glutathione beads were incubated with G-actin as in A. The supernatant and the pellet fractions were separated on SDS as above. Variations in loading were due to inaccurate pipetting.

Results were obtained from a single experiment.

4.3 Analysis of the effect of Las17-PWCA-S588D mutant on actin binding using microscale thermophoresis

To further investigate whether the binding between the PWCA-S588D and G-actin was affected by the mutation, Microscale thermophoresis (MST) technique was used. MST analysis is based on measuring the changes of the mobility of fluorescently labelled molecules along temperature gradients (22-45˚C) by detecting the changes in intrinsic properties such as size, charge, and hydration shell of the labelled molecule.

In this experiment, the GST fusions of Las17-PWCA (wt) and PWCA-S588D phosphomutant were purified and cleaved from the GST tag using precission protease. The wild type and S588D proteins were dialysed into G-buffer, and then labelled using the Monolith™ protein labelling kit RED. The binding experiment was performed by preparing 2 fold dilution series of G-actin (unlabelled) in MST buffer an equivalent volume of a 1/10 dilution of fluorescently labelled Las17-PWCA wild type fragments or PWCA-S588D mutant was added (section 2.7.6). Samples were loaded into glass capillaries and the movement of the fluorescent molecules (G-actin/Las17-PWCA or G-actin/PWCA-S588D) was measured by NanoTemper Monolit -115 instrument.

Data were obtained from experiment that has been done once.

Figure 4.2.A, shows curve fits for Las17-PWCA (wt) and G-actin which allowed a K_d of 0.27 µM to be calculated for the binding affinity of Las17-PWCA to the monomeric actin. This value was comparable to the affinity of WCA domain of WASP to actin monomer with affinity of 0.4 µM (Higgs and Pollard, 1999).

In contrast, MST analysis of PWCA-S588D showed that, the PWCA-S588D fragment had a lower affinity for G-actin with a K_d value of 2.1 µM (shown in figure 4.2.B). This data and the GST pull down assay confirmed that, S588D is essential for G-actin binding.

A. MST of Las17-PWCA

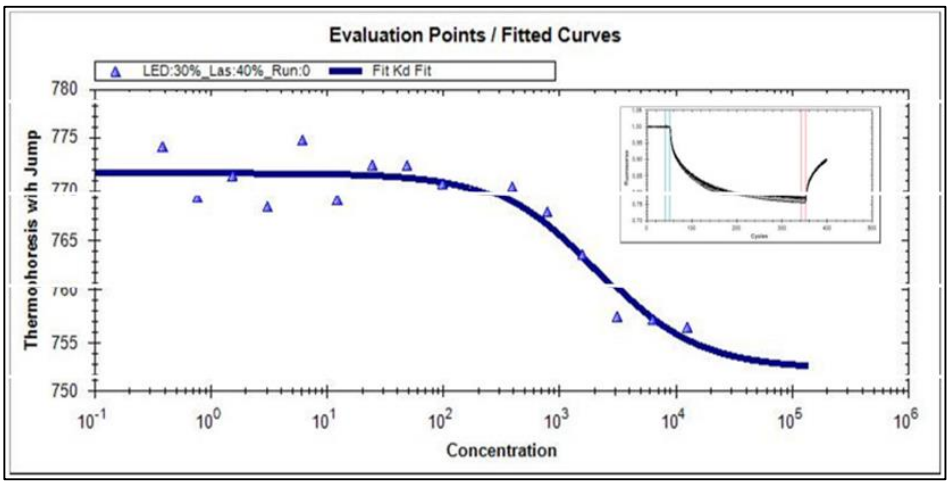

B. MST of PWCA-S588D

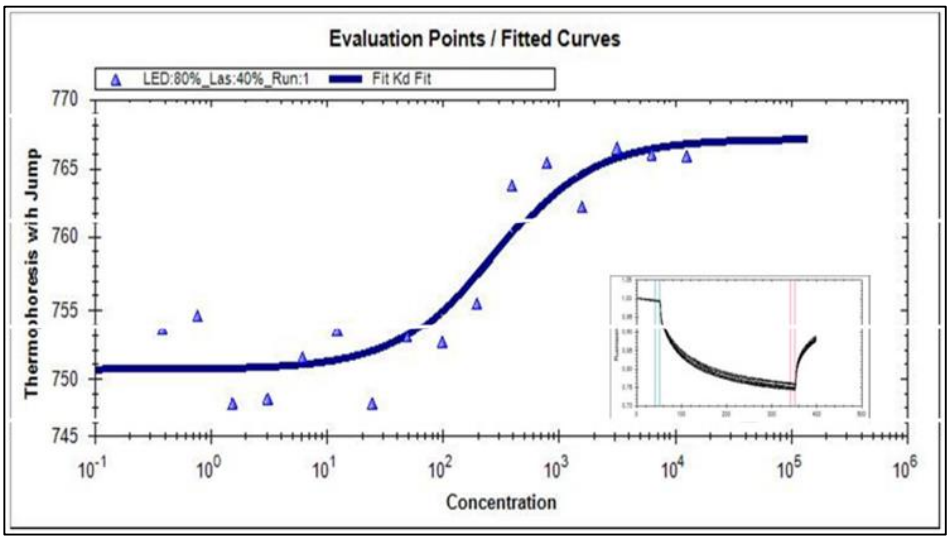

Figure 4.2: Thermophoretic analysis of the interaction of Las17-PWCA and S588D mutant with G-actin

(A) MST traces and curve fits for a1/10 dilution of Las17-PWCA (wt) into the titration of actin monomers. A k_d of 0.27 µM can be derived from the MST assay. Inset triangle (on the right) showed normalised fluorescence of imaged fluorescence inside capillaries that is plotted against time. At the initial state, IR-laser is switched on at *t* = 5 sec., and the fluorescence decrease as the temperature increases, and the labelled complex diffuses away from the heat spot due to thermophoresis.

(B) MST traces analysis of the interaction of PWCA-S588D and G-actin, fitting of the data allowed to determine a k_d of 2.1 µM.

4.4 Analysis of the effect of Las17-PWCA-I555D mutant on the kinetics of actin polymerisation

The process of actin polymerisation can also be studied by following the incorporation of pyrene-actin into actin filaments in the presence of salt. Incorporation of pyrene-actin into a filament produces fluorescence signals that can be detected fluorimetically (Cooper and Pollard, 1982).

Before analysing the effect of the S588 mutants on actin polymerisation, it was important to know what effect of G-actin non binding contributed by Las17PWCA-I555D mutant would have in these experimental conditions. This would allow us to determine whether the S588 reduced actin binding has a similar effect on G-actin polymerisation. A previous PhD student from the Ayscough lab confirmed that, like S588D the I555D at WH2 domain of Las17 inhibited the ability of Las17-PWCA to bind actin in GST pull down assay. Suggesting that, mutation into aspartate at I555D contributes to the majority of actin binding ability of Las17.

Las17-PWCA (wt) and Las17-PWCA-I555D fragments were purified and cleaved from GST-tag. The proteins were buffer exchanged into G-buffer and mixed with, 3 µM G-actin and 3% pyrene-actin in G-buffer or in the presence or absence of 2 nM of Arp2/3 complex. Prior to salt addition, measurements were taken by fluorescence spectrophotometer (Cary Eclipse VARIAN) for 5 minutes to ensure that, there was no polymerisation taking place before the actual experiment. The fluorimeter experiment of the tested proteins was started upon addition of 1x KME salts and the measurements were taken for 120 minutes (section 2.7.6). The polymerisation assays were analysed using two parameters, lag time (first 2 min) and elongation time up to 10 minutes.

Figure 4.3.A, shows the polymerisation profile of the control G-actin+ salt exhibited a lag of about 2 minutes followed by polymerisation. Addition of G-actin+ salt to Arp2/3 complex caused a marked increase in polymerisation rate but no significant effect on nucleation as demonstrated previously (Higgs

and Pollard, 2001).

The effect of addition of Las17-PWCA is also shown in figure 4.3.A. left panel. In this case PWCA causes an increase in polymerisation rate while addition of Arp2/3 is accompanied by a reduction in the lag and therefore nucleation was enhanced. The graph on the right depicted the initial 10 min of actin polymerisation whereby Las17-PWCA solely did not affect the lag and the elongation phase of actin polymerisation. However, the presence of Arp2/3 complex caused a noticeable decrease in the lag time, and the elongation of actin was greatly elevated. This indicates that, the nucleation ability of Arp2/3 complex was enhanced by PWCA fragment of Las17.

Figure 4.3.B depicts the effect of the non G-actin binding mutant Las17-PWCA-I555D, in this case PWCA-I555D addition appeared to decrease the lag in the absence of Ap2/3, but addition of Arp2/3 did not have an effect. Therefore if WH2 can not bind actin, the PWCA fragment cannot activate Arp2/3 complex but its Arp2/3 independent function for nucleation of F-actin is promoted.

4.5 Analysis of the effect of Las17-PWCA-S588 mutants on actin polymerisation

The mutant S588D inhibited binding of G-actin, but the S588A mutant exhibited normal actin binding broadly similar to wild type as judged by GST pull down assay (section 4.2). To investigate whether the binding effects of the phosphomutants (S588A/D) impact on actin-nucleation and filament formation, a pyrene-actin assay was undertaken as described in section 4.4.

As shown in the left graph in figure 4.4.A, the polymerisation level of PWCA-S588A alone was not affected, but the polymerisation rate was slightly enhanced in the presence of Arp2/3 complex. To analyse the effect S588A in

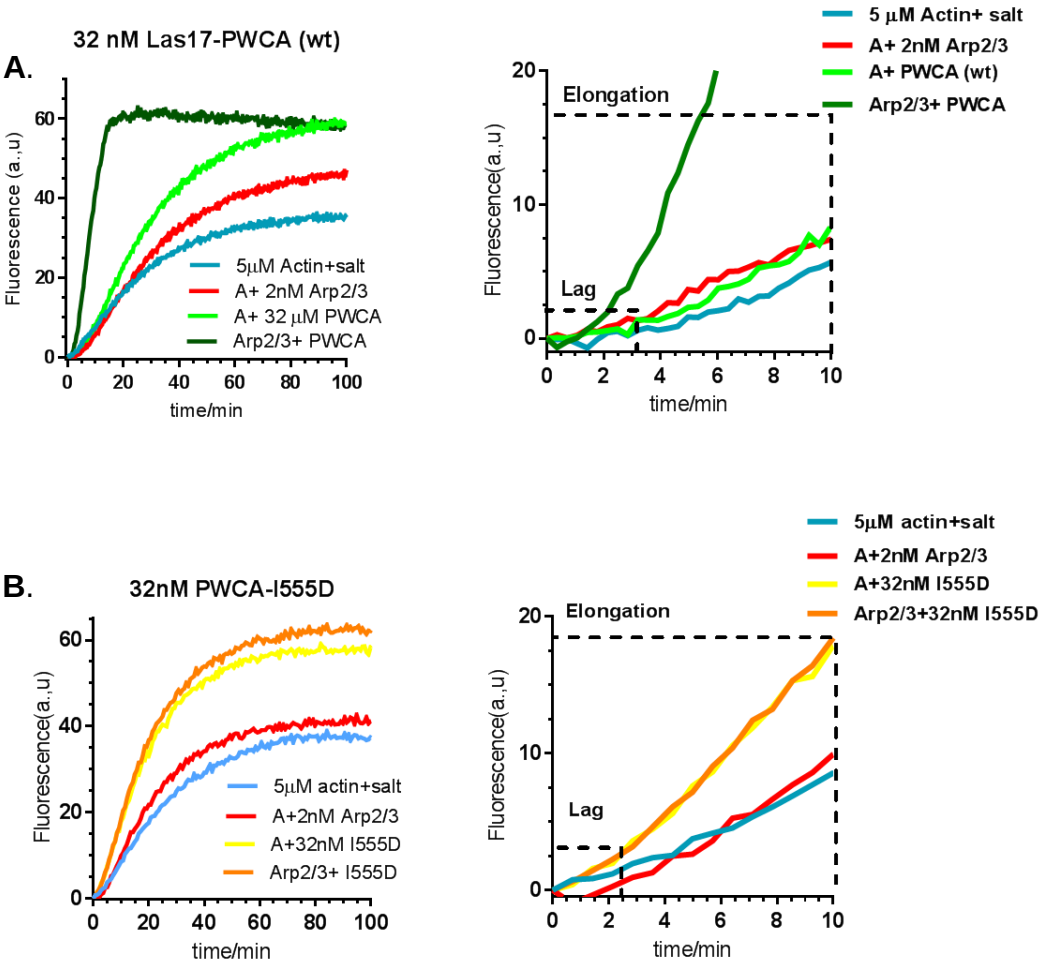

Figure 4.3: G-actin polymerisation of Las17-PWCA and PWCA-I555D mutant.

Polymerisation 5 µM of G-actin (A) (10% labelled pyrene) in the absence or presence of 2 nM of Ap2/3 complex. **(A)** In the left panel, Las17-PWCA was added to 32 nM (the optimum concentration to investigate the changes of the tested parameters) alone causes a small shift of actin polymerisation, but the addition of 2 nM Arp2/3 complex (Arp) enhances the Las17-PWCA to nucleate actin monomers. The right panels are expansions part of figure in the left panels, but the changes in polymerisation kinetic were observed at the first 10 minutes of the assay and this was important to determine whether lag/elongation phases were affected. Upon addition of Arp2/3 complex there was a noticeable decrease in the lag time, and it increases the rate of actin elongation by Las17-PWCA (wt). **(B)** Graph line of polymerisation activities of I555D mutants which revealed similar effect as Las17-PWCA wild type, but it has no additive effects on the polymerisation rate of actin in the presence of Arp2/3 complex (left panel). The right panel showed the changes on actin polymerisation at 10 min of pyrene-actin assay.

The data shown were obtained from a single experiment

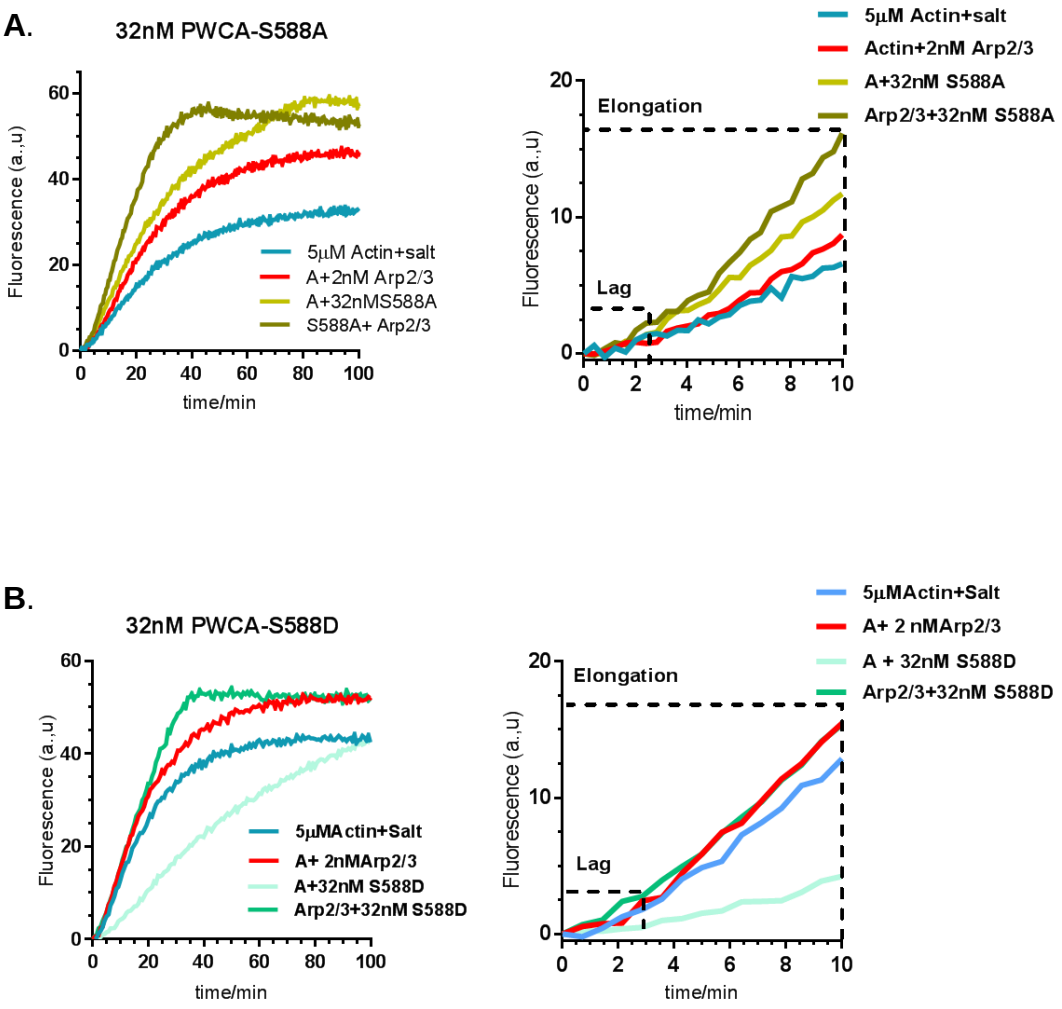

Figure 4.4: G-actin polymerisation of the phosphomutants S588A/D.

(A) Pyrene–actin assay of Las17-PWCA- S588A mutants which showed similar rate of actin nucleation and F-actin elongation as the PWCA (wt) fragment (figure 4.3.A).

(B) Pyrene-actin assay in the presence of Las17-PWCA-S588D.

The data shown were obtained from a single experiment

more details, the first 10 min of the reaction was observed. As shown in the right graph, neither the PWCA-S588A alone nor the PWCA-S588A+Arp2/3 revealed any alteration in the lag time, but the elongation of F-actin by S588A+Arp2/3 was visible at approximately 5-6 minutes of the reaction.

Figure 4.4.B (left panel) showed that, PWCA-S588D alone had a prolonged lag time and a delay in elongation. PWCA-S588D showed no additional increase in polymerisation rate when Arp2/3 was added.

The overall data suggested that, introducing of the S588D mutation reduces actin binding and similar to the I555D mutation does not activate Arp2/3 complex. However, unlike the I555D mutation in the absence of Arp2/3 the S588D also reduces the polymerisation rate. Given the low concentration of All PWCA fragments in this assay, the reason for PWCA-S588D inhibitory effect on polymerisation kinetic is currently unclear.

4.6 Analysis of the effect of Las17-WCA-S588 mutants on actin polymerisation

Given the overall polymerisation rate of Las17-PWCA was impaired by S588D mutation, it was important to determine whether this defect is due to inability of Las17-WCA domain to function. To address this, the coding sequence of *LAS17-WCA* domain was amplified using oligonucleotide OKA 1183 and OKA1184. Sequence corresponds to DNA encoding Las17-WCA (529-633 a.a) was cloned into pGEX6P-1 plasmid (pKA114) using BamH1 and Sal1 restriction enzymes and then verified by sequencing.

In order to examine whether S588A/D phosphomutants influence the ability of Arp2/3 to nucleate and polymerise actin, Mutations at S588 to alanine (S588A) or Aspartate (S588D) were generated in plasmids carrying GST fusion of Las17-WCA and prepared as above.

The effect of S588A/D on actin polymerisation was assessed fluorimetically in the presence of different concentrations of Arp2/3 complex. The polymerisation assay was monitored for up to 150 minutes, and the rate of

actin polymerisation was quantified for each WCA fragment in the presence of Arp2/3 complex. The differences between the tested variants were analysed by quantifying the fitted linear regression of each variant obtained from 2 experiments. Statistics were performed using PrismPad 6 software.

Figure 4.5.A (left panel) showed that, Las17-WCA alone inhibited the actin polymerisation due to the presence of the actin binding domain (WH2). Upon addition of Arp2/3 complex in a concentration dependent manner, the lag phase was reduced resulting in an increase in the polymerisation rate of actin. As displayed in the right graph, the rate of actin elongation of Las17-WCA+Arp2/3 showed a 2 fold increase in the fluorescent intensity indicating effective polymerisation.

Figure 4.5.B, revealed that, WCA-S588A alone appeared to sequester G-actin to a greater extent but it could function with Arp2/3 to increase polymerisation to similar extent as wild type WCA.

Figure 4.5.C showed that, the sequestering ability of Las17-WCA-S588D truncation was similar to that observed in the wild type (figure 4.5.A). In contrast, the rate of polymerisation of actin in the presence of WCA-S588D and Arp2/3 complex was decreased even at higher levels of Arp2/3. Graph on right panel showed that, the rate of actin elongation shown by addition of the WCA-S588D mutant was significantly inhibited, which would indicate that, mutation to aspartate may preclude nucleation and actin filament formation by inhibiting binding of actin and Arp2/3 complex accordingly the rate of actin polymerisation was significantly slowed down.

These data would suggest that, Las17-S588D negatively regulates the function of the WCA domain possibly by inhibiting the Arp2/3 complex binding.

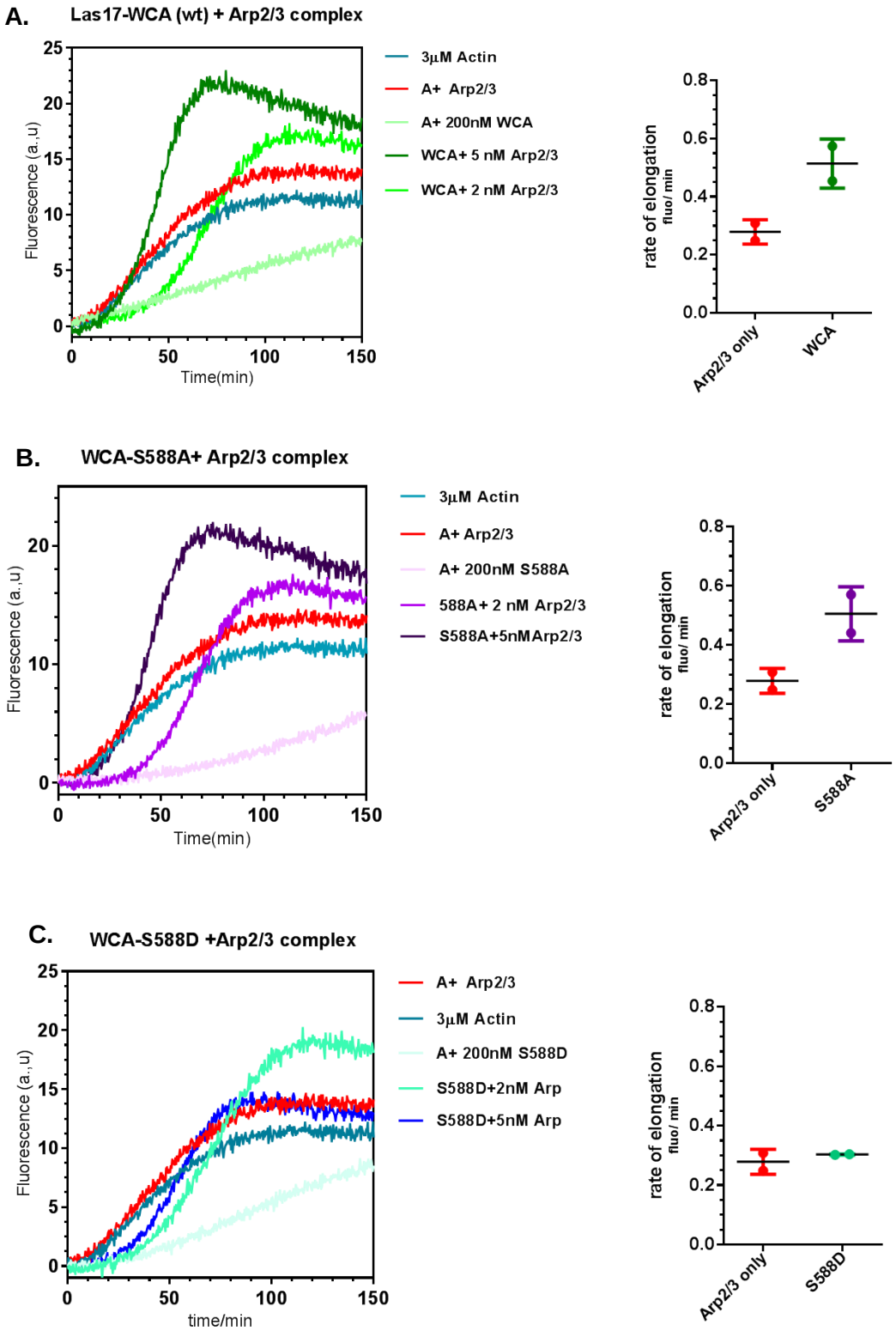

Figure 4.5: Pyrene actin assay of Las17-WCA (A) polymerisation of Las17-WCA wild type, **(B)** LAS17-WCA-S588A, and, **(C)** Las17-WCA-S588D in the presence of two different concentrations of Arp2/3 complex (Arp) 2 nM and 5 nM. Graph bars revealed the elongation rate of each fragment once Arp2/3 was added (average elongation rates were obtained from three data sets).

4.7 Investigation of the intramolecular binding between the PP region and the WCA domain of Las17

The recognition of Arp2/3 independent mechanism activity through the poly-proline (PP) domain indicated possible interplay between PP and the Las17 C-terminal region (WCA domain). In this report it was hypothesised that, Las17 might undergo conformational change which might regulate its Arp2/3 dependent and independent actin-based function. The intramolecular interaction of Las17 was investigated using in vitro and in vivo binding approaches.

4.7.1 Determination of WCA-PP intramolecular binding in vitro

The intramolecular interaction of Las17-WCA domain and its central PP region was examined using GST pull down assay whereby, GST fusion of Las17-PP (a.a 300-536) and Las17-WCA (a.a 529-633) were expressed in BL21 (DE3) cells and purified as described in materials and methods. The GST tag was cleaved from the WCA while GST fusion of Las17-PP fragment was left attached to the beads.

To investigate WCA-PP intramolecular interaction, an equivalent volume of Las17-WCA and Las17-PP immobilised on GST beads were mixed and incubated for 1 hour. The protein samples were sedimented by centrifugation at 3000xg for 3 minutes. The supernatant was removed and transferred into separate tubes, and the beads were washed with buffer to remove the unbound material. Supernatant and pellet were separated by SDS-PAGE gel. As shown in figure 4.6.A, the GST control was unable to bind WCA. In contrast, addition of Las17-WCA fragment to GST-PP fusion resulted in a marked shift of WCA fragment into the pellet fraction along with the GST-PP beads which suggested a binding of these two Las17 domains.

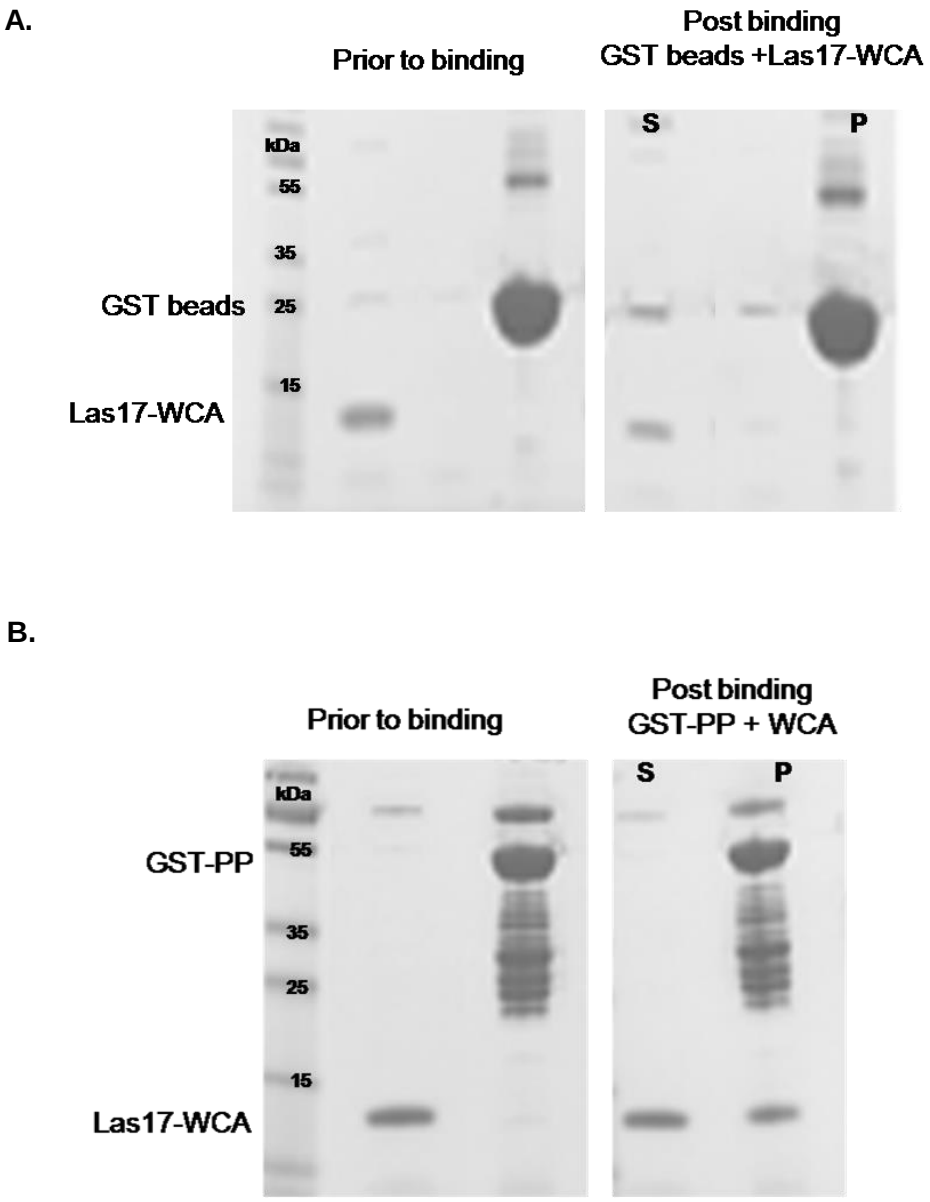

Figure 4.6: Las17-WCA truncation binds to Las17-PP fused GST

(A) GST only and Las17- WCA were purified using GST purification, GST was left on beads while LAS17-WCA fragment was eluted and GST tag and eluted using precession protease enzyme to be detached from GST beads. The gel on the left shows the individual proteins. Gel on the right shows proteins after incubation and serial washes with Las17 buffer.

(B) Las17-PP-GST fusion was left bound to glutathione sepharose beads. The gel on the right showed the proteins individually, whereas the gel on the right clarify Las17-WCA (wt) bound to Las17-PP on GST beads.

Pull down assay was done twice and similar results were obtained in each run.

4.7.2 S588D is essential for intramolecular binding

Results presented above provided evidence of intramolecular interaction of Las17-PP and WCA domains. Therefore, it was of interest to determine whether S588A/D mutants contribute to the WCA-PP intramolecular binding and this was examined in the presence of Las17-WCA with S588A and S588D mutations. Binding assay of the WCA-S588 mutants and PP fused GST was performed as described in 4.7.1.

Figure 4.7.A shows binding of the WCA-S588A fragment with GST fused Las17-PP on beads where a fraction of WCA-S588A truncation is shifted along with GST-PP fusion into the pellet (arrow), suggesting that, S588A did not affect WCA-PP interaction. In contrast, Las17-WCA-S588D truncation displayed a reduced level of binding as the majority of WCA-S588D remained in the supernatant whilst, GST-PP fusion and traces of Las17-WCA were shifted into the pellet fraction (arrow). This indicates that the S588D inhibits an intramolecular interaction between WCA and PP regions of Las17.

4.7.3 Testing WCA-PP intramolecular binding using Yeast Two Hybrid analysis

The mutation S588D in the WCA domain of Las17 inhibited the intramolecular interaction with Las17-PP region in vitro. Therefore to corroborate these results in vivo, yeast two hybrid assays were used. A plasmid expressing Las17-PP fused to Gal4-activation domain (pGAD) was obtained from the lab plasmid collection, whereas Las17-WCA fragment was amplified, and sub cloned into pGBDU-C1 plasmid (pKA168) expressing Gal4-binding domain (pGBD) and verified by sequencing.

Las17-PP fused pGAD plasmid was transformed into MAT a yeast 2 hybrid strain (KAY 711), and the pGAD fusion of Las17-WCA was transformed into α strain (KAY 712). The transformation of each strain was performed using Lithium acetate method and then selected on suitable synthetic drop out

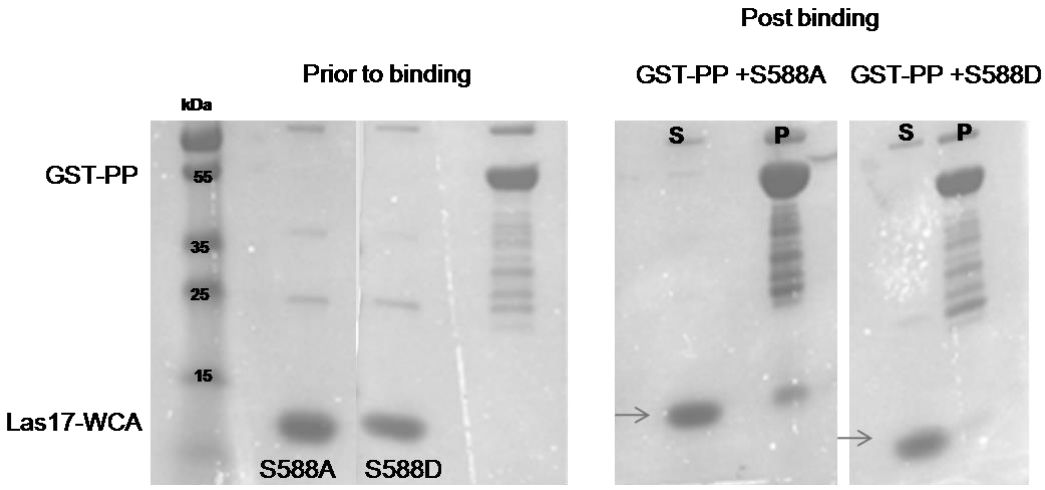

Figure 4.7: Binding assay of WCA-S588 mutant and Las17-PP fused GST

Las17-WCA containing S588A and 588D mutations were purified as GST fragments together with Las17-PP fragment. GST tag was removed from WCA-S588A/D fragments while Las17-PP was left attached to GST beads. Gel on the left shows proteins before binding while gel on the right, shows proteins after interaction. This might suggest that, S588 phosphorylation is important for the stability of the PP-WCA intramolecular interaction.

media. MAT α strain expressing pGAD fused Las17-PP was mated with MAT a strain expressing pGBD fused Las17-WCA, and the grown cells were selected on drop out uracil, leucine plates to select for diploid strain that carried both plasmids. The cells were inoculated into SD liquid media and grown until OD_{600} = 0.6. the culture was then 1/10 serially diluted and spotted into drop out Histidine, uracil, leucine (HUL) plates containing 4 mM or 8 mM of 3-amino1, 2,4-triazole (3AT).

An interaction between the proteins can be determined when the cells are able to grow on a media lacking histidine due to the presence reporter genes which can only be activated upon interaction of the Gal4 activation and binding domains which are fused to the proteins of interest (see figure 2.1, page 86). In this case, the reporter genes used were for histidine biosynthesis and β-galactosidase biosynthesis. Therefore, by growing the cells on drop out his, ura, leu (HUL) plate and interactions can be detected due to the ability of cells to make histidine. However, growth cannot occur if interactions are lost. 3-AT is a competitive inhibitor of Imidazoleglycerol-phosphate dehydratase enzyme required for histidine biosynthesis pathway. 3-AT is commonly used in yeast two hybrid screens to examine for the strength of the interaction between the tested proteins, and also to check for protein-self activation. Alternatively, β-galactosidase assay was also used to screen for β-galactosidase reporter gene whereby the strength of the interaction can be investigated by measuring absorbance at OD_{420nm} of o-nitrophenyl-β-D-galactoside (OPNG) products including O-nitrophenol (yellow product) and galactose.

All figures show representative data obtained from at least three independent experiments.

Figure 4.8.A shows that, except the control cells (Sla1 and Lsb5 hybrid), all the tested strains were unable to grow on plates lacking histidine + 4 mM or 8 mM of 3-AT, which may suggest that, the level of interaction between the tested proteins is insufficient to be detected using this approach. Thus, it was

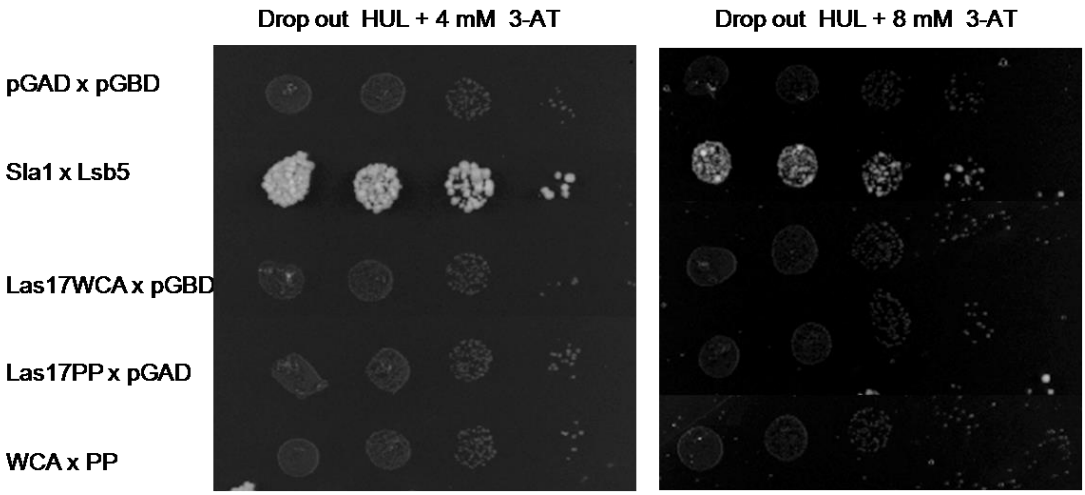

Figure 4.8: Yeast two hybrid analysis of Las17-PP interaction with Las17-WCA domain

Plasmid expressing Las17-WCA fused to Gal4-activation domain (pGAD) truncation or LAS17-PP fused to Gal4-binding domain (pGBD) fragment was transformed into pJ-69-4 (a) and (α) strains and grown on selective media. Strains containing the following hybrid: pGAD x pGBD, LAS17-WCA x pGAD, Las17-PP x pGBD, Sla1xLsb3 (as a positive control), and LAS17-WCA x LAS17-PP were grown until OD_{600}= 0.5 and then 1:10 serially diluted onto drop out ($^{-}$his, $^{-}$ura, $^{-}$leu) plates containing 4 µM or 8 µM 3-AT and incubated at 30˚C for 48 hours. Strain expressing Sla1 xLsb5 was the growth was seen on the tested plates.

thought to quantify the expression level of β-galactosidase activity which might be more sensitive to inspect for this interaction.

Diploid strains expressing the following crosses: empty, Las17-WCA x pGAD; Las17-PP x pGBD; Sla1 x Lsb5; and WCA x PP hybrids were grown in an appropriate liquid media and OD_{600} = 0.6 was taken to account for all numbers. Cells were assayed for β-galactosidase activity as described in section 2.5.9.

As shown in figure 4.9.A, there was a high level of Ortho-nitrophenol production from cells expressing WCA x pGAD, Sla1 x Lsb5, and WCA x PP. However, cells expressing the negative control: WCA x pGAD and PP x pGBD exhibited low activity of β-galactosidase. These result suggested self activation as judged by increasing rate of β-galactosidase activity of the strain harbouring the empty Gal4 DNA binding domain fused Las17-WCA.

To optimise the conditions for protein self-activation, the WCA truncation of Las17 was fused into Gal4-activation domain, whereas the Las17-PP truncation was amplified using PCR and cloned into pGBDU-C1 plasmid. Plasmids were sent to be verified by sequencing. Each successful clone was transformed into the recommended strains above and, then tested for β-galactosidase activity. Results obtained from at least 2 different experiments were shown in figure 4.9.B.

Although the level of O-nitrophenol production was significantly increased in the cells expressing Sla1 x Lsb5, which reflect the validity of the assay at least for this interaction, there was low level of β-galactosidase activity in cells expressing WCA x PP cross which would suggest no interaction between WCA domain and PP region of Las17. Therefore it was concluded that, yeast two hybrid analysis is perhaps inadequate method to be undertaken to analyse for this interaction. The reason for this could be that, PP-WCA interaction is too weak to be detected, or could be that the binding domain (BD) or the activation domain (AD) interferes with the interaction and thus an interaction between the two domains though was not possible.

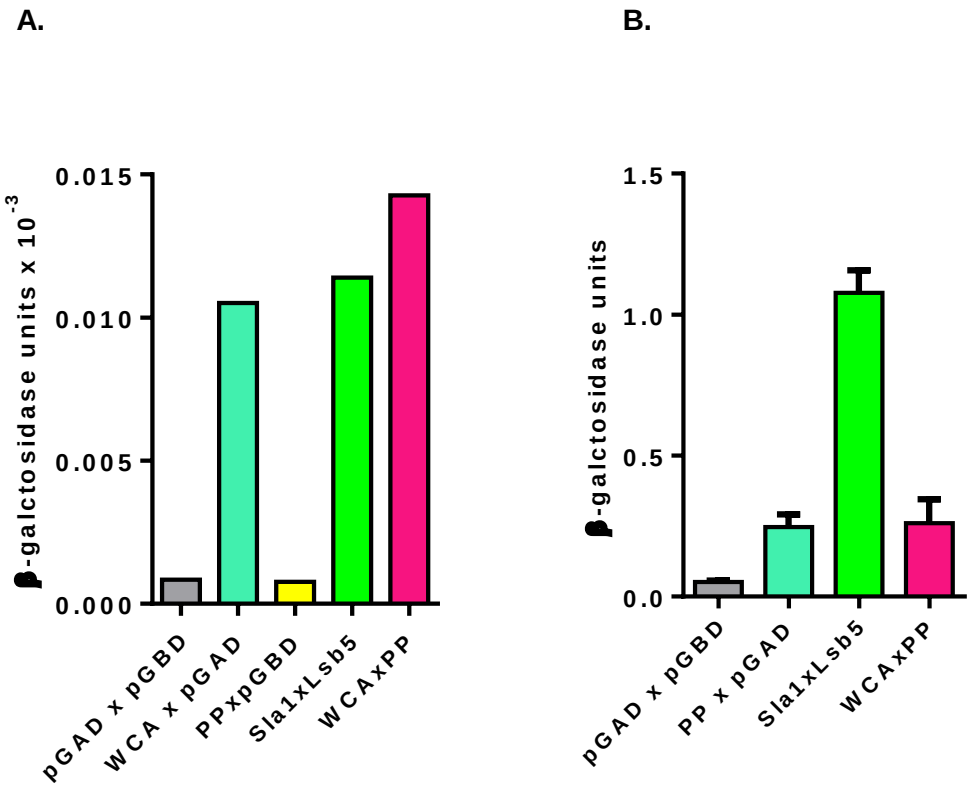

Figure 4.9: β-galactosidase of Las17-PP interaction with Las17-WCA domain

(A) Strains in figure 4.7 were grown in drop out (-ura and -leu) liquid media and assayed for β-galactosidase. Results confirmed self activation.

(B) Plasmid expressing Las17-WCA truncation fused to Gal4-AD and or Las17-PP fused to Gla4-Binding domain were transformed into pJ-69-4 a, and α strains. These cells along with PP x pGBD, Sla1xLsb3, and WCA x PP were grown in SD liquid media and β-galactosidase was assayed. Error bars are standard deviation.

4.8 Discussion

As in mammalian WASP, Las17 in yeast has WCA domain at its C-terminal which is involved in G-actin binding, and nucleation of actin monomers mediated by Arp2/3 complex activation (Winter et al., 1999). In addition, Las17 contains a region with multiple proline tracts and within this the last 36 amino acids (500-536 a.a) were shown to exhibit the greatest contribution for actin binding. This region contains novel actin binding sites that are able to bind either G-actin or F-actin, and allow nucleation and actin filament assembly through a mechanism independent of Las17 –WCA (Robertson et al., 2009; Urbanek et al., 2013).

4.8.1 S588D inhibits binding of monomeric actin

One of the purposes of this work was to determine whether the S588A/D phosphomutants contribute to Las17-WCA domain ability for actin binding, and also to examine whether presence of Arp2/3 complex is essential for actin nucleation and stimulation of actin polymerisation. In this study, it was suggested that, S588 is crucial for the majority of actin based-Las17 functions as changing S588 into aspartate in the Las17PWCA perturbed G-actin association to the Las17-WCA domain, and this may inhibit actin nucleation mediated by Las17-PP region. This conclusion was further validated by MST analysis in which the Las17PWCA-S588D interacting with G-actin revealed reduced disassociation constant (to 2 µM) which might suggest that, S588D hampered the Las17-PWCA ability to bind G-actin. How this binding is affected is however still unknown. It is possible that the conformation of the region allows the ser588 residue to directly affect actin binding at the WH2 domain. Alternatively, there could be another actin binding site that is available in the central domain.

4.8.2 The effect of I555D mutation on Las17-PWCA on Arp2/3 independent and dependent function

Before testing the effect of S588A/D mutants on Las17 NPF activity in vitro, it was of interest to determine the effect of I555D mutation on the kinetics of actin polymerisation mediated by Arp2/3 complex. As judged by pyrene-actin

assay it was found that perturbing the WH2 domain actin binding site through I555D did not disrupt the ability of Las17PWCA to nucleate actin filaments. However, it was absolutely required to enhance actin polymerisation mediated by the Arp2/3 complex. This means that Arp2/3 can only increase polymerization if actin is present at the WH2 site (Urbanek et al., 2013).

4.8.3 S588D inhibits actin nucleation mediated by Arp2/3 complex activity

If S588 mutations affected actin nucleation by blocking actin binding at the WH2 site, this would be expected to mimic the I555D mutation described above. Changing S588 to alanine in Las17PWCA exhibited a relatively mild effect and the addition of Arp2/3 continued to induce an increase in polymerization rate. In contrast, Las17-PWCA-S588D fragment showed a striking inhibition of actin polymerisation mediated by Arp2/3 complex. This would confirm that phosphorylation of S588 is important to enhance Las17 NPF to activate Arp2/3 complex. The Las17 polymerisation activity mediated by Arp2/3 complex was further examined by introducing S588A/D mutations into Las17–WCA fragment. The G-actin binding ability of Las17-WCA wild type and S588A/D mutants were similar suggesting that in this context there was little or no effect on the interaction of S588A/D mutants with G-actin. This was surprising as the GST pull down and MST data indicated that S588D affected the interaction with actin, at least in the context of the PWCA fragment. This might suggest that the proline rich region was somehow influencing the actin binding properties of the WCA region.

4.8.4 Intramolecular interactions of Las17-PP region and Las17-WCA domain can be detected

Regulation of actin and Arp2/3 interaction with Las17 based on data presented in this chapter led to the hypothesis of a possible intramolecular binding between PP and WCA domains. As shown by pull down assay the Las17-WCA fragment was shifted into the pellet with PP fragment which would suggest a binding between the two domains. Furthermore, MST assay

was performed by Dr. Ellen Allwood in the Ayscough lab in which an interaction between PP and WCA domains was suggested with a K_d in the nM range. However, further experiments would be required to confirm this result. The possible role of phosphorylation in regulation of the WCA-PP intramolecular binding was investigated in the presence of WCA fragment containing S588A and S588D mutations. It was found that, the binding was not altered by S588A mutation. However, S588D mutation, which mimics the constitutively phosphorylated Las17-WCA, disrupted binding to the Las17-PP region. This result leads us to build a preliminary conclusion in which the WCA-PP intramolecular binding of Las17 is possibly regulated by phosphorylation of S588 which is required to modulate binding of actin monomers and Arp2/3.

Chapter 5:

Further Analysis of Las17 Phosphorylation

Chapter: 5

5.1 Introduction

Endocytosis involves sequential recruitment of more than 60 proteins that form the endocytic patch and regulate membrane invagination, and vesicle scission. Actin polymerisation is required during endocytosis to provide the force that drives membrane internalisation and vesicle scission. In eukaryotes the Arp2/3 complex is central to regulate remodelling of the actin filaments at sites of endocytosis. The Arp2/3 complex activation in yeast is dependent upon various NPFs including Las17, Myo3/5, and Pan1. However, the WASP homologue, Las17 is considered to be the prime activator of the Arp2/3 complex that promotes actin polymerisation during endocytosis. As well as the G-actin binding WH2 domain, the presence of additional actin binding regions in its poly-proline PP region has been shown to add to Las17 NPF activity (Urbanek et al., 2013). As shown in chapter 4, unlike the WCA domain, the actin binding motifs in the PP region can nucleate actin independently of Arp2/3 complex activity (figure 4.3.B). This may suggest that, Las17 functions in a sequential manner whereby actin nucleation mediated by Las17PP region occurred independently of Arp2/3 activity at early stage of endocytosis while actin nucleation mediated by WCA domain and Arp2/3 complex exhibits the major NPF activity of Las17. The mechanism whereby these functions are regulated is not clear. Unlike WASP itself, the GBD domain is absent in the WAVE protein similar to Las17. WAVE is believed to exist in trans-inhibitory state forming a complex with other ligands and it acts downstream of the Rac GTPase pathway (see section 1.4.7.1.3). Thus, it seems likely that regulatory routes, other than GTPase binding are involved in activating and modulating Las17 and probably other WASP family proteins such as WAVE. However, the role of Las17 activation by signalling pathway has not been shown in yeast endocytosis. The major aim of this part of the study was to investigate the phosphorylation state of Las17 and to identify the possibly kinases that phosphorylate Las17.

5.2 Generation of Las17 antibodies

Western blotting is a frequently used analytical technique that recognises specific proteins when blotted onto a membrane. A specific antibody against the protein of interest is required to visualize the protein. Both levels of expression and post translation modification can be indicated by this approach. Often proteins are tagged with epitopes in order to facilitate western blotting; such tag can however interfere with protein function. Therefore, in order to avoid the use of epitope tags and to investigate the possibility of Las17 phosphorylation, polyclonal antibodies were raised against the PWCA fragment of recombinant Las17. The PWCA region was chosen as it is relatively easy to purify in comparison to the full length version of the protein.

5.2.1 Purification of recombinant Las17-PWCA fragment

The Las17 PWCA (amino acids 300-633) fragment was overexpressed in C41-(DE3) *E*. *coli* strain and then purified using a GST fusion purification method (section 2.6.4). The use of commercial C41-(DE3) competent cells was effective for induction of the recombinant Las17 protein and reduced the toxicity caused to the host cells. However, the recombinant Las17 fragment was commonly co-purified with a higher molecular weight protein. The co-purified contaminant was about 70 kDa and was considered most probably a chaperone (70kDa Heat shock protein) expressed in *E*. *coli* strains (5.1. left panel). The co-purification of the chaperone in *E. coli* may facilitate the correct folding of proteins and maintain protein in the native state. However, co-purification is also a possible indication that the protein alone might have folding or solubility problems.

As purified material was preferable for raising antibodies; it was important to remove the contaminating band from the protein. Several different methods were used, including gel filtration which was performed by a post doctoral research assistant in the lab (Personal communication with Dr. Ellen

Allwood). Elimination of the chaperone band however also resulted in loss of a vast majority of Las17.

An alternative method was undertaken in which Las17 was separated from the contaminating band by SDS-PAGE. The band corresponding to Las17 (~45 kDa) was excised from the gel and then subjected to the electro-elution. The electro-elution of the protein was carried out in a horizontal gel tank in the presence of detergent (1x SDS PAGE running buffer). The gel slices containing Las17-PWCA bands were electrophoresed at 20mA overnight at 4˚C. Prior to analysing the purity of the electro-eluted Las17-PWCA, the dilute protein mixture was concentrated by mixing the protein sample with Strata Clean resins (Stratagen), briefly centrifuged, and then analysed on SDS-PAGE gel (figure 5.1, right panel).

Several Las17-PWCA purifications were performed with the purpose of obtaining a final concentration of 1 mg/ml protein cleaved from GST. To this end, the electro-elution method led to very significant loss of Las17, and was therefore considered to be unsuitable.

Eventually it was decided to raise the antibodies by injecting post-mashed gel slice containing Las17 fragment into the host animals directly.

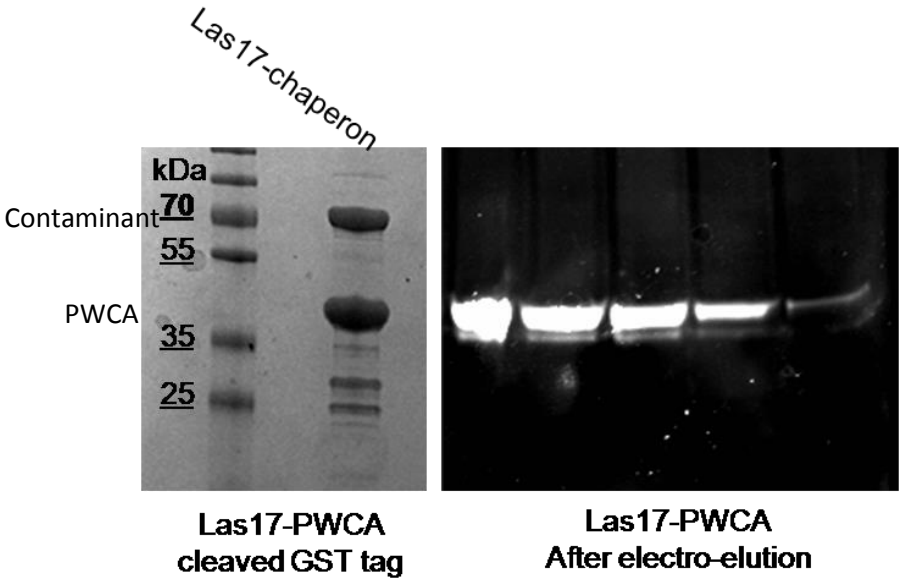

Figure 5.1: Purification of Las17-PWCA fragment to generate Las17 antibodies.

Las17-PWCA was GST purified from *E.coli* bacterial cell, the GST tag was cleaved using by incubation GST-LAS17 fusion on beads with precission protease overnight at 4˚C. The cleaved Las17 –PWCA was run on SDS-PAGE and the gel was stained with Coomassie and destained to visualise the protein (left panel). Las17-PWCA band was excised from the gel and the protein was electro-eluted in the presence of SDS buffer at 20mA overnight at 4˚C. The protein was concentrated using strata resins. Fractions of Las17-PWCA were checked for purity by running on SDS-UV gel (right panel). The Las17-PWCA was then buffer exchanged into PBS buffer.

5.2.2 Immunization of the antigen

The procedures for producing Las17 antibodies were carried out in Cambridge Research Biochemical institute. Three rats were chosen for raising Las17-PWCA polyclonal antibodies. Three rats were injected in a period of 4 weeks intervals so that a total of 8 immunizations were performed and 3 bleeds were harvested subsequently. The pre-immune bleed was also collected to serve as negative control in the tests.

Three week gaps were allowed between the first and the second injections to ensure that the response of the IgG antibodies to the antigen is boosted. One week later the rats were subjected to the third injection and 0.5 ml of the first bleed was harvested. The fourth and the fifth immunization were carried out in 2 week intervals and 2 ml of the second bleed was collected afterwards. The rats were injected once more and a test blot at this stage revealed no specific antibody binding and so a one month rest period was allowed before proceeding with further injections. Next, subsequent immunization was performed with Las17PWCA in solution instead of the post mashed-gel materials. This step was carried out to test whether this would induce the immune-system of the hosts further. The rats were injected twice with a one week interval between injections and 8 ml of the third bleed was harvested.

The sera of the second and the third bleeds obtained from the three rats were examined against different fragments of Las17 as described below.

5.2.3 Testing the rat sera for Las17 antibodies

To determine the specificity of the purified polyclonal antibodies against the PWCA fragment of Las17, whole yeast cell extracts were prepared from yeast strains expressing the endogenous *LAS17* as a positive control (KAY446) and from a strain lacking *las17* (KAY 472). This acted as a negative control. The purified Las17-PWCA fragment cleaved from GST was examined alongside. 200 µl of each sample was loaded across the width of a single lane 10% SDS-PAGE. The electrophoresed proteins were then

transferred onto PDVF membrane and subjected to a titration experiment.
To determine the optimum concentration of the antibodies, 10 fold dilutions were prepared from the pre-immunized, and bleed 2 sera of the three rats. Dilutions of 1:1000, 1:5000, 1:10000, and 1:20.000 were made up in blocking buffer (depicted in figure 5.2). The membranes were placed on top of the slot blotter and 500 µl of each dilution bleed was loaded onto a separate well and incubated for an hour at room temperature with shaking. The membranes were washed and then incubated with HRP conjugate secondary antibodies for an hour. The proteins on each membrane were then detected using ECL reagents (see section 2.6.10).

The blot of the wild type extract in figure 5.2.A showed that, 1/1000 concentration of the Las17 antibodies obtained from the second bleed of rat 1 and rat 2 were able to recognise a band which corresponded to the Las17 full length size (67 kDa). In contrast, the 67 kDa band was completely absent in the negative control (arrow indicated in figure 5.2.B).

In addition, the antibodies detected further higher molecular Weight bands suggesting that, other proteins are recognised by the antibodies.

The sera obtained from rat 3 did not show antigenicity to any of the tested extracts, therefore it was not examined further.

Figure 5.3 shows blotting analysis of the Las17 antibodies against the purified recombinant Las17-PWCA fragment. The antibodies obtained from rat 1 and 2 were able to recognise a protein at ~34kDa and this band is comparable to the size of Las17-PWCA fragment (arrow). As in the control, other high molecular weight bands were detected.

The Las17 antibodies obtained from the third bleed of rat 1 and 2 were also analysed as described above. Various different dilutions were prepared (1:500, 1:1000, 1:2000, and 1:3000) and tested against different parts of recombinant Las17 including PWCA, PP, and WCA fragments.

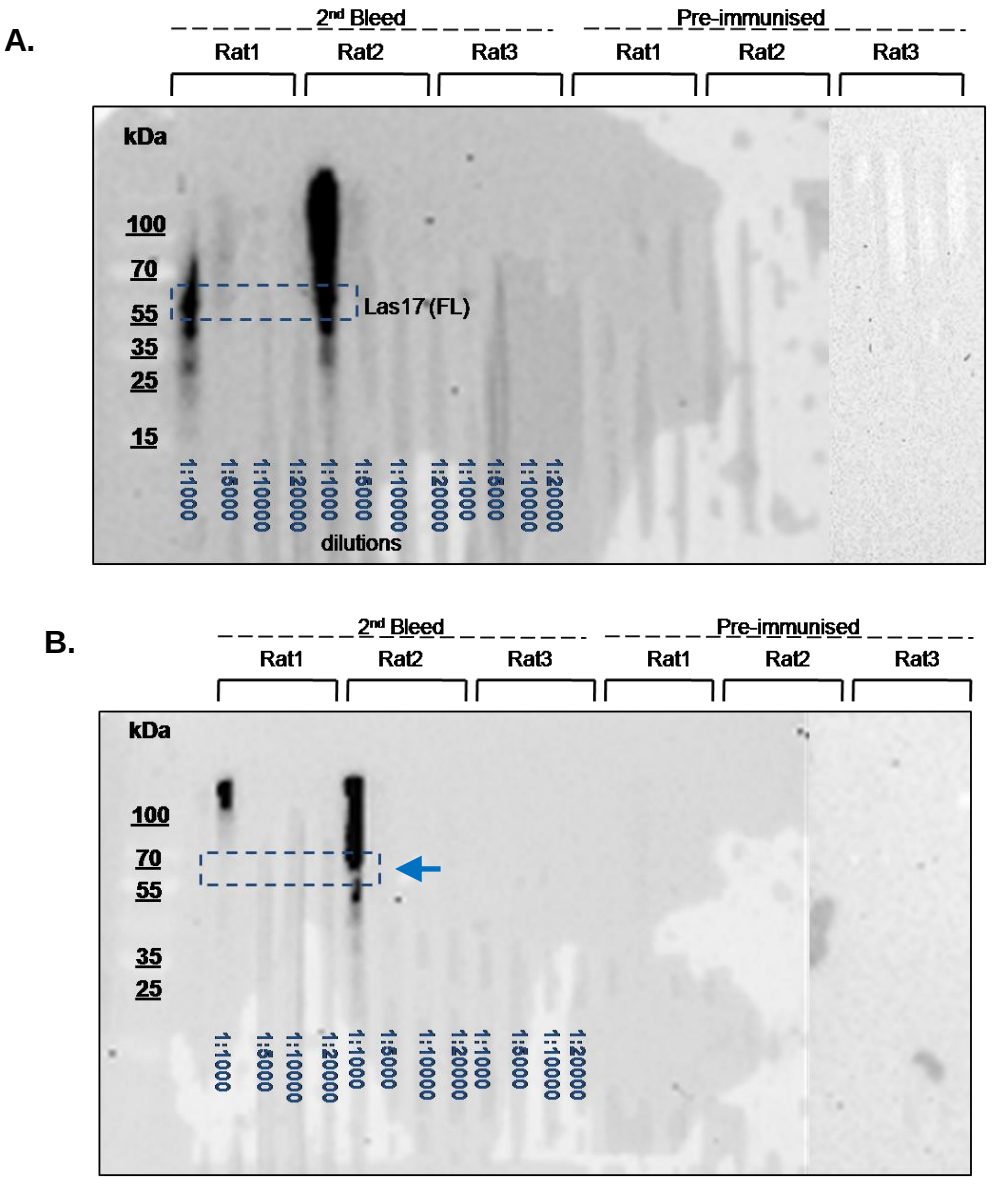

Figure 5.2: Immunobloting analysis of Las17PWCA antibodies

(A) Analysis of yeast extracts prepared from the wild type strain; Serial dilutions were prepared from the antiserum of the second bleed and the pre-immunized anti sera (control) from rat 1,2 and 3. Band between 35 and 55 kDa correspond to Las17PWCA size can be observed from 1:1000 of the second bleed from rat1,rat 2 but this band was absent in rat3

(B) Immunobloting analysis of yeast extract prepared from *las17* deletion strain as in (A).

As shown in figure 5.4.A, the Las17 antibodies of the third bleed recognised the 34 kDa band corresponded to Las17-PWCA fragment (arrow). As well as detecting likely chaperones, lower molecular bands can be observed which may be degradation of Las17.

Immunobloting in figure 5.4.B shows analysis of Las17 antibodies against the central polyproline (PP) region of Las17. A protein band corresponding to Las17-PP size = 24 kDa was visible in each lane (arrow). However, the Las17 antibodies from rat 2 at 1/500 and 1/1000 dilution exhibited higher immunogenicity against the PP fragment as the intensity of the band was elevated (arrow).

Immunobloting analysis of Las17-WCA fragment in figure 5.4.C shows that Las17 antibodies obtained from rat1 had no antigenicity against WCA fragment as only the chaperone bands were observed on the blot. In contrast, a small molecular weight band at 10.5 kDa was recognised by the Las17 antibodies from rat 2. These bands are the expected size of Las17-WCA (arrow) indicating that the Las17 antibodies can detect the Las17-WCA fragment.

Due to time constraints of the study and the problem of visualization of the non-Las17 bands using the antibodies an alternative strategy was considered, in which the full length *LAS17* gene was cloned into a plasmid bearing 3 copies of Influenza Hemagglutinin epitope (3x-HA). The plasmid Las17-3x-HA (KAY1037) expressed *LAS17* under its own promoter and this would then allow for the use of the commercial HA antibodies.

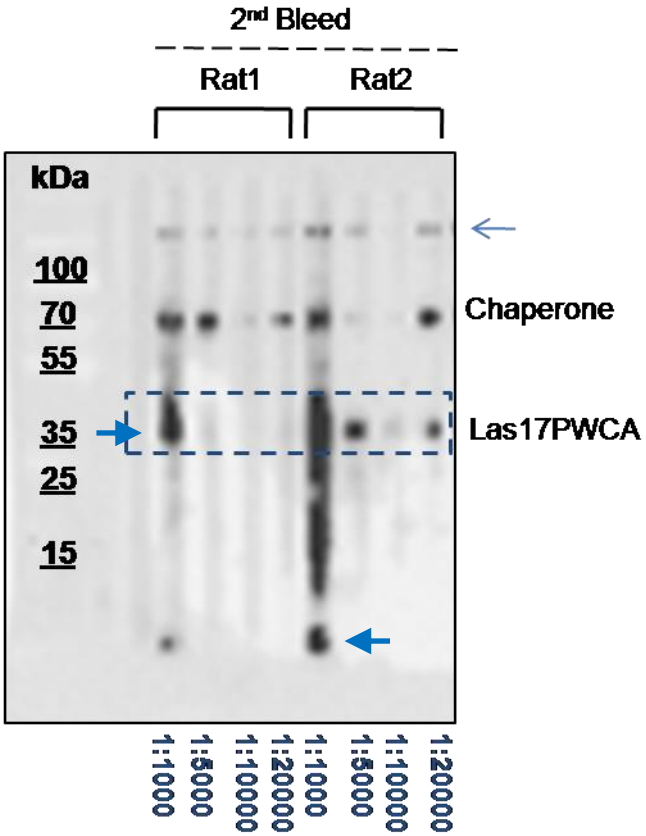

Figure 5.3: Immunobloting analysis of the Las17 antibodies from the second bleed of rat1 and rat 2.

Serial dilutions of the second bleed were prepared and tested against the recombinant Las17PWCA. A protein band corresponded to the size of PWCA fragment was detected and, higher and lower molecular weight bands were also observed.

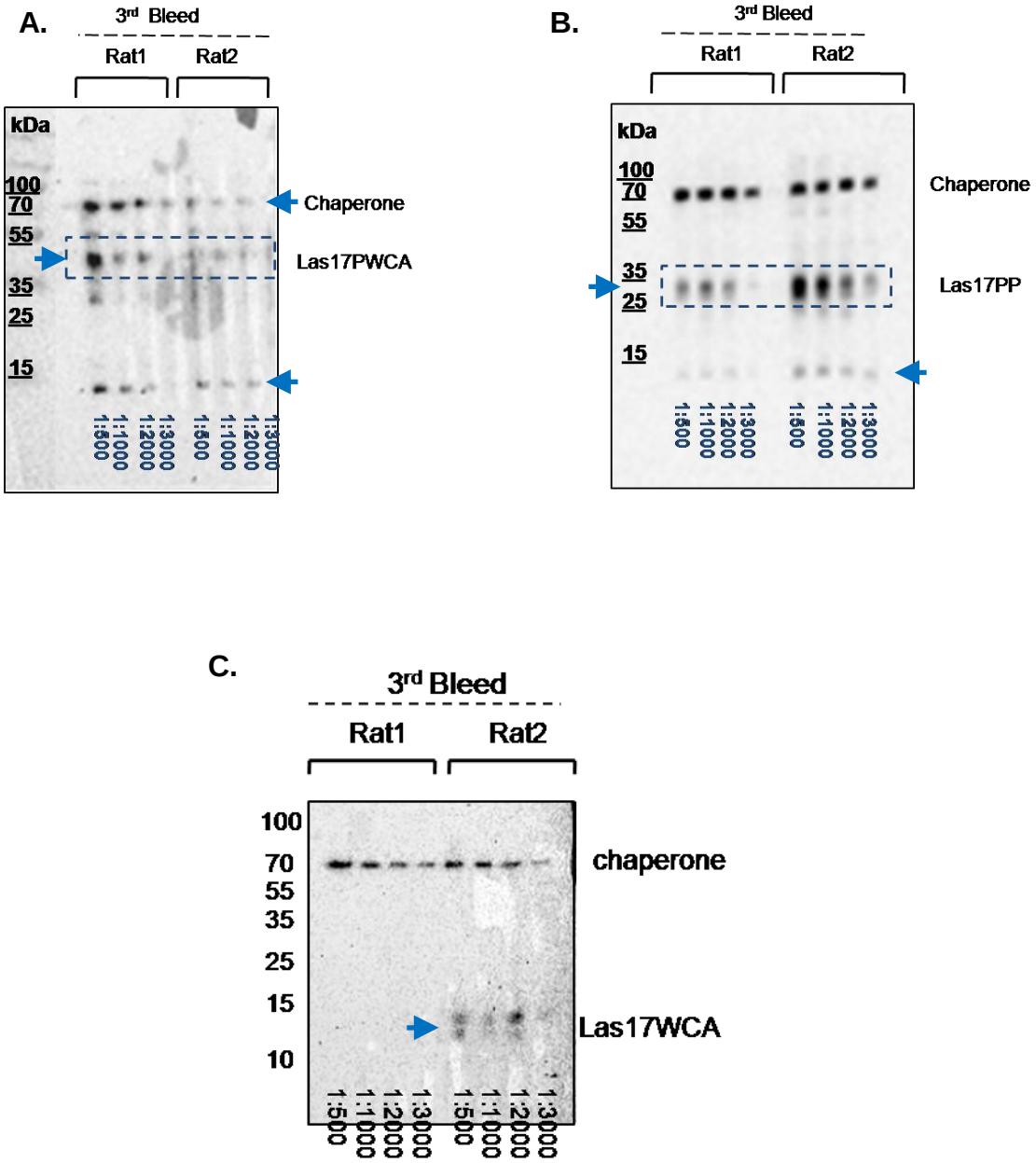

Figure 5.4: Immunobloting analysis of the third bleed of rat 1 and rat 2.

(A) 1:500, 1:1000, 1:2000, and 1:3000 Serial dilutions of the final bleed was prepared from rat1 and rat2 and the specificity of the Las17 antibodies were examined against the recombinant Las17PWCA
(B) The Las17 antibodies tested against the recombinant Las17PP as in A.
(C) Immunobloting analysis of small WCA fragment of Las17.

5.3 Visualization of Las17-3xHA from yeast extract

Activation of human WASP through phosphorylation is well studied but phosphoregulation of the WASP homologue Las17 in yeast is yet to be specifically reported therefore, in this report it was sought to investigate the phosphorylation status of Las17 in vivo.

Wild type strain expressing Las17-3xHA plasmid or *las17* deletion strains carrying either 3xHA empty plasmid or Las17-3xHA plasmid were grown to late log phase OD_{600}= 0.8-1. Pellet of each strain were treated with proteases and phosphatase inhibitors to prevent protein degradation and dephosphorylation by endogenous enzymes. The whole cell extract of the above yeast strains were prepared as described in section 2.6.1 and an equal amount of each lysate was then separated on 6% SDS-PAGE gel. To determine possible modification of Las17, the proteins were transferred onto nitrocellulose membrane and detected by western blot using alkaline phosphatase conjugated secondary antibodies. Figure 5.5.A shows immunobloting analysis of Las17-3xHA expressed in wild type strain or *las17* deletion strain whereby the Las17 appeared as a broad band (lane 1 and lane 2). The appearance of this band suggested the possibility of a doublet which would suggest that Las17 may be modified by phosphorylation.

To investigate whether this hypothesis is true the migration of Las17-3xHA expressed in the above strains was examined using Phos-tag $^{Mg2+}$ -SDS-PAGE. The Phos-Tag is 1, 3-bis [pyridine-2-ylmethyl) amino] propan-2olate, which contains two sites for binding of divalent such as Mn^{2+} or Zn^{2+}. In aqueous solution the complex Mn^{2+}-Phos-Tag forms a phosphomonoester bond with the phosphate group bound to serine (S) or threonine (T) residue at pH ≥7. Following Phos-Tag binding, the migration of the modified proteins is retarded, permitting the phosphorylated proteins to be separated from their non phosphorylated counterparts.

(A) Analysis of Las17 phospho-species on SDS-PAGE

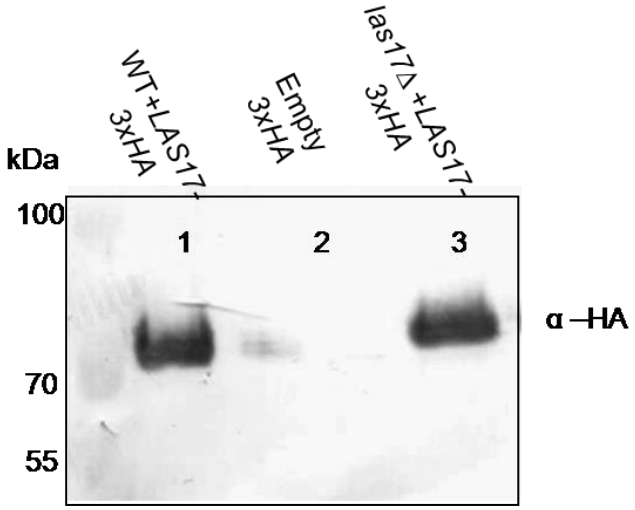

(B) Analysis of Las17 phospho-species on Phos-tag gel

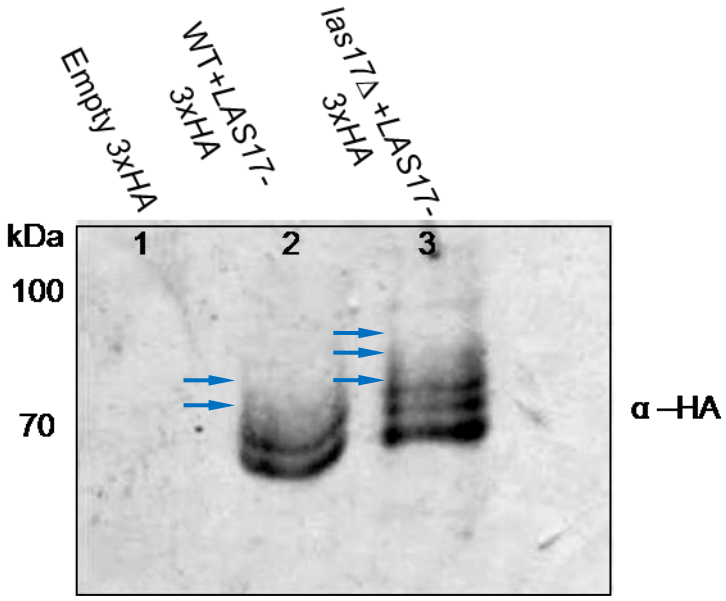

Figure 5.5: Analysis of Las17 phosphoforms in vivo

(A) Yeast crude extracts were prepared from late log phase *las17* deletion cells expressing HA- plasmid (negative control (lane 1), lane 2 wild type cells expressing HA-empty plasmid (positive control), and *las17* deletion cells expressing *LAS17* (lane 3). Samples were loaded on 6% SDS-PAGE and analysed by western blot using α-rat a primary antibodies and alkaline phosphatase conjugated secondary antibodies.
(B) Western blot analysis of set of samples in (A) were analysed on a 10% Phos-tag^{+2}Mn gel. Experiment was repeated at least 3 times.

As shown in figure 5.5.B, Las17-3xHA expressed in wild type strain appeared as two major bands in the blot whereby bands were separated due to phosphate binding indicating phosphorylation (arrows). In contrast, Las17-3xHA expressed in las17 deletion strain showed three major bands can be observed (arrows). This pattern indicates that other species of Las17 are present. These data support the idea that, Las17-3xHA is phosphorylated in vivo. In addition to the major bands there is also a higher molecular weight smear possibly indicating further minor phosphorylation events. The reason for the presence of extra phosphoforms of Las17-3xHA expressed in *las17* null background is unclear but it could be that, these cells undergo compensatory changes due to the loss of the endogenous *LAS17* or that, the HA tag potentially interferes with the normal function of Las17 and in these cells there is no endogenous Las17 present.

To examine the second possibility, the function of the actin marker Abp1-GFP was assessed in cells carrying just the HA tagged Las17.

5.4 Effect of the 3xHA tagged Las17 expression on the behaviour of Abp1-GFP actin marker

As described in section 5.1.2, the number of Las17 phosphorylated forms was different in wild type and *las17* null strains which could be attributed to the defects in a number of cellular functions. Las17 is a component of actin cortical patches where the process of endocytosis actively occurs, therefore the impact on the Abp1-GFP lifetime and movement was assessed in wild type or *las17* deletion strains carrying the Las17-3xHA plasmid.

The wild type (KAY 446) or *las17* null (KAY472) yeast strains expressing Las17-3xHA plasmid were transformed with plasmid carrying Abp1-GFP marker (pKA88). An overnight culture was prepared from the grown colonies of each strain and refreshed next day in SD medium until the cell growth reached to the logarithmic phase. The yeast strains (wild type and *las17* null)

expressing both Las17-3xHA and Abp1-GFP marker were then visualised and time lapse movies of Abp1-GFP patches were recorded over periods of 90 seconds. Kymographs of single patches were generated which showed the movement of an endocytic patch at the plasma membrane followed by invagination into the cell.

Figure 5.6.A showed that the Abp1-GFP marker expressed in the wild type had an average lifetime of 19.6 seconds a value comparable to that published elsewhere (Aghamohammadzadeh, et al., 2014; Kaksonen et al., 2005). In contrast, the Abp1-mRFP marker in *las17* null strain carrying Las17-3xHA exhibited a significant increase in the patch lifetime to 31.1 seconds. This indicates that the absence of the endogenous *LAS17* leads to a delay in the assembly and disassembly of components at the endocytic site.

Figure 5.6.B showed kymographs of Abp1 patch in wild type strain in which an individual endocytic patch revealed a small steep movement at the membrane indicating invagination. Around 76% of Abp1 patches in wild type cells exhibited invagination (n=25). In contrast, the Abp1 patches in null strain exhibited pronounced defects in patch movement with only 36% of the patches showing normal invagination. This suggested that, internalisation of Abp1 actin marker was severely defective in the cells in which Las17 was HA tagged. For this reason it was considered most appropriate to investigate phosphorylation in strains also expressing endogenous protein.

A. Abp1- GFP lifetime

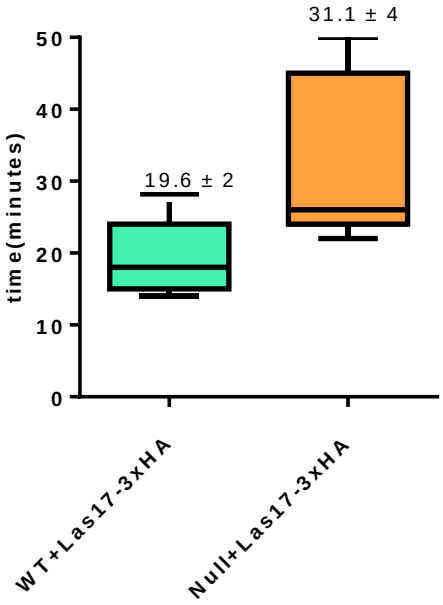

B. Kymographs of the endocytic reporter Abp1-GFP

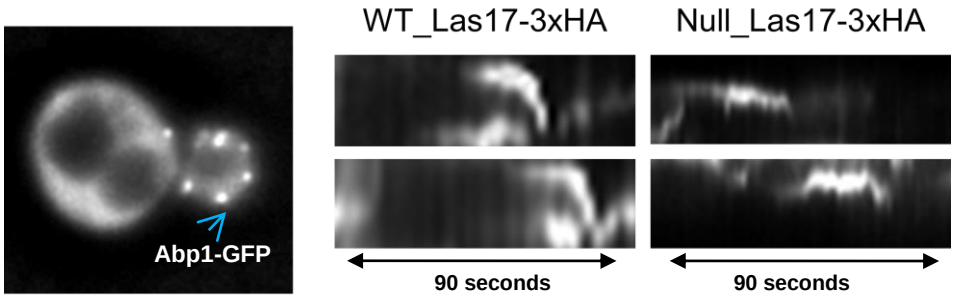

Figure 5.6: Analysis of Abp1-GFP behaviour in wild type and null strains expressing Las17-3xHA plasmid.

(A) The lifespan of Abp1-GFP patches in wild type and *las17* null strains carrying Las17-3xHA plasmid. Error bars are standard deviation.

(B) Time lapse movies of wild type or las17 deletion strains expressing Las17-3xHA plasmids were acquired and kymographs of a single Abp1-GFP patch in each strain were generated using ImageJ software.

5.5 Determination of the kinases responsible for Las17 phosphorylation

Protein kinases in *S. cerevisiae* play an important role in regulation of multiple signalling pathways by phosphorylating specific threonine/serine residues of their substrates. Results in section 5.1.5 confirm that, in cells Las17 can exists in multiple states as the band patterns of Las17 was altered on Phos-tag-SDS gels. To identify the possible kinases that are involved in Las17 phosphorylation in vivo, cells carrying deletion of kinase genes *ark1*, *prk1*, *pho85*, *yck1/2*, and *yak1* were transformed with plasmid bearing Las17-3xHA alongside a wild type strain (KAY446) to serve as a positive control. The cells were grown to log phase, Lysates of each strain was prepared as described in section 2.6.1. Proteins were separated on 10% Mn^{2+}-Phos-tag gel and then analysed by western blot and visualised using alkaline phosphatase.

Most of the kinases investigated had previously been shown to interact genetically or physically with Las17 (Spoko et al., 2006, Michelot et al., 2010; Mok et al., 2010; Ptacek et al., 2005). Yak1 interaction with Las17 has not been reported yet, but the *yak1* deletion strain was in our lab collection. Table (A) in figure 5.7 shows a brief description of the kinases used in this study.

Figure 5.7.B shows western blotting analysis of Las17-3xHA in a wild type strain alongside the kinase deletion backgrounds. In the wild type strain, Las17-3xHA appears as two separated bands indicating phosphorylation. Neither *ark1* nor *prk1* deletion strains revealed any change in Las17 band pattern compared to the wild type strain (lane 2 and 3). In contrast, the loss of *pho85*, *yck1* and its paralogue *yck2* and *yak1* caused changes in the Las17-3xHA band pattern (lanes 3, 4, 5, and 6). The characteristic phosphorylation bands in Las17-3xHA in these kinase backgrounds were more similar to *las17* null strain bearing La17-3xHA plasmid as a sole source of Las17 with 3 main bands.

It is not clear why kinase deletion of *phos85*, *yck1/2*, and *yak1* leads to an increase in the phosphorylation state of the Las17-3xHA. It may indicate that phosphorylation by these kinases is required for progression through endocytosis and that their absence might cause a block in the pathway allowing accumulation of a minor phosphorylated species.

5.6 Separation of Las17 phosphoforms using 2D gel

Distinct phospho-species of Las17 were observed upon expression of Las17-3xHA in *las17* null strain. To investigate these Las17 phospho-species further, 2 dimensional PAGE (2D gel) was undertaken. 2D-gel analysis is used to investigate post translational modifications such as phosphorylation of proteins in more details. The 2D gel mapping system allows separation of the phosphorylated proteins from the protein mixture by generating spots of focused protein. Therefore, the *las17* deletion strain expressing Las17-3xHA (wild type) plasmid was grown to logarithmic phase and then crude extracts were prepared using liquid nitrogen grinding method (described in section 2.6.2). Las17-3xHA was immunopreciptated using anti HA Agarose conjugate and eluted with the hydration buffer. The isoelectric focusing electrophoresis (IEF) was performed with 7 cm neutral dry gel strips (pH 3-10) using Ettan IPGphor3. Proteins were separated on 12% SDS-PAGE gel and then transferred onto PDVF membrane followed by immunobloting using anti HA-rat antibodies. The Las17-3xHA was probed using ECL reagents. The focusing position of the phospho-species in the immobilized pH gradients was first predicted from the Las17 amino acids sequence using the website http://scansite.mit.edu/calc_mw_pi.html where a maximum of 8 of SP or ST forms were suggested. These CdK consensus motifs were searched along the peptide sequence of Las17 (table (A) in figure 5.8).

As shown in figure 5.9, the Las17-3xHA appeared as 2 major spots and a more minor spot similar to bands on the 1 D gel towards the more acidic (+) pI of the gel. However, due to problems optimising spot resolution in each experiment as well as time limits, this approach was not examined further.

A. Kinases used in this study

Kinase	orthologue	family	Function
Ark1/Prk1	AAK/GAK	Ark1/Akl1/Prk1	Regulating actin cortical patches and endocytosis
Pho85	CDK5	cyclin dependent kinase (CDK)	Regulating the cellular response to nutrients and cell cycle establishment
Yck1/2	CKγ1/2	casein kinase1 (CK1)	Endocytosis, and glucose sensing
Yak1	DYRK1A	casein like kinase(CLK)	functions downstream to Ras/PKA signalling pathway in response to glucose sensing

B. deletion kinases expressing Las17-3xHA

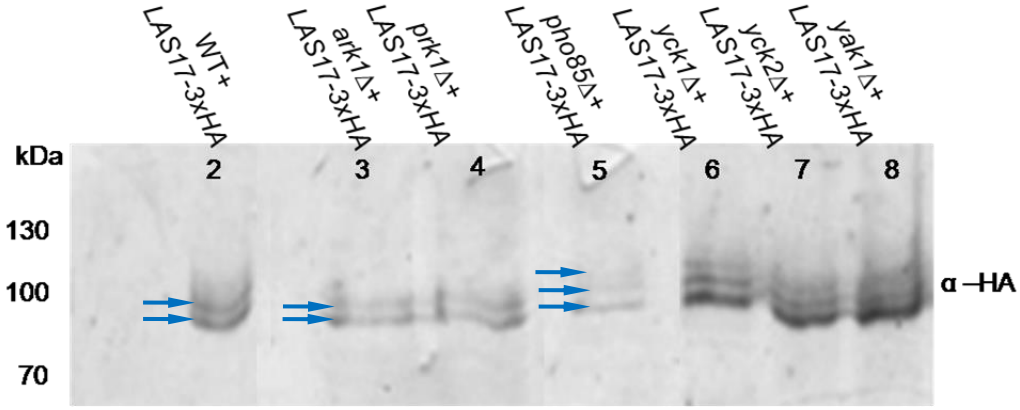

Figure 5.7: Effect of various deletion kinases on Las17-3xHA phosphorylation forms.

(A) A table represents identification of the kinases used in this study.
(B) Las17-3xHA plasmid was transformed into wild type strain (1), or deletion kinases strains such as *pho85*Δ (2), *ark1*Δ (3), *prk1*Δ (4), *yck1*Δ (5), *yck2*Δ (6), and *yak1*Δ (7). Log phase cells were collected, treated with protease and phosphatase inhibitors, and then lysed. 15 µl of each crude extract was loaded and run on 10% phos-tag gel. The proteins were probed with alpha HA antibodies and detected using alkaline phosphatase.

A. pI of predictable phosphosites within Las17 protein

Phosphate	Molecular Weight	Isoelectric Point
0	67589.0690	9.25
1	67667.0330	9.04
2	67744.9970	8.73
3	67822.9610	8.13
4	67900.9250	7.52
5	67978.8890	7.16
6	68056.8530	6.91
7	68134.8170	6.72
8	68212.7810	6.55

B. separation of Las17 phospho-species using 2D gel electrophoresis

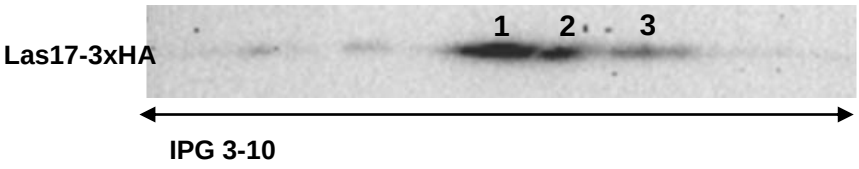

Figure 5.8: two dimensional gel analysis of Las17-3xHA.

(A) Table shown the pI of the potential phosphoresidues within Las17 peptide sequence.

(B) Las17-3xHA was immunopreciptated from *las17* null strain and then separated according to its charge (first dimension) and then to its MW in the second dimension. The Las17-3xHA was probed by rat anti-HA antibodies and the resulted spots 1 and 2 were indicated in the figure.
2D results were based on 3 experiments but interpretable data was obtained only once.

5.7 Identification of a novel Las17 phosphosites by Mass Spectrometry (MS) analysis

Whole phosphproteome mass spec studies have reported that Las17 phosphorylation takes place at multiple serines or threonines (Swaney et al., 2013; Holt., et al 2009; Smolka., et al 2007), but the functional relevance of Las17 phosphorylation has yet to b fully investigated. In conjunction with protein database alogarithms, Mass spectrometry (MS) is used for mapping multiple phosphosites within proteins and has contributed greatly to our understanding of protein regulation. The aim of this section was to verify or detect phosphoresidues within Las17 using MS approach.

Crude extracts were prepared from a large scale culture of *las17* null cells expressing LAS17- 3xHA plasmid, followed by an immunoprecipitation step. The protein was eluted with sample buffer and then run on SDS-PAGE. The gel was stained with Coomassie safe stain™ followed by destaining by several changes with Milli-Q water. The band corresponding to Las17-3xHA was excised and subjected to Trypsin digestion (see section 2.6.14). The extracted peptide mixture was concentrated with formic acid and then analysed by liquid chromatography-tandem mass spectrometry (LC-MS/MS) in cooperation with the biological mass spectrometry facility (biOMICS), Faculty of Science at the University of Sheffield.

In order to boost the analysis for phosphorylated peptides, two mass spectroscopic experiments were employed: multidimensional protein identification technology (MudPIT) and neutral loss multi stage activation (MSA) (Macek et al., 2009; Wu and MacCoss, 2002). In the first mass experiment MudPIT analysis was performed whereby the complex peptide mixture was separated by a triphasic micro-capillary column (reverse phased, cataion exchange, and reversed phase HPLC) and this was placed in line with the tandem mass spectroscopy. The tandem mass spectra generated by the MudPIT were then searched by matching the spectral data and the peptide sequence databases. The MSA method was undertaken as second mass trial in which the search was more directed towards serine (S)

and threonine (T) phosphopeptides if present. S/T peptides can be identified through the loss of H_3PO_4 group which results in 89 Dalton a loss shift from phosphorylated S/T residues while 80 Dalton loss shift occurs by phosphorylated tyrosine. Phosphorylation site localisation probabilities for all peptide match spectra were calculated by phosphoRS algorithm, where the sum of all sequence probabilities had to be equal to 100%.

The raw MS/MS spectra was searched against the Swissprot database with a taxonomy filter of *S. cerevisiae* and interpreted with either Sequest or Mascot for peptide identification. The search applied forward and reverse (decoy database) to allow an estimate of the false positive rate, with mass tolerance of 10 ppm and 0.8kDa for MS1 and MS2. Up to 2 missed cleavages sites per tryptic peptide were allowed in each search. During protein degradation semi tryptic peptides can be generated. Therefore, the analysis was re-run for the second data set with Semi-Trypsin. The search included methionine for oxidation and peptide phosphorylation of serine, tyrosine, and threonine. All the results were filtered to reporter proteins with a minimum of 2 peptides per protein of at least 95% confidence.

The presence of multiple proline repeats within Las17 peptide sequence prevents Trypsin digest. Trypsin digestion occurs effectively after Arginine (K) or Lysine (R) residues, but proline (P) residue can bind to the carboxyl side of either K or R residues thereby inhibiting Trypsin activity. For this reason the outcome of peptide coverage in both experiments was low (25%). The resulting tryptic peptides of Las17 are shown in figure 5.9.A, in which 5 peptides were shown to be phosphorylated at single or multiple sites (headed arrows). MudPIT analysis detected an individual phosphorylated peptide, but the other 4 phosphopeptides were identified by neutral loss search (described below). The Localisation probabilities of the phosphorylated sites by PhosphoRS are depicted in the schematic diagram of Las17 in figure 5.9.B.

A. Las17 peptides resulted from in gel tryptic digestion

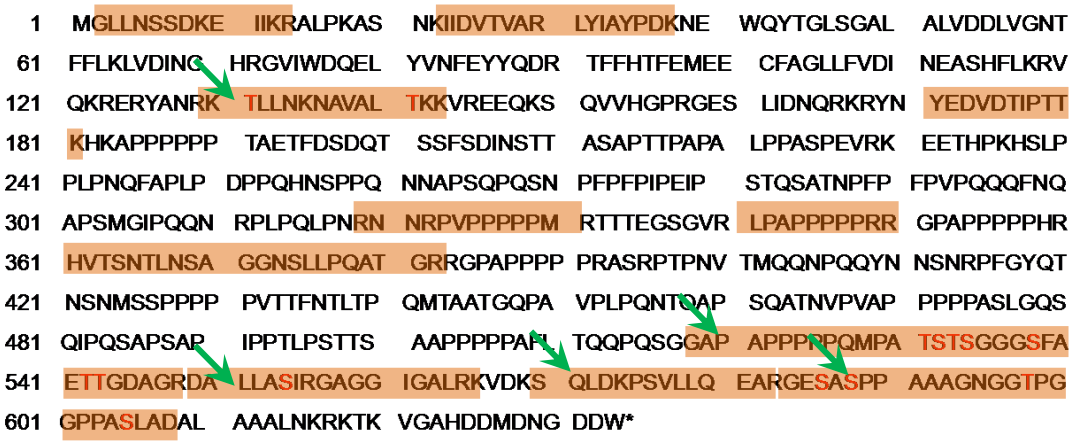

B. Position of phosphorylation sites within the domains of Las17

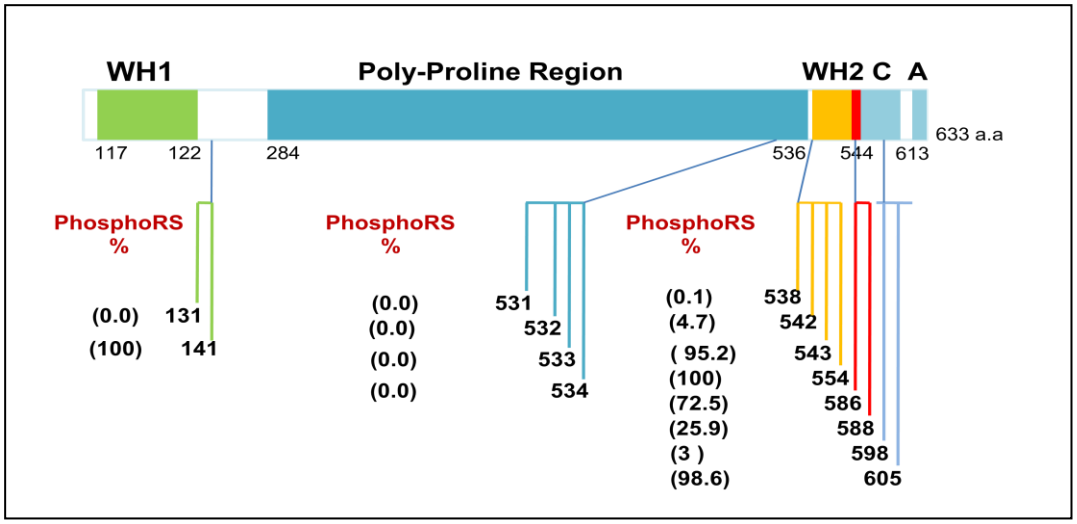

Figure 5.9: Detection and identification of phosphosites in Las17.

(A) Amino acids sequence of Las17 shows the proteolytic tryptic peptides resulted from this study (arrows). The residue labelled in red represents the MS identified phosphosites detected in this study.

(B) Schematic diagram of Las17 domain structures, the layout below illustrates the phosphoresidues recovered from MudPIT or Neutral Loss alogarithms. The phosphoRS software was utilized to find the potential phosphosites localisation of sum of 100 probabilities in each sequence. The colour line in each group set was matched to the Las17 domains through which these residues are positioned.

As shown in figure 5.9.B, just after the end of WH1 domain two threonine residues (T131/141) in a single peptide were scored for phosphorylation. In this case the phosphoRS probability of T141 was indicated as 100% confidence of phosphorylation. Further residues were identified as phosphosites including T531/S532/T534/S535, 538, and T542/543. These residues located within a large peptide that initiate from the C-terminus of PP region and terminates prior to the beginning of the WH2 domain. Among all of these residues, the T543 was rated as the phosphorylated residue with the highest phosphoRS scores (95.2%) suggesting that it is most likely to be phosphorylated.

One peptide containing the conserved RDALLASIR motif lies within the WH2 domain, this was the only phosphopeptide identified by MudPIT and was given a score of 100% at Ser554 as a phosphorylated residue.

The residues S586/588, T598, and S605 were found within the tryptic peptide GESASPPAAAGNGGTPGGPPASL and were scored for phosphorylation. The residues S586/S588 were previously reported as Las17 phosphorylation sites (Holt et al., 2009; Smolka et al., 2007), while the phospho T598 and S605 were not previously reported in this region. S605 displayed the highest confidence of phosphorylation (98.6%) possibly suggesting that, S605 is functionally significant.

The overall MS data would suggest that, the residues T141, T543, S554, S586/588, and S605 are likely to be phosphorylated and might contribute to regulation of Las17 function.

5.8 In vivo analysis of T543 and S554 phosphomutants

Two of the phosphoresidues (T543 and S554) identified lie within the G-actin binding WH2 domain. The conserved I555 residue is also in this region (figure 5.10.A), and I555 mutation into aspartate was shown to be detrimental in nucleation of G-actin in vitro (unpublished work has been done by previous PhD student Adam Smith). Therefore, it was thought valuable to assess the functional importance of these amino acids through changing T543 or S554 into non-phosphorylatable alanine (A) and phosphomimetic aspartate (D). Point mutations were made on a centromeric plasmid carrying Las17 full length expressing Las17 under its own promoter. The phosphomutants (*T543A/D* and *S554A/D*) were verified by sequencing and then transformed into *las17* deletion strains to be analysed in vivo. Due to time constraint all experiments have been done only once.

The temperature sensitivity of *T543A/D* and *S554A/D* mutants was assessed by growing *las17* deletion strains carrying an empty, wild type, *T543A/D*, and *S554A/D* plasmids to logarithmic phase. 1:10 serial dilution of each cell culture was prepared and spotted onto plates containing synthetic media.

Figure 5.10.B. (on the left panel) reveals that, neither *las17-T543A/D* nor *S554A/D* mutant was temperature sensitive as the mutants exhibited similar pattern of growth at 30˚C and 37C˚. As well as growing on plates, the same set of cells were grown in SD liquid medium to investigate their growth rate over time. In all cases cells exhibited wild type or near wild type growth. Indicating that, *las17-T543* and *las17-S554* mutants are not temperature sensitive as they were able to grow normally at 37˚C.

A. Sequence alignment of WH2 in WASP family members

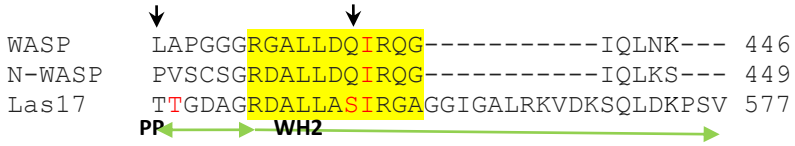

B. Growth of *T543A/D* and *S554A/D* mutants

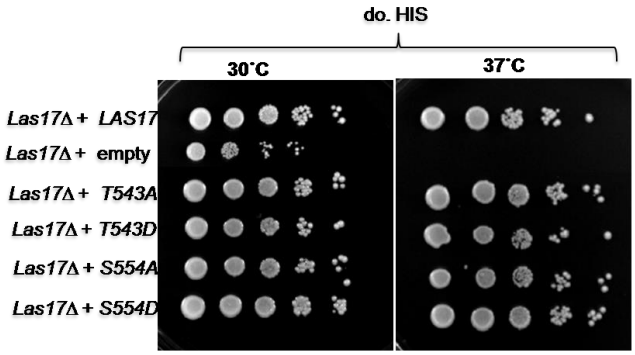

C. Growth curve of *T543A/D* and *S554A/D* mutants

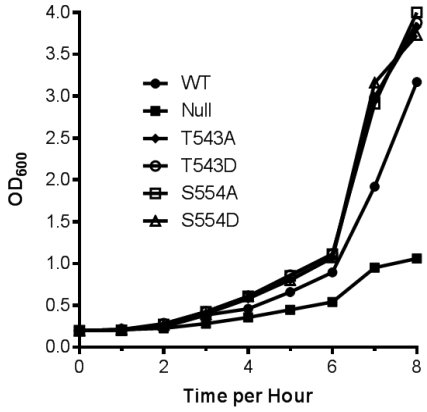

Figure 5.10: in vivo analysis of *las17-T380* phosphomutants

(A) Sequence alignment of WH2 domain of human WASP/N-WASP and homologue in yeast Las17. Conserved DALLAS motif was highlighted (yellow) and T543 and S554 (arrows) and the conserved I555 residue were labelled in red.

(B) log phase *las17* deletion cells carrying wild type, empty, *T543A/D*, and *S554A/D* plasmids were serially diluted (1/10) and then spotted onto SD agar plates, and then incubated at 30˚C and 37˚C for 48 hours.

(C) Growth curve of cells in (B) on SD liquid medium at 30˚C over a period of 8 hours.

Further investigations were undertaken in which the effects of *las17* phosphomutants *T543A/D* and *S554A/D* on the actin cytoskeleton was examined. As above, yeast stains lacking *las17* carrying *LAS17*, empty, *T543A/D*, and *S554A*/*D* plasmids were grown to OD_{600}=0.5-0.6. 1 ml of the actively grown culture of each strain was stained with Rhodamine-Phalloidin for 30 minutes. The cell pellet was washed several times with the recommended buffers and then viewed under fluorescent microscope (described in section 2.8.1).

Again the actin organisation of the cells carrying *T543A/D* and *S554A/D* mutations was not affected as shown in figure 5.11.A. Cells expressing *T543A/D* and *S554A/D* mutants exhibited normal actin patches whereby the majority of these cells had polarised actin cables in the bud and actin cables aligned along the mother. The graph bar in figure 5.11.B, revealed the percentage of cells in *las17-T543A/D* and *las17-S554A/D* mutants with and without polarised actin patches thus confirming neither *T543A/D* nor *S554A/D* mutants have an effect on the actin cytoskeleton in yeast cells.

A. Rhodamine-phalloidin staining of *T543A/D* and *S554A/D*

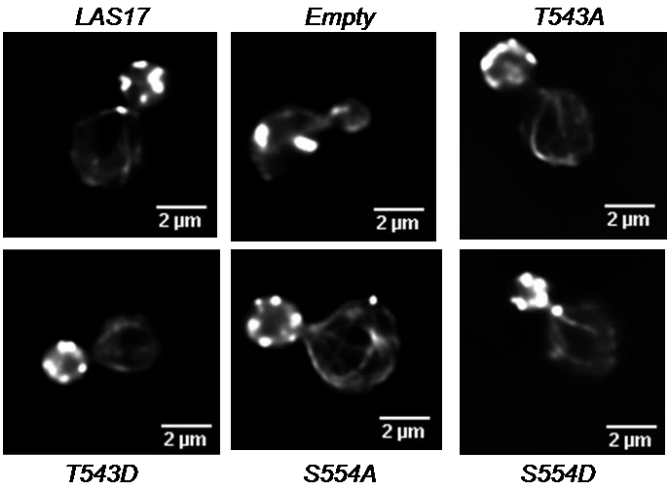

B.

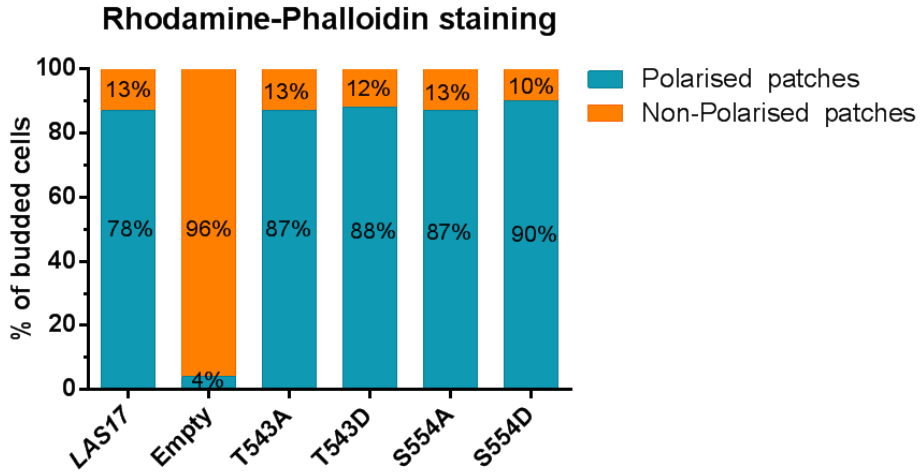

Figure 5.11: Actin cytoskeleton of *T543A/D* and *S554A/D* mutants.

(A) Images showed the actin cytoskeleton of las17 null strains carrying *LAS17* (wt), an empty, *T543A/D* and *S554A/D* plasmids. Cells were grown to log phase at 30˚C and then stained with rhodamine-phalloidin for 30 minutes and then viewed. Scale bar 2 µm.

(B) Percent representation of the actin patches polarity for the cells in (A) n=100. Graph bar was generated using Prism graph-Pad 6 software.

5.9 In vivo study of T380 residue as a potential phosphorylation site

The actin regulating kinases Ark1/Prk1 kinases in yeast are the homologue of the AAK/GAK family in mammals. Ark1/Prk1 kinases localised at actin cortical patches and play an important role in regulation of the endocytic coat disassembly during scission. The Ark1 consensus phosphorylation site (L(I)xxQxTG) is similar to that of Prk1 suggesting that, both Ark1 and Prk1 are functionally redundant (Cope et al., 1999; Zeng et al., 2001). The Las17 amino acids sequence was searched for LxxQxTG Prk1 recognition motif and a single Prk1 recognition motif was found within Las17-PP region (see figure 5.12.A). Prk1 kinase regulates several endocytic proteins by phosphorylating threonine residue within its recognition motif (Mok et al., 2010).

5.9.1 Temperature sensitivity test of *las17-T380A/D* mutants

Las17 contains a single Prk1 recognition motif which lies within the poly-proline (PP) region of Las17 (figure 5.12). The T380 residue lies within the Prk1 motif was previously reported as a site of phosphorylation (Swaney et al., 2013), though it was not found in the MS analysis carried out in this study. Phosphomutants were generated using site directed mutagenesis to change the T380 to non phosphorylatable alanine (*T380A*) or to aspartate (*T380D*) to mimic the constitutive phosphorylation of Las17. Mutations were made on a plasmid harbouring *Las17* full length that expresses *LAS17* under its own promoter. The mutants were verified by sequencing and then transformed into *las17* deletion strains. Cells were grown to logarithmic phase, and the effects of T380A/D mutants on growth at 37˚C was assessed by spotting 1/10 dilution of each cells on SD plates, SD with 1M sorbitol or 0.9M NaCl. Plates were incubated at 30˚C and 37˚C for 48 hours.

As shown in figure 5.12.B, in *las17* deletion strain complemented with *LAS17* wild type was able to grow at permissive and restrictive temperature (left panel) and the growth was normal also at hyper osmotic pressure (right panel) as well as hypertonic shock (bottom panel).

A. Prk1kinase recognition motif in PP region

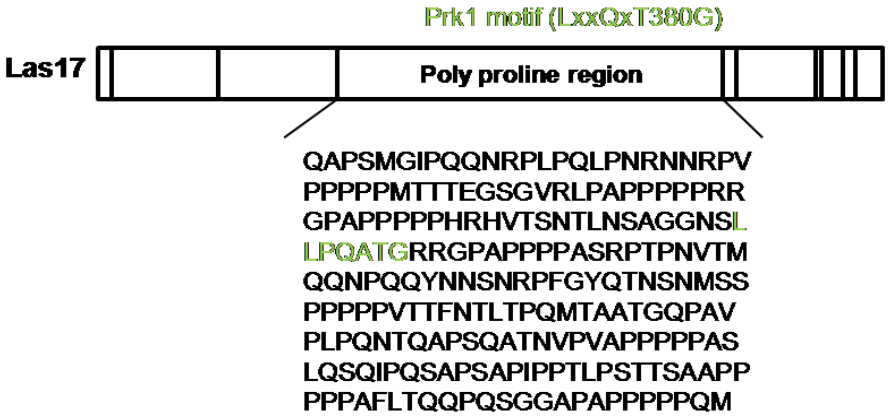

B. Growth assay of *T380A/D* mutants

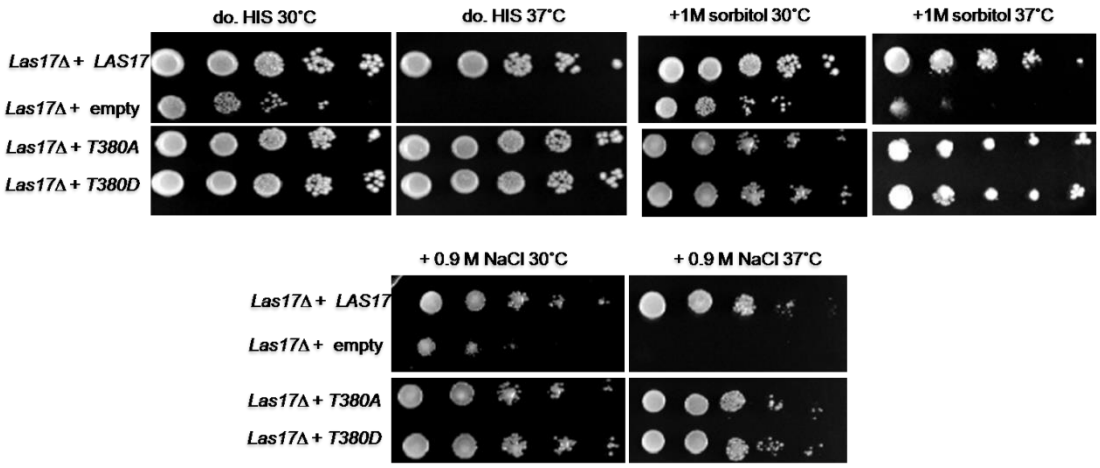

Figure 5.12: in vivo analysis of *las17-T380* mutants

(A) Schematic diagram of Las17 showing the location of the putative phospho threonine 380 in Prk1 recognition motif LxxQxTG. The amino acid sequence of the poly proline region (PP) was depicted as well.

(B) The *las17* null strains were transformed with the plasmids as indicated. The resulted cells were grown to log phase and 10 fold dilution of the cell culture was spotted onto SD medium (top left), + 1M sorbitol (top right) and 0.9M NaCl (below). The plates were then incubated at 30 and 37˚C for 48 hours. Results were based on a single experiment.

In contrast, cells carrying an empty plasmid were temperature sensitive at 37˚C (right panel) and the growth was partially rescued in the presence of 1M sorbitol at 37˚C (left panel). The growth of *Las17* null cells was impaired at 37˚C in the presence of salt (bottom panel). Cells expressing *las17-T380A/D* mutants were not temperature sensitive as the mutants were able to grow at 37˚C. In addition both *T380A* and *T380D* mutants exhibited similar growth as that observed in wild type cells in the presence of sorbitol or salt, suggesting that, T380 is not required for cell growth at restrictive conditions.

5.9. 2 Effect of T380 mutants on actin cytoskeleton

The effect of *las17-T380A/D* mutants on actin organisation of *las17* null cells was examined. Images of *T380A/D* mutants stained with rhodamine-phalloidin are depicted in figure 5.13.A. Both *las17-T380A/D* mutants exhibited normal actin organisation similar to that observed in wild type cells. Likewise the number of cells expressing *T380A/D* mutants with polarised actin patches was over 70% for each mutant, but the percentage of mutants with no-polarised actin patches was less than 30% (figure 5.13.B). Indicating that, neither *T380A* nor *T380D* mutants is essential for actin cytoskeleton in yeast cells.

5.9.3 Effect of *T380A/D* mutants on lucifer yellow uptake

To further extend the analysis for *T380A/D* mutants, the uptake of the fluorescent Lucifer yellow dye was determined. The Lucifer yellow is a soluble dye that is able to enter cells by endocytosis and accumulate into the vacuole. The extent of a defect in fluid phase endocytosis can be monitored microscopically (Munn and Riezman, 1985). The above set of *las17* null strains were stained with lucifer yellow and incubated for 30 and 90 minutes to follow internalisation and trafficking into the vacuole (described in section 2.8.2).

A. Actin organisation of *las17-T380A/D*

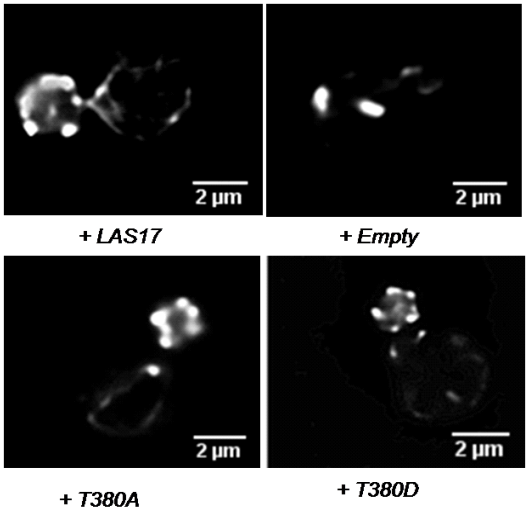

B.

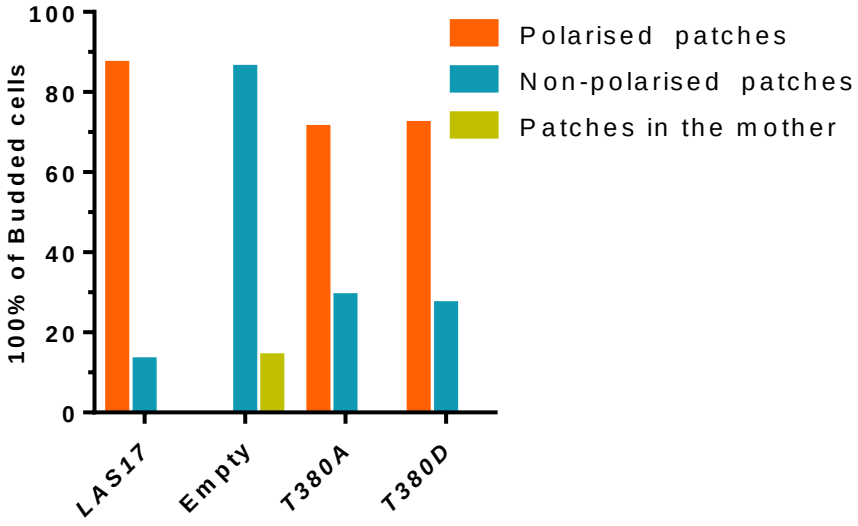

Figure 5.13: Rhodamine-Phalloidin staining of *las17-T380* mutants.

(A) The *las17* deletion strains carrying *LAS17*, an empty, *T380A* and *T380D* plasmids were grown to logarithmic phase and stained with Rh-Ph stain for 30 minutes. The cells were then viewed under the fluorescent microscope. Scale bar 2µm. The *T380A/D* phosphomutants showed wild type phenotype.

(B) Quantification of actin cortical patches of the same sets of cells in (A). The graph bar was generated using Prism graph-Pad programme.

Results are based on a single assay.

Lucifer yellow (LY) uptake into cells expressing *LAS17* as well as the *T380A/D* mutants was assessed graphically as represented in figure 5.14 (upper panel). After 30 minutes incubation, the number of cells expressing *LAS17 (*wt) that were able to internalise LY into vacuole was increased to 53%. Other cells showed endosomal or plasma membrane staining. In contrast, the majority of *las17* null cells exhibited a bright membrane with some endosomal staining (59%) and a much lower number of cells that had stained vacuoles (4%). Around 16% of cells expressing the *las17-T380A* mutant had vacuolar staining, whereas 23% of *las17-T380D* mutants were trafficked the dye into the vacuole. This suggests that, both *T380A/D* mutants affect endocytosis due to delay in LY trafficking from the membrane to the vacuole.

At 90 minutes neither *las17-T380A* nor *las17-T380D* expressing cells exhibited any phenotypic effect on lucifer uptake (figure 5.14. right lower panel). This would suggest that the mutations cause a delay in uptake and trafficking rather than a complete block.

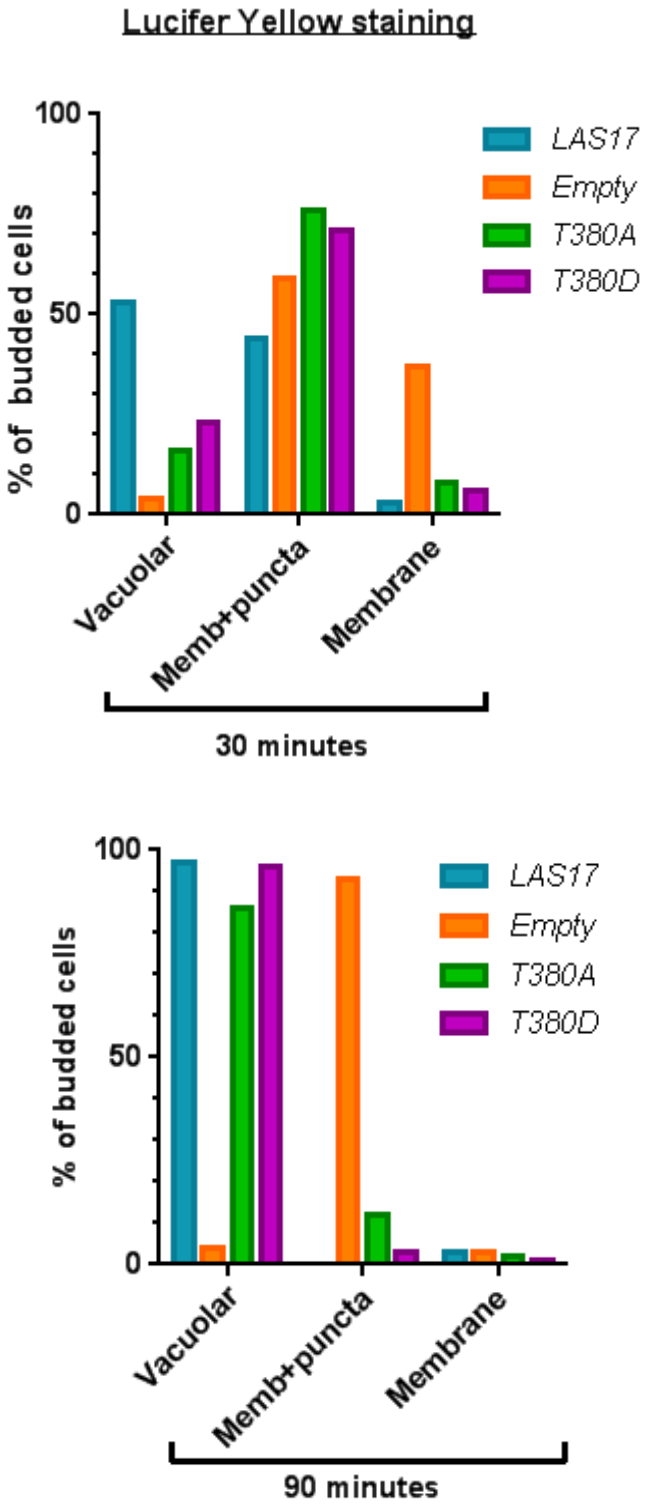

Figure 5.14: Rhodamine-Phalloidin staining of *las17-T380* mutants.

Quantification of the LY uptake of *las17* null cells carrying *LAS17*, empty, *T380A/D* plasmids. Cells were grown to log phase and then incubated with 4mg/ml of Lucifer yellow for 30 minutes or 90 minutes at 30˚C. The graph bar was analysed using Prism graph-Pad 6.

Quantifications were based on a single assay.

5.10 Discussion

This chapter focussed on further analysis of the phosphorylation of Las17 both to determine effective ways to analyse the phosphorylation and to map specific phosphorylated residues. The data presented in chapters 3 and 4 indicated that phosphorylation of serine 588 is important in regulating Las17 function in vivo. This mechanistic insight into regulation is important because like other WASP family members such as Scar/WAVE, Las17 does not have a GTPase binding site involved in its regulation, thus must rely on alternative mechanisms such as phosphorylation to ensure that it is active only at the correct places in the cell.

The major achievements outlined in this chapter are -

1. Generation of Las17 antibodies
2. Demonstration of Las17 phosphorylation using gel based approaches and use of these methods for investigating kinases that might be involved in Las17 regulation.
3. Identification of previously unknown phosphorylation sites and preliminary analyses on the importance of these

Generation of Las17 antibodies

The first aim of this chapter was to generate Las17 antibodies in rat in order to allow clear in vivo analysis of Las17 phosphorylation. There are no reported antibodies to Las17 in the literature so such tools would allow analysis of Las17 in the absence of tagging. Given the importance of the C-terminal region for key interactions of Las17 it would be preferable to use untagged Las17 in studies. Antibodies were raised to the PWCA region of Las17 and antisera obtained were tested against PWCA, the PP fragment or with WCA alone. The 3rd bleed of rat 2 seemed to show recognition of epitopes in PP and in WCA, while the recognition of WCA by the rat 1 antisera was less clear. Attempts to use antibodies against yeast extracts did not show clear differences between extracts from wild type or *las17* null strains. Work is currently being carried out in the Ayscough lab to purify the antibodies for future studies.

Demonstration of Phosphorylation using HA tagged Las17 in gel based assays

Because of the problems with the antibodies raised directly to Las17, it was decided that investigations would proceed using Las17 HA-tagged at its C-terminus that could be detected with commercial anti-HA antibodies. Extracts were made from cells expressing Las17-HA from a plasmid. On our normal SDS-poly acrylamide gels it was difficult to discern distinct bands. However use of PhosTag, which binds to phosphate groups on proteins and retards their movement in gels, allowed distinct phosphorylated forms of Las17 to be distinguished. The fact that different bands could be seen in the presence of the PhosTag additive is good evidence that the Las17 protein in the extracts is phosphorylated. Another experiment that could be done to demonstrate phosphorylation would be to make extracts and then to treat them with lambda phosphatase. This should lead to the dephosphorylation and should result in a single band on a gel, if the others were due to this modification. The reason that this was not done was that the conditions required for the lambda phosphatase affected running on the PhosTag gels.

An unexpected result was that extracts from cells containing endogenous *LAS17* or cells in which *LAS17* had been deleted carried different number of Las17 bands. This suggested that when HA tagged Las17 was the only Las17 in cells, it was differentially exposed to kinases than when it was co-expressed with endogenous protein. To determine whether this difference had functional consequences the behaviour of an endocytic reporter Abp1-GFP was analysed. Interestingly the lifetime of this protein in patches at the plasma membrane increased in the absence of endogenous Las17. The exact reason for the difference is not clear, but it would be of interest to immunoprecipitate the HA-tagged protein from the wild type and deletion strain to determine what the phosphorylation difference between the proteins is as it is clear that this difference impacts on endocytosis. At this time however it is not known whether the differences observed are because the

HA tagged protein is not having to function in the wild type cells so is less exposed to relevant kinases, or whether the HA tag causes a defect which means that when this protein is having to function in all aspects of Las17 function its exposure to kinases is increased (or to phosphatases is decreased).

The presence of multiple phosphorylation forms of Las17-3xHA suggests the possibility of action of more than one kinase. Phosphorylation sites of protein commonly fall within a consensus peptide sequence that is defined for a specific kinases. Genetic and physical studies have identified several kinases that may act on a number of endocytic proteins including Las17. Therefore several kinase deletion strains were obtained and tested for their effect on the Las17-HA phosphorylation pattern. Specifically, extracts from *ark1/prk1*, *pho85*, *yck1/2*, and *yak1* null strains were tested using phos-tag gel approach. In all cases the strains contained endogenous *LAS17*. The Ark1/Prk1 kinases have been shown to link the actin cytoskeleton to endocytosis as mutations in the catalytic domain of Prk1 led to formation of large endocytic clumps in the cytosol (Zeng and Cai, 1999). Here, expression of Las17-3xHA in either *ark1* or *prk1* deletion background exhibited a Las17 wild type phosphorylation pattern (figure 5.7). This result was unexpected as Las17 contains a consensus site for these kinases (T380) and phosphorylation has been previously suggested (Mok et al., 2010). However, it is possible that phosphorylation is very transient and difficult to capture by this approach. In addition, if the HA tagging affects incorporation of the Las17 into endocytic complexes in the presence of the untagged protein, we simply might not be able to see the effect of the kinase deletion in these cells. The other kinase deletions (*pho85*, *yck1/2*, and *yak1* (figure 5.7) lead to an increase in the number of bands compared to wild type and in fact the pattern was more similar to that obtained in the absence of endogenous protein. An increase in number of phosphorylated bands might indicate that the kinase deletion has directly or indirectly affected the progress of endocytosis such that there is an accumulation of a Las17 species specific

for that endocytic stage. Further analysis of phosphorylated residues would indicate whether these mutants are likely to be enriched for the Las17 at a certain endocytic stage, rather than resulting from distinct differences in the kinases present in the cells.

Mapping of Las17 phosphorylation sites using Mass spectrometry

The mass spectrometry (MS) analysis allows us to reveal the presence of further phosphorylation sites in the Las17 amino acid sequence. Following the WH1 domain a phospho-peptide containing T131 and T141 was detected and the localisation probability calculated using PhosphoRS was 100% for T141 modification. Thus, confirming that, T141 residue is phosphorylated. This site is close to where the yeast homologue of WASP interacting protein, WIP (verprolin, Vrp1) is thought to bind (Naqvi et al., 1998). In the analysis peptide coverage of the polyproline region was not very high so it is possible that if alternative approaches were used to cleave the protein, further phosphorylation sites would be identified in this region. Beyond the PP region of Las17, multiple serine, or threonine residues were identified. One of the sites with highest probability from the phosphoRS was at T543 (figure 5.9.B). It was hypothesized that T543 might contribute to Las17 function as it located within a motif that links the PP region with WH2 domain. Additionally, the MudPIT analysis revealed that the S554 residue as a phosphorylation site. S554 lies within the highly conserved RDALLASIR motif in the WH2 domain. Given the importance of WH2 for actin binding it is of interest to determine whether phosphorylation at this site affects the actin binding proteins of this domain. Interestingly, we were able to demonstrate that S586 and S588 are phosphosites and this result corresponded to the previously published phosphoproteomic data (Holt et al., 2009; Smolka et al., 2007). Although the phosphorylation probability of S588 was lower than some of the other sites. This may reflect its transience or the fact that it functions only at specific stages in the cell cycle or life span. The in vivo and in vitro analysis of *S588* mutants showed clear detrimental phenotypic consequences (chapter 3 and 4). Finally, a peptide carrying T598 and S609

was also detected by MS with the PhosphoRS indicating a probability of 100% for S609 modification. As with S586 and S588, this residue lies in the central (C) motif. This region has been suggested to be involved in both actin and Arp2/3 binding but the exact function of the region is not well defined (Kelly et al., 2006).

Having established that the Las17 Thr543 and Ser554 are phosphorylated based on our MS data; the effect of the *T543A/D* and *S554A/D* mutants was assessed in vivo (section 5.1.7). The growth assays revealed that each mutant was able to complement the growth defect in *las17* null strain at elevated temperatures and that actin organisation was normal. Therefore, it was concluded that single mutations at T543 or S544 are not sufficient to cause any detectable change in Las17 activity. However, assays investigating the behaviour of individual endocytic events might reveal more subtle defects.

Finally, Ark1/PrK1 kinases are known to be involved in regulating actin assembly. At the endocytic sites Las17 localises to cortical patches and contains single repeat of Prk1 recognition motif (figure 5.12.A). The recognition Prk1 motif in Las17-PP region contains T380 residue that has been shown to be phosphorylated (Sawayn et al., 2013). Despite not being identified in our MS analysis it was considered appropriate to investigate the effect of T380 mutants on Las17 function. Phenotypic analysis of growth and actin cytoskeleton organization indicated that *T380A/D* mutants do not behave significantly differently from wild type cells. Preliminary data did show that both mutants (*T380A/D*) caused a mild phenotype in lucifer-yellow internalisation during a period of 30 min incubation thus further experiments using this approach and also those analysing endocytic reporters might indicate further defects.

Chapter 6:

General Discussion

Chapter: 6

6.1 Functional significance of Las17 phosphorylation

Regulation of the endocytic machinery through post translation modification is still not well understood. The key Arp2/3 complex activator, Las17 in yeast is required to drive the formation of membrane invaginations at endocytic sites. The Las17 N-terminal region is known to bind the WIP homologue Vrp1 which can bind actin monomers but is itself unable to bind Arp2/3 complex (Takenawa and Miki, 2001) while the C-terminal WCA region is crucial for its NPF activity mediated by monomeric actin and Arp2/3 binding. The main aim of this work was to investigate whether phosphorylation plays a role in modulating Las17 function in *S. cerevisiae*. I have shown that Las17 is indeed phosphorylated at a number of Ser/Thr sites. Currently the kinases responsible for Las17 phosphorylation are not yet clear. However, attempts have been taken to define these kinases (see section 5.5). Preliminary data indicate some differences in Las17 phosphorylation status when analysed in some of the kinase deletion strains. However, further analysis will be required to determine which kinase(s) function in modifying Las17 at distinct sites.

One specific phosphorylation event was investigated in more detail and experiments indicated that Ser588 phosphorylation plays a significant role in regulation of Las17 function during endocytosis. Ser588 within the Las17WCA domain was previously identified in global phospho-proteome studies as a phosphorylation site but the significance of the modification had not been investigated (Smolka et al., 2007; Holt et al 2009). It is likely that some phosphorylation events are more central to specific regulatory events than others. For example, the initial analysis investigated both Ser586 and Ser588. However, changing Ser586 to alanine or aspartate did not make any marked changes that were detectable in growth, or other assays. In the context of the Ser588 mutation the additional S586 mutation did appear to slightly increase the extent of temperature sensitivity phenotype suggesting that the additional charge in this region did influence function, but alone was not sufficient to cause any changes.

Chapter: 6

Chapter 3 in this study describes the major effects of S588 mutations in vivo. The phosphomimetic *las17-S588D* mutation caused the cells to be unable to grow at elevated temperature similar to cells with a deletion of *LAS17* gene (Li et al., 1999). *Las17-S588D* mutants have also shown striking changes in actin patch polarisation as judged by rhodamine-phalloidin staining, though this was not as severe as the complete null strain (Li et al., 1997; Madania et al,. 1999). Las17-S588A/D mutant proteins are still able to localize to endocytic sites and there is some rescue of Lucifer yellow uptake supporting the idea that some interactions may still happen appropriately. Previously published data revealed that, as opposed to deletion of the entire *LAS17* gene, neither *las17*Δ*WCA* nor Δ*CA* mutants has a severe cellular phenotype suggesting that, Las17 does not function solely through its interaction with the Arp2/3 complex but there are other factors that act redundantly with Las17 to activate Arp2/3 (Winter et al., 1999; Sun et al., 2006; Galletta et al., 2008). The Las17Nt (a.a 1-368) which interacts with Vrp1 is able to suppress the growth defect associated with *las17*Δ cells at 37˚C in vivo (Takenawa and Miki, 2001). This raises a question as to why Ser588D has such a significant impact in vivo as this mutation lies in the regions deleted in these various mutations. It suggests that the presence of Ser588 has a dominant effect and is more severe than when the region is completely removed. Urbanek et al., (2013) showed that, a combination of mutations that affect actin binding by both the WH2 domain and the PP region causes a severe phenotype similar to the defect caused by *las17-S588D* (see section 3.6 for further details).On the other hand, the defect caused by S588A mutant was relatively mild but erratic movement of the Sla1 marker was seen in the plane of the plasma membrane and also a delay in Sla1 patch inward progression and this would indicate a defect in actin polymerisation after Las17 recruitment to the endocytic site (see figure 3.8.A). From these data it can be suggested that phosphorylation of S588 might affect the ability of the Sla1 reporter to remain at the site and that the negative charge of the phosphate group needs to be neutralised (presumably by removal of the group) for Las17 to function.

Overall the in vivo data suggest that Ser588 is a key regulatory residue of Las17and its phosphorylation could be function at early stage of endocytosis to influence the Arp2/3-independent function of Las17.

The effect of S588A/D in vitro was more subtle than the effects observed in vivo. As judged by GST-pull down assay and MST analysis, the Las17PWCA-S588D showed reduced binding to G-actin, but this result conflicts with that observed using the pyrene-actin polymerisation assay. Polymerisation of actin in the presence of S588D mutation either in Las17PWCA or WCA showed actin sequestering ability in the mutants comparable to the wild type. The exact reason for the differences is not clear but may lie in the buffer conditions during the specific assays which might stimulate nuclei formation and thus allowing further actin monomers to incorporate into filaments. However, the impact of S588D mutant was predominant upon Arp2/3 addition (section 4.5 and 4.6). One possible reason for the lack of a strong phenotype in vitro is that simply the proteins most affected by the mutation were not present in the assay but they are present in vivo.

The C-terminus of all WASPs is well-conserved and is composed of the WH2 G-actin binding domain followed by CA domain. The function of the C region is less well understood but it was suggested to have affinity for G-actin and it may play a role in the transfer of the actin monomers to the Arp2/3 binding (A) domain (Kelly et al., 2006). The region that connects WH2 with CA domain called a linker is not conserved among WASPs. The linker region in human WASP contains multiple proline residues that are known to break the secondary structure of this region of the protein thus acting as a spacer (see Figure 6.1) (Veltman and Insall, 2010). On the other hand, the linker region in yeast WASP (Las17) seems to extend to be part of the central domain and interestingly encompasses the Ser588 residue.

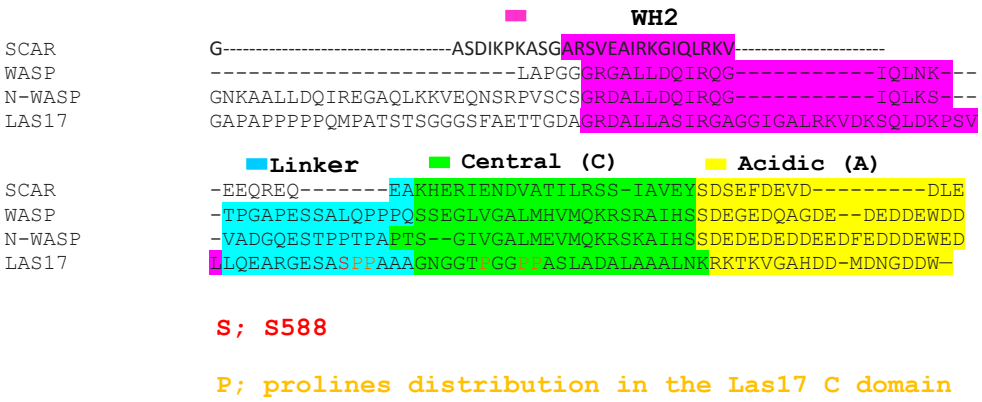

Figure 6.1: Multiple sequence alignment of the WASPs WCA domain

The data in chapter 4 indicate that an intramolecular interaction between PP and WCA domains might occur in Las17 which has been shown experimentally to be inhibited upon addition of S588D mutant (see figure 4.7). If this interaction is favoured in the presence of another protein, for example an SH3 domain binding protein or Vrp1 then the mutation might preclude their binding in vivo. Future experiments aim to determine whether other endocytic proteins known to bind to Las17 are mislocalized in the Ser 588 mutant strain.

Based on data available so far a molecular model could be suggested, in which S588 phosphorylation regulates the WCA domain function by promoting a conformation whereby the WCA domain folds on the PP domain .This structure might favourLas17PP driven actin nucleation. This disposition of the WCA domain maybe responsible for reducing the affinity towards the G-actin monomers by reducing the exposure of G-actin binding sites within the WH2 domain and this would therefore leads to a subsequent decrease in the transfer of the actin monomers to the Arp2/3 complex. This S588 inhibitory model does not seem to affect F-actin assembly by PP506/507 actin binding sites published by Ayscough lab (Urbanek et al., 2013). Again, in support of this assumption, the Las17 G-actin Motif (LGM) suggested by Feliciano et al., 2015 whereby the second actin binding site in the PP (300-404 a.a) is important to facilitate actin monomer transfer to the WCA domain but existence of Sla1-binding site in this region may reduce G-actin binding and thus preventing actin polymerisation mediated by the Arp2/3 complex (Feliciano et al., 2015). This is possible as the concentration of the cytoplasmic G-actin pool in yeast is relatively smaller than that in the mammalian cells (Karpova et al., 1995). Concerning our model, Las17 might then need to be dephosphorylated by unknown phosphatases to allow a conformational change in Las17 which then enhances the ability of Las17 to activate Arp2/3 complex and increase the rate of actin polymerisation to drive membrane invagination.

Ark1/Prk1 kinases target endocytic coat model components such kinases target endocytic coat model components such as Sla1, and Pan1 and phosphorylation is important for disassembly and dissociation of these proteins from the endocytic site (Zeng et al., 2007). Sites phosphorylated by these kinases are then dephosphorylated by Glc7 a yeast PP1 phosphatase and its targeting adaptor Scd5 (Chiet al., 2012). This dephosphorylation of the patch components is necessary to allow new rounds of endocytosis. Our preliminary data provide evidence that indicates how Las17 is negatively regulated by phosphorylation but it is also important in the future to consider its dephosphorylation

With regards to available data, one possible model for phosphoregulation of Las17 can be suggested (depicted in figure 6.2). (1) Upon Las17recruitment to the endocytic site phosphorylation at S588 by kinases takes place and this would trigger an intramolecular interaction of the Las17 molecule. Preliminary data shows that Sla1 might play a role in holding intramolecular conformation of Las17 but further investigations are required to support this idea. At this stage however, Las17 is able to generate new unbranched-actin filaments mediated by its poly-proline rich region. These filaments have been proposed to stabilise the endocytic site and provide a platform for membrane invagination and would be responsible for Arp2/3 complex recruitment to the site (Urbanek et al., 2013). After a few seconds, S588 dephosphorylation by unidentified phosphatases occurs and this would stimulate Arp2/3-driven branched actin formation (step 2). Together, preformed filaments and the branched F-actin would generate a force to drive membrane invagination against turgor pressure. (Steps 3 and 4) pathway of S588A/D mutations based on in vivo and in vitro data whereby both mutants affect invagination due to defects in actin assembly but this affect was major by S588D.

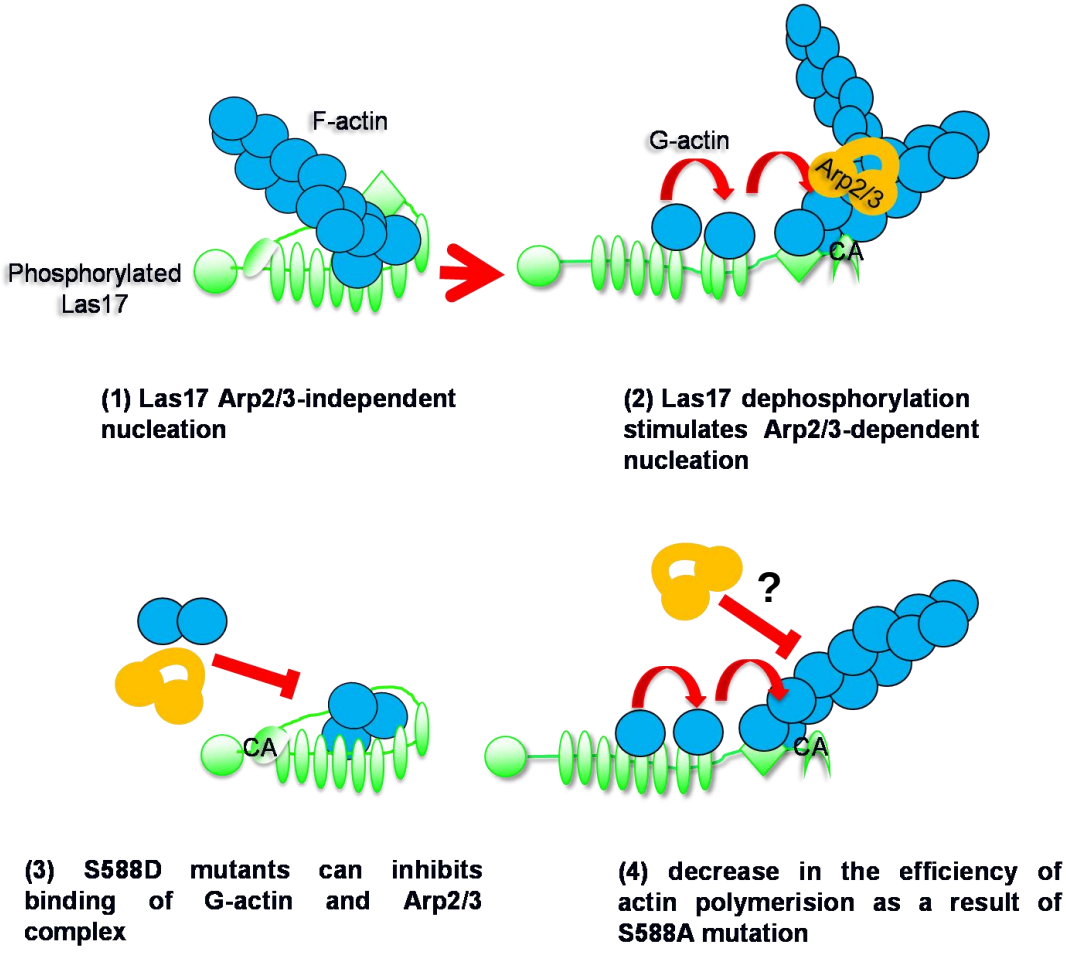

Figure 6.2: model of Las17 endocytic function and regulation of actin assembly.

(1) New actin filaments generated stabilize endocytic site and provide a platform for invaginationSer588 phosphorylation may not affect this step. (2) Arp2/3-driven branched actin filaments drive membrane invagination. (3) Constitutive phosphorylation of S588 inhibits step (2) so inhibits invagination. (4) Inappropriate invagination due to defects in actin assembly resulted from S588A.

6.2 Future investigations of Las17 regulation and function

Testing the model

This work and the suggested model allow a new hypothesis to be proposed and tested. For the model to represent the situation in cells, we would have to demonstrate that Arp2/3 binding is affected in the S588A/D mutants. Given that both Ser588 and Ser 605 were identified in the mass spec analysis it will be worth making both mutants singly and together to investigate this interaction. An epitope tag on an outer subunit of the Arp2/3 complex (e.g. Arc40) would allow immunoprecipitation of Arp2/3 and subsequent western blotting could be used to determine whether Las17 and the mutants interact to similar levels.

Integration of mutants

The work outlined in the project has used mutant versions of Las17 carried on plasmids but under control of the Las17 promoter. The expression levels do not look very different from the wild type endogenous protein levels but to ensure that phenotypes are not due to slight overexpression of the mutants from plasmids the S588A/D mutations can be generated within the genome by allele replacement strategies. In order to do this a strain carrying *LAS17* with *URA*3 marker has now been generated and DNA cassettes with Ser588 mutations were amplified. This work has been completed by Dr. Aga Urbanek who integrated the *las17-S588D/A* mutants successfully. The integrated mutant *las17-S588* showed similar temperature sensitivity for the growth as that observed when this mutation expressed by a centromeric plasmid (pKA 606).This supports the current data associated with Ser588 as a key regulatory residue in Las17.

Use of Las17 antibodies

Chapter 5 focused on investigating whether Las17 is phosphorylated in vivo and work was carried to generate Las17 antibodies. Preliminary testing suggested antibodies from the third bleed of rat 2 against recombinant Las17 fragments might be useful for further studies. Now this has been

demonstrated as Las17 antibodies were further examined against crude whole cell extracts prepared from a wild type strain or *las17* null strain. were further examined against crude whole cell extracts prepared from a wild type strain or *las17* null strain.

Figure 6.3 shows that, Las17 antibodies at 1:2000 dilution is sufficient to recognise Las17 from wt extracts. The protein band appears to run higher than the predicted Las17 size but this is frequently seen with other endocytic proteins Sla1 runs at 175kDa but is calculated size is136 kDa. The absence of this band in the null strain extracts supports the specificity of the antibodies.

This finding is important as studies published on Las17 interaction and localization so far have all used tagged protein. Now it is possible to investigate Las17 phosphorylation forms without the need of tags as the detection will be direct against the endogenous Las17. In the future It would be interesting to determine whether Las17 phosphorylation varies under different conditions e.g. of stress, in stationary cells or in mitosis as these might all be conditions in which endocytosis might be reduced.

Identification of Las17 interactions by mass spectrometry analysis

The mass spec data generated in this study to determine phosphorylation sites also allowed us to investigate the proteins that interact with Las17. Due to time constraints, the controls for this analysis to eliminate false positive binding have not been completed and so the data were not presented as part of the main body of this thesis. However, many of the proteins identified as interacting have previously been found to interact genetically or physically with Las17 (table 6.1) and also include a number of kinases (table 6.2).

Future studies however would need to complete the necessary controls and also to use other methods such as immuno-precipitation or yeast 2-hybrid

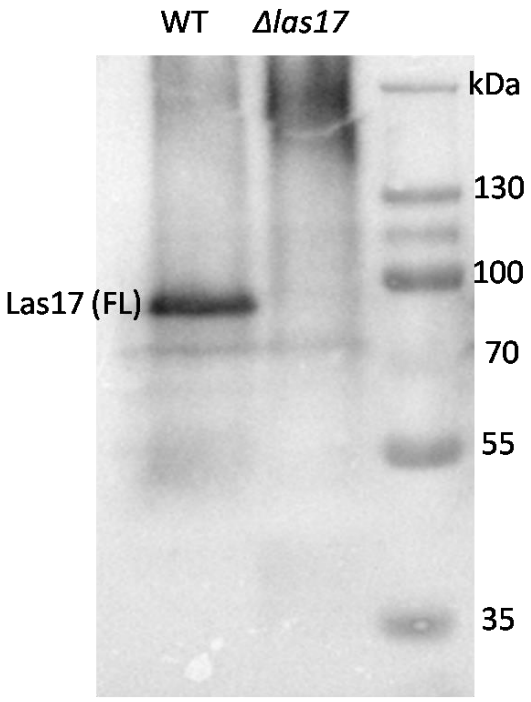

Figure 6.3: Immunobloting analysis of the Las17 antibodies from the 3rd bleed of rat 2.

That was prepared and tested against the crude extract made from wild type strain (KAY 389) or null strain (KAY1801) and run on 8% SDS-PAGE. Las17 was probed by preparing 1:2000 dilution of Las17 antibodies obtained from 3rd bleed of rat1 and 1:10000 secondary anti-rat antibodies. Blot was obtained from: Dr. Aga Urbanek

analysis to confirm these interactions. Confirmation of the significance of kinase interactions would use in vitro kinase assays to determine whether certain kinases are able to phosphorylate Las17 on specific residues.

Overall the data presented in this thesis have demonstrated that Las17 is phosphorylated in vivo and that phosphorylation at position serine 588 is important for its function during endocytosis. Future studies will allow us to determine how phosphorylation at Ser588 and other residues influence the molecular mechanism of Las17 function on the absence and presence of Arp2/3 complex.

Table 6.1: Las17 interactors detected by MS analysis in this study

Interactor	Cellular process	Type of interaction	Reference
Abp1	endocytosis	Genetic and physical	D´Agostino & good, 2005; Michelot et al., 2010
Act1	endocytosis	Genetic and physical	Michelot et al., 2010; Madania et al., 1999; Li et al., 1997
Bbc1	endocytosis	Physical	Michelot et al., 2010; Rodal et al., 2003; Tong et al., 2002
Bzz1	endocytosis	Genetic and physical	Kishimoto et al., 2012; Michelot et al., 2010; Ho et al., 2002; Tong et al., 2002, Soulard et al., 2002
Chc1	endocytosis	genetic	Gavin et al., 2002; Feliciano & De Pietro, 2012
Cof1	endocytosis	physical	Li et al., 1997
Crn1	endocytosis	physical	Michelot et al., 2010
Myo1	cytokinesis	genetic	Roumanie et al., 2002
Myo3	endocytosis	Genetic and physical	Galletta et al., 2008; Lechler et al., 2000; Tong et al., 2002; Michelot et al., 2010
Myo4	mRNA transport	physical	Ho et al., 2002
Pan1	endocytosis	Genetic and physical	Galletta et al., 2008; Feliciano & E Pietro, 2012
Rsp5	endocytosis	Genetic and physical	Kaminska et al., 20011; Tong et al., 2002
Sac6	endocytosis	physical	Michelot et al., 2010
Sec16	exocytosis	Physical	Michelot et al., 2010
Sla1	endocytosis	Genetic and physical	Chi et al., 2012; Michelot et al., 2010; Tonikian et al., 2009; Li et al., 1997
Sla2	endocytosis	physical	Gavin et al., 2002
Syp1	endocytosis	physical	Michelot et al., 2010
Vps5,13	Vacuolar sorting	physical	Michelot et al., 2010; Tong et al., 2002
Vrp1	endocytosis	Genetic and physical	Ho et al., 2002; Soulard et al., 2002; Evangelista et al., 2000; Roumanie et al., 2000; Naqvi et al., 1998
Ypp1	Cargo transport	physical	Michelot et al., 2010

Table 6.2: Kinases identified by MS analysis in this study

Interactor	Cellular process	interaction	Modification	Reference
Gin4	Bud growth	genetic	-	Sharifpoor et al., 2012
Akl1(Ark1 /Prk1)	endocytosis	physical	phosphorylation	Michelot et al., 2010; Mok et al., 2010
Yck1/2	endocytosis	physical	phosphorylation	Ptacek et al., 2005
Tor2	Cell cycle	physical	-	Michelot et al,. 2010
Pho85 /pho81	cell cycle , osmotic tolerance	physical	-	Ho et al., 2002
Ksp1	DNA replication	physical	phosphorylation	Ptacek et al., 2005

References

Achard, V., Martiel, J. L., Michelot, A., Guerin, C., Reymann, A. C., Blanchoin, L. and Boujemaa-Paterski, R. (2010) A "primer"-based mechanism underlies branched actin filament network formation and motility. *Curr Biol* 20, 423-8.

Adams, A. E. and Pringle, J. R. (1984) Relationship of actin and tubulin distribution to bud growth in wild-type and morphogenetic-mutant Saccharomyces cerevisiae. *J Cell Biol* 98, 934-45.

Adams, D.W., Errington J. (2009) Bacterial cell division: assembly, maintenance, and disassembly of the Z ring. *Nat Rev Microbiol* 7:642–653.

Aghamohammadzadeh, S. and Ayscough, K. R. (2009) Differential requirements for actin during yeast and mammalian endocytosis. *Nat Cell Biol* 11, 1039-42.

Aghamohammadzadeh, S., Smaczynska-de Rooij, I. I., & Ayscough, K. R. (2014) An Abp1-Dependent Route of Endocytosis Functions when the Classical Endocytic Pathway in Yeast Is Inhibited. *PLoS ONE* 9(7), e103311.

Aguilar, R. C., Watson, H. A., and Wendland, B. (2003) The yeast Epsin Ent1 is recruited to membranes through multiple independent interactions. *J Biol Chem* 278, 10737-43.

Amann, K. J. and Pollard, T. D. (2001) The Arp2/3 complex nucleates actin filament branches from the sides of pre-existing filaments. *Nat Cell Biol* 3, 306-10.

Amatruda JF, Cannon JF, Tatchell K, Hug C, Cooper JA (1990) Disruption of the actin cytoskeleton in yeast capping protein mutants. *Nature* 344:352–354.

Amberg, D. C. (1998) Three-dimensional imaging of the yeast actin cytoskeleton through the budding cell cycle. *Mol Biol Cell* 9, 3259-62.

Ampe, C., Markey, F., Lindberg, U. and Vandekerckhove, J. (1988) The primary structure of human platelet profilin: reinvestigation of the calf spleen profilin sequence. *FEBS Lett* 228, 17-21.

Ayscough KR (2000) Endocytosis and the development of cell polarity in yeast require a dynamic F-actin cytoskeleton. *Curr Biol* 10:1587–1590.

Ayscough KR, Eby JJ, Lila T, Dewar H, Kozminski KG, Drubin DG. (1999) Sla1p is a functionally modular component of the yeast cortical actin cytoskeleton required for correct localization of both Rho1p-GTPase and Sla2p, a protein with talin homology. Mol Biol *Cell* 10:1061-1075.

Ayscough KR, Stryker J, Pokala N, Sanders M, Crews P, Drubin DG (1997) High rates of actin filament turnover in budding yeast and roles for actin in establishment and maintenance of cell polarity revealed using the actin inhibitor latrunculin-A. *J Cell Biol* 137:399–416.

References

Baba Y,Nonoyama S, Matsushita M, Yamadori T, Hashimoto S, Imai K, et al. (1999) Involvement of Wiskottaldrich syndrome protein in B-cell cytoplasmic tyrosine kinase pathway. *Blood* 93:2003-2012.

Balasubramanian MK, Bi E, Glotzer M. (2004)Comparative analysis of cytokinesis in budding yeast, fission yeast and animal cells. Curr Biol 14(18):R806-18.

Balcer HI, Goodman AL, Rodal AA, Smith E, Kugler J, Heuser JE, Goode BL (2003) Coordinated regulation of actin filament turnover by a high-molecular-weight Srv2/CAP complex, cofilin, profilin, and Aip1. *Curr Biol* 13:2159–2169.

Balcer, H. I., Goodman, A. L., Rodal, A. A., Smith, E., Kugler, J., Heuser, J. E. and Goode, B. L. (2003) Coordinated regulation of actin filament turnover by a high-molecular-weight Srv2/CAP complex, cofilin, profilin, and Aip1. *Curr Biol 13*, 2159-69.

Ballweber E, Hannappel E, Huff T, Mannherz HG. (1997) Mapping the binding site of Thymosin beta4 on actin by completion with G-actin binding proteins indicates negative co-operativity between binding sites located on opposite subdomains of actin. *Biochem J* 327:787-93.

Ballweber, E., Hannappel, E., Huff, T., Stephan, H., Haener, M., Taschner, N., Stoffler, D., Aebi, U. and Mannherz, H. G. (2002) Polymerisation of chemically cross-linked actin:thymosin beta(4) complex to filamentous actin: alteration in helical parameters and visualisation of thymosin beta(4) binding on F-actin. *J Mol Biol* 315, 613-25.

Bamburg, J. R. (1999) Proteins of the ADF/cofilin family: essential regulators of actin dynamics. *Annu Rev Cell Dev Biol* 15, 185-230.

Beach DL, Salmon ED, Bloom K. (1999) Localization and anchoring of mRNA in budding yeast. *Curr Biol* 9(11):569-78.

Belmont LD, Patterson GM, Drubin DG. (1999) New actin mutants allow further characterization of the nucleotide binding cleft and drug binding sites. *J Cell Sci* 112 (Pt 9):1325-36.

Beltzner CC, Pollard TD. 2004 Identification of functionally important residues of Arp2/3 complex by analysis of homology models from diverse species. *J Mol Biol* 336(2):551-65.

Bertling, E., Hotulainen, P., Mattila, P. K., Matilainen, T., Salminen, M. and Lappalainen, P. (2004) Cyclase-associated protein 1 (CAP1) promotes cofilin-induced actin dynamics in mammalian nonmuscle cells. *Mol Biol Cell* 15, 2324-34.

Benedetti, H., Raths, S., Crausaz, F. and Riezman, H. (1994). The END3 gene encodes a protein that is required for the internalization step of endocytosis and for actin cytoskeleton organization in yeast. Mol Biol Cell 5, 1023-37.

Bisi S, Disanza A, Malinveron C, Frittoli E, Palamidessi A, Scita G. (2013) Membrane and actin dynamics interplay at lamellipodia leading edge. *Curr Opin Cell Biol* 25:565-573.

References

Boettner, D. R., D'Agostino, J. L., Torres, O. T., Daugherty-Clarke, K., Uygur, A., Reider, A., Wendland, B., Lemmon, S. K. and Goode, B. L. (2009) The 228 F-BAR protein Syp1 negatively regulates WASp-Arp2/3 complex activity during endocytic patch formation. *Curr Biol* 19, 1979-87.

Bork, P., Sander, C., and Valencia, A. (1992) An ATPase domain common to prokaryotic cell cycle proteins, sugar kinases, actin, and hsp70 heat shock proteins. *Proc Natl Acad Sci USA* 89, 7290−7294.

Bosticardo, M., Marangoni, F., Aiuti, A., Villa, A. and Grazia Roncarolo, M. (2009) Recent advances in understanding the pathophysiology of Wiskott-Aldrich syndrome. *Blood* 113, 6288-95.

Bramhill D, Thompson CM. (1994) GTP-dependent polymerization of *Escherichia coli* FtZ protein to form tubules. Proc. *NatI Acad USA* 91:5813-5817.

Broschat KO, Weber A, Burgess DR. (1989) Tropomyosin stabilizes the pointed end of the actin filaments by slowing depolymerization. *Biochemistry* 28:8501-8506.

Broschat KO. (1990) Tropomyosin prevents depolymerization of actin filaments from the pointed end. *J Biol Chem* 265:21323-21329.

Bryce NS, Schevzov G, Ferguson V, Percival JM, Lin JJ, Matsumura F, Bamburg JR, Jeffry PL, Hardman EC, Gunning P, Weinberger RP. (2003) Specification of actin filament function and molecular composition by tropomyosin isoforms. *Mol Biol Cell* 14:1002-1016.

Buck M, Xu W, Rosen MK. (2001) Global disruption of the WASP autoinhibited fold on Cdc42 binding. Ligands displacement as a novel method to monitor amide hydrogen exchange. *Biochemistry* 40, 14115-14122.

Bugyi B, Carlier MF. (2010) Control of actin filament treadmilling in cell motility. *Annu Rev Biophys* 39:449-70.

Burbelo, P. D., Drechsel, D., and Hall, A. (1995) A conserved binding motif defines numerous candidate target proteins for both Cdc42 and Rac GTPases. *J Biol Chem* 270, 29071-4.

Buzan JM, Frieden C. (1996). Yeast actin: polymerization kinetic studies of wild type and a poorly polymerizing mutant. Proc Natl Acad Sci U S A. 93(1):91-5.

Cai, L., Makhov, A. M., and Bear, J. E. (2007) F-actin binding is essential for coronin 1B function in vivo. *J Cell Sci* 120, 1779-90.

Campbell, C. S., and Mullins, R. D. (2007) In vivo visualization of type II plasmid segregation: Bacterial actin filaments pushing plasmids. *J Cell Biol* 179, 1059−1066.

Campellone, K. G., and Welch, M. D. (2010) A nucleator arms race: cellular control of actin assembly. *Nat Rev Mol Cell Biol* 11, 237-51.

References

Campellone, K. G., Webb, N. J., Znameroski, E. A., and Welch, M. D. (2008) WHAMM is an Arp2/3 complex activator that binds microtubules and functions in ER to Golgi transport. *Cell* 134, 148-61.

Carlier MF (1991) Actin - Protein-Structure and Filament Dynamics. Journal of Biological *Chemistry* 266:1-4.

Carlier MF, Pantaloni D. (1986) Direct evidence for ADP-Pi-F-actin as the major intermediate in ATP-actin polymerization. Rate of dissociation of Pi from actin filaments. *Biochemistry* 25(24):7789-92.

Carlier, M. F. and Pantaloni, D. (1997) Control of actin dynamics in cell motility. *J Mol Biol* 269, 459-67.

Carlier, M. F., Didry, D., Erk, I., Lepault, J., Van Troys, M. L., Vandekerckhove, J., Perelroizen, I., Yin, H., Doi, Y. and Pantaloni, D. (1996) The beta 4 is not a simple G-actin sequestering protein and interacts with F-actin at high concentration. *J Biol Chem* 271, 9231-9.

Carlier, M. F., Jean, C., Rieger, K. J., Lenfant, M. and Pantaloni, D. (1993) Modulation of the interaction between G-actin and thymosin beta 4 by the ATP/ADP ratio: possible implication in the regulation of actin dynamics. *Proc Natl Acad Sci USA* 90, 5034-8.

Carlier, M. F., Laurent, V., Santolini, J., Melki, R., Didry, D., Xia, G. X., Hong, Y., Chua, N. H. and Pantaloni, D. (1997) Actin depolymerizing factor (ADF/cofilin) enhances the rate of filament turnover: implication in actin-based motility. *J Cell Biol* 136, 1307-22.

Carlsson L, Nystrom LE, Sundkvist I, Markey F and Lindberg U. (1977) Actin polymerizability is influenced by profilin, a low molecular weight protein in non-muscle cells. *J Mol Biol* 115, 465–483.

Casella, J. F., and Torres, M. A. (1994) Interaction of Cap Z with actin. The NH2-terminal domains of the alpha 1 and beta subunits are not required for actin capping, and alpha 1 beta and alpha 2 beta heterodimers bind differentially to actin. *J Biol Chem* 269, 6992-8.

Chang FS, Stefan CJ, Blumer KJ. (2003) A WASp homologue powers actin polymerisation-dependent motility of endosomes in vivo. *Curr. Biol*.; 13(6):455-63.

Chang FS, Han GS, Carman GM., Blumer KJ. (2005) A WASP-binding type II phosphatidylinositol 4-kinase required for actin polymerisation driven endosome motility. *J Cell Biol*., 171(1), 133-142.

Chant J, Pringle JR. (1995) Patterns of bud-site selection in the yeast Saccharomyces cerevisiae. *J Cell Biol* 129(3):751-65.

Chhabra ES, Higgs HN. (2007) The many faces of actin: matching assembly factors with cellular structures. *Nat Cell Biol* 9:1110-1121.

Chi RJ., Torres OT., Segarra VA., Lansely T., Chang JS., et al., (2012)Role of Cdc5, a protein phosphatase-1 targeting protein, in phosphoregulation of Sla1 during endocytosis. *J Cell Sci* 125:4728-4739.

References

Chowdhury S, Smith KW, Gustin MC. (1992) Osmotic stress and the yeast cytoskeleton: phenotype-specific suppression of an actin mutation. *J Cell Biol* 118(3):561-71

.Cooper JA, Wear MA, Weaver AM. (2001) Arp2/3 complex: advanced on the inner workings of a molecular machine. *Cell* 107(6):703-5. Review.

Cooper JA, Pollard TD. (1985).Effect of capping protein on the kinetics of actin polymerization. *Biochemistry* 24(3):793-9.

Cooper JA and Pollard TD (1982), Methods to measure actin polymerisation. *Methods Enzymol*85, p.182-210.

Cope M, Yang S, Shang C, Drubin DG (1999) Novel protein kinases Ark1p and Prk1p associate with and regulate the cortical actin cytoskeleton in budding yeast. *J Cell Biol* 144:1203–1218

Cory GO, Garg R, Cramer R, Ridley AJ. (2002) Phosphorylation of tyrosine 291 enhances the ability of WASP polymerisation and filopodium formation. Wiskott-Aldrich syndrome protein. *J Biol Chem* 277: 45115-54121.

Cory GOC, Cramer R, Ridley AJ. (2003). Phosphorylation of the WASP-VCA domain increases its affinity for the Arp2/3 complex and enhances actin polymerization by WASP. *Mol Cell* 11:1229-1239.

Costa, R., Warren, D. T. and Ayscough, K. R. (2005) Lsb5p interacts with actin regulators Sla1p and Las17p, ubiquitin and Arf3p to couple actin dynamics to membrane trafficking processes. *Biochem J* 387, 649-58.

Coutts AS, Weston L, La Thangue NB (2009) A transcription co-factor integrates cell adhesion and motility with the p53 response. *Proc Natl Acad Sci USA* 106:19872–19877.

D'Agostino JL and Goode BL (2005) Dissection of Arp2/3 complex actin nucleation mechanism and distinct roles for its nucleation-promoting factors in Saccharomyces cerevisiae. *Genetics* 171(1):35-47

Daniel, R. A., and Errington, J. (2003) Control of cell morphogenesis in bacteria: Two distinct ways to make a rod-shaped cell. *Cell* 113, 767−776.

Dawson JC, Legg JA, Machesky LM (2006) Bar domain proteins: a role in tubulation, scission and actin assembly in clathrin-mediated endocytosis. *Trends Cell Biol* 16, 493-498.

De Bore P, Crossley R, Rothfield L. (1992) The essential bacteria cell-division protein FtsZ is a GTPase. *Nature* 359:254-256.

De la Fuente, M. A., Sasahara, Y., Calamito, M., Anton, I. M., Elkhal, A., Gallego, M. D., Suresh, K., Siminovitch, K., Ochs, H. D., Anderson, K. C. et al. (2007) WIP is a chaperone for Wiskott-Aldrich syndrome protein (WASP). *Proc Natl Acad Sci US A* 104, 926-31.

Derivery, E., Lombard, B., Loew, D. and Gautreau, A. (2009a) The Wave complex is intrinsically inactive. *Cell Motil Cytoskeleton* 66, 777-90.

References

Derivery, E., Sousa, C., Gautier, J. J., Lombard, B., Loew, D. and Gautreau, A. (2009b) The Arp2/3 activator WASH controls the fission of endosomes through a large multiprotein complex. *Dev Cell* 17, 712-23.

Derman, A. I., Becker, E. C., Truong, B. D., Fujioka, A., Tucey, T. M., Erb, M. L., Patterson, P. C. and Pogliano, J. (2009) Phylogenetic analysis identifies many uncharacterized actin-like proteins (Alps) in bacteria: regulated polymerization, dynamic instability, and treadmilling in Alp7A. *Mol Microbiol* 73, 534-552.

Dewar, H., Warren, D. T., Gardiner, F. C., Gourlay, C. G., Satish, N., Richardson, M. R., Andrews, P. D. and Ayscough, K. R. (2002) Novel proteins linking the actin cytoskeleton to the endocytic machinery in Saccharomyces cerevisiae. *Mol Biol Cell* 13, 3646-61.

Didry, D., Carlier, M. F. and Pantaloni, D. (1998) Synergy between actin depolymerizing factor/cofilin and profilin in increasing actin filament turnover. *J Biol Chem* 273, 25602-11.

Divakaruni AV, Ogorzalek Loo RR, Xie Y, Loo JA, Gober JW (2005) The cell-shape protein MreC interacts with extracytoplasmic proteins including cell wall assembly complexes in *Caulobacter crescentus*. *PNAS* 102: 18602–18607.

Doherty, G. J. and McMahon, H. T. (2009) Mechanisms of endocytosis. *Annu Rev Biochem* 78, 857-902.

dos Remedios, C. G., Chhabra, D., Kekic, M., Dedova, I. V., Tsubakihara, M., Berry, D. A. and Nosworthy, N. J. (2003). Actin binding proteins: regulation of cytoskeletal microfilaments. *Physiol Rev* 83, 433-73.

Dovas A, Cox D.(2010). Regulation of WASp by phosphorylation: Activation or other functions? *Commun Integr Biol* 3(2):101-5.

Doyle, T. and Botstein, D. (1996) Movement of yeast cortical actin cytoskeleton visualized in vivo. *Proc Natl Acad Sci USA* 93, 3886-91.

Drubin DG. (1990) Actin and actin-binding proteins in yeast. *Cell Motil Cytoskeleton* 15(1):7-11. Review.

Duleh SN, Welch MD. (2010) WASH and the Arp2/3 complex regulate endosome shape and trafficking. *Cytoskeleton (Hoboken)* 67(3):193-206.

Dulic V, Egerton M, Elgundi I, Raths S, Singer B, et al. (1991) Yeast endocytosis Assays. *Meths Enzymol* 194:697-710.

Duncan MC, Cope M, Goode BL, Wendland B, Drubin DG (2001) Yeast Eps15-like endocytic protein, Pan1p, activates the Arp2/3 complex. *Nat Cell Biol* 3:687–690.

Dey P, Togra J, Mitra S. (2014) Intermediate filament: structure, function, and applications in cytology. *Diagn Cytopathol* 42(7):628-35.

References

Echarri A., Lai MJ., Robinson MR., and Pendergast AM. (2004) Abl interactor 1 (Abi-1) wave-binding and SNARE domains regulate its nucleocytoplasmic shuttling, lamellipodium localization, and wave-1 levels. *Mol Cell Biol* 24, 4979–4993.

Eden, S., Rohatgi, R., Podtelejnikov, A.V., Mann, M. and Kirschner, M.W.(2002) Mechanism of regulation of WAVE1-induced actin nucleation by Rac1 and Nck. *Nature (London)* 418, 790–793.

Erickson HP, O'Brien ET (1992) Microtubule dynamic instability and GTP hydrolysis Ann. Rev. Biophys. *Bipmol Struct* 21:145-166

Erin D. Goley and Matthew D. Welch. (2006) The Arp2/3 complex: an actin nucleator comes of age. *Nature reviews Molecular Cell Biology* 7, 713-726.

Esue O, Cordero M, Wirtz D, Tseng Y. (2005) The assembly of MreB, a prokaryotic homolog of actin. *J Biol Chem* 280:2628-2635.

Eitzen, G., Wang, L., Thorngren, N., and Wickner, W. (2002).Remodeling of organelle-bound actin is required for yeast vacuole fusion. J. Cell Biol. 158, 669–679.

Enggvist-Goldstein AE, Drubin DG. (2003) Actin assembly and endocytosis: from yeast to mammals. *Annu Rev Cell Dev Biol* 19:287-332. Review.

Evangelista M, Zigmond S, Boone C.(2003).Formins: signaling effectors for assembly and polarization of actin filaments. J Cell Sci 116(Pt 13):2603-11. Review.

Evangelista M., Pruyne D., Amberg DC., Boone C., and Bretscher, A. (2002) Formins direct Arp2/3-independent actin filament assembly to polarize cell growth in yeast. *Nat Cell Biol* 4, 260-9.

Falzone TT, Lenz M, Kovar DR, Gardel ML.(2012) Assembly kinetics determine the architecture of alpha-actinin crosslinked F-actin networks. *Nat Commun* 3:861.

Feliciano D, Di Pietro SM. (2012) SLAC, complex between Sla1 and Las17, regulates actin polymerization during clathrin-mediated endocytosis. *Mol Biol Cell* (21):4256-72.

Firat-Karalar EN, Hsiue PP, Welch MD. (2011) The actin nucleation factor JMY is a negative regulator of neuritogenesis. *Mol Biol Cell* 22(23):4563-74.

Fitzen G, Wang L, Thorngren N, Wickner W. (2002) Remodelling of organelle-bound actin is required for yeast vacuole fusion. *J Cell Biol*., 158(4):669-679.

Foth BJ et al., (2006) New insights into myosin evolution and classification. *Proc Natl Acad Sci USA* 103:3681-3686.

Fukuoka M, Suetsugu S, Miki H, Fukami K, Endo T, Takenawa T. (2001) A novel neural Wiskott-Aldrich syndrome protein (N-WASP) binding protein, WISH, indices Arp2/3 complex activation independent of Cdc42. *J Cell Biol* 152, 471-482.

References

Frieden C, Goddette DW. (1983) Polymerization of actin and actin-like systems: evaluation of the time course of polymerization in relation to the mechanism. *Biochemistry* 22(25):5836-43.

Friesen H, Murphy K, Breitkreutz A, Tyers M, Andrews B. (2003) Regulation of the yeast amphiphysin homologue Rvs167p by phosphorylation. *Mol Biol Cell* 14(7):3027-40.

Fujiwara, I., Takahashi, S., Tadakuma, H., Funatsu, T. and Ishiwata, S. (2002) Microscopic analysis of polymerization dynamics with individual actin filaments. *Nat Cell Biol* 4, 666-73.

Fujii T, Iwane AH, Yanagida T, Namba K (2010) Direct visualization of secondary structures of F-actin by electron cryomicroscopy. *Nature* 467:724-728.

Galletta BJ, Cooper JA (2009) Actin and endocytosis: mechanisms and phylogeny. *Curr Opin Cell Biol* 21:20-27.

Galletta, B. J., Chuang, D. Y. and Cooper, J. A. (2008) Distinct roles for Arp2/3 regulators in actin assembly and endocytosis. *PLoS Biol* 6, e1.

Gallwitz D, Sures I. (1980) Structure of a split yeast gene: complete nucleotide sequence of the actin gene in Saccharomyces cerevisiae. *Proc Natl Acad Sci USA* 77(5):2546-50.

Gandhi M., Jangi M. and Goode, B. L. (2010) Functional surfaces on the actin-binding protein coronin revealed by systematic mutagenesis. *J Biol Chem* 285, 34899-908.

Gaucher, J. F., Mauge, C., Didry, D., Guichard, B., Renault, L. and Carlier, M. F. (2012) Interactions of isolated C-terminal fragments of Neural Wiskott-Aldrich Syndrome Protein (N-WASP) with actin and Arp2/3 complex. *J Biol Chem* 287(41):34646-59.

Gavin AC, et al. (2002) Functional organization of the yeast proteome by systematic analysis of protein complexes. *Nature* 415(6868):141-7

Gavin AC, et al. (2006) Proteome survey reveals modularity of the yeast cell machinery. *Nature* 440(7084):631-6

Geese M, Loureiro JJ, Bear JE, Wehland J, Gertler FB, Sechi S. (2002) Contribution of Ena/VASP proteins intracellular motility of listeria requires phosphorylation and protein –rich core but not F-actin binding or multimerization. *Mol Biol Cell* 13, 2383-2396.

Gelkin VE, Orlva A, Lukoyanova N, Wriggers W, Egelman EH (2001) Actin depolymerisation factor stabilizes an existing state of F-actin and can change the tilt of F-actin subunits. *J Cell Biol* 153, 75-86.

Gheorghe D. M., Aghamohammadzadeh S., Smaczynska-de, R. II, Allwood, E. G., Winder, S. J. and Ayscough, K. R. (2008) Interactions between the yeast SM22 homologue Scp1 and actin demonstrate the importance of actin bundling in endocytosis. *J Biol Chem* 283, 15037-46.

References

Gietz RD, Schiestl RH. (2007) High-efficiency yeast transformation using the LiAc/SS carrier DNA/PEG method. *Nat Protoc* 2(1):31-4.

Gitai Z., Dye N. A., Reisenauer A., Wachi M., and Shapiro L. (2005) MreB actin-mediated segregation of a specific region of a bacterial chromosome. *Cell* 120, 329–341.

Goldschmidt-Clermont PJ, Machesky LM, Baldassare JJ Pollard TD. (1990) The actin-binding protein profilin binds to PIP2 and inhibits its hydrolysis by phospholipase C. *Science* 247:1575–1578.

Goldschmidt-Clermont, P. J., Furman, M. I., Wachsstock, D., Safer, D., Nachmias, V. T. and Pollard, T. D. (1992) The control of actin nucleotide exchange by thymosin beta 4 and profilin. A potential regulatory mechanism for actin polymerization in cells. *Mol Biol Cell* 3, 1015-24.

Goldschmidt-Clermont, P. J., Machesky, L. M., Baldassare, J. J., and Pollard, T. D. (1990) The actin-binding protein profilin binds to PIP2 and inhibits its hydrolysis by phospholipase C. *Science* 247, 1575-8.

Gomez TS., and Billadeau DD. (2009) A FAM21-containing WASH complex regulates retromer-dependent sorting. *Dev Cell* 17, 699-711.

Goode, B. L., and Rodal, A. A. (2001) Modular complexes that regulate actin assembly in budding yeast. *Curr Opin Microbiol 4*, 703-12.

Goodman A, Goode BL, Matsudaira P, Fink GR (2003) The *Saccharomyces cerevisiae* calponin/transgelin homolog Scp1 functions with fimbrin to regulate stability and organization of the actin cytoskeleton. *Mol Biol Cell* 14:2617–2629.

Greer C, Schekman S. (1982) Actin from *Saccharomyces cerevisiae*. *Mol Cell Biol* 2(10)1270-8.

Gremm D, Wegner A. (2000) Gelsolin as a calcium-regulated actin filament-capping protein. *Eur J Biochem* 267(14):4339-45.

Guarente L. (1983) Yeast promoters and lacZ fusions designed to study expression of cloned genes in yeast. Methods Enzymol. 101:181-91.

Han Choe, Leslie D. Burtnick, Marisan Mejillano Helen L Yin, Robert C Robinson, Senyon Choe. (2002). The calcium activation of Gelsolin: insights from the 3 Å structure of the G4-G6/actin complex. *J Mol Bio* 324(4): 691-702.

Hanson, J. and Lowy, J. (1964) The Structure of Actin Filaments and the Origin of the Axial Periodicity in the I-Substance of Vertebrate Striated Muscle. *Proc R Soc Lond B Biol Sci* 160, 449-60.

Helfman DM, Cheley S, Kuismanen E, Finn LA, and Yamawaki-Kataoka Y. (1986) Nonmuscle and muscle tropomyosin isoforms are expressed from a single gene by alternative RNA splicing and polyadenylation. *Mol Cell Biol* 6(11): 3582–3595.

References

Helwani FM, Kovacs EM, Paterson AD, Verma S, Ali RG, Fanning AS, Weed SA, Yap AS.(2004). Cortactin is necessary for E-cadherin-mediated contact formation and actin reorganization. *J Cell Biol* 164(6):899-910.

Herman IM. (1993) Actin isoforms. *Curr Opin Cell Biol*; 5(1):48-55.

Herrmann H, Bär H, Kreplak L, Strelkov SV, Aebi U (2007) Intermediate filaments: from cell architecture to nanomechanics. *Nat Rev Mol Cell Biol* 8 (7): 562–73.

Higgs HN, Blanchoin L, Pollard TD.(1999) Influence of the C terminus of Wiskott-Aldrich syndrome protein (WASp) and the Arp2/3 complex on actin polymerization. *Biochemistry* 38:15212-15222.

Higgs, H. N., and Pollard, T. D. (2000) Activation by Cdc42 and PIP(2) of Wiskott-Aldrich syndrome protein (WASp) stimulates actin nucleation by Arp2/3 complex. *J Cell Biol* 150, 1311-20.

Hitchcock-DeGregori SE, Sampath P, Pollard TD. (1988). Tropomyosin inhibits the rate of actin polymerization by stabilizing actin filaments. *Biochemistry* 27:9182-9185.

Ho, H. Y., Rohatgi, R., Lebensohn, A. M., Le, M., Li, J., Gygi, S. P. and Kirschner, M. W. (2004) Toca-1 mediates Cdc42-dependent actin nucleation by activating the N-WASP-WIP complex. *Cell* 118, 203-16.

Holmes KC, Angert I, Kull FJ, Jahn W, Schroder RR (2003) Electron cryo-microscopy shows how strong binding of myosin to actin releases nucleotide. *Nature* 425:423-427.

Holmes, K. C., Popp, D., Gebhard, W. and Kabsch, W. (1990) Atomic model of the actin filament. *Nature* 347, 44-9.

Holt LJ, Tuch BB, Villén J, Johnson AD, Gygi SP, Morgan DO. (2009) Global analysis of Cdk1 substrate phosphorylation sites provides insights into evolution. *Science* 325(5948):1682-6.

Holtzman DA, Yang S, Drubin DG (1993) Synthetic-lethal interactions identify two novel genes, *SLA1* and *SLA2,* that control membrane cytoskeleton assembly in *Saccharomyces cerevisiae*. *J Cell Biol* 122:635–644.

Howard J, Hyman AA (2003) Dynamics and mechanics of the microtubule plus end. *Nature* 422:753-758 10.1038.

Howard J, Hyman AA (2009) Growth, fluctuation, and switching at microtubule plus ends. *Nat Mol CellBiol* 10:569-574.

Huang, B., Zeng, G., Ng, A. Y. & Cai, M. (2003) Identification of novel recognition motifs and regulatory targets for the yeast actin-regulating kinase Prk1p. *Mol Biol Cell* 14, 4871–4884.

References

Huang F, Khvorova A, Marshall W, Sorkin A. (2004) Analysis of clathrin-mediated endocytosis of epidermal growth factor receptor by RNA interference. *J Biol Chem* 276:16657-16661.

Hufner, K., Higgs, H. N., Pollard, T. D., Jacobi, C., Aepfelbacher, M. and Linder, S. (2001) The verprolin-like central (vc) region of Wiskott-Aldrich syndrome protein induces Arp2/3 complex-dependent actin nucleation. *J Biol Chem* 276, 35761-7.

Hurley JH. (1996) The sugar kinase/heat shock protein 7O/Actin superfamily: implications of Conserved Structure for Mechanism. *Annu Rev Biophys Biomol Struct* 25, 137-62.

Idissi FZ, Grotsch H, Fernandez-Golbano IM, Presciatto-Baschong C, Riezman H, Geli MI (2008). Distinct acto/myosin-I structure associate with endocytic profiles at the plasma membrane. *J Cell Biol*. 180:1219-1232

Ishikawa, R., Yamashiro, S., and Matsumura F. (1989) Differential modulation of actin-severing activity of gelsolin by multiple isoforms of cultured rat cell tropomyosin. Potentiation of protective ability of tropomyosins by 83-kDa nonmuscle caldesmon. *J Biol Chem* 264, 7490-7497.

Jia D, Gomez TS, Billadeau DD, Rosen MK. (2012) Multiple repeat elements within the FAM21 tail link the WASH actin regulatory complex to the retromer. *Mol Biol Cell* 23(12):2352-61.

Kabsch, W., Mannherz, H. G. and Suck, D. (1985). Three-dimensional structure of the complex of actin and DNase I at 4.5 A resolution. *EMBO J* 4, 2113-8.

Kabsch, W., Mannherz, H. G., Suck, D., Pai, E. F., and Holmes, K. C. (1990) Atomic structure of the actin: DNase I complex. *Nature* 347, 37-44.

Kaiser, C., Michaelis, S., and Mitchell, A. (1994) Meths in Yeast Genetics: A Laboratory Course Manual, (*Cold Spring Harbor Laboratory Press*).

Karpova, T.S., Tatchell, K., and Cooper, J.A. (1995). Actin filaments in yeast are unstable in the absence of capping proteinor fimbrin. J. Cell Biol. 131, 1483–1493.

Kaksonen, M., Sun, Y., and Drubin, D. G. (2003) A pathway for association of receptors, adaptors, and actin during endocytic internalization. *Cell* 115, 475-87.

Kaksonen, M., Toret, C. P. and Drubin, D. G. (2005) A modular design for the clathrin- and actin-mediated endocytosis machinery. *Cell* 123, 305-20.

Kaminska J, et al. (2011) Yeast Rsp5 ubiquitin ligase affects the actin cytoskeleton in vivo and in vitro. *Eur J Cell Biol* 90(12):1016-28

Kelly AE. Kranitz H, Dötsch V, Mullins RD. (2006) Actin binding to the central domain of WASP/Scar proteins plays a critical role in the activation of the Arp2/3 complex. *J Biol Chem* 281:10589-10597.

References

Kenneth G, Campellone, Neil J. Webb, Elizabith A, Znameroski, Matthew D. Welch. (2008) WHAMM Is an Arp2/3 Complex Activator that Binds Microtubules and Functions in ER to Golgi Transport. *Cell* 134(1): 148-61.

Kim K, Galletta BJ, Schmidt KO, Chang FS, Blumer KJ, Cooper JA (2006) Actin-based motility during endocytosis in budding yeast. *Mol Biol Cell* 17:1354–1363.

Kim AS, Kakalis LT, Abdul-Manan N, Liu GA, Rosen MK. (2000) Autoinhibition and activation mechanisms of the Wiskott-Aldrich syndrome protein. *Nature* 404(6774):151-8.

Kinley AW, Weed SA, Weaver AM, Karginov AV, Bissonette E, Cooper JA, Parsons JT. (2003) Cortactin interacts with WIP in regulating Arp2/3 activation and membrane protrusion. *Curr Biol* 13(5):384-93.

Kishimoto T, et al. (2011) Determinants of endocytic membrane geometry, stability, and scission. *Proc Natl Acad Sci USA 108*(44):E979-88.

Kollmar M, Lbik D, Enge S. (2012) Evolution of the eukaryotic ARP2/3 activators of the WASP family: WASP, WAVE, WASH, and WHAMM, and the proposed new family members WAWH and WAML.*BMC Res Notes* 5:88.

Kovar DR, Pollard TD. (2004) Insertional assembly of actin filament barbed ends in association with formins produces piconewton forces. *Proc Natl Acad Sci USA* 101(41):14725-30.

Kovar DR. (2006) Cell polarity: formin on the move. *Curr Biol* 16(14):R535-8.

Kozma R, Ahmed S, Best A, Lim L (1995) The Ras-related protein Cdc42Hs and bradykinin promote formation of peripheral actin microspikes and filopodia in Swiss 3T3 fibroblasts. *Mol Cell Bio*15:1942-1952.

Kruse T, Bork-Jensen J, Gerdes K. (2005) The morphogenetic MreBCD proteins of *Escherichia coli* form an essential membrane-bound complex. *Mol Microbial* 55:78-89.

Kübler E, Riezman H (1993) Actin, and fimbrin are required for the internalization step of endocytosis in yeast. *EMBO J* 12:2855–2862.

Kuhn JR, Pollard TD (2005) Real-time measurements of actin filament polymerization by total internal reflection fluorescence microscopy. *Biophysical Journal* 88:1387-1402.

Kusano K, Abe H, Obinata T. (1999) Detection of a sequence involved in actin-binding and phosphoinositides-binding in the N-terminal side of cofilin. *Mol Cell Biochem* 190 (1-2): 133-41.

Kwiatkowski DJ, Stossel TP, Orkin SH, Mole JE, Colten HR, Yin HL. (1986) Plasma and cytoplasm gelsolins are encoded by a single gen and contain a duplicated actin-binding domain. *Nature* 323 (6087):455-8.

Lal AA, Korn ED. (1986) Effect of muscle tropomyosin on the kinetics of polymerization muscle actin. *Biochemistry* 25:1154-1158.

References

Lanier LM, Gertler FB. (2000) Actin cytoskeleton: thinking globally, actin' locally. *Curr Biol* 10(18):R655-7.

Lappalainen P, Drubin DG. (1997) Cofilin promotes rapid actin filament turnover in vivo. *Nature* 388 (6637), 78-82.

Lappalainen, P., Kessels, M. M., Cope, M. J. and Drubin, D. G. (1998) The ADF homology (ADF-H) domain: a highly exploited actin-binding module. *Mol Biol Cell* 9, 1951-9.

Lassing I, Lindberg U. (1990) Polyphosphoinositide synthesis in platelets stimulated with low concentrations of thrombin is enhanced before the activation of phospholipase C. *FEBS Lett* 262 (2):231-3.

Lechler, T., Shevchenko, A. and Li, R. (2000) Direct involvement of yeast type I myosins in Cdc42-dependent actin polymerization. *J Cell Biol* 148, 363-73.

Lechler, T., Jonsdottir, G. A., Klee, S. K., Pellman, D., & Li, R. (2001) A two-tiered mechanism by which Cdc42 controls the localization and activation of an Arp2/3-activating motor complex in yeast. *The Journal of Cell Biology* 155(2), 261–270.

Lee, S. H., & Dominguez, R. (2010) Regulation of Actin Cytoskeleton Dynamics in Cells. *Molecules and Cells 29*(4), 311–325.

Li, R. (1997) Bee1, a yeast protein with homology to Wiskott-Aldrich syndrome protein, is critical for the assembly of cortical actin cytoskeleton. *J Cell Biol* 136, 649-58.

Lin, M. C., Galletta, B. J., Sept, D. and Cooper, J. A. (2010) Overlapping and distinct functions for cofilin, coronin, and Aip1 in actin dynamics in vivo. *J Cell Sci* 123, 1329-42.

Linardopoulou, E. V., Parghi, S. S., Friedman, C., Osborn, G. E., Parkhurst, S. M. and Trask, B. J. (2007) Human subtelomeric WASH genes encode a new subclass of the WASP family. *PLoS Genet* 3, e237.

Liu, W., Santiago-Tirado, F. H., and Bretscher, A. (2012) Yeast formin Bni1p has multiple localization regions that function in polarized growth and spindle orientation. Mol Biol *Cell* 23, 412-22.

Lord M, Laves E, Pollard TD. (2005) Cytokinesis depends on the motor domains of myosin-II in fission yeast but not in budding yeast. *Mol Biol Cell* 16(11):5346-55.

Löwe J., Amos LA. (1999)Tubulin-like protofilaments in Ca^{2+}-induced FtsZ sheets. *EMBO J* 18:2364-2371.

Lu, J., and Pollard, T. D. (2001) Profilin binding to poly-L-proline and actin monomers along with ability to catalyze actin nucleotide exchange is required for viability of fission yeast. *Mol Biol Cell* 12, 1161-75.

Macek B, Mann M, and Olsen JV (2009) Global and Site-Specific Quantitative Phosphoproteomics: Principles and Applications. *Annual Rev Pharmacol Toxicol*; 49: 199-221.

References

Machesky, L. M., Mullins, R. D., Higgs, H. N., Kaiser, D. A., Blanchoin, L., May, R. C., Hall, M. E. and Pollard, T. D. (1999) Scar, a WASp-related protein, activates nucleation of actin filaments by the Arp2/3 complex. *Proc Natl Acad Sci USA* 96, 3739-44.

Madania, A., Dumoulin, P., Grava, S., Kitamoto, H., Scharer-Brodbeck, C., Soulard, A., Moreau, V. and Winsor, B. (1999) The Saccharomyces cerevisiae homologue of human Wiskott-Aldrich syndrome protein Las17p interacts with the Arp2/3 complex. *Mol Biol Cell* 10, 3521-38.

Maldonado-Báez L, Dores MR, Perkins EM, Drivas TG, Hicke L, Wendland B. (2008) Interaction between Epsin/Yap180 adaptors and the scaffolds Ede1/Pan1 is required for endocytosis. *Mol Biol Cell* 19(7):2936-48.

Manneville S. (2004) Actin and Microtubules in Cell Motility: Which One is in Control? *Traffic* 5: 470 – 477.

Marchand JB, Kaiser DA, Pollard TD, Higgs HN. (2001) Interaction of WASP/Scar proteins with actin and vertebrate Arp2/3 complex. *Nat Cell Biol* 3:76-82.

McGough A, Pope B, Chiu W, Weeds A. (1997) Cofilin changes the twist of F-actin: implications for actin filament dynamics and cellular function. *J Cell Biol* 138, 771-781.

McGough, A. (1998) F-actin-binding proteins. *Curr Opin Struct Biol* 8, 166-76.

Michelot A, Costanzo M, Sarkeshik A, Boone C, Yates JR 3rd, Drubin DG. (2010) Reconstitution and protein composition analysis of endocytic actin patches. *Curr Biol* 20(21):1890-9.

Miki, H., Sasaki, T., Takai, Y. and Takenawa, T. (1998a) Induction of filopodium formation by a WASP-related actin-depolymerizing protein N-WASP. *Nature* 391, 93-6.

Miki, H., Suetsugu, S. and Takenawa, T. (1998b) WAVE, a novel WASP-family protein involved in actin reorganization induced by Rac. *EMBO J* 17, 6932-41.

Mok J, et al. (2010) Deciphering protein kinase specificity through large-scale analysis of yeast phosphorylation site motifs. *Sci Signal* 3(109):ra12

Moller-Jensen, J., Borch, J., Dam, M., Jensen, R. B., Roepstorff P., and Gerdes, K. (2003) Bacterial mitosis: ParM of plasmid R1moves plasmid DNA by an actin-like insertional polymerization mechanism. *Mol Cell* 12, 1477−1487.

Moon, A. L., Janmey, P. A., Louie, K. A., and Drubin, D. G. (1993) Cofilin is an essential component of the yeast cortical cytoskeleton. *J Cell Biol* 120, 421-35.

Moreau V, Frischknecht F, Reckmann I, Vincentelli R, Rabut G, Stewart D, et al (2000) A complex of N-WASP and WIP integrates signaling cascades that lead to actin polymerization. *Nature Cell Biology* 2:441-448.

Moseley JB., Goode BL. (2006) The yeast actin cytoskeleton: from cellular function to biochemical mechanism. *Microbiol Mol Bio Rev* 70, 605-645.

References

Mukherjee A, Lutkenhaus J. (1994) Guanine nucleotide-dependent assembly of FtZ into filaments. *J Bcteriol* 176:2754-2758.

Mulholland J, Preuss D, Moon A, Wong A, Drubin D, Botsteib D. (1994) Ultrastructural of the yeast actin cytoskeleton and its association with plasma membrane. *J Cell Biol* 125(2): 381-91.

Mullins, R. D., Heuser, J. A. and Pollard, T. D. (1998) The interaction of Arp2/3 complex with actin: nucleation, high affinity pointed end capping, and formation of branching networks of filaments. *Proc Natl Acad Sci USA* 95, 6181-6.

Munn AL, Riezman H. (1994) Endocytosis is required for the growth of vacuolar H(+)-ATPase-defective yeast: identification of six new END genes. *J Cell Biol* 127(2):373-86.

Munn, A. L., Stevenson, B. J., Geli, M. I., and Riezman, H. (1995) end5, end6, and end7: mutations that cause actin delocalization and block the internalization step of endocytosis in Saccharomyces cerevisiae. *Mol Biol Cell* 6, 1721-42.

Namgoong, S., Boczkowska, M., Glista, M. J., Winkelman, J. D., Rebowski, G., Kovar, D. R. and Dominguez, R. (2011) Mechanism of actin filament nucleation by Vibrio VopL and implications for tandem W domain nucleation. *Nat Struct Mol Biol* 18, 1060-7.

Naqvi, S. N., Zahn, R., Mitchell, D. A., Stevenson, B. J. and Munn, A. L. (1998) The WASp homologue Las17p functions with the WIP homologue End5p/verprolin and is essential for endocytosis in yeast. *Curr Biol* 8, 959-62.

Narayanan A, LeClaire LL 3rd, Barber DL, Jacobson MP.(2011) Phosphorylation of the Arp2 subunit relieves auto-inhibitory interactions for Arp2/3 complex activation. *PLoS Comput Biol* (11):e1002226.

Newpher, T. M. Lemmon, S. K. (2006) Clathrin is important for normal actin dynamics and progression of Sla2p-containing patches during endocytosis in yeast. *Traffic* 7, 574-88.

Newpher, T. M., Smith, R. P., Lemmon, V. and Lemmon, S. K. (2005) In vivo dynamics of clathrin and its adaptor-dependent recruitment to the actin-based endocytic machinery in yeast. *Dev Cell* 9, 87-98.

Ng R, Abelson J. (1980) Isolation and sequence of the gene for actin in *Saccharomyces cerevisiae*. *Proc Natl Acad Sci USA* 77(7):3912-6.

Nishida E, Maekawa S, Sakai H. (1984) Cofilin, a protein in porcine brain that binds to actin filaments and inhibits their interactions with myosin and tropomyosin. *Biochemistry* 23:5307–5313.

Novick P, Botstein D. (1985) Phenotypic analysis of temperature-sensitive yeast actin mutants. *Cell* 40(2):405-16.

Oda, T. (2009) Conformational change of actin induced by polymerization. Tanpakushitsu *Kakusan Koso* 54, 1864-9.

References

Okreglak V, Drubin DG. (2007) Cofilin recruitment and function during actin-mediated endocytosis directed by actin nucleotide state. *J Cell Biol* 178(7):1251-1264.

Ono, S. (2007) Mechanism of depolymerization and severing of actin filaments and its significance in cytoskeletal dynamics. *Int Rev Cytol* 258, 1-82.

Oosawa F, Kasia M. (1962) A theory of linear and helical aggregations of macromolecules. *J Mol Biol* 4:10-21.

Orlova A., Garner EC., Galkin VE., Heuser J., Mullins RD., Egelman EH. (2007)The structure of bacteria ParM filaments. *Nat. Struct. Mol. Biol*. 14:921-926.

Otterbein LR, Graceffa P, Dominguez R. (2001) The crystal structure of uncomplexed actin in ADP state. *Science* 293:708-711

Paavilainen, V. O., Bertling, E., Falck, S. and Lappalainen, P. (2004) Regulation of cytoskeletal dynamics by actin-monomer-binding proteins. *Trends Cell Biol* 14, 386-94.

Palmgren, S., Ojala, P. J., Wear, M. A., Cooper, J. A., and Lappalainen, P. (2001) Interactions with PIP_2, ADP-actin monomers, and capping protein regulate the activity and localization of yeast twinfilin. *J. Cell Biol.* 155, 251-260.

Pantaloni, D. and Carlier, M. F. (1993) How profilin promotes actin filament assembly in the presence of thymosin beta 4. *Cell* 75, 1007-14.

Pantaloni, et al., (2001) Mechanism of actin-based motility. *Science* 292, 1502-1506.

Pantaloni D, Carlier MF, Coue M, Lal AA, Brenner SL, Korn ED (1984) The Critical Concentration of Actin in the Presence of Atp Increases with the Number Concentration of Filaments and Approaches the Critical Concentration of Actin.Adp. *Journal of Biological Chemistry* 259:6274-6283.

Paul AS, Pollard TD. (2009) Review of the mechanism of processive actin filament elongation by formins. *Cell Motil Cytoskeleton.* Review 66 (8):606-17.

Pollard TD (1986) Rate Constants for the Reactions of Atp-Actin and Adp-Actin with the Ends of Actin-Filaments. *Journal of Cell Biology* 103:A264-A264.

Pollard TD and Borisy GG (2003) Cellular motility driven by assembly and disassembly of actin filaments. *Cell* 112:453-465.

Pollard, T. D. (2007) Regulation of actin filament assembly by Arp2/3 complex and formins. *Annu Rev Biophys Biomol Struct* 36, 451-77.

Pollard, T. D., Blanchoin, L. and Mullins, R. D. (2000) Molecular mechanisms controlling actin filament dynamics in nonmuscle cells. *Annu Rev Biophys Biomol Struct* 29, 545-76.

Prehoda, K. E., Scott, J. A., Mullins, D. R. & Lim, W. A. (2000) Integration of multiple signals through cooperative regulation of the N-WASP–Arp2/3 complex. *Science* 290, 801–806.

References

Pruyne DW, Schott DH, Bretscher A. (1998) Tropomyosin-containing actin cables direct the Myo2p-dependent polarized delivery of secretory vesicles in budding yeast. *J Cell Biol* 143(7):1931-45.

Pruyne, D., Evangelista, M., Yang, C., Bi, E., Zigmond, S., Bretscher, A. and Boone, C. (2002) Role of formins in actin assembly: nucleation and barbed-end association. *Science* 297, 612-5.

Ptacek J, et al. (2005) Global analysis of protein phosphorylation in yeast. *Nature* 438(7068):679-84

Puius, Y. A., Mahoney, N. M. and Almo, S. C. (1998) The modular structure of actin-regulatory proteins. *Curr Opin Cell Biol* 10, 23-34.

Quintero-Monzon, O., Jonasson, E. M., Bertling, E., Talarico, L., Chaudhry, F., Sihvo, M., Lappalainen, P. and Goode, B. L. (2009) Reconstitution and dissection of the 600-kDa Srv2/CAP complex: roles for oligomerization and cofilin-actin binding in driving actin turnover. *J Biol Chem* 284, 10923-34.

Quintero-Monzon, O., Rodal, A. A., Strokopytov, B., Almo, S. C. and Goode, B. L. (2005) Structural and functional dissection of the Abp1 ADFH actin-binding domain reveals versatile in vivo adapter functions. *Mol Biol Cell* 16, 3128-39.

Qualmann, B. & Kelly, R. B. (2000) Syndapin isoforms participate in receptor-mediated endocytosis and actin organization. *J. Cell Biol.* 148, 1047–1062.

Rajmohan R, Meng L, Yu S & Thanabalu T (2006) WASP suppresses the growth defect of Saccharomyces cerevisiae las17 Delta strain in the presence of WIP. *Biochem Bioph Res Co* 342: 529–536.

Revenu C, Athman R, Robine S, Louvard D (2004) The co-workers of actin filaments: from cell structure to signals. *Nat Rev Mol Cell Biol* 5:635-646.

Ridley AJ, Paterson HF, Jhonston CL, Diekmann D, Hall A (1992) The small GTP-binding protein rac regulates growth factor-induced membrane ruffling. *Cell* 70:401-401.

Robertson AS, Smythe E, Ayscough KR. (2009) Function of actin in endocytosis. *Cell Mol Life sci* 66(13):2049-65.

Robertson AS, Smythe E, Ayscough KR. (2010) Functions of actin in endocytosis. *Cell Mol Life Sci*. 66(13):2049-65.

Robertson, AS., Allwood, E. G., Smith, A. P., Gardiner, F. C., Costa, R., Winder, S. J. and Ayscough, K. R. (2009) The WASP homologue Las17 activates the novel actin-regulatory activity of Ysc84 to promote endocytosis in yeast. *Mol Biol Cell* 20, 1618-28.

Robinson RC, Turbedasky K, Kaiser DA, et al. (2001) Crystal structure of Arp2/3 complex. *Science* 294 (5547):1679-84.

Rodal, A. A., Manning, A. L., Goode, B. L. and Drubin, D. G. (2003) Negative regulation of yeast WASp by two SH3 domain-containing proteins. *Curr Biol* 13, 1000-8.

References

Rohatgi R, Ho HY, Kirschner MW. (2000) Mechanism of N-WASP activation by Cdc42 and phosphoatidylinositol 4.5-bisphosphate. *J Cell Biol* 150(6):1299-310.

Rohatgi, R., Ho, H. Y., and Kirschner, M. W. (2000) Mechanism of N-WASP activation by CDC42 and phosphatidylinositol 4, 5-bisphosphate. *J Cell Biol* 150, 1299-310.

Rottner, K., Hanisch, J., and Campellone, K. G. (2010) WASH, WHAMM and JMY: regulation of Arp2/3 complex and beyond. *Trends Cell Biol* 20, 650-61. 242.

Roumanie O, et al. (2000) Evidence for the genetic interaction between the actin-binding protein Vrp1 and the RhoGAP Rgd1 mediated through Rho3p and Rho4p in Saccharomyces cerevisiae. *Mol Microbiol* 36(6):1403-14.

Roumanie O, et al. (2002) Functional interactions between the VRP1-LAS17 and RHO3-RHO4 genes involved in actin cytoskeleton organization in Saccharomyces cerevisiae*. Curr Genet* 40(5):317-25.

Rubenstein PA. (1990) The functional importance of multiple actin isoforms. *Bioessays* Review 12(7):309-15.

Safer D, Elzinga M, Nachmias VT (1991) Thymosin beta 4 and Fx, an actin- sequestering peptide, are indistinguishable. *J Biol Chem* 266: 4029–4032.

Samarin S, Romero S, Kocks C, Didry D, Panttaloni D, Carlier MF. (2003) How VASP enhances actin –based motility. *J Cell Biol* 163, 131-142.

Schafer, D. A., Jennings, P. B. and Cooper, J. A. (1996) Dynamics of capping protein and actin assembly in vitro: uncapping barbed ends by polyphosphoinositides. *J Cell Biol* 135, 169-79.

Schlüter K, Waschbüsch D, Anft M, Hügging D, Kind S, Hänisch J, Lakisic G, Gautreau A, Barnekow A, Stradal TE. (2014) JMY is involved in anterograde vesicle trafficking from the trans-Golgi network. *Eur J Cell Biol* 93(5-6):194-204.

Schutt CE, Myslik JC, Rozycki MD, Goonesekere NC, Lindberg U.(1993) The structure of crystalline profilin-beta-actin. *Nature* 28; 365(6449):810-6.

Selden, L. A., Kinosian, H. J., Newman, J., Lincoln, B., Hurwitz, C., Gershman, L. C. and Estes, J. E. (1998) Severing of F-actin by the amino-terminal half of gelsolin suggests internal cooperativity in gelsolin. *Biophys J* 75, 3092-100.

Sept, D. and McCammon, J. A. (2001) Thermodynamics and kinetics of actin filament nucleation. *Biophys J* 81, 667-74.

Sharifpoor S, et al. (2012) Functional wiring of the yeast kinome revealed by global analysis of genetic network motifs. Genome Res 22(4):791-801

Shikama, N., Lee, C. W., France, S., Delavaine, L., Lyon, J., Krstic-Demonacos, M. and La Thangue, N. B. (1999). A novel cofactor for p300 that regulates the p53 response. *Mol Cell* 4, 365-76.

References

Shortle DJ, Haber J, Botstein D. (1982) Lethal disruption of the yeast actin gene by integrative DNA transformation. *Science* 217:371-373.

Siomi D, Sakai M, Niki H. (2008) Determination of bacterial rod shape by a novel cytoskeleton membrane pprotein. *EMBO J* 27:3081-3091.

Siton O, Bernheim-Groswasser A. (2014) Reconstitution of actin-based mortility by Vasodilator-stimulated phosphoprotein (VASP) depends on the recruitment of F-actin seeds from the solution produced by cofilin. *J Biol Chem* 289(45): 31274-86.

Siton O, Ideses Y, Albeck S, Unger T, Bershadsky AD, Gov NS, Bernheim-Groswasser A. (2011). Cortactin releases the brakes in actin- based motility by enhancing WASP-VCA detachment from Arp2/3 branches. *Curr Biol* 21(24):2092-7.

Skoble J, Auerbuch V, Goley D, Welch MD, Portnoy DA. (2001) Pivotal role of VASP in Arp2/3 complex-mediated actin nucleation, actin brnch-formation, and Listeria monocytogenes motility. *J Cell Biol* 155, 89-100.

Smaczynska-de, R., II, Allwood, E. G., Aghamohammadzadeh, S., Hettema, E. H., Goldberg, M. W. and Ayscough, K. R. (2010) A role for the dynamin-like protein Vps1 during endocytosis in yeast. *J Cell Sci* 123, 3496-506.

Smaczynska-de, R., II, Allwood, E. G., Mishra, R., Booth, W. I., Aghamohammadzadeh, S., Goldberg, M. W. and Ayscough, K. R. (2012) Yeast dynamin Vps1 and amphiphysin Rvs167 function together during endocytosis. *Traffic* 13, 317-28.

Smaczynska-de, R., II, Costa, R. and Ayscough, K. R. (2008) Yeast Arf3p modulates plasma membrane PtdIns(4,5)P2 levels to facilitate endocytosis. *Traffic* 9, 559-73.

Smolka MB, Albuquerque CP, Chen SH, Zhou H.(2007) Proteome-wide identification of in vivo targets of DNA damage checkpoint kinases. *Proc Natl Acad Sci USA* 104(25):10364-9.

Smythe E, Ayscough KR. (2003) The Ark1/Prk1 family of protein kinases. Regulators of endocytosis and the actin skeleton. *EMBO Rep* (3):246-51. Review.

Snapper, S. B., Takeshima, F., Anton, I., Liu, C. H., Thomas, S. M., Nguyen, D., Dudley, D., Fraser, H., Purich, D., Lopez-Ilasaca, M. et al. (2001) N-WASP deficiency reveals distinct pathways for cell surface projections and microbial actin-based motility. *Nat Cell Biol* 3, 897-904.

Sopko R, et al. (2006) Mapping pathways and phenotypes by systematic gene overexpression. *Mol Cell* 21(3):319-30

Soulard, A., Friant, S., Fitterer, C., Orange, C., Kaneva, G., Mirey, G. and Winsor, B. (2005) The WASP/Las17p-interacting protein Bzz1p functions with Myo5p in an early stage of endocytosis. *Protoplasma* 226, 89-101.

Stovold, C.F., Millard, T.H. and Machesky, L.M. (2005) Inclusion of Scar/WAVE3 in a similar complex to Scar/WAVE1 and 2. *BMC Cell Biol* 6(1), 11.

References

Stradal TE, Scita G. (2006) Protein complexes regulating Arp2/3-mediated actin assembly. *Curr Opin Cell Biol* 18(1):4-10.

Straub F (1942) Actin. . *Studies from the Institute of Medical Chemistry University Szeged*, II:3-15.

Strelkov, S. V., Herrmann H and Aebi, U. (2003) Molecular architecture of intermediate filaments. *Bioessays* 25, 243-251.2003).

Strzelecka-Golaszewska, H. (2001). Divalent cations, nucleotides, and actin structure. *Results Probl Cell Differ* 32, 23-41.

Suck, D., Kabsch, W. and Mannherz, H. G. (1981) Three-dimensional structure of the complex of skeletal muscle actin and bovine pancreatic DNAse I at 6-A resolution. *Proc Natl Acad Sci USA* 78, 4319-23.

Suetsugu S (2013) Activation of nucleation promoting factors for directional actin filament elongation: allosteric regulation and multimerization on the membrane. *Semin Cell Dev Biol* 4: 267-71.

Suetsugu S, Miki H, Takenawa T. (2001) Identification of another actin-related protein (Arp) 2/3 complex binding site in neural Wiskott-Aldrich syndrome protein (N-WASP) that complements actin polymerization induced by the Arp2/3 complex activating (VCA) domain of N-WASP*. J Biol Chem* 276, 33175-33180a.

Suetsugu S, Hattori M, Miki H, Tezuka T, Yamamoto T, Mikoshiba K, Takenawa T. (2002) Sustained activation of N-WASP through phosphorylation is essential for neurite extension. *Dev Cell* 3(5):645-58.

Suetsugu, S., Miki, H., Yamaguchi, H., Obinata, T. and Takenawa, T. (2001) Enhancement of branching efficiency by the actin filament-binding activity of N-WASP/WAVE2*. J Cell Sci* 114, 4533-42.

Sun HQ, Yamamoto M, Mejillano M, Yin HL. (1999) Gelsolin, multifunctional actin regulatory protein*. J Biol Chem* 274:33179-33182.

Sun, Y., Carroll, S., Kaksonen, M., Toshima, J. Y. and Drubin, D. G. (2007) PtdIns(4,5)P2 turnover is required for multiple stages during clathrin- and actin-dependent endocytic internalization*. J Cell Biol* 177, 355-67.

Sun, Y., Kaksonen, M., Madden, D. T., Schekman, R. and Drubin, D. G. (2005). Interaction of Sla2p's ANTH domain with PtdIns(4,5)P2 is important for actin-dependent endocytic internalization*. Mol Biol Cell* 16, 717-30.

Sun, Y., Martin, A. C. and Drubin, D. G. (2006) Endocytic internalization in budding yeast requires coordinated actin nucleation and myosin motor activity. *Dev Cell* 11, 33-46.

Swaney DL, et al. (2013) Global analysis of phosphorylation and ubiquitylation cross-talk in protein degradation. *Nat Methods* 10(7):676-82

References

Ti SC, Jurgenson CT, Nolen BJ, Pollard TD. (2011) Structural and biochemical characterization of two binding sites for nucleation-promoting factor WASp-VCA on Arp2/3 complex. *Proc Natl Acad Sci USA* 108(33):E463-71.

Tojkander S, Gergana Gateva and Pekka Lappalainen. (2012) Actin stress fibers – assembly, dynamics, and biological roles*. Journal of Cell Science* 125, 1-10.

Tomasevic, N., Jia, Z., Russell, A., Fujii, T., Hartman, J. J., Clancy, S., Wang, M., Beraud, C., Wood, K. W. and Sakowicz, R. (2007) Differential regulation of WASP and N-WASP by Cdc42, Rac1, Nck, and PI(4,5)P2. *Biochemistry* 46, 3494-502.

Tondeleir, D., Vandamme, D., Vandekerckhove, J., Ampe, C., and Lambrechts, A. (2009) Actin isoforms expression patterns during mammalian development and in pathology: insights from mouse models. *Cell Motil Cytoskeleton* 66, 798-815.

Tong, A. H., Drees, B., Nardelli, G., Bader, G. D., Brannetti, B., Castagnoli, L., Evangelista, M., Ferracuti, S., Nelson, B., Paoluzi, S. et al. (2002) A combined experimental and computational strategy to define protein interaction networks for peptide recognition modules. *Science* 295, 321-4.

Tong, A. H., Evangelista, M., Parsons, A. B., Xu, H., Bader, G. D., Page, N., Robinson, M., Raghibizadeh, S., Hogue, C. W., Bussey, H. et al. (2001) Systematic genetic analysis with ordered arrays of yeast deletion mutants. *Science* 294, 2364-8.

Tonikian, R., Xin, X., Toret, C. P., Gfeller, D., Landgraf, C., Panni, S., Paoluzi, S., Castagnoli, L., Currell, B., Seshagiri, S. et al. (2009) Bayesian modeling of the yeast SH3 domain interactome predicts spatiotemporal dynamics of endocytosis proteins. *PLoS Biol* 7, e1000218.

Torres, E., and Rosen, M. K. (2003) Contingent phosphorylation/dephosphorylation provides a mechanism of molecular memory in WASP. *Mol Cell* 11, 1215-27.

Torres, E., and Rosen, M. K. (2006). Protein-tyrosine kinase and GTPase signals cooperate to phosphorylate and activate Wiskott-Aldrich syndrome protein (WASP)/neuronal WASP. J *Biol Chem* 281, 3513-20.

Toshima, J., Toshima, J. Y., Martin, A. C. and Drubin, D. G. (2005) Phosphoregulation of Arp2/3-dependent actin assembly during receptor-mediated endocytosis. *Nat Cell Biol* 7, 246-54.

Tysca MJ, Warshaw DM. (2002) The myosin power stroke. *Cell Motil Cytoskeleton* . Review51(1):1-15. Review.

Urbanek AN, Smith AP, Allwood EG, Booth WI, Ayscough KR. (2012)A novel actin-binding motif in Las17/WASP nucleates actin filaments independently of Arp2/3.*Curr Biol*. 23(3):196-203.

van den Ent, F., Amos, L. A. and Lowe, J. (2001) Prokaryotic

References

origin of the actin cytoskeleton. *Nature* 413, 39-44.

van den Ent, F., Moller-Jensen, J., Amos, L. A., Gerdes, K., and Lowe, J. (2002) F-actin-like filaments formed by plasmid segregation protein ParM. *EMBO J* 21, 6935−6943.

Van Troys, M., Huyck, L., Leyman, S., Dhaese, S., Vandekerkhove, J. and Ampe, C. (2008) Ins and outs of ADF/cofilin activity and regulation. *Eur J Cell Biol* 87, 649-67.

Vartiainen, M. K., Mustonen, T., Mattila, P. K., Ojala, P. J., Thesleff, I., Partanen, J. and Lappalainen, P. (2002) The three mouse actin-depolymerizing factor/cofilins evolved to fulfil cell-type-specific requirements for actin dynamics. *Mol Biol Cell* 13, 183-94.

Vavylonis D, Kovar DR, O'Shaughnessy B, Pollard TD.(2006) Model of formin-associated actin filament elongation. *Mol Cell* 21(4):455-66.

Veltman DM and Insall RH (2010) WASP family proteins: their evolution and its physiological importance. *Mol Biol of the Cell* 21, 2880-2893.

Vida TA, Emr SD. (1995) A new vital stain for visualizing vacuolar membrane dynamics and endocytosis in yeast. *J Cell Biol* 128(5):779-92.

Volkmann, N., Amann, K. J., Stoilova-McPhie, S., Egile, C., Winter, D. C., Hazelwood, L., Heuser, J. E., Li, R., Pollard, T. D. and Hanein, D. (2001) Structure of Arp2/3 complex in its activated state and in actin filament branch junctions. *Science* 293, 2456-9.

Waddle J, Karpova T, Waterson R, Cooper J (1996) Movement of cortical actin patches in yeast. *J Cell Biol* 132:861–870.

Waddle, J. A., Karpova, T. S., Waterston, R. H. and Cooper, J. A. (1996) Movement of cortical actin patches in yeast. *J Cell Biol* 132, 861-70.

Wallar BJ, Stropich BN, Schoenherr JA, Holman HA, Kitchen SM, Alberts AS. (2006) The basic region of the diaphanous-autoregulatory domain (DAD) is required for autoregulatory interactions with the diaphanous-related formin inhibitory domain. *J Biol Chem*. 281(7):4300-7.

Walter F., PhD. Boron (2003). Medical physiology: A cellular and Molecular Approach. Elsevier/Saunders. P.1300. ISBN 1-4160-2328-3.Page 25

Wang, H., Robinson, R. C. and Burtnick, L. D. (2010) The structure of native G-actin. *Cytoskeleton (Hoboken)* 67, 456-65.

Warren DT, Andrews PD, Gourlay CG, Ayscough KR (2002) Sla1p couples the yeast endocytic machinery to proteins regulating actin dynamics. *J Cell Sci* 115:1703–1715.

Weaver AM, Heuser JE, Karginov AV, Lee WL, Parsons JT, Cooper JA. (2002) Interaction of cortactin and N-WASp with Arp2/3 complex. *Curr Biol* 6; 12(15):1270-8.

References

Weed SA, Karginov AV, Schafer DA, Weaver AM, Kinley AW, Cooper JA, Parsons JT. (2000) Cortactin localization to sites of actin assembly in lamellipodia requires interactions with F-actin and the Arp2/3 complex. *J Cell Biol* 151(1):29-40.

Wegner A, Engle J. (1975) Kinetics of the cooperative association of actin to actin filaments. *Biophys Chem* 3(3):215-25.

Weinberg J, Drubin DG. (2012)Clathrin-mediated endocytosis in budding yeast. *Trends Cell* 22(1):1-13.

Welch MD, Mullins RD.(2002) Cellular control of actin nucleation. *Annu Rev Cell Dev Biol*. 18:247-88.

Wendland B, Steece KE, Emr SD (1999)Yeast epsins contain an essential N-terminal ENTH domain, bind clathrin and are required for endocytosis. *EMBO J* 18:4383-4393.

Wendland, B., Steece, K. E. and Emr, S. D. (1999) Yeast epsins contain an essential N-terminal ENTH domain, bind clathrin and are required for endocytosis. *EMBO J* 18, 4383-93.

Whitacre J, Davis D, Toenjes K, Brower S, Adams A. (2001) Generation of an isogenic collection of yeast actin mutants and identification of three interrelated phenotypes. *Genetics* 157(2):533-43.

Wickstead B, Gull K. (2011)The evolution of the cytoskeleton. *J Cell Biol* 2; 194(4):513-25.

Winder SJ, Jess T, Ayscough KR (2003) SCP1 encodes an actin-bundling protein in yeast. *Biochem J* 375:287–295.

Winder, S. J. and Ayscough, K. R. (2005) Actin-binding proteins. *J Cell Sci* 118, 651-4.

Winder, S. J., Jess, T. and Ayscough, K. R. (2003) SCP1 encodes an actin-bundling protein in yeast. *Biochem J* 375, 287-95.

Winter, D., Lechler, T. and Li, R. (1999) Activation of the yeast Arp2/3 complex by Bee1p, a WASP-family protein. *Curr Biol* 9, 501-4.

Winter, D., Podtelejnikov, A. V., Mann, M. and Li, R. (1997) The complex containing actin-related proteins Arp2 and Arp3 is required for the motility and integrity of yeast actin patches. *Curr Biol* 7, 519-29.

Witke W. (2004) The role of profilin complexes in cell motility and other cellular processes. *Trends Cell Biol* 14:461–469.

Wu CC, MacCoss MJ. (2002) Shotgun proteomics: tools for the analysis of complex biological systems. *Curr Opin Mol Ther*; 4(3):242-50.

Wu H, Parsons JT. (1993) Cortactin, an 80/85-kilodalton pp60src substrate, is a filamentous actin-binding protein enriched in the cell cortex. *J Cell Biol* 120(6):1417-26.

References

Wu, J. Q., and T. D. Pollard. (2005) Counting cytokinesis proteins globally and locally in fission yeast. *Science* 310:310-314.

Xing Judy Chen, Anna Julia Squarr, Raiko Stephan, Baoyu Chen, Theresa E, Higgins, David J.Barry, Morag C. Martin, Michael K. Rosen, Sven Bogdan, Michael WAY. (2014) Ena/VASP proteins cooperate with the WAVE complex to regulate the actin cytoskeleton. *Dev. Cell* 30(5):569-584.

Yang C, Svitkina T. (2011a) Visualizing branched actin filaments in lamellipodia by electron tomography. *Nat Cell Biol* 13:1012-1013.

Yang C, Svitkina T. (2011b) Filopodia initiation focus on the Arp2/3 complex and formins. *Cell Adh Migr* 5:402-408.

Yao X, Rubenstein PA. (2001) F-actin-like ATPase activity in a polymerization-defective mutant yeast actin (V266G/L267G). *J Biol Chem* 276(27):25598-604.

Young, M. E., Cooper, J. A., and Bridgman, P. C. (2004) Yeast actin patches are networks of branched actin filaments. *J Cell Biol* 166, 629-35.

Yu, X. and Cai, M. (2004) The yeast dynamin-related GTPase Vps1p functions in the organization of the actin cytoskeleton via interaction with Sla1p. *J Cell Sci* 117, 3839-53.

Zalevsky J, Lempert L, Kranitz H, Mullins RD. (2001) Different WASP family proteins stimulate different Arp2/3 complex dependent actin –nucleating activities. *Curr Biol* 11, 1903-1913.

Zeng G. Cai M. (1999) Regulation of actin cytoskeleton organization in yeast by a novel serine/threonine kinase Prk1p. *J Cell Biol*. 11:71-82.

Zeng G., Huang B., Neo SP., Wang J., Cai M. (2007) Scd5p mediates phosphoregulation of actin and endocytosis by the type 1 phosphatases Glc7p in yeast. *Mol. Biol. Cell* 18:4885-4898.

Zeng, G., Yu, X. and Cai, M. (2001) Regulation of yeast actin cytoskeleton-regulatory complex Pan1p/Sla1p/End3p by serine/threonine kinase Prk1p. *Mol Biol Cell* 12, 3759-72.

Zheng, B., Han, M., Bernier, M. and Wen, J. K. (2009) Nuclear actin and actin-binding proteins in the regulation of transcription and gene expression. *FEBS J* 276, 2669-85.

Zimmerle CT, Frieden C. (1986) Effect of temperature on the mechanism of actin polymerization. *Biochemistry* 25(21):6432-8.

Zuchero, J. B., Coutts, A. S., Quinlan, M. E., Thangue, N. B. and Mullins, R. D. (2009) p53-cofactor JMY is a multifunctional actin nucleation factor. *Nat Cell Biol* 11, 451-9.